TRIBHUVAN UNIVERSITY

INSTITUTE OF ENGINEERING

PULCHOWK CAMPUS

Assessment of the Land Use/Cover and Climate Change Impacts in the Urbanized River Basin

The Case of Bagmati River Basin, Nepal

Suraj Lamichhane

(2073/Ph.CE/105)

A THESIS SUBMITTED TO THE DEPARTMENT OF CIVIL IN PARTIAL FULFILLMENT OF THE REQUIREMENTS FOR THE DEGREE OF DOCTOR OF PHILOSOPHY

DEPARTMENT OF CIVIL ENGINEERING,

December, 2020

COPYRIGHT

DECLARATION

Thesis entitled **"Assessment of the Land Use/Cover and Climate Change Impacts in the Urbanized River Basin, The Case of Bagmati River Basin, Nepal"** which is being submitted to Department of Civil Engineering, Pulchowk Campus, Institute of Engineering, Tribhuvan University; Nepal for the award of the degree of Doctor of Philosophy (Ph.D.) is a research work carried out by me under the supervision of **Prof. Dr. Narendra Man Shakya**, Department of Civil Engineering, Institute of Engineering, Tribhuvan University between April 2017 to December 2020. I declare that the work is my own and has not been submitted for a degree of another university.

Suraj Lamichhane
Campus Roll No: 073-Ph.CE-105
Department of Civil Engineering
Pulchowk Campus,
Institute of Engineering
Tribhuvan University,
Lalitpur, Nepal

RECOMMENDATION

This is to recommend that **Mr. Suraj Lamichhane** has carried out research entitled **"Assessment of the Land Use/Cover and Climate Change Impacts in the Urbanized River Basin; The Case of Bagmati River Basin, Nepal"** under my supervision. To my knowledge, this work has not been submitted for any other degree. He has fulfilled the entire requirement laid down by the Institute of Engineering, Tribhuvan University, for the submission of thesis and for the award of the degree.

_____

Prof. Dr. Narendra Man Shakya
Department of Civil Engineering
Pulchowk Campus,
Institute of Engineering
Tribhuvan University,
Lalitpur, Nepal

Tribhuvan University

INSTITUTE OF ENGINEERING

The thesis entitled **"Assessment of the Land Use/Cover and Climate Change Impacts in the Urbanized River Basin; The Case of Bagmati River Basin, Nepal"** submitted by **Mr. Suraj Lamichhane** for partial fulfillment of the requirement for the degree of Doctor of Philosophy in Civil Engineering and specialization in Water Resources Engineering has been accepted by the Institute of Engineering Research Committee upon the recommendation of the supervisor and Departmental Research Committee and approved by the following examiners

External Examiner

Prof. Dr. Hiroshi Ishidaira

University of Yamanashi

Kofu, Japan

Internal Examiners

1. Dr. Divas Bahadur Basnyat

Nepal Development Research Institution (NDRI), Lalitpur

2. Dr. Laxmi Prasad Devkota
Academician,
Nepal Academy of Science and Technology

.....

Prof. Dr. Shashidhar Ram Joshi

Committee Chairperson,

Dean

Institute of Engineering

Date: - December 15, 2020

Tribhuvan University

INSTITUTE OF ENGINEERING

The undersigned certify that they have evaluated the thesis entitled **"Assessment of the Land Use/Cover and Climate Change Impacts in the Urbanized River Basin; The Case of Bagmati River Basin, Nepal"** submitted by Mr. Suraj Lamichhane and have external oral presentation for partial fulfillment of the requirement for the degree of Doctor of Philosophy and recommended to the Institute of Engineering for acceptance of this thesis

……

External Examiner

Prof. Dr. Hiroshi Ishidaira

University of Yamanashi

Kofu, Japan

……..……..…

Internal Examiner

Dr. Divas Bahadur Basnyat

Nepal Development Research Institution (NDRI), Lalitpur

……

Internal Examiner

Dr. Laxmi Prasad Devkota

Academician,

Nepal Academy of Science and Technology (NAST), Lalitpur

Acknowledgement

I express sincere appreciation towards my respected supervisor Prof. Dr. Narendra Man Shakya, for his guidance and insight during the entire research. I appreciate his contribution of time and ideas to make my research productive and stimulating. It gives me pleasure to extend my sincere gratitude to Institute of Engineering (IOE), Pulchowk Campus, Department of Civil Engineering, Tribhuvan University for providing me an opportunity to accomplish my Ph.D. degree. This Ph.D. research had been supported by MSESSD program, a joint collaboration between IOE and Norwegian University of Science and Technology (NTNU) and supported by Energy and Petroleum Program (En Pe), Norway. I also thank Prof Dr. Martina Keitsch, Professor at the NTNU; Associate Prof. Dr. Hiroshi Ishidaira at the University of Yamanashi; Prof. Dr. K.N.Jha at the Indian Institute of Technology (IIT) Delhi; and so on during my foreign study with concerning institutions. I always remember their contribution to making my research an "international." Again, I am very appreciating to Dr. K.N. Dulal for the valuable suggestion as an external examiner during DRC presentation.

I am very grateful to the Chairperson of DRC Associate Prof. Dr. Bharat Mandal, and Committee Members Prof. Dr. Gokarna Bahadur Motra, Associate Prof. Dr. Rajan Suwal, and Professor Dr. Laxman Prasad Poudel (Campus Chief, Pulchowk Campus) for their comments on the research and suggestions during my presentations in DRC. Similarly, I am gratified to the Heads of Department of Civil Engineering during my study period Associate Prof. Dr. Kamal Bahadur Thapa and Associate Prof. Dr. Bharat Mandal for their well-managed prerequisite courses for my Ph.D. study and other organizational support given to me. Most important, I would like to express my sincere appreciation to the course teachers Prof. Dr. Balkrishna Sapakota, Associate Prof. Nagendra Bahadur Amatya, prof. Dr. Hem Raj Sharma, Dr. Pawan Bhattrai, and others for their wonderful instructions to succeed in the academic course matters. The administrative personnel at Department of Civil Engineering are thankful for their friendly behavior, and administrative support rendered to me. Similarly, I would like to thank Dean of the IoE Prof. Dr. S.R. Joshi and Ast. Dean Prof. Dr. Sushil B Bajracharya, former Dean of the IoE, Prof. Dr. Tri Ratna Bajracharya, Prof. Ram Chandra Sapakota, for their continuous encouragement and moral support at IOE. Likewise, I am thankful to Campus administrative staff at Pulchowk Campus for their honest support during my Ph. D. study.

I express my sincere thanks to Dr. Vishnu Prasad Pandey, Dr. Bhesh Raj Thapa, Dr. Aakash Dawadee, Dipendra Gautam, and Dr. Anil Aryal for his continuous guidance and support during the doctoral studies since the very beginning. I am grateful to my colleagues Pradip Adhikari, Sanjeeb Baral, Tikaram Baral, Dr. Ananta Man Pradhan, Dr. Bishnu Prasad Bhattrai, Indra Narayan Yadav, Babu Ram Dawadi, Bindu Shrestha, Hari Prasad poudel, Sarashwoti Thapa, and others for their continuous support since starting of my study.

Lastly, I would like to thank my family for their love and continuous encouragement. For my parents who raised me with a love of engineering and supported me in all my pursuits and most of all for my loving, supportive, and encouraging wife Sarita Dawadi, daughter Sukriti, son Suprit, whose faithful support during my Ph. D. work is appreciated.

Thank You

Suraj Lamichhane

CRN: 073/Ph.CE/105

December, 2020

Abstract

Land use/cover (LULC) change in the form of urbanization and climate change are affecting water resources in many urbanized basins around the world, and the Bagmati River Basin in central Nepal is not an exception. Kathmandu Valley (KV) watershed located in the headwaters of the Bagmati River Basin is urbanizing at a higher rate and hosting 29% of the urban population in the country. Urbanization and associated land use/cover (LULC) change, population increase, excess water demand, encroachment of open land, and climate change results over-stress in the surface as well as subsurface water balance of the basin. Rise in impervious built-up area, excess surface runoff, reduction of groundwater recharge dynamics and corresponding impacts in the river runoff exacerbate water scarcity, more specifically in the dry period. Groundwater is, and will continue to be, the main source of water supply in the KV, however, both supply side (i.e., recharge) and demand side (i.e., pumping) of groundwater are affected due to urbanization, thus, putting more pressure on the groundwater resources in the KV. However, there is no comprehensive understanding of groundwater dynamics under the scenarios of changing LULC, climate, and pumping rates. This study therefore develops projected future scenarios of LULC, climate, recharge areas, and pumping rates and then uses multiple models to assess impacts of – i) LULC change on potential recharge areas; ii) projected climate change and LULC change on spatio-temporal distribution of surface water availability; and iii) urbanization on groundwater dynamics.

The LULC change was modeled using CLUE-S model. Results showed 6.51% decrease and 4.9% increase in agricultural and built-up areas, respectively, during 2010 - 2018; however, projected to change by +21.4%, -20.5%, and -0.9% in built-up, agricultural, and forest areas, respectively, during 2020-2050. In terms of recharge areas, 6% of the open land is projected to convert into impervious areas every decade. Future climate was projected based on an ensemble multiple Regional Climate Models (RCMs) under Representative Concentration Pathways (RCP) scenarios. Results revealed that average annual values of maximum temperature, minimum temperature, and precipitation in the KV watershed for the period of 2010 to 2050 are projected to increase by 0.19^{o}C, 0.33^{o}C, and 24%, respectively, for RCP4.5 scenarios and 0.89^{o}C, 0.96^{o}C and 1%, respectively, for RCP8.5 scenarios.

Current and future water balances under the scenarios of LULC change and climate change were simulated by developing a hydrological model in the Soil and Water Assessment Tool (SWAT) platform. Simulated future mean annual river discharge under RCP4.5 scenario

showed projected increase by 37%, 21%, and 36%, due to climate change (CC) alone, LULC change alone, and combined (both LULC and CC) scenarios at the Khokana station for 2050. Similarly, under the RCP8.5 scenario, future runoff is projected to change by -14%, +21%, and -14% for the aforementioned scenarios during the same period. LULC change resulted increase in average annual flow, however, decrease in base-flow. The decadal average rate of groundwater contribution to the river discharge for the RCP4.5 and RCP8.5 scenarios declined with 58% and 68%, respectively, for the integrated scenario due to less infiltration by the expansion of the built-up area.

Finally, impacts of urbanization on groundwater dynamics were evaluated by developing a groundwater flow model using MODFLOW code. Urbanization was reflected in the model as encroachment in groundwater recharge areas as various pumping rate scenarios. The pumping rate included the integrated pumping from the deep and shallow aquifer. Finally, future pumping scenarios were developed using three types of population growth rates; 1% for the developed areas (with greater pumping rate of > 100 m^3/day), 1.5% for newly developing areas (pumping rate between 50 to 100 m^3/day), and 3 % for the areas in the peripheral parts of the valley (pumping rate less than the 50 m^3/day). Simulated results showed significant drawdown in the inner and northern areas compared to the other parts. Except the cases of dry pocket areas, maximum drawdowns in the basin for the combined and only pumping scenarios for the dry season are -5.25 m and -4.87 m, respectively during 2020-2050. The drawdowns induced due to encroachment of recharge areas -1.09 m, -3.63 m for dry and wet seasons, respectively.

Findings from this study using multiple models and scenarios indicate changes in water balance, potential shrinking of recharge area and subsequent decrease in recharge volume, and depletion in groundwater levels in some areas. These phenomena have implications in river basin hydrology. Therefore, appropriate planning and management of watershed conservation activities, water resources, and water supply systems are essential to use both surface and groundwater resources in the valley in a sustainable way.

Abbreviations and Acronyms

Abbreviations

AF	Adjusted Factor
AHP	Analytic Hierarchy Process
ASCE	American Society of Civil Engineers
ASSESS	the Australian Community Climate and Earth-System Simulator
BTOPMC	Block-wise use of TOPMODEL with Muskingum-Cunge Routing
CC	Climate Change
CFUGs	Community Forest User Groups
CG	Center of Gravity
CGD	Central Groundwater District
CI	Consistency Index
CLUE	Conversion of Land Use and its Effects
CLUE-S	the Conversion of Land Use and its Effects at Small regional extent
CN	Curve Number
CR	Consistency Ratio
DEM	Digital Elevation Model
DHM	Department of Hydrology and Meteorology
ET	Evapo-Transpiration
GCMs	General Circulation Models
GDEM	Global Digital Elevation Map
GIS	Geographical Information System
GoN	Government of Nepal
GW	Ground-Water
GWF	Ground-Water Flow
GWPRA	Groundwater Potential Recharge Area

GWT	Ground Water Table
HBV	Hydrologiska Byrans Vattenbalansavdelning
HEC-HMS	Hydrologic Engineering Center’s Hydrologic Modeling System
HRUs	Hydrological Response Units
ICIMOD	International Center for Integrated Mountain Development
IGB	Indus, Ganges, and Brahmaputra
IPCC	Intergovernmental Panel on Climate Change
KGE	Kling-Gupta Efficiency
KUKL	Kathmandu Upatyaka Khanepani Limited
KV	Kathmandu Valley
KVWSMB	Kathmandu Valley Water Supply Management Board
LCM	Land Change Modeler
lpcd	liter per capita day
LS	Linear Scaling
LULC	Land Use Land Cover
MAE	Mean Absolute Error
MCDM	Multi-Criteria Decision Making
MCM	Million-Cubic-Meters
ME	Mean Error
MODFLOW	MODular groundwater FLOW
MWSP	Mealchi Water Supply Project
NGD	Northern Groundwater District
nos	Numbers
NSE	Nash–Sutcliffe Efficiency
NWT	Newton Solver Technique
PBIAS	Percent BIAS

PET	Potential Evapo-Transpiration
PRMS	Precipitation Runoff Modeling System
QM	Quantile Mapping
RCMs	Regional Climate Models
RCP	Representative Concentration Pathway
RMSE	Root Mean Square Error
ROC	Receiver Operating Characteristic
SCS-CN	Soil Conservation Service Curve Number
SD	Standard Deviation
SDGs	Sustainable Development Goals
SGD	Southern Groundwater District
SSPs	Shared Socioeconomic Pathways
SWAT	Soil and Water Assessment Tool
TWS	Total Water Storage
USGS	United States Geological Survey
VDCs	Village Development Committees

Acronyms

A2	Regionally oriented economic development
B2	Local environmental sustainability
-	Minus (Negative)
'	Minute
"	Second
%	Percent
+	Plus (Positive)
<	Less than
>	Greater than
±	Plus minus
Δh	Change in head
ΔH	Change in head due to pumping
Δt	Chanage in time
ΔV	Change in volume
$\sum$	Sum
^{0}/daily	Degree per day
^{0}	Degree
^{0}C	Degree celsius
2-D	Two dimensional
3-D	Three dimensional
F^{-1}	Inverse cumulative distribution function
H_2O	Water
hr	Hour
K	Hydraulic conductivity
km^2	Square kilometer

L	Length unit
L/T	Lenth per unit time
L^{-1}	Per unit length
L^3	Length cube (Volume)
L^3T^{-1}	Length cube per time
m/year	meter per year
m	meter
m^2/day	Meter square per day
m^3/s	Meter cube per second
masl	Meter above sea level
mm	Millimeter
mm/hr	Millimeter per hour
mm/yr	Milimeter per year
Obs	Observed
P	Precipitation
p. p. m	parts per millions
Qi	Discharge
r	Correlation coefficients
S1	Pre-monsoon
S2	Monsoon
S3	Post-monsoon
Sim	Simulated
sq.km	Square kilometer
S_S	Specific storage
T	Temperature
T^{-1}	Per unit time

W	Well
W/m^2	Watt per meter square
Wj	Weightage factor
α	Alfa (Permissible limit factor)
β1	Beta (Coefficients of explanatory varibles)
λmax	Lambda (Eigen value)
μ	Mean
σ	Standard deviation
*	Asterisk (Corrected value)

List of Tables

List of Figures

Table of Contents

Chapter 1. Introduction

1.1 Background

Climate change and land use/cover (LULC) change, more specifically, urbanization, are the dominant phenomena across the globe in the recent decades. Urbanization, which pertains shifting of the rural population towards the urban area, increases the population density and leads to social changes in the area (UN DESA, 2018). Urbanization fundamentally tends to increase the built-up area and population density for economic activities. Principally, urbanization is governed by the migration of people with the pull and push factors related to environmental, economic, cultural, and socio-political changes (Van Hear et al., 2018). In 1950 only 30% of the world population lived in the urban area and it reached 55% in 2018. If similar trend continues, 68% of total people are expected to be in urban areas by 2050 (UN DESA, 2018). Continuation of urbanization process may translate the urban centers into megacities (with over 10 million populations). By 2030, number of megacities are expected to reach 41, occupying only 2% of the world's land area, accommodating more than half of the global population, and consuming 75% of the global resources (Nambiar et al., 2018). Urbanization may increase the global water and food demands by 30% and 60%, respectively, in 2050 (Boretti and Rosa, 2019). The rates of increase in water and food demands are higher in the African and Asian continents.

Nepal is among the ten least urbanized countries in the Asia, however, is one of the top ten countries with highest rate of urbanization (UN DESA, 2018). The Kathmandu Valley (KV), Pokhara Valley, inner Tarai Valleys, and border towns near the East-West Highway are the major urban centers in Nepal (MoUD, 2017) as shown in Figure 1-1. The KV located at headwater of the Bagmati River Basin in central Nepal, is the most populated and fast-growing urban area in Nepal hosting about 29% of urban population in the country (MoUD, 2017). The urbanization pattern can be observed through increase in population density, changes in LULC, and change in urban facilities and environmental (Lamichhane and Shakya, 2019a). The valley has a population density of over 10,000 persons/sq.km, whereas, the core city area has much higher than the average density. For example, the population densities of Kathmandu, Lalitpur, and Bhaktapur cities are 19,726 persons/sq.km, 14,574 persons/sq.km, and 12,662 persons/sq.km, respectively (CBS, 2011). Peri-urban areas of the KV too have high population density of 4,445 persons/sq.km on an average, which is expected to increase at a faster rate in near to mid-future for various reasons such as

availability of land and lower cost (Lamichhane and Shakya, 2019a), and therefore, further contribute to urbanization.

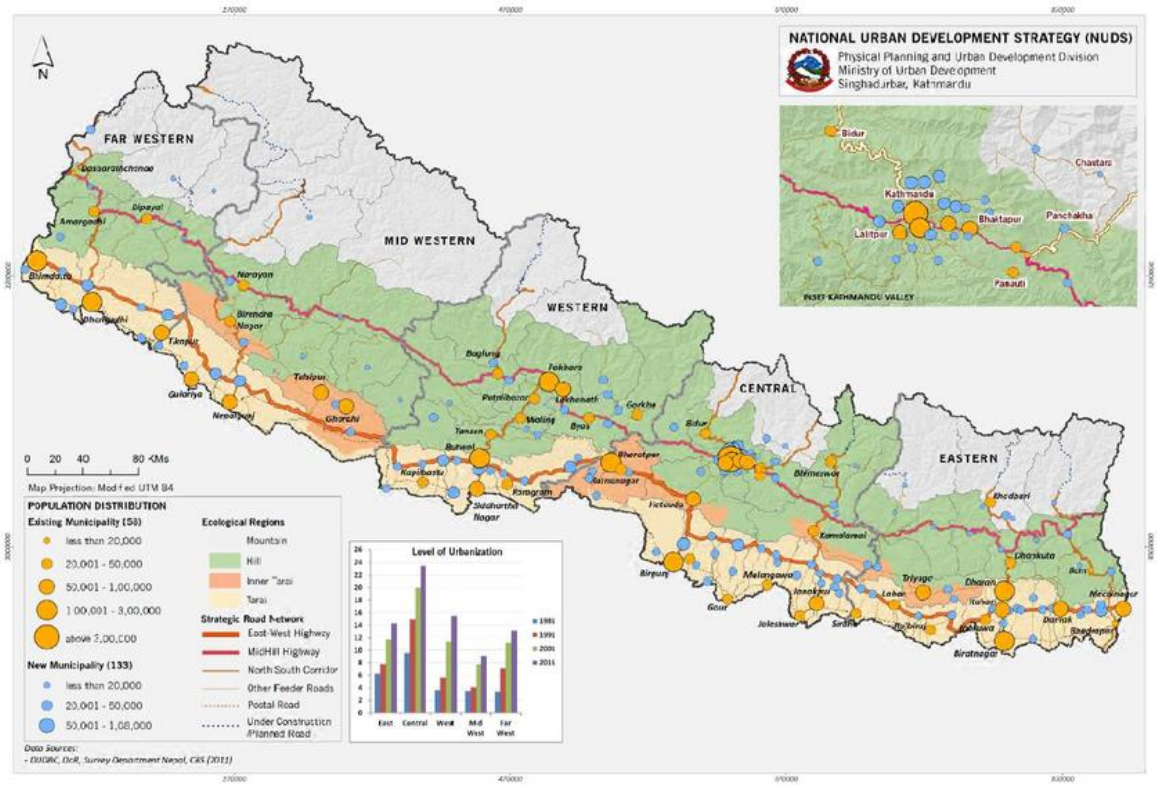

Figure 1-1 Urban areas in Nepal

(Source: MoUD, (2017)*)*

Urbanization has both positive and negative consequences, but in the context of water resources, it has always created more challenges than opportunities. Conversion of the LULC type due to urbanization has affected sustainable management of water resources (Mohammady et al., 2017). The urbanization process is translating permeable land surface into impervious one and ultimately changing regional hydrological characteristics (Zhou et al., 2013). Furthermore, LULC plays a significant role in the hydrological process by directly influencing the surface runoff, infiltration, groundwater flow, and interflow. These hydrological phenomena affect the hydrology of the river in terms of runoff volume, flood frequency, and base flow (Aich et al., 2016). As water is central to achieve the Sustainable Development Goals (SDGs) and groundwater is a key source to supply water in many areas, it plays a vital role in achieving the SDGs. People use subsurface water in various forms, such as well, stone spout, and others from history to the hitherto for multiple purposes such as domestic, agriculture, and industrial, among others (Gautam and Prajapati, 2014). Existing sources and water supply system in the KV can meet only 19% and 31% of water demands in

the dry and wet seasons, respectively (Thapa et al., 2018). The deficit in water supply as well as a major share in the supplied water comes from the groundwater resources in the valley. Projected increase in population and subsequent increase in water demand is expected to exert more pressure in water resources in the valley in general, and groundwater resources in particular, and therefore exacerbate the future water crisis.

Groundwater, the renewable reserve of freshwater in many cases, is stored in aquifers. Groundwater is also the primary source of water in the river during lean seasons, mainly when rainfall is nominal (Belhassan, 2011). LULC change such as urbanization increases proportion of impervious surface leading to excess runoff and less groundwater flow (Schilling et al., 2010). The changes in the surface LULC conditions influence the runoff, infiltration, and recharge capacity of that area. Due to high surface runoff, groundwater recharge is not well assured to refill the enormous amount of extraction. To maintain the natural recharge condition in the basin, recharge areas need to be protected. Groundwater use is governed by factors such as availability, accessibility, transportability, and cost-effectiveness. Reliable sources and affordable cost are the primary factors that prompt people to use subsurface water (Shrestha et al., 2016a). Groundwater use in the KV is also increasing over the years, however, recharge to aquifers are limiting due to urbanization. Appropriate management of groundwater resources in the KV is crucial for ensuring water security in the valley. It requires an elaborate understanding of groundwater storage and recharge potentials as well as optimal groundwater pumping rates.

Surface water as well as groundwater availability and use are affected by factors such as LULC change, climate change (Zipper et al., 2017), population growth, and associated increase in water demand. Water availability is varied by both changes in demand as well as supply. From the supply perspective, changes in hydrological cycle through the change in vegetation cover, runoff, groundwater recharge, and evapotranspiration (Bhaskar and Welty, 2015) affects water availability. Whereas from demand side, water abstraction to meets various demands alters water availability. In case of groundwater in the KV, groundwater pumping rate is six times greater than the recharge rate and it is declining the groundwater table by approximately 2.5 m/year at some locations (Pandey et al., 2010). In addition, Pandey and Kazama (2011) highlighted that anthropogenic activities are the main driving forces that pressurize the change in the groundwater environment. Shrestha et al. (2020) revealed that groundwater in the majority of the core urban areas of the KV are more vulnerable in comparison with the peri-urban areas due to rapidity of urbanization. The

groundwater system is overstressed due to lack of effective management of the resources in the context of over-pumping, population growth, urbanization, LULC change, reduced recharge, and climate change (Foster and Macdonald, 2014).

Climate change is another driver that affects water availability as well as demand. Climate change is the integrated, multi-sectorial, and multi-disciplinary response in society, and that change with the external forces such as economic, environmental, demographic, social, and technological changes. The global and regional climate changes and associated risks are projected to increase due to rise in global and regional mean temperatures (IPCC, 2014). Climate change impacts have been observed in several sectors in Nepal, and the water resources sector is not an exception. Changes in climatic parameters such as temperature and precipitation alter the river discharge, regional and local water availability, and water supply (Beskow et al., 2013). As per the IPCC (2007), the average temperature and precipitation in Asia by the end of the century are projected to increase from 1.8°C to 3.9°C and from 1% to 12%, respectively. In the case of the Hindu Kush Himalayan region (Indus, Ganges, and Brahmaputra river basins), mean temperature is projected to rise to 3.5°C and 6.3°C for Representative Concentration Pathways (RCPs) scenarios 4.5 and 8.5, respectively (Guo-yu and Bhakta, 2017). Precipitation is expected to change from 3% to 37% under the RCP4.5 and RCP8.5 scenarios, but with a higher level of uncertainty (Lutz et al., 2016). Changes in precipitations and temperature alter water balance components, sediment concentration, and water quality (Pokhrel, 2018). Though earlier studies have shed light on impact of climate change on runoff and flooding (magnitude, frequency, and duration) in the Bagmati River Basin (e.g., Sharma and Shakya, 2006), there are no studies related to the impacts on groundwater. Furthermore, impacts of LULC change on surface and groundwater availability are not yet known. As both climate and LULC changes create a more realistic scenario, it is imperative to evaluate separate as well as combined impacts of climate and LULC change on surface and groundwater resources (Shrestha et al., 2018).

1.2 Statement of the problem

The sixth goal among the 17 sustainable development goals (SDGs) has set targets for universal, equitable, safe, and affordable drinking water and sanitation to achieve by 2030. The essential water requirement of 50 liters per capita per day (lpcd) for human life is recommended by various international health organizations (UN, 2010). The Government of Nepal (GoN) has planned 135 lpcd for the domestic consumption purpose for the KV, located in the headwaters of the Bagmati Basin, through the service provider Kathmandu Upatyaka

Khanepani Limited (KUKL) after implementation of Malachi Water Supply Project (MWSP) (ADB, 2015). The existing service area of the KUKL gets only a quarter of annual demand supplied, and the remaining deficit of water must be fulfilled by the groundwater pumping. Even after Melamchi, which is pending already for decades, it would not be able to fulfill water demands in the KV and therefore groundwater pumping will continue (Thapa et al., 2018).

Groundwater is, and will continue to be, a key source of water to meet continuously increasing water demand in the KV. Over four million people in the KV rely on groundwater as the main source of water supply. Due to limited surface water resources, groundwater has become a natural choice of water supply. Industries, hotels, and housing colonies in the valley are using groundwater as a safe, reliable, and cost-effective source of water since the 1980s (Pandey et al., 2010). The high rate of in-migration from diverse cultural backgrounds, dramatic socioeconomic change, and haphazard urbanization is creating an imbalance in the urban environmental health, use of natural resources, and change in land-use practices in the KV. Groundwater pumping is estimated at more than six times higher than estimated recharge, which is alarming in terms of long-term sustainability of groundwater use.

Similarly, Pandey et al. (2010) reported the water table declination by 1.38 to 7.5 m between 2000 and 2008. In that period, the rate of groundwater extraction was quantified as 21.56 million cubic meters (MCM), and the recharge as 9.6 MCM. Urbanization pattern and accelerated pumping of groundwater resources to meet various water demands in the city, if continued with historical trends, is expected to have adverse impacts on groundwater balance of the basin (D€oll et al., 2014). However, a comprehensive understanding of groundwater dynamics under the scenarios of change in LULC, climate, and pumping rates are yet to develop.

LULC in the KV is changing over the historical period. The open land (cultivated, bush area, open field, and water body) has decreased by 12.8% between 1976 and 2015 (Rimal et al., 2017) due to increase in the built-up areas (Figure 2-8). If the trends in LULC change, population growth, and urbanization continued at the same rate (as per Figure 1-2), management of land, water, and energy resources would be more challenging in the near future (Dahal et al., 2019). Furthermore, LULC plays a significant role in the hydrological process by directly influencing the surface runoff, infiltration, groundwater flow, and interflow.

The increase of urban are by 6.46% from 2000 to 2010 has changed the river flows, lateral flows and groundwater flows by the +27%, -25%, and -21% of annual flow, respectively (Pokhrel, 2018). So, increase in urban area creates challenges for both surface as well as surface water availability, leading to more scarce in the future. Urbanization process affects the quality and quantity of groundwater in an area (Wakode et al., 2018), and subsequently affect the socio-economic development as well as the eco-environment of the surroundings in many ways (Han et al., 2017). The case is true for the KV as well. To regulate the LULC change drivers, scientific understanding of the extent of changes and associated impacts, and optimal level of groundwater pumping are needed (Singh et al., 2018).

Furthermore, change in the precipitation pattern and increase in the temperature can affect runoff characteristics, alter the water balance, including groundwater resources, and their seasonality. Extreme events are expected to increase with more intense precipitation and associated flooding events. Storing surplus runoff during monsoon season in groundwater reservoirs and using them in dry periods could be a potential option as they are environmentally friendly, however, it needs a detailed understanding of hydrogeological characteristics, groundwater flow dynamics, current and future climatic characteristics. LULC changes and associated impacts on runoff characteristics, recharge, and groundwater dynamics can be found through the surface and subsurface hydrological modeling. It can generate useful evidences for future water resources planning.

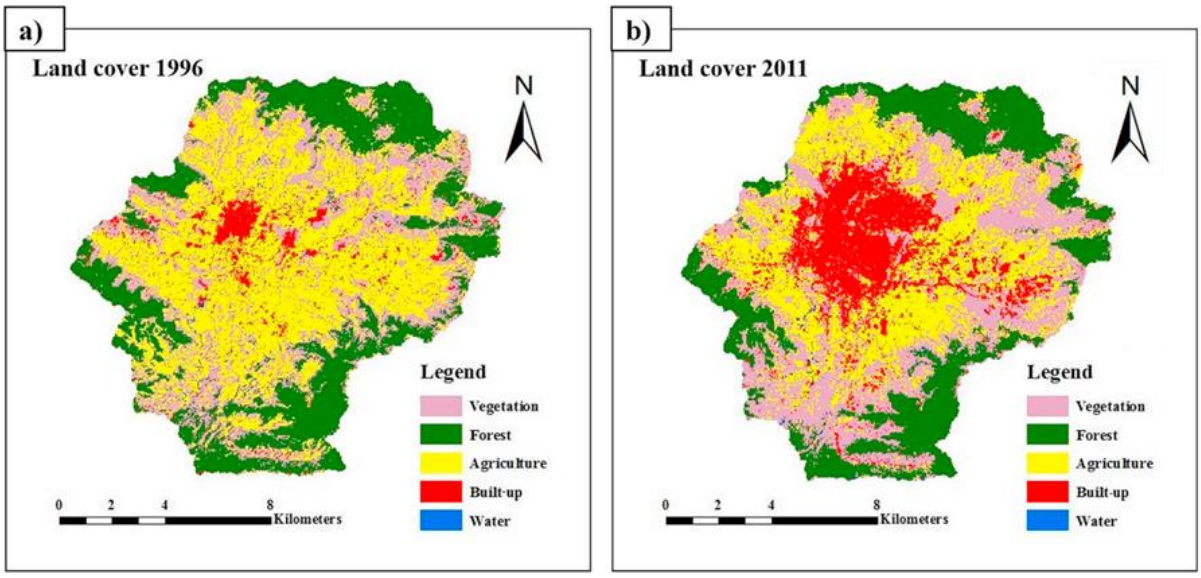

Figure 1-2 LULC change in the Kathmandu Valley a) 1996 and b) 2011

(Dahal et al., 2019)

Therefore, a comprehensive study integrating multiple models such as LULC projection model, hydrological model, climate model, and groundwater flow model is required to develop a comprehensive understanding of water balance, recharge characteristics, and groundwater dynamics, under multiple set of scenarios related to LULC change, climate change, and urban population growth.

1.3 Objectives

This study aims to develop a comprehensive understanding of LULC change projection, water balance, recharge characteristics, and groundwater flow dynamics in the KV located in the headwaters of the Bagmati River Basin in central Nepal using an integrated modeling approach. It has three specific objectives.

i. To assess impacts of projected LULC change on potential recharge areas.

ii. To evaluate impacts of projected climate and LULC change in spatial-temporal distribution of surface water availability.

iii. To assess impacts of urbanization in groundwater dynamics.

1.4 Scope of works

To achieve the specific objectives, the following sequential studies have been performed.

a) Formulation of present and past LULC map and quantification of the current LULC change pattern in the KV using Landsat image and Geographical Information System (GIS) tools.
b) Projection of future urbanization pattern for five different scenarios (normal built-up area growth, double of normal growth, half of normal growth, population growth rate, half of population growth rate) used to simulate the land-use model.
c) Set up the Conversion of Land Use and its Effects at Small regional extent (CLUE-S) model corresponding to the scenarios and project the future LULC map for each decade (2020, 2030, 2040, and 2050).
d) Delineation of potential groundwater recharge areas using Multi-Criteria Decision Making (MCDM), Analytic Hierarchy Process (AHP) techniques, and GIS tools in the present and future decadal series.
e) Quantification of the encroachment of potential recharge area using future LULC map and GIS tools

f) Estimation of the water balance components under current and future scenarios, by using a well-calibrated and validated hydrological model in Soil and Water Assessment Tool (SWAT).
g) Projection of future climate, multiple climate models are used after appropriately correcting the biases.
h) The climate and LULC change impact on the spatio-temporal distribution of river runoff and the water balance in the river basin are assessed.
i) Characterization of groundwater flow dynamics under current and projected future urbanization scenarios by developing a well-calibrated and validated groundwater flow model in MODular groundwater FLOW (MODFLOW).
j) Development of future scenarios of pumping rate and decadal recharge is based on projected future LULC map.
k) Estimation of the groundwater flow dynamics under current and future scenarios, and device recommendations of strategies for regulating groundwater use and protecting groundwater recharge areas.

1.5. Limitations of the study

For the integrated assessment of surface and sub-surface hydrological analysis of Bagmati River basin system, land use/cover change, climate change, and pumping rate change analysis using multi-model approach was considered. The following are the limitations of the study:

a) Due to lack of adequate data in land use change analysis, the neighborhood data parcel significantly affect the entire output in terms of confined settlements instead of scattered settlements. So, more detailed land use data may improve the output.
b) The database to create layers in land use model gravely depends on the quality of data and resolution, so precise and high-resolution data may improve model output. This study uses commonly available database for analysis, which could be improved using more sophisticated data.
c) Limited field test data are used in this study. Spatially more distributed and large number of test data are needed for precise outputs.
d) Recharge fundamentally depends on the soil characteristics. This study does not perform experimental delineation of the characteristics of subsurface soil that may alter the recharge characteristics.

e) Reliability analysis of different MCDMs is not performed in this study. Calibration of available model may be valuable for selection of the approach rather than sole selection of AHP.
f) Updated data and regular time-series data will be crucial for precise outputs. The data considered in this study are not regular after 2014 due to the 2015 Gorkha earthquake.
g) Limited climatic data except temperature and precipitation is used in this study. Limited data may lead to uncertainties in the model parameters.
h) Sensitivity and uncertainties analysis are not considered in this study and the same are considered from previously published works. Rigorous sensitivity and uncertainty analysis may improve the outputs.
i) The grid size of the LULC projection if scaled down in smaller extent will improve the outputs.
j) Calibration and validation of groundwater model is done using single year data. Multi-year data will be helpful to better calibrate the model.
k) The observations as well as pumping well data used in this study are not in proper grid. The data if obtained in unsteady state may be helpful for improvement in the outputs.
l) Field based hydrogeological characteristics, parameters, and geological settings if generated in actual form would result better outputs. This study uses existing data from literature that may not exactly represent the field conditions.

1.6 Thesis structure

To achieve the objectives, the thesis is organized into six chapters as the main body, followed by references and annexes. The thesis structure is presented in Figure 1-3 and briefly summarized hereunder.

Chapter 1 deals with the background, statement of the problem, and objectives. Chapter 1 describes the current population and built-up area in the KV and their corresponding impacts on the river flow and groundwater table.

Chapter 2 presents a review of published articles, research reports, and books relevant to the objectives. Past and future LULC and climate change studies have been reviewed. The study carried with the climate and LULC changes in the surface (hydrological models), and sub-surface (groundwater flow models) water system studies are also reviewed in this chapter.

Chapter 3 deals with the details of the study area in terms of topography, demography, climate, drainage network of the basin, and the other information of the river basin.

Chapter 4 provides a methodological framework as well as a detailed description of the methodology adopted in this study.

Chapter 5 provides results and discussions in line with the three objectives of this study. The results of LULC change, climate change, recharge area variation, and increased pumping rate and their impacts on the water resources are quantified and discussed adequately with reference to the findings of other relevant studies.

Chapter 6 comprises a summary of conclusions and recommendations.

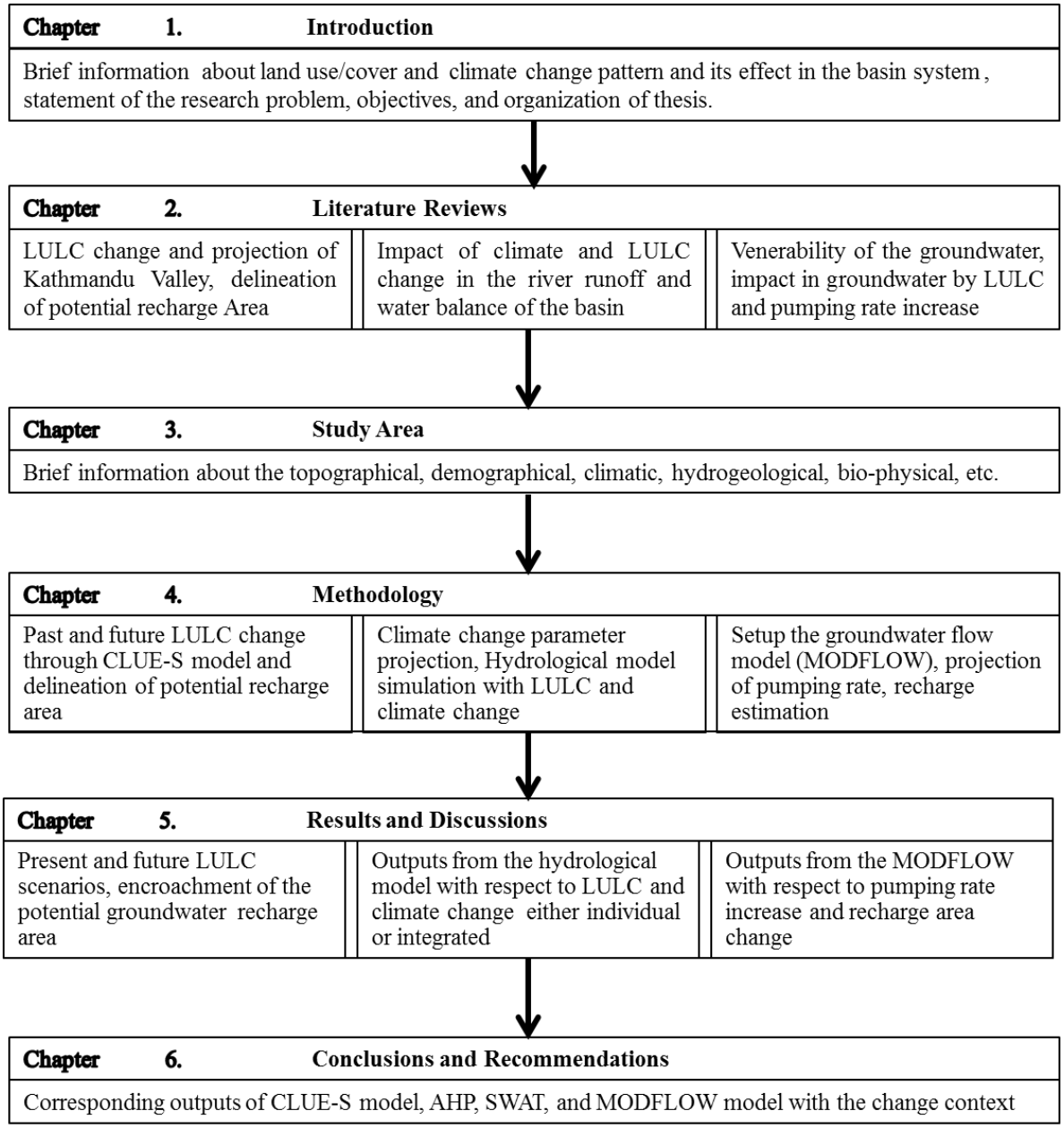

Figure 1-3 Flow diagram of the organization of thesis

Chapter 2. Literature Review

This chapter presents literature review on various aspects related to the objectives and conceptual framework used in this study. They are elaborated in following sub-chapters. They include developing future scenarios (land use/cover, climate, and groundwater pumping), hydrological models and groundwater models; water resources assessments under current and future scenarios, and earlier studies in the Kathmandu Valley (KV).

2.1 Developing land use/cover scenarios

2.1.1 Approaches for LULC projection

Due to urbanization, the rate of land use/cover (LULC) change is univocal across the globe. If proper LULC planning and management is not enforced, it is expected to impact various aspects of society and ecosystem. For future planning, projected future LULC map is required. Modeling-based approaches are generally applied to project future LULC scenarios with respect to spatial policies, conversion setting, land use requirements and location characteristics. In this regard, various principles, relationships, and models are developed for the projection of future LULC change by several researches. The population growth rate in urban areas has exhaustive relationships with urbanization, and physical facility reflects another dynamics of urbanization pattern. LULC change in the developing areas has an empirical positive exponential relation with urbanization, and it could be observed in the historical urban areas and their corresponding LULC changes (Paudel et al., 2016). All LULC change models are conceptualized through this principle. The urbanization pattern and LULC change have complicated relationships with economic development, and such complex phenomenon is discretized to the small driving forces for solving (Zhou et al., 2016). Biophysical and socioeconomic factors are considered as the driving forces of the change (Yin et al., 2011), and the analysis is functioned as the probabilistic approach of each LULC change with respect to the weightage of each driving forces as per Equation 2.1 (Verburg et al., 2002).

$$R_{ki} = a_k X_{1,i} + b_k X_{2,i} \quad (2.1)$$

Where R_{ki} is the weightage for the location i to land use type k,

$X_{1,i}$, is the characteristics of driving forces for location i and

a_k and b_k are the relative weightage of the characteristics with corresponding land use type k.

Future urban growth or LULC change models are developed to simulate the spatial and temporal dynamics of LULC change. Various driving forces are involved in LULC change, and their relationships are nonlinear. They are represented in the models like Markov Chain and genetic algorithm (Tang et al., 2007), cellular automata coupling with fuzzy logic (Liu et al., 2011), statistical model (Tran et al., 2017), artificial neural network (Almeida et al., 2008; Li and Yeh, 2002), weight of evidence (Thapa and Murayama, 2011), CLUE-S (Verburg et al., 2002), Land Change Modeler (LCM) (Kim, 2010), GEOMOD (Praskievicz and Chang, 2011), Dinamica EGO (Soares-Filho et al., 2009), and Landuse Sim (Pratomoatmojo, 2018), etc. All of these models use the socioeconomic and biophysical aspects (e.g., topography, slope, aspect, population settlements, river networks, road networks, etc.) as driving forces that play the spatio-temporal change effects in the area. Most of the aforementioned LULC change models are useful for a large area, and the model cannot provide satisfactory performance for a small scale. The Conversion of Land Use and its Effects modeling framework (CLUE) was developed to simulate LULC change based on an empirical relationship between different LULC types and its driving factors (Veldkamp and Fresco, 1996). For the small extent area, the CLUE model is not applicable. Then the CLUE model is modified and called the Conversion of Land Use and its Effects at Small regional extent (CLUE-S) model.

The CLUE-S is an empirical model to simulate the LULC change based on change in local characteristics with the dynamic temporal and spatial distribution of land requirements. The study area can be divided into a small grid with defined land-use characteristics. The driving forces are then identified, and input data of each driving forces (geology, slope, aspect, population density, settlement, river network, road network, etc.) are prepared by using appropriate geo-spatial tools. The relation of driving forces and land use type can be found by the Receiver Operating Characteristic (ROC) values (Pointius and Schneider, 2001). In each grid LULC change probability can be found by the auto-logistic regression models by using the driving forces. The demand characteristics and conversion elasticity provides the actual demand in the area and LULC change restriction for LULC type. The total probability can then be calculated as a sum of each land use type.

Numerous studies have been conducted with the application of CLUE-S model for the future analysis of LULC change, urban growth rate and pattern, change in agricultural pattern, and LULC changes with the special restriction. The CLUE-S model has been commonly used and the performance of the model is more robust than the other for the small scale LULC change

(Jiang et al., 2015; Verburg, 2010; Verburg et al., 2002; Zhou et al., 2013). Therefore, CLUE-S is appropriate to simulate LULC and project future LULC in the KV.

Shrestha et al. (2018) showed that the LULC change in a river basin can have a significant impact in the flow pattern. The study assessed the LULC change in the basin by the dynamic, spatially explicit, land use change model (Dyna-CLUE) with the two scenarios "economic" (proceed past conversion trend) and "conversion" (restriction for the certain field type). The model was functional based on the demand of the land requirement (non-spatial) and the probability of the LULC change in that period (spatial allocation). The analysis showed that the economic conversion gives the robust output when any restriction is not in the any agriculture field type and the future LULC change in the upstream part of the river basin should not be overlooked for sustainable development of the river basin. In the context of the KV several LULC projection study has been conducted by assuming the different driving forces and the models; the observational outputs from the analysis showed that the expansion of the built-up area in the peri-urban area of the valley and that creates the more impervious in the open land (Rimal et al., 2017; Thapa and Murayama, 2012).

2.1.2 Implication of urbanization in water resources

Increase in population will create excessive demand for resources (water, food, energy, etc.). In the future, the pumping rate may increase due to urbanization, recharge may decline with reduction of the open land, and excess runoff may occur due to increase in the impervious surface. Pokhrel (2018) using a well calibrated SWAT model, showed that 6% increase in the built-up area leads to an increase in 27% surface runoff and 5% sediment flow. Similarly, the adverse effect would occur in lateral and groundwater flow contributions. The land-use change effect in the river basin has a serious threat in terms of upstream river degradation and downstream aggradation, increase in the peak river flood and decrease in the lean flow, and increase in the surface runoff and decrease in the groundwater recharge characteristics.

Furthermore, an increase in the population of the valley creates the gap in water supply and demand. The sustainable development goals (SDGs) have set the goal for universal, equitable, safe, and affordable drinking water for everyone by 2030. The primary water requirement for human life is 50 lpcd as recommended by various international organizations (UN, 2010). The government of Nepal (GoN) has planned for 135 lpcd for domestic purpose in Kathmandu Valley that would be supplied by Kathmandu Upatyaka Khanepani Limited (KUKL) after the implementation of Melamchi Water Supply Project (MWSP) (ADB, 2015).

The existing service areas of the KUKL supply is nearly one-fourth of the demand. Remaining deficit must be fulfilled by the groundwater pumping. All the demand side stress will be managed by the groundwater pumping. Pandey et al. (2010) mentioned that anthropogenic activities (urbanization, population growth, and increase in tourism and hotels, intensive improvement in lifestyle, inadequate surface water resources and Land cover change) are the major driving forces to pressurize the alter in the groundwater environment. Shrestha et al. (2020) revealed that groundwater is more vulnerable in the core city areas when compared to the peri-urban areas of the valley due to urbanization. They concluded that due to urbanization, the rate of increase in population and built-up area is quite high. This ultimately leads to an increase in the pumping demand and decrease in the recharge distress in the groundwater table, and the water balance in the surface and sub-surface of the valley will be more critical in the upcoming days.

2.2 Identifying potential areas for groundwater recharge

2.2.1 Hydrological principle for groundwater recharge

For the sustainable development and management of the water resources, the potentiality of the resources must be found in the different qualitative forms. Potentiality of the resources will be found by the appropriate tools, scientific principles and model techniques. All the methods are functions with the hydrological balance and the bio-physical characteristics of the basin as described below.

The hydrological cycle and its response in the hydrological components (precipitation, runoff, infiltration, evapo-transpiration, groundwater flow etc.) have been more multifaceted by the complex interrelation between the spatial variation varied land use/cover, soil characteristics and climatic variables. The basic hydrological cycle (Figure 2-1) and the water balance equation (Equation 2-2) reveals that the groundwater recharge and river flow of a catchment/basin mostly depends upon physical and climatic characteristics of the catchment/basin.

$$P = R + I + I_f + ET \qquad 2.2$$

Where, P, R, I, I_f, and ET means precipitation (L), surface runoff (L), interflow (L), ground infiltration (change in storage) (L), and evapotranspiration (L) of the basin respectively.

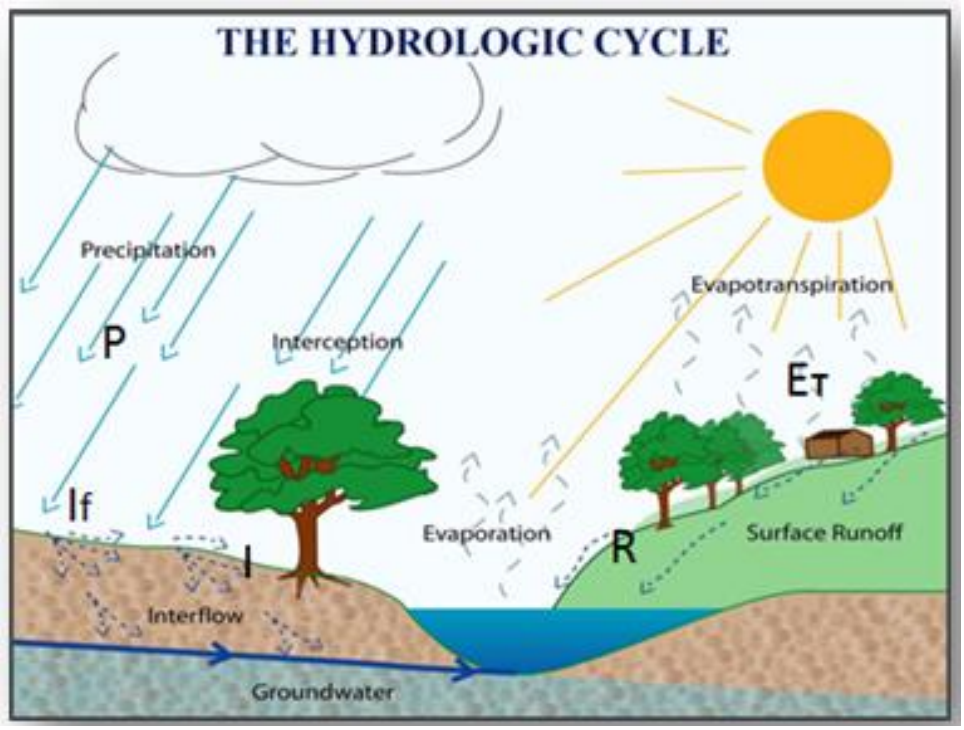

Figure 2-1 Hydrological cycle of the basin

Groundwater recharge areas are those having high infiltration and deep percolation capacity to increase the water table and the water pass through the lateral flow in the river channel or the vadose zone to groundwater aquifer. Many hydrological model studies show that, base flow and the lateral flow of the river basin have increased by increasing the groundwater recharge (Aryal et al., 2017; Thapa et al., 2017; Bajracharya et al., 2018).

2.2.2 Approaches for identifying groundwater recharge potential areas

Groundwater recharge capacity mostly depends up on infiltration capacity and surface coverage. Similarly, without precipitation recharge is not possible. There are many factors that influence the groundwater recharge capacity. Representing those factors in the form of indicators/variables and aggregating together using appropriate weights to each of them is called as indicator-based approach, which is widely used for the studies involving delineating potential areas for groundwater recharge (Kaliraj et al., 2014; Lamichhane and Shakya, 2019a; Singh et al., 2018; Singh and Nachtnebel, 2016; Tiwari et al., 2019; Wakode et al., 2018).

The indicators used in most of those studies are summarized in Table 2-1. Though different names are used in different studies, they more or less fall under those 10 indicators (three in first hierarchies and 10 in second or total), in general. The indicators cover following three broad categories: topography, climate and socio-economy. For an area of interest, a suitable

set of indicators are generally decided based on literature review, their relation to the recharge potential, expert view/consultation, availability of data, and statistical performance of the data (e.g., ROC test).

Table 2 -1 Various layers and relation with groundwater recharge

S.N.	First hierarchy	Layers	Relation	Reference
1	Topography	Slope	The steep slope area have low contact period and creates more runoff resulting less recharge	(Bashir et al., 2008; Rukundo and Doğan, 2019)
2		River Distance	Banks of the river have more recharge capacity than the farther	(Bashir et al., 2008; Rukundo and Doğan, 2019)
3		Geology	Gravel and send have more recharge tendency than the clay and rocky area.	(Bashir et al., 2008; Rukundo and Doğan, 2019)
4		Land Use/Cover (LULC)	The open land (like, forest and agriculture) have high recharge tendency compare the built-up areas	(Bashir et al., 2008; Rukundo and Doğan, 2019)
6		Aspect	North and west facing are wetter and have high recharge capacity compare the other aspects	(Bashir et al., 2008)
7		Elevation	Plane areas have high inundation time compare to the sloppy land and creates more recharge.	(Bashir et al., 2008)
5	Climate	Precipitation	Larger duration, high frequency, and less intensity of precipitation have less runoff.	(Bashir et al., 2008; Rukundo and Doğan, 2019)

8	Socio-economic	Population Density	High density means the more impervious land and less recharge potential.	(Bashir et al., 2008)
9		Market Distance	Near the market has highly urbanized area having less recharge.	(Bashir et al., 2008)
10		Road Distance	Near the road network mostly represents the settlements and impervious area.	(Bashir et al., 2008)

2.2.3 Identifying weights to the indicators

Multi-criteria decision making (MCDM) techniques are often used to assign weights to indicators and parameters while computing index (Aher et al., 2013). MCDM techniques can solve the issue of assigning weights by combing several criteria (Malczewski, 2004). Each individual criteria has unique values which represent all features and then reflects in the output (Chow et al., 2010). Numerous types of MCDM techniques are in practice, they include - 1) Multi-Attribute Utility Theory (Fishburn, 1967), 2) Fuzzy Set Theory (Zadesh, 1965), 3) PROMETHEE (Behzadian et al., 2010), 4) Analytic Hierarchy Process (Saaty, 2004), 5) Goal Programming (Romero, 1997), 6) Case-based Reasoning (Li and Sun, 2008), 7) Data Envelopment Analysis (Hermans et al., 2009), 8) Simple Additive Weighting (SAW) Technique (Qin et al., 2008), 9) Elimination and Choice Translating Reality (ELECTRE) (Konidari and Mavrakis, 2007), 10) Simple Multi-Attribute Rating Technique (SMART) (Y. Chen et al., 2010), and 11) Technique for Order of Preference by Similarity to Ideal Solution (TOPSIS) (Qin et al., 2008).

Actual delineation of groundwater recharge area based on field-based data is complicated and resource-intensive. Therefore, theoretical techniques such as MCDM are more applied considering their reliability, cost-effectiveness, and less-time consuming for the region where data availability of data is more difficulties an issue. Such practice is well established and applied in many earlier studies in different parts of the globe to delineations suitable areas (Kaliraj et al., 2014; Singh et al., 2018; Singh and Nachtnebel, 2016). Analytic Hierarchy Process (AHP) (Saaty, 2004) is one of the most widely used MCDM techniques in the water resources sector. The main three principles of this method are – problem discretization,

comparative analysis, and prioritize the various choices against others during the evaluation. The simplicity of this method is that it assigns weight based on pair-wise comparison matrix developed based on preferences of the experts to one indicator against the other. A scale value of each event is given in odd numbers (1 to 9) and the intermediate value is signed if the compromise is needed. The details of methodology and equations are described in the section 4.2.2.

A study by Jhariya et al. (2016) concluded that a combination of GIS, MCDM and AHP techniques is a powerful tool for the delineation of potential groundwater recharge areas. Numerous bio-physical layer (geomorphology, slope, aspect, geology, drainage density, precipitation, soil type, LULC, etc.) was used and the weightage of the each layer was found by the application of AHP techniques. The weightage of each factor is assigned by the expert knowledge and experience, therefore the consistency of each layer or composite outputs of the weightage, has been checked by the statistical evaluating indicator (Consistency Ratio (CR)) with the acceptable limit (Saaty, 2004). Similarly, GIS based MCDM techniques (AHP) is a high capacity to integrate large number of diverse layer data as a simple manner for the suitability analysis of any resources (Chaudhary et al., 2016; Y. Chen et al., 2010; Jhariya et al., 2016). AHP method is extensively used as it is easy to handle; scale is simple; easily sets hierarchy to one against others, and easy to solve. It is mostly used in the performance-type problems, corporate policy and strategy, natural resource management (like water resources), and political strategy and planning (Velasquez and Hester, 2013).

AHP method, as elaborated and used in other studies (e.g., Kaliraj et al., 2014; Chaudhary et al., 2016; Singh and Nachtnebel, 2016), has been adopted in this study to estimate weights to different layers to compute potential groundwater recharge area index. The weights factor is obtained through pair-wise comparison matrix of each layer compare the layers (Saaty, 2004). Finally, indicator values are multiplied by respective weights to compute an index for groundwater potential recharge areas as shown in Equation 2-3 (Malczewski, 2004).

$$\text{GWPRA} = \sum_{j=1}^{m} \sum_{i=1}^{n} (w_j \times x_i) \qquad 2.3$$

Where, GWPRA is the Groundwater Potential Recharge Area (GWPRA); x_i is the i^{th} class of the thematic layer normalized weight; w_j is the weight layer found from AHP of the j^{th} thematic layer; and m and n represents the total number of thematic layer and total number of class in a thematic layer.

A similar technique is adopted for the potential recharge area delineation in various locations (Kaliraj et al., 2014; Wakode et al., 2018). Chaudhary et al. (2016) has used the technique for the delineation of a suitable location for the fire station in the Kathmandu Valley and its service area. Four factors (distance from roads, settlements, land cover, distance from rivers, and population density) were considered for analysis. The weightage in that study was identified using the GIS tools as well as group discussions in the study area.

2.2.4 LULC change impact in surface runoff/groundwater recharge

Future scenarios of the KV indicate more encroachment of agricultural and open lands which implies reduction in recharge capacity of these areas. Population growth in the future may increase the pumping rate and LULC change which subsequently reduce the recharge capacity. In this case, the groundwater balance will change with the changed context (Rimal et al., 2017; Thapa and Murayama, 2012). Dahal et al. (2019) demonstrated that the recharge capacity of the northern and southern part of the KV, which have high potential to recharge the groundwater, could be reduced due to urban growth. The analysis was based on the past (1996 to 2011) and projected LULC map upto 2030 by using land use change model. The potentiality of the recharge area was identified by the runoff characteristics of Soil Conservation Service Curve Number (SCS-CN) method. It is simple and empirical approach that easily integrates the runoff coefficient with respect to basin LULC and hydrological parameters (Precipitation, infiltration, detention storage, evaporation, evapotranspiration etc.) as per Equations 2.4 and 2.5.

$$Q = \frac{(P - I_a)^2}{P - I_a + S} \qquad 2.4$$

Where $S = \frac{100}{CN} - 10$ 2.5

If $P \leq I_a$ whereas $Q = 0$

Q, P, I_a, S, and CN are the surface runoff (L), precipitation (L), initial abstraction (L), potential maximum soil moisture retention after runoff begins (L), and curve number value respectively.

In the study area, all the biophysical and hydrological characteristics of the basin were integrated with the Curve Number (CN) value. The higher CN value (range 30 - 100) indicates the maximum runoff characteristics and vice-versa. After the simulation, the result revealed that the change in CN value with the corresponding LULC change, in the core urban

and outer peripheral area the initial value was considered as high (85) and low (33) respectively. Before and after projection, the average CN values were changed from 63 to 65 in between 29 years. In the final outputs from the study, the potential recharge area has located for future protection in the northward (Lapsephedi, Bhadrakali, Nayapati, Budalinilkantha, Sundarijal, Gagalphedi, Chapali, and Baluwa) and southward (Devichour, Bhardv, Nallu, and Godawari) of the Kathmandu basin such as the JICA (1990) and Pandey et al. (2013) study. These studies indicate that the runoff of the basin will increase in the future and reduce the recharge volume by reducing the potential recharge area as per Figure 2-2. The major limitation of the study is that, the CN value of the study area is not to properly incorporating temporal and spatial changes in all biophysical and hydrological parameters. Both studies are based on the physical evaluation of the map despite the fact that the recharge volume mainly depends upon the infiltration tendency in that area.

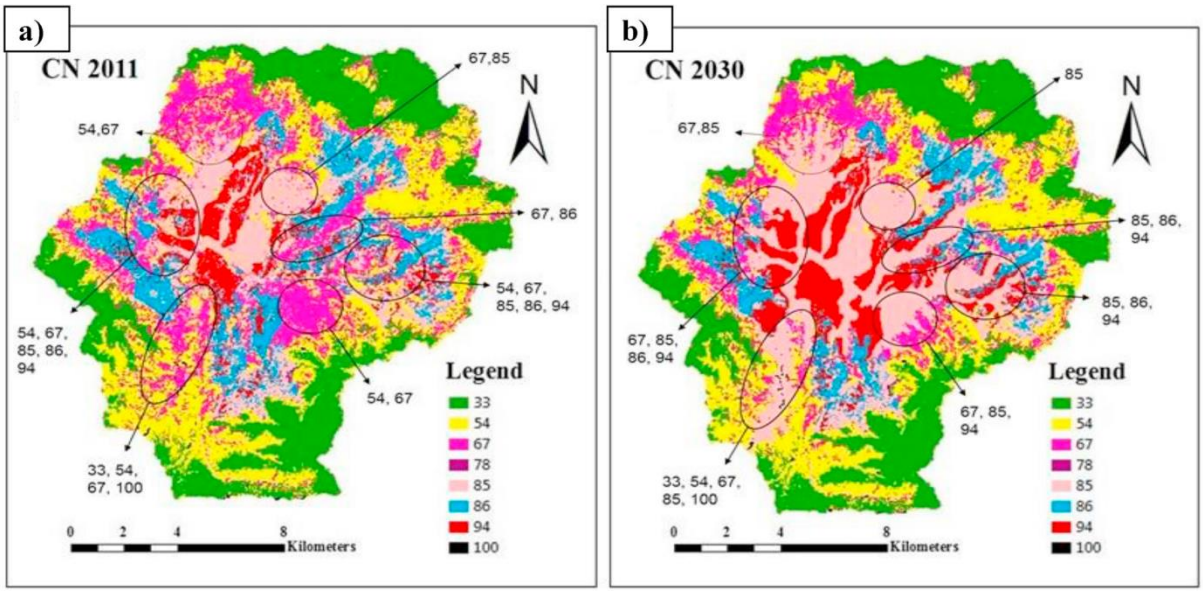

Figure 2-2 Present and future generated CN characteristics of the KV in a) 2011 and b) 2030 *(source:- (Dahal et al., 2019)*

The water balance of the groundwater hydrology will be maintained by the volume of input and output. But the current trend of pumping rate is greater than the recharge due to the increase in impervious surface area and population density. Numerous literatures have also highlighted that for maintaining the groundwater hydrology either artificial recharge or enhancing the recharge capacity by protecting the natural recharge area (Rukundo and Doğan, 2019; Shrestha, 2009; Shrestha et al., 2020). The actual identification of recharge area is more complicated and various field and lab tests were required. So, theoretical delineation

of recharge area is an appropriate and powerful tool in such area having lesser data available as per above discussion.

2.3 Hydrological modeling

To identify the natural hydrological response of the river basin, many studies have been conducted to establish the relation between climate and watershed characteristics in the hydrological process by rainfall runoff models (Bormann et al., 2009). All available hydrological models are used for the generation of flow for river basin management, flood mitigation, reservoir operation plan, design of hydraulic structures, and many other water resources aspects based on catchment and climatic characteristics (Ye et al., 2013). The hydrological model of a basin plays an important role for assessing the daily, seasonal and yearly flow and water balance within the basin or river reach. The simulation of temporal and spatial water balance data of the basin can give necessary information for the decision-maker to water resources management (Dwarakish and Ganasri, 2015; Pandey et al., 2019).

The hydrological models are generally classified based on criteria such as principles, structures, and their capability (Jajarmizadeh et al., 2012). Many hydrological models have been developed with unique or common properties. The entire model functions with the principle of water balance within the area as per Equation 2-6.

$$\textit{Inflow of water} - \textit{Outflow of water} = \textit{Change in storage} \qquad 2.6$$

2.3.1 Different types of hydrological models

Dingman (2002) classified the hydrological model in two types, namely, physical and mathematical models. The physical model works in natural or human-created form as a scaled-down frame, whereas mathematical model works as per logical numerical steps. Now, numerous hydrological models are developed with higher resolution due to availability of powerful computers for easy calculations and iterations. American Society of Civil Engineers (ASCE), 1982 provided some mathematical model as deterministic, analytical, dynamic, empirical heuristic, interactive, linear and nonlinear, probabilistic, numerical, simulation, theoretical and semi-empirical (Table 2-2).

Table 2-2 Classification of hydrological models

S.N.	Sources	Categories	Subcategories	Based on
1	Dingman (2002)	Simulation Basis	Physical based	Logic is based on the physical process
			Conceptual based	Logic is based on the conceptual process
			Empirical or regression based	The relation between input and output based on observed events
			Stochastic time series based	Prediction of the output based on the historical data
		Spatial Basis	Lumped model	Output response is in single basin
			Distributed model	Output based on the changing parameters and scale in sub basin level
			Coordinate system model	Output response is in coordinate system
		Temporal Basis	Steady state	Event is considered in steady state
			Steady state seasonal	Consider as a seasonal
			Single event	Consider in the single event
			Continuous	Multiple events
		Method of	Non dimensional	Like an empirical

S.N.	Sources	Categories	Subcategories	Based on
		Solution	Formal analytical	Like an analytical
			Formal numerical	Like numerical
			Hybrid solution	Combination of numerical and analytical
2	Shaw et al. (2010)	Deterministic Model	Conceptual Model	As per the above
		Stochastic Model		As per the above
3	Chow (1988)	Physical Based Model	Scale Model	Scale down the real system
			Analog Model	Same physical system and characteristics
		Mathematical Model	Deterministic Model	Based input data for all a time and create the same output
			Lumped Model	Output response is in single basin
			Semi-distributed	Output response is divided in to sub basins
			Distributed	Output based on the changing parameters and scale in sub basin level
			Stochastic Model	Based on the prediction of the output
4	Oogathoo (2006)	Empirical Method	Deterministic Model	As per the above

S.N.	Sources	Categories	Subcategories	Based on
			Stochastic Model	As per the above
		Theoretical Method	Physical Based	As per the above
5	Jajarmizadeh et al. (2012)	Black Box Model		Only the relation between input and output, no consideration between the physical process
		Conceptual Model	Distributed model	As per the above
			Semi - distributed model	As per the above
			Lumped model	As per the above
		Deterministic Model		As per the above
6	Wagener et al. (2004)	Metric Based		Database model same like a black box or empirical
		Parametric Based		Parameter calibration based on concept like conceptual
		Mechanistic Based		Parameter calibration based on physical process like physical model
7	Lewarne (2009)	Linear or non-linear		Output based on relationship of input data.
		Deterministic and Stochastic		Initial given data define the parameter output and probabilistic output based on the random value

S.N.	Sources	Categories	Subcategories	Based on
		Dynamic or Static		Output depends on time or not
		Lumped or distributed		Basin is homogenous or not
		Physical based or conceptual		As per the above

Most of the researches state that the application of the hydrological models is based on the available data and the required outputs. For better estimation, a mathematical model is more realistic than the others (Singh and Woolhiser, 2003). In the context of the high mountainous topographical area with no or limited data availability, semi-distributed model or lump model are more reliable (Bajracharya et al., 2018; Mishra et al., 2018; Pandey et al., 2019). As per the studies conducted by the several researchers (Babel et al., 2014; Mishra and Herath, 2014; Pokhrel, 2018), future flow is generated by optimizing the model parameters .

2.3.2 Application of hydrological models

The use of enlarged hydrological model was started after the development of the Stanford Watershed Model (Crawford and Linsley, 1966). After that lump or conceptual hydrological model was developed with processing by the simple differential equation, hydraulic law, and other empirical equations like Computer based Stream flow Synthesis and Reservoir Regulation (COSSARR) model (Rockwood et al., 1972), the Sacramento model (Burnash et al., 1973), the tank model (Sugawara, 1976); HEC-1 (Hydrologic Engineering Center (US), 1981), HYMO (Williams and Hann, 1973), and RORB (Laurenson et al., 1983). Some models are developed based on conservation of mass, energy, and momentum like SHE (Abbott et al., 1986), IDHM (Beven et al., 1984), and Hill slope model (Binley et al., 1989).CREAMS model (Knisel, 1980) was formulated for the integration of impact of soil characteristics on water, nutrient, sediment in the channel.

Solving the hydrological phenomenon and water quality is often complicated for the complex watershed, especially when integrating the surface flow, groundwater recharge, evapotranspiration, sediment, nutrients, etc. Soil Water Assessment Tool (SWAT) model (Arnold et al., 1998) was formulated for integrating the hydrological parameters (e.g. weather, soil, sediment characteristics, nutrient, plant growth, pesticides, etc.). It is semi-distributed conceptual hydrological model, which is divided into the sub-basin and the hydrological response of each basin was connected by the drainage network. The sub-basins

are formed by the combination of Hydrological Response Units (HRUs) having similar LULC and topographical characteristics. Each HRUs have a unique value and hydrological characteristics that generates the runoff, sediment, and nutrient based on the climatic data, soil properties, topographical characteristics, and land use practices (Arnold et al., 1998). SWAT calculation was based on the principle of the water balance of the basin as following Equation 2-7

$$SW_t = SW_0 + \sum_{i=o}^{t+1} R_{dayi} - Q_{surfi} - E_{ai} - W_{seepi} - Q_{lati} - Q_{gwi} \quad 2.7$$

where SW_t is the final soil water content (mm H_2O) in the outlet, SW_0 is the initial soil water content on day i (mm H_2O), t is the time (days) in the outlet, R_{day} is the amount of precipitation on day i (mm H_2O) on the basin, Q_{surf} is the amount of surface runoff on day i (mm H_2O) from the basin, E_a is the amount of evapotranspiration on day i (mm H_2O) from the basin, W_{seep} is the amount of water entering the vadose zone from the soil profile on day i (mm H_2O) from the surface, Q_{lat} is lateral flow from unit to channel and Q_{gw} is the amount of return flow on a day i (mm H_2O) from the groundwater unit.

The hydrological processes of each unit surface runoff volume, potential evapotranspiration, lateral flow, and channel routing in SWAT are calculated based on the Soil Conservation Service Curve Number (SCS-CN) method (Bosznay, 1989), Penman–Monteith method (Neitsch et al., 2011), creating a shallow aquifer (Arnold et al., 1998), and Muskingum method (Chow, 1988) respectively. Spruill et al. (2000) used SWAT model for assessing the daily and monthly discharge of Karst river watershed by optimizing the model parameter. The sensitivity of each parameter was then identified during model calibration and validation. It concluded that hydraulic conductivity of soil, base flow factor from sub-basin, channel characteristics (area, length, roughness, etc.), and drainage area were more sensitive than the other model parameters. Aryal et al. (2017) showed the various uncertainties related to climate in the Tamakoshi basin (nearby the Bagmati basin) hydrology by comparing the output from the SWAT and Hydrologic Engineering Center's Hydrologic Modeling System (HEC-HMS) model. HEC-HMS is a semi-distributed model and operates based on the basin model, meteorological model, control specification, and time data series management (McColl and Aggett, 2007). The solving operation of the model is based on the continuity equation as per Equation 2.8.

$$\frac{dS(e)}{dt} - \sum_i Q_i(t) + \sum_j Q_j(e,t) = 0 \quad 2.8$$

Where S, t, e, Q_i , and Q_j, is reservoir storage (L^3), time (T), water elevation (L) in the reservoir, flow for each inflow i, and outflow for each outlet j in each time steps t respectively.

In Aryal et al. (2017) Other parameters were assigned for loss (based on constant loss method with parameters of constant loss rate in mm/h, maximum soil storage in mm, percentage of imperviousness, and initial deficits in mm), transformation parameters (based on Clark unit-hydrograph) with the information of storage coefficient, concentration time in (hr), and routing (based on Muskingum K (hr) and X) (Scharffenberg et al., 2003). Study revealed that the SWAT model performs better than the HEC-HMS because the HEC-HMS prefers the better for low flow scenario or the model is more preferable where the loss through the basin and channel is more. HEC-HMS is performing better for the reservoir operational area compared to other (Gyawali and Watkins, 2013; Sardoii et al., 2012).

SWAT was successfully used by researchers in the world (including Bagmati basin) for hydrologic modeling and water resources management in watersheds with various climatic and topographic characteristics. After calibrating the model parameter with the physically observed database, model gave reasonably better performance (Aryal et al., 2017; Mishra et al., 2018; Pandey et al., 2019; Pokhrel, 2018; Shrestha et al., 2018). Besides the above-cited studies, all the results have not been perfect due to simplifying the assumption, model parameters, and statistical indicator during calibration and validation of the model. So a single model of the basin cannot give the superior output or response of hydrological component. Hence multi-model output should be visualized the perfect hydrological response through the model parameters of the watershed (Nasseri et al., 2014).

Thapa et al. (2017) assessed from the calibration of parameters and analysis based on seasonal variation in water balance components of three different hydrological model of Bagmati basin, the outputs of the SWAT model had greater accuracy compared to the Hydrologiska Byrans Vattenbalansavdelning (HBV) (Bergström, 2006), and Block-wise use of TOPMODEL model with Muskingum - Cunge routing (BTOPMC) (Takeuchi et al., 2007).

HBV model is a lump and simple conceptual hydrological model based on the relation between rainfall and runoff. The water balance of the basin was described by the concept of three reservoirs tank model concept, first is the soil moisture zone reservoir, second is upper

zone storage or sub-surface flow, and third is lower zone storage or groundwater recharge. The basic operating water balance Equation 2.9 of the model is the following.

$$P - E - Q = \frac{d(SP+SM+UZ+LZ+Lakes)}{dt} \quad 2.9$$

Where $P, E, Q, SP, SM, UZ, and\ LZ$ refers precipitation (LT^{-1}), evaporation (LT^{-1}), flow (LT^{-1}), snow pack (L), snow moisture (L), and upper/lower groundwater zone (L) with respect the time (T). In this basin snow contribution is negligible and two reservoirs have been assumed for the analysis. The upper reservoir was used for simulating the surface runoff and the lower was groundwater flow and storage. For obtaining the better statistical performance indicator important parameters (FC (maximum soil storage), LP (evaporation reduction factor), BETA (shape indicator), PERC (rate of percolation), UZL (limiting factor), K0, K1, and K2 area recession coefficient, MAXBS (triangular weighting function) were calibrated.

BTOPMC is physically distributed rainfall-runoff model. The runoff estimate is based on the principle of TOPMODEL by assuming the catchment in block-wise and the channel routing is calculated based on the Muskingum-Cunge method. The TOPMODEL was formed by the concept of hill slope model (Kirkby, 1976) with the base of the topographical index γ_{i-top} found by following Equation 2.10

$$\gamma_{i-top} = \ln \langle (a_i | dl_i) | tan\beta_i \rangle \quad 2.10$$

Where a_i, dl_i, $tan\beta_i$, is the upstream drainage area from the outlet, contour line length, and stream slope respectively.

After dividing the whole catchment into grid cells, the effective runoff generation area of each grid cell (i) is calculated from the product of effective contribution factor and total catchment area and the TOP model is redefined by Equations 2.11 and 2-12 and Figures 2-3.

$$q_{bi} = \frac{\{a_i f(a_i) r_k\}}{a_{0i}} \quad 2.11$$

$$\gamma_i = \ln \langle (a_i f(a_i) | a_{0i}) | tan\beta_i \rangle \quad 2.12$$

Where q_{bi}, $f(a_i)$, r_k, a_{0i}, γ_i, is refer the specific base flow of the reach per unit area, function of upstream area runoff contributor, recharge rate of the block K, area of the grid, and topographical index of the grid (i) respectively.

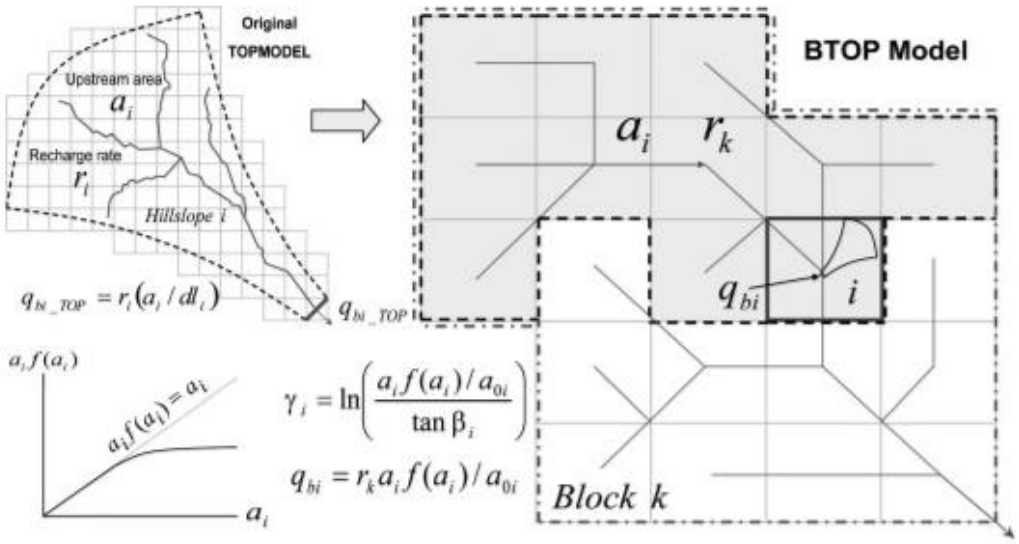

Figure 2-3 Concept of BTOP model

(source:- (Takeuchi et al., 2007)*)*

Base-flow and overland flow of each cell is depending on the local saturation deficit of the cell and it has been varied with the reference of average saturation deficit and soil topographic index (Takeuchi et al., 2007). Potential Evapo-Transpiration (PET) input is calculated separately by using Snyder's equation with daily evapotranspiration data (Snyder, 1993). The final future discharge was generated after optimizing the main sensitive parameter of the model like; m (coefficient of delay), n_0 (roughness coefficient), alpha (empirical constant), SD_{bar} (average saturation deficit), T_0 (soil saturated transmissivity), and S_{rmax} (maximum root depth of plant).

After coupling the SWAT model with GIS to analyze the raster and vector input data features of the model, fast simulation, user-friendly integration, and easy to optimization the parameters and analysis of the outputs would be easy (Pandey et al., 2019). Major sensitive parameters (Table 2.3) of the model were optimized manually during the calibration and the validation period. The water balance of the model output is the basis of the conservation of mass as per Equation 2.6.

Table 2-3 Description of SWAT model parameters

S.N.	Parameter	Description	Relation to outputs
1	CN2	SCS runoff characteristics curve number (CN) for	Positive function of surface runoff, increase the surface runoff by

S.N.	Parameter	Description	Relation to outputs
		moisture condition II	increasing the CN2 value and vice-versa
2	CH_N (1,2)	Manning roughness coefficient in channel	Negative relation to surface runoff, if CH_N value is increased; increase the roughness of reach, decrease the channel velocity, increase the time of concentration, decrease the peak discharge, and vice versa
3	CH_K (1,2)	Effective hydraulic conductivity channel	The relation is depends upon the soil type and the type of channel.
4	CANMX	Maximum canopy water storage when canopy is fully	Negative relation to surface runoff but positive in base flow, rise the CANMX more water will be evaporates and decrease the surface runoff
5	GW_REVAP	Groundwater evaporation coefficient; movement of water coefficient from shallow aquifer to the root zone	Adverse effect to base flow, rise the value means increase the evaporation from shallow aquifer and fall the groundwater recharge.
6	GWQMN	Groundwater (shallow aquifer) minimum depth for return to flow	Adverse impact in stream base flow, high GWQMN means high storage in aquifer and lower the base flow and vice versa
7	GW_DELAY	Groundwater delay (time taken by the water to flow subsurface surface to river reach)	Negative impact in base flow, high GW_DELYA means take more time to travel for passing to channel and reduce the base flow and vice versa

2.3.3 Calibration and validation of hydrological models

Generally, model performance is judged by comparing the calculated values and the corresponding measured or numerical benchmark data. When using the single indicator the analysis may misguide the outcomes of the model, so the combination of indicators like; scatter plot method, Percent BIAS (PBIAS), Root Mean Squire Error (RMSE), The index of agreement (D-index), and Nash–Sutcliffe Efficiency (NSE) coefficient, are currently used in the hydrological models. The threshold value of the indicator shows the model output is reliable or not within the test hypothesis (Ritter and Muñoz-Carpena, 2013).

The scatter plot or graphical representation method was also used for the visual evaluation of the model performance between the observed and simulated on the same scale (1:1), where higher scatter means the wrong evaluations. The "c" value is evaluated by fitting the best fit regression line to the scatter plot. The intercept value showed the lag or leads the simulated output with the observed value. Willmott (1984) had a slope of 1 which means the perfect in the match. The zero intercept means the perfectly generate the data in the same magnitude. Nyeko (2015) accessed the performance of the intercept method in SWAT model output, it indicated the good judgment between magnitude and direction of observed data but it had no ability to direct which parameter was more sensible for the outfit of the generated data. Therefore, more care is required when using this method.

The index of agreement (d-index) method was firstly introduced by Willmott (1984) based on the degree of agreement between the observed and simulated value. It is the ratio of mean square error and the potential error as per Equation 2.13.

$$d = 1 - \frac{\sum_{i=1}^{n}(O_i - P_i)^2}{\sum_{i=1}^{n}(|P_i - \bar{O}| + |O_i - \bar{O}|)^2} \qquad 2.13$$

Where O_i, P_i, and $\bar{O}$, is the observed, simulated and mean of observed discharge in each step i respectively.

Computed value one shows the perfect agreement and zero means no significance. This method has been used widely as it overcomes the insensitivities of the R^2 and NSE. Biondi et al. (2012) explained the performance of d-index was more useful and gave better performance in the hydrological model but it was unresponsive in the case of low flow and prefers high efficiency even the model is poorly calibrated (Krause et al., 2005).

Percent BIAS (PBIAS) measures the output data based on zero tolerance meaning the average variation between the observed and simulated data would be zero. Low magnitude

percentage value of the PBIAS means towards the better generation, the positive value suggests the model output is underestimated and vice versa. The governing equation of the method is shown in Equation 2.14 (Moriasi et al., 2007).

$$PBIAS = \frac{\sum_{i=1}^{n}(O_i - P_i)}{\sum_{i=1}^{n} O_i} \times 100 \qquad 2.14$$

Where O_i, and P_i, is the observed, simulated discharge in each step i respectively.

In the water balance analysis, it is easy to express the errors in which components of the model parameters are present. It has also a tendency to evaluate the model with the large value and variation between observed and measured data. With these kinds of properties of method, it was extensively used in the groundwater model performance by the other researchers (Fonseca et al., 2014; Nyeko, 2015) also. Large variation of positives and negatives data and its cumulative effect may be creates the minimum value of the PBIAS means the better performance. In such type of uncertainty of the model performance is minimized through the use of multiple statistical indicators.

Pearson's correlation coefficient (r) and coefficient of determination (R^2) value have been used to identify the degree of co-linearity between the observed and simulated data and it was found in the fraction with the range of zero to one. The R^2 value one indicated the prefect correlation and the zero means the no relation between the data (Legates and McCabe, 1999). The R^2 value, greater than 0.5 is assumed the acceptable range as per Equation 2.15.

$$R^2 = \left\{ \frac{\sum_{i=1}^{n}(O_i - \bar{O}) \times (P_i - \bar{P})}{\left[\sum_{i=1}^{n}(O_i - \bar{O})^2\right]^{0.5} \times \left[\sum_{i=1}^{n}(P_i - \bar{P})^2\right]^{0.5}} \right\} \qquad 2.15$$

Where as O_i, $\bar{O}$, P_i, and $\bar{P}$ is the observed, mean of observed, simulated and mean of simulated discharge in time steps i respectively. Pearson's correlation coefficient (r) and coefficient of determination (R^2) method has major limitation that the model evaluates the outputs as the linear relationship between the variables (Santhi et al., 2001). It is more sensitive during the high flow condition in the hydrological model evaluation. But in lean seasons the variation has no significance in the model parameters. In fact, the model shows better performance during the mean monthly flow simulation (Mishra et al., 2018; Pandey et al., 2019).

RMSE generates deviation of the simulated value with respect to the mean error and also found the degree of correlation between the simulated and observed value. The output value ranging from zero to one, the value greater than 0.5 means the considerable acceptable and

greater value refers to less error (Moriasi et al., 2007; Santhi et al., 2001). Nash-Sutcliffe Efficiency (NSE) (Nash and Sutcliffe, 1970) is the dimensionless goodness of fit indicator and the unit value represents the perfect fit between the data. It was used to determine the magnitude of the output by comparing the residual variance to the observed variance. This was a commonly used method during the calibration and validation process of the hydrological models and showed better information from the simulated data. The NSE performance value within the range (Moriasi et al., 2007) can be reflected in the model output and the details of the indicators are described in the methodology section 4.4.2.

Kling-Gupta Efficiency (KGE) (Gupta et al., 2009) method was generated for the decomposing of the biased factor (correlation, variability and mean biased) in the various component (Equation 2.16) of the simplifying the NSE method.

$$KGF = 1 - \sqrt{(r-1)^2 + (\frac{\sigma_{sim}}{\sigma_{obs}} - 1)^2 + (\frac{\mu_{sim}}{\mu_{obs}} - 1)^2} \qquad 2.16$$

Where r, σ_{sim} , σ_{obs}, μ_{sim}, and μ_{obs} is the linear correlation between simulated and observed data, standard deviation of simulated data, standard deviation of observed data, simulated mean and the observed mean respectively. KGE is perfect when its value is one, if the KGE value is less than zero indicate that mean of observation is better than the simulation (Castaneda-Gonzalez et al., 2018). Various studies revealed that positive KGE value means good results from simulation and the negative value is considered as bad. Rogelis et al. (2016) the study performed KGE value in-between 0.5 to 0 indicated the poor but it cannot give the significance in negative value and negative KGE values were not mentioned. But Schönfelder et al. (2017) suggested that the negative was not satisfactory. Andersson et al. (2017) stated that the positive and negative value in the definition likes NSE. Up to now, KGE outputs value is not compared to the NSE value and the performance value is not translated into the qualitative matrix. So, the description of model output depends upon the modeler experience and interpretation. Now a days, NSE, R^2, RSME, and $PBIAS$ are the most commonly used indicators for the performance assessment of the hydrological models (Adhikari, 2017; Moriasi et al., 2007; Pandey et al., 2019; Santhi et al., 2001; Shrestha et al., 2018).

2.4 Developing future climate scenarios

Assessment Reports (ARs) from the Intergovernmental Panel on Climate Change (IPCC) provides latest status of global and regional climate projection, scenarios, and risks associated

with increase in global and regional mean temperature rises (IPCC, 2014). The special report of IPCC published in 2018 (IPCC, 2018) highlights that the pre-industrial levels and related stage would enforce 1.5^0C rise in temperature (global warming) by 2100. Anthropogenic activities are the major drivers of climate change. Urbanization and its corresponding LULC changes are the key factors of the urban climate change through temperature and precipitation. Satellite-driven land-sat data of the urban surface temperature and the LULC data from 1990 to 2010 found that the spatial-temporal change in urban surface temperature with respect to land surface condition in China. There was a strong relation between them (Shi et al., 2015). Similarly, comparing the urban and rural precipitation, significant change has been detected in the intensity, duration, daily and seasonal precipitation variation in that region (Chen et al., 2015). Therefore, it is imperative to develop suitable set of future climatic scenarios and assess impacts under those scenarios.

2.4.1 Climate models

Various climatic models are available, and each model has its own computing features. The future climatic input value of each model has been generated by the General Circulation Models (GCMs) and Regional Climate Models (RCMs) with the different emission scenarios. Numerous techniques are available for downscale and bias correction. The selection of the appropriate scenario, technique, and model for the climate change impact study is not straight forward (Lutz et al., 2016). The selection of the model depends upon historical climatic data source, skills of a modeler, and the climatic variables of the model. The output of each model is varying due to the selection of model, data, downscaling, and biased correction techniques (Kharin et al., 2013).

GCMs simulate the three-dimensional physical properties of the climate by solving numerical conservation equations of mass, energy, momentum and water vapor including equation of state. The GCMs have a coarse resolution in the horizontal and vertical scale and the output of the model mainly variable with the resolution. After reducing the uncertainty of the climatic variables, the resolution and the information in the grid was finer than the GCMs. The downscaled data level in the fine grid for the regional level analysis as a RCMs is shown in Figure 2.4. The function of RCMs is also same as GCMs but it takes a limited area for acquiring high-resolution data.

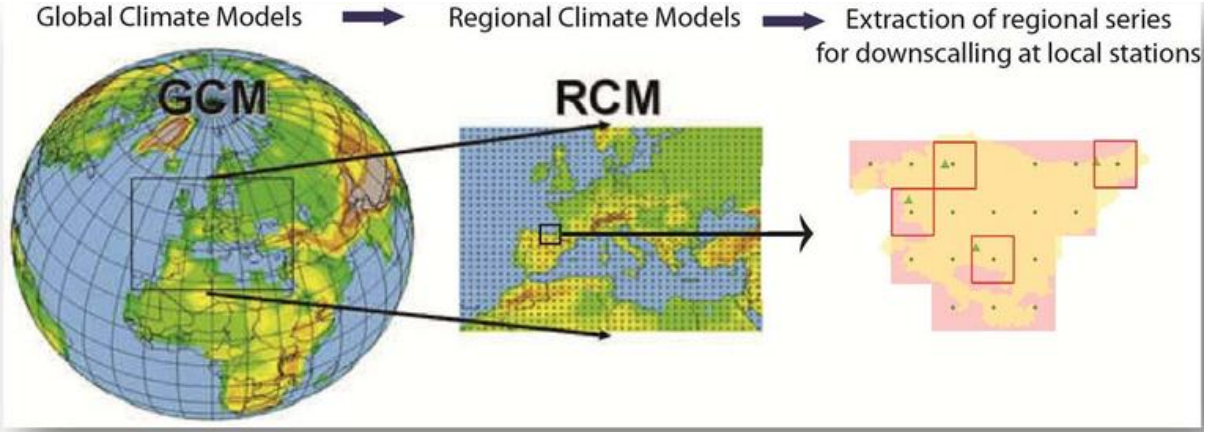

Figure 2-4 Concept of downscale from GCMs to RCMs and local levels

(source:- (Gonzalez-Aparicio and Zucker, 2015)*)*

A list of literatures reviewed with respect to the use of GCMs and RCMs in the areas similar to the study area is provided in Table 2.4. Such a climatic variation, topographical conditions and climate change scenario are analyzed in the different basin and from the analysis, Aryal et al. (2017) concluded that the RCMs (ACCESS-CSIRO-CCAM, CNRM-CM5, and CCSM4) generated from the respective GCMs are more reliable for the mountainous region like Bagmati basin.

Table 2-4 List of used RCMs and GCMs in a similar region of the study area

S.N.	RCMs/GCMs	Sources	Resolution	Used Location	Reference
1	ACCESS-CSIRO-CCAM	Collaboration for Australia Weather and Climate Research, Australian Government	0.5^0/daily	Tamakoshi Basin, Songkhram River Basin	(Aryal et al., 2017; Shrestha et al., 2018)
2	CNRM-CM5-CCAM	National Centre for Meteorological Research (CNRM), France	0.5^0/daily	Tamakoshi Basin, Songkhram River Basin	(Aryal et al., 2017; Shrestha et al., 2018)
3	CCSM4	National Center for Atmospheric Research (NCAR), USA	0.9424 × 1.25°	Tamakoshi Basin	(Aryal et al., 2019)
4	CMIP5	Coupled Model Inter-comparison Project	10 km x 10 km	IGB, Kaligandaki Basin	(Bajracharya et al., 2018; Lutz et al., 2016)
5	MPI-ESM-LR-CCAM	European Network for Earth System Modeling	0.5^0/daily	Kaligandaki, Tamakoshi, Songkhram River Basin	(Aryal et al., 2017; M. Shrestha et al., 2017; Shrestha et al., 2018)
6	GFDL-CM3	Institute for Atmospheric and Environmental Sciences (IAES),		Tamakoshi Basin	(Aryal et al., 2017)

S.N.	RCMs/GCMs	Sources	Resolution	Used Location	Reference
		Goethe University, Germany			
7	MPI-ESM-LR	Atmospheric Research, Melbourne, Australia		Tamakoshi Basin	(Aryal et al., 2017)
8	Nor ESM-M			Tamakoshi Basin	(Aryal et al., 2017)
9	MRI-GCM	Meteorological Research Institute (MRI), Japan	20 km	Bagmati Basin	(Mishra and Herath, 2014)
10	HadGEM3-RA		0.44^0 x 0.44^0	Indrawati Basin,	(Shrestha et al., 2016b)
11	MIROC-ESM		2.79^0 x 2.8125^0	Indrawati Basin,	(Shrestha et al., 2016b)
12	MRI-CGCM3		1.875^0 1.875^0	Indrawati Basin,	(Shrestha et al., 2016b)

2.4.2 Climate scenarios

Global or regional climate models project future climate based on various climatic scenarios, which are defined based on population growth, economic development, LULC change, and atmospheric conditions. The scenarios are evolving over the time and elaborated hereunder.

Special Reports on Emission Scenarios (SRES): The SRES scenario was issued by the Intergovernmental Panel on Climate Change (IPCC) in 2000. The SRES scenarios describe four scenario families to describe a range of possible future conditions. Referred to by letter-number combinations such as A1, A2, B1, and B2, each scenario was based on a complex relationship between the socioeconomic forces driving greenhouse gas and aerosol emissions and the levels to which those emissions would climb during the 21st century. The SRES scenarios have been in use for more than a decade, so many climate model results describe their inputs using the letter-number combinations. For example Babel et al. (2014) projected future climate in the Bagmati River Basin using SRES scenarios and found that the maximum temperature is projected to increase by 2.1^{o}C and 1.5^{o}C and precipitation by 13.2% and 17.5% under A2 and B2 scenarios by the end of 2080.

Representative Concentration Pathways (RCPs) scenarios: In the IPCC assessment reports published in 2013 used a new set of scenarios, which are termed as RCP scenarios, which are defined based on the concentration of greenhouse gases (GHG) in the atmosphere by the end of decades (IPCC, 2014). The concentration of GHG changes the solar radiation rate in Watts per m^2 in the earth atmosphere. After generating the RCPs based on the radiative forcing, SRES scenarios are no more in practice. Each RCP indicates the range of increase in the radiation in the earth surface due to increase in GHG in Earth's atmosphere at the end of decade. Four RCP scenarios are defined, which are RCP2.6 (low emission), RCP4.5 (moderate emission), RCP6.0 (moderate high emission), and RCP8.5 (high emission). Detail of the RCPs is described in the Table 2-5 (IPCC, 2014). For example, Shrestha et al. (2017b) used RCP scenarios to assess climate change impact in the water balance of Melmchi River based on climate data from a set of GCMs, and concluded that temperature and precipitation are projected to increase by 2.35^{o}C and 4.25^{o}C, and 6% and 18% by the end of 2085s under RCP4.5 and RCP8.5 scenarios, respectively. Most of the literatures showed that, in the context of Nepal, the medium and high RCP scenarios (RCP4.5 and RCP8.5) provide the better information for future climate change analysis (Aryal et al., 2017; Babel et al., 2014; Bajracharya et al., 2018).

Table 2-5 Types of representative concentration pathway (RCP) scenarios

Name	Radiative forcing	CO_2 equivalent (p.p.m.)	Temp anomaly (°C)	Pathway
RCP8.5	8.5 W/m^2 in 2100	1370	4.9	Rising
RCP6.0	6 W/m^2 post 2100	850	3.0	Stabilization without overshoot
RCP4.5	4.5 W/m^2 post 2100	650	2.4	Stabilization without overshoot
RCP 2.6	3 W/m^2 before 2100, declining to 2.6 W/m^2 by 2100	490	1.5	Peak and decline

Shared Socioeconomic Pathways (SSPs): This is a new set of future scenarios that integrates social development and economic development aspects together by combining climate models, climate policies, population growth, inequality across, governance efficiency, and within countries, institutional factors, socio-economic developments, technology change, and environmental conditions (O'Neill et al., 2014). These new framework is widely used in the community level for the future climate change impact, vulnerability, adaption and mitigation. The analysis of SSPs is in the framework/matrix base having the one axis with climate forcing (RCPs) and the other dimension is socioeconomic conditions. The SSPs analysis is based on the socioeconomic development with the five narratives; sustainable development, regional rivalry, inequality, fossil-fueled development, and middle-of-the-road development as per Table 2-6 (O'Neill et al., 2014; Riahi et al., 2017; Yang and Cui, 2019). The SSPs can easily transformation the qualitative narratives into the quantitative projections of the socioeconomic (population, urbanization, education, and socioeconomic development) drivers. Since SSPs are newly developed and projected future climate from climate models under SSP scenarios are yet to be available in public domain, SSP scenarios are not considered in this study.

Table 2-6 Summary of SSPs narratives

S.N.	SSP	Narratives	SRES
1	SSP1	Sustainability – Taking the Green Road (Low challenges to mitigation and adaptation)	B1
2	SSP2	Middle of the Road (Medium challenges to mitigation and adaptation)	B2
3	SSP3	Regional Rivalry – A Rocky Road (High challenges to mitigation and adaptation)	A2
4	SSP4	Inequality – A Road Divided (Low challenges to mitigation, high challenges to adaptation)	No analogue
5	SSP5	Fossil-fueled Development – Taking the Highway (High challenges to mitigation, low challenges to adaptation)	A1F1

2.4.3 Bias correction

The climatic model outputs depend on the used method of downscaling and bias correction techniques. Numerous studies have been conducted for the bias correction of the climatic parameters during the downscaling of the data (Aryal et al., 2017; Lutz et al., 2016; Mishra et al., 2018; M. Shrestha et al., 2017; Shrestha et al., 2018). Table 2-7 lists various methods of bias correction along with their pros and cons.

Table 2-7: Methods of bias correction

(Source: Chen et al., 2013)

S.N	Methods	Advantage	Disadvantage
1.	Linear scaling (LS)	• Mean-based • Simple correction techniques	• The RCM-simulated data have same sequence in daily precipitation • Could not address the frequency change distribution in precipitation.
2.	Local intensity scaling (LOCI)	• It is also mean-based techniques • The mean monthly factor is used for the correction to RCM simulated data and wet day frequency is corrected.	• The changes of frequency distribution of precipitation are not account. • Temporal structure of daily precipitation occurrence is not adjusted.
3.	Daily translation (DT)	• Distribution-based techniques • Different correction factors are used to correct the frequency distribution in daily precipitation of RCM-simulated data.	• It used the same sequence of daily precipitation which simulates through the RCM • The temporal structure of daily precipitation occurrence is not adjusted.
4.	Daily bias correction (DBC)	• Distribution-based techniques • Combines the daily translation and local intensity scaling approaches to take into account for further analysis.	• Temporal structure of daily precipitation occurrence is not adjusted.
5.	Quantile mapping based on an empirical distribution	• Distribution-based techniques • The RCM Simulated precipitation is corrected based on the point-wise daily constructed empirical cumulative distribution functions and precipitation frequency is also	• Temporal structure of daily precipitation occurrence is not adjusted.

S.N	Methods	Advantage	Disadvantage
	(QME)	corrected in same time	
6.	Quantile mapping based on a gamma distribution (QMG)	• Distribution-based techniques • Corrects the RCM-simulated precipitation based on a gamma distribution. The frequency of precipitation occurrence is corrected using the LOCI method. • Gama distribution function is used for the correction of RCM generated precipitation and the precipitation frequency occurrence is corrected using the local intensity scaling method	• Temporal structure of daily precipitation occurrence is not adjusted. • The observed and RCM generated precipitation characteristics varies the performance.

Principally two types of techniques have been used for bias correction; one is a simple method like the delta change method and Linear Scaling (LS) method based on the linear relationship between the data and the other is the complex method with the power transformation basis Quantile Mapping (QM) techniques. The selection of techniques for researchers is nearby similar to the ground measured data with the temporal variation (Bajracharya et al., 2018; Pandey et al., 2019; Shrestha et al., 2020).

Delta change method is a simple method and it is used based on the relation between the observed and simulated result. If the relation is simply linear with the zero initial value, then the correction is done as per Equations 2.17 and 2.18.

$$P_{adj} = \alpha P_{obs} \quad 2.17$$

$$\alpha = \frac{\overline{P_{sim}}}{\overline{P_{Fut}}} \quad 2.18$$

Where P and $\bar{P}$ referees the precipitation and mean precipitation, adj, obs, and fut, is the adjusted, observed and future precipitation. The main highlight of the method is that the precipitation is not in the negative terms and its mainly relative change is considered. If the

future changes of the parameter have a constant base value then equation is changed as follows Equations 2.19 and 2.20 (Engen-Skaugen, 2007).

$$P_{adj} = (P_{Obs} - \bar{P}_{obs}) + \gamma\, \bar{P}_{obs} \quad 2.19$$

$$\gamma = {}^{\sigma_{sim}}/_{\sigma_{fut}} \quad 2.20$$

Where, σ represent the standard deviation of the concern data.

If the distribution of the data is nonlinear and the transformation equation is changed with respect to the exponential relationship of the observed data as per Equation 2.21 (Terink et al., 2009).

$$P_{adj} = \alpha\, P_{obs}^{b} \quad 2.21$$

Where, b is the power non parametric constant.

For linear scaling, the temperature is in an additive correction basis, and precipitation is in multiplier basis as pre below Equations 2.22 and 2.23

$$P_{fut}(d)^{*} = P_{obs}(d) \,.\, [\,\{P_{fut}(d)\}/\,\{P_{ref}\,(d)\}] \quad 2.22$$

$$T_{fut}(d)^{*} = T_{obs}(d) + [\,\{T_{fut}(d)\} - \{T_{ref}\,(d)\}] \quad 2.23$$

where, P, T, and d indicates the precipitation, temperature, and daily value respectively, the fut, obs, and ref refers to future, observed, and reference period respectively and asterisk indicates the biased corrected RCMs data. The above mentioned methods are not properly correct the bias of the simulated parameters and also difficult to find the relation of the each data, to reduce such effect quantile mapping techniques is more useful.

Quantiles mapping (QM) techniques operate in the principle that the quantiles of the downloaded data to match the quantiles of the ground observed data by using the transfer function (Gudmundsson et al., 2012) as per Equation 2.24.

$$Y_{sim}(d)^{*} = Y_{sim}(d) + CF(d) \quad 2.24$$

Where, CF is the cumulative distribution function with reference day.

2.5 Water resources assessment

Water resources assessment primarily involves estimating long-term average and monthly/season water volumes at different spatial scales for current as well as projected

future scenarios. There are a large number of studies related to water resources assessment across the world as well as in Nepal. Some of the studies related to water resources assessment in Nepal include (Aryal et al., 2017; Babel et al., 2014; Bajracharya et al., 2018; Bhatt et al., 2014; Mishra et al., 2018; Pandey et al., 2019; Sangam. Shrestha et al., 2017; Thapa et al., 2017). Future water resources can be assessed using scenarios such as climate change, LULC change, population changes, and combination of various changes. Following sub-sections presents literature review related to assessing impacts of selected scenarios on water resources.

2.5.1 Assessing climate change impacts

Change in the precipitation pattern and increase in the temperature of a region affect runoff characteristics as well as alter the water balance throughout the basin (Bolch et al., 2012). Lutz et al. (2016) concluded that the positive variation range in temperature and precipitation under the RCP4.5 and RCP8.5 scenarios in the Indus, Ganges, and Brahmaputra (IGB) basin at the end of the century varied from 3.5°C to 6.3°C and from 3% to 37% respectively. A study by Bajracharya et al. (2018) suggested that for the Kaligandaki basin, the extreme increase in average annual temperature and precipitation by 4°C and 26% by late century under RCP8.5. The change dynamics of the river basin climate has increased the water yield by 50% at the outlet of basin.

Terink et al. (2009) explained that the precipitation pattern, intensity, duration, and frequency have more uncertainty, in those parameters power transformation techniques are more reliable. But in temperature follow the previous pattern with a slight change that reflects the relation is more linear. Most of the researchers, indicated the performance of the biased correction significance has been checked by the statistical indices (R^2, RMS, PBIAS, etc.) (Gautam et al., 2010; Lutz et al., 2016; Mishra and Herath, 2014; Pandey et al., 2019; Shrestha et al., 2018). Most of the researchers outlined that the climate change effect is mostly changing the dynamics of the water balance and runoff characteristics in the basin that has been quantified by inputting the climate models outputs in the hydrological rainfall-runoff model (HEC-HMS, SWAT, HBV, etc.) (Aryal et al., 2017; Mishra and Herath, 2014; Pandey et al., 2019; Shrestha et al., 2018; Thapa et al., 2017).

Aryal et al. (2017) explained the changing pattern of the climatic variables and its implication in the water balance as well as river runoff of the Tamakoshi River by using the HEC-HMS and SWAT model. The maximum temperature change under RCP4.5 and RCP8.5 is expected

by +1.75^{0}C and +3.52^{0}C, similarly in minimum temperature change has been detected by +2.1^{0}C and +3.73^{0}C under both scenarios. But the annual average precipitation has decreasing trend under both RCP4.5 and RCP8.5 with -2.5% and -2.44% respectively. From the results of the study, it has been concluded that the uncertainty of river hydrological characteristics mostly depends on the choice of RCPs scenario, bias correction, climatic models and hydrological models. Mishra et al. (2018) concluded that climate change has positive and negative impacts on river flow. Bheri river discharge has been decreasing in the month of July and August by 20% and increasing upto 70% in dry period due to an increase in the annual precipitation upto 15.2% at the end of the century. Similarly, the average annual temperature has been detected to increase in the RCP4.5 and RCP8.5 upto 0.029^{0}C/year and 0.068^{0}C/year respectively. The above studies clearly define the selection of the suitable climatic models, process use for refining the data to reduce the uncertainty of the parameters and the selection of suitable hydrological mode is the prime performance indicator of the research.

2.5.2 Assessing LULC change impacts

Climate change, urbanization, population growth, and the LULC change are reciprocal to each other. Some studies assume that the LULC is not a stationary event (Mohammady et al., 2018; Pokhrel, 2018; Zhou et al., 2013). Land-use change transformation from the open land to the settlement area that changes the hydrological regime by decreasing the infiltration capacity, groundwater recharge, base-flow and increasing the surface runoff, peak flood magnitude, and average flow of the stream (Sahin and Hall, 1996). Jennings and Jarnagin (2002) found that the change in LULC by increasing the impervious surface in the catchment area grew 3 to 33% of surface runoff of the stream in the Virginia state. Wang et al. (2018) concluded that the hydrological response of the Xitiaoxi River Basin (XRB) changed due to increase in the impervious surface of the basin and the analysis during the period from 1985 to 2008 by using the SWAT model. The output was simulated by increased impervious area 11.45% and that caused an increase in the average annual surface runoff and water yield by 11.87% and 1.09%, respectively. Similarly, average annual percolation, evapotranspiration (ET), and base flow of the basin were reduced by 16.53%, 0.73%, and 17.26%, respectively due to the LULC change effect. The LULC change has a positive correlation with the water yield and surface runoff related parameter, and vice versa to ET, base flow and percolation parameters. All of the above literature were analyzed based on the past land-use change in the

basin and its corresponding effect in the river hydrology but they cannot foresee the future scenario with respect to projected LULC change in the basin in the mountainous terrain.

2.5.3 Assessing integrated impacts of both climate and LULC changes

Urbanization reduces the surface water and affects the groundwater recharge due to excess demand and LULC change. The integrated impact of climate change and LULC change in the basin is facing the imbalance of the natural system and the effect will be rise exponentially in the future (Lamichhane and Shakya, 2019b). Bosch and Hewlett (1982) experienced that reduced agricultural land and increased urban area have been creating an imbalance in river discharge from the study of 94 catchments in the world. The combined changes amplify the uncertainty effect in the climatic variability in the hydrological regime.

Yang et al. (2017) highlighted the integrated impact on the Heihe River basin using the SWAT model, historical LULC, and corresponding climatic data between 1980 to 2010. Increasing the agricultural land (Adverse of urban development) and the climatic variables (precipitation and temperature increased up to 15.7 mm and 0.38°C), ET and surface runoff of the basin was increased by 3.2% and 6.6% respectively. The outcomes of the study visualized that the effect of LULC change was not significant than the climate change but the effect in the hydrological parameter through the LULC change cannot be overlooked in the future. Shrestha et al. (2018) quantified the future climate change and corresponding LULC change effect in the Songkhram River Basin Thailand having a tropical semi-arid climate zone. The climatic parameters impact was more significant than the LULC. Future climate projection was generated from the RCMs of CCAM GCM and the land-use change projection was done in the two (Economic scenario and Conversion scenario) projection scenarios by using the Dyna-CLUE land-use change model. The economic scenario is based on the current growth pattern. From the climatic model, precipitation was increased by 16.8% and 8.1% in the RCP4.5 and RCP8.5 respectively. The SWAT model was used for the simulation of future LULC and climate data. Individual climate change had a negative impact on the average annual surface runoff of the river even increases in precipitation patterns in the future with the base LULC data. Similarly in LULC change only, the average annual surface runoff at the outlet of the basin has a positive impact with the base year climatic condition. From these observations, the groundwater-related parameters have a high impact due to less recharge from the surface and thus generate more runoff from the basin. Integration scenarios that also decrease the average annual runoff of the river system but reduce the gap of the decrement with respect to baseline. From the results, it is observed that the water balance and

river runoff are more sensitive for climate rather than LULC change. But both phenomena will occur simultaneously and cannot be avoided. The runoff characteristics of the basin are varying with the climatic and biophysical conditions of the basin. Even increase in the precipitations in the basin (Shrestha et al., 2018) reduces the average annual runoff due to the high rate of evapotranspiration and recharge capacity.

The combine LULC and climate change effect in the basin is not superimposed. It may be smoothing the effect on each other. All the above cited studies of the individual and integrated change impact are not directly associated with the groundwater simulation for assessing the future groundwater scenario.

2.5.4 Uncertainty in the water resources assessment

The water resources assessment through the hydrological model represents the complex watershed properties in the simple hydrological process and therefor there includes uncertainties in various aspects (Nasseri et al., 2014). Different sources of uncertainties are related to the selection of climate models, downscaling process, and the bias correction techniques used. The uncertainty is accumulated in the data through the GHG emission scenarios or it is also an inherent part of the model with associating through the input data, model structure, input model parameters, and others (Pandey et al., 2019). Nasseri et al. (2014), the uncertainty evaluation principles was mainly grouped in the three types; probabilistic (based on the cumulative distribution function, probable distribution function, and input/output variables), possibility (based on the fuzzy logic) and hybrid (combination of two methods) method. The recent studies performed that the management and representation of the uncertainty in the climate data or the hydrological model through the probabilistic approach taken in the model with the combination of GCMs/RCMs data (Iizumi et al., 2009). The uncertainty of the input data (like temperature and precipitation) and its corresponding impact in the water resources assessment of the model output can be seen during the calibration and the validation of the model with the acceptable limit (Pandey et al., 2019).

The climate change and hydrologic stationarity in the model or assumption that can be taken during the analysis create more uncertainty. The uncertainty can be easily characterized through probabilistic terms and also provided the knowledge of deep uncertainty associated with climate change, demand in a different social scenario, population growth, and others (Brown et al., 2020). From these analyses, generate the concept of resilience to improve the water resources design for future uncertainty by combining persistence, adaptability, and

transformability. For minimizing the effect of uncertainty of the climate change in the hydrological model, multiple data of RCMs/GCMs are used and compare for better performance. Aryal et al. (2017) study of the Tamakoshi River in the Nepal, conclude that the multiple model (SWAT, HEC-HMS), various climate data from GCMs/RCMs, appropriate downscaling methods, multiple biased correction technics (quantile mapping), projection scenarios (RCP4.5 and RCP8.5) provides the reliable and robust output through the minimizing the uncertainty effect. MoFE, (2019) report in "Climate Change Scenarios for Nepal National Adaptation Plan," uncertainty analysis of projected temperature and precipitation can be calculated through the multiple models used, analysis through the standard deviation or coefficient variation, and inter-quantile range among the models. For the uncertainty analysis for future climate and discharge of the river of the study was done by using the two-way and three-way ANOVA methods. In the water resources assessment the cumulative uncertainty impact was assessed and tries to minimize during the model simulation. Pandey et al. (2019), also stated that the effect of input data uncertainty has higher degree than the model parameters, so, the higher quality of observed, downloaded, and projected data performed the better results.

Higher uncertainty is seen in the stream flow data in small time (daily) due to precipitation prediction. Similarly, Nasseri et al. (2014), study used the different techniques (multi model, one probabilistic model, Modified Bootstrap Ensemble Model (MBEM), one possibility, FUzzy C-means Ensemble based on data Pattern (FUCEP), Ordinary Kriging (OK), Weighted Average (WA) methods, and Bayesian Model Averaging (BMA)) for the uncertainty analysis in the water resources assessment. From the above techniques MBEM and FUCEP provides the better preference than the other for the uncertainty. So, for the better future assessment of water resources the uncertainty has been removed the phase which it occurs during the simulation.

2.6 Groundwater modeling

Groundwater is the largest water resource which is sufficient and accessible. The global change has an adverse effect on this resource (Aeschbach-Hertig and Gleeson, 2012). Urbanization, increase in population, increase water use, excessive use of water for irrigation, industrialization, LULC change, increase rate of drilling and pumping, and change of climatic variability are continuously creating a cumulative impact in water resources around the world (Gorelick, S.M. and Zhen, 2016). Exploitation and contamination of groundwater is a global problem and the KV is not an exception. In many urban areas, groundwater is the key source

of water supply. For example Thapa et al. (2018) showed that water deficit when considering the existing sources and systems in the KV is nearly two-third. The deficit as well as supply water depends upon the groundwater resources. For the sustainable management and planning of the groundwater resources, groundwater models have played a vital role to satisfy the planning of demand and supply of sources with maintaining groundwater hydrology (Refsgaard et al., 2010). Excessive research has been directed in the field of groundwater modeling for balancing the groundwater ecosystem in the change context (Adhikari, 2017; Pandey and Kazama, 2014; Shrestha et al., 2020; Zipper et al., 2017). Following sub-sections presents literature review on various aspects of groundwater modeling.

2.6.1 Evolution of groundwater modeling

Groundwater flow modeling is a conceptual computational techniques used for the simulation of the underground hydrological system. In the present day, the groundwater models are extensively used for addressing the groundwater problem and show the complex phenomenon below the surface. Historically, Hagen (1839) and Poiseuille (1840) pioneered the fundamental equation of groundwater flow in the viscous flow through the capillary tube. Later Darcy (1856) derived the fundamental equation based on the conservation of mass theory for simulating the flow of the liquid in the porous medium (soil is homogenous, incompressible and isotropic). After formulating of the Darcy law, many other equations were derived in with this concept (Groundwater flow equation, Heat transfer equation, Laplace equation). Toth (1963) investigated the groundwater flow in the small drainage basin. In his hypothesis he found that the existence of the nested groundwater region in the hierarchically of local flow, sub-regional flow, and regional flow with the application of the topographical, geological, and climate data of the catchment. This sub-flow system could be easily predicted the recharge area, discharge from the basin, variation of groundwater depth and volume etc.

Freeze and Witherspoon (1966) used a numerical model of the layered aquifer system by solving the three-dimensional equation in steady-state groundwater flow with heterogeneous and isotropic groundwater basins. The model quantified the basin yield from the analysis of hydraulic conductivity properties and water table configuration of the basin. Later Freeze (1971) used the numerical model in transient condition with the relation of the water table, infiltration characteristics and the base flow hydrograph of the basin. The model was used for finding the basin water yield based on pumping rate, recharge capacity and discharge characteristics of the basin. Trescott and Larson (1976) used a 3D finite-difference equation

with principal of the conservation of mass for groundwater flow simulation by using computer code.

The first version of the simulation code was generated by the United States Geological Survey (USGS) in 1983 and the code was called USGS Modular Three-Dimensional Finite-Difference Ground-Water Flow Model (MODFLOW) and initially the code was written in the FORTRAN-66 programming language (McDonald and Harbaugh, 1984).

After formulation of the 3D groundwater flow models, the simulation of the groundwater potential and the associated flow characteristics was done in the different sectors since 1988. To enhance the model capability was created by including the other associate like observation, parameter estimation, calibration and evaluation of the model up to MODFLOW-2000. Rapid growth of computer programming languages and computing technology, and associated packages (Groundwater transport process and groundwater management process) in the model or process was inbuilt in the model after releasing the MODFLOW-2005. This version included the saturated and unsaturated flow simulation process, irrigation process, groundwater simulation-optimization process, parameter optimization process, density-dependent flow process, and solute transport process, etc. After releasing a free version of the MODFLOW-2005, the simulation of Groundwater was done in the various basin and objectives (Loudyi, 2005; Adhikari, 2017; Zipper et al., 2017; Shrestha et al., 2020). Currently, thousands of computer program codes have been developed for the analysis of the groundwater problem. Further expansion has been done in the groundwater simulation with the other dynamics like; integrating the surface and sub-surface groundwater modeling (Barlow and Harbaugh, 2006), Windows-based graphic user interfaces Visual MODflow, Groundwater Modeling Systems (GMS) (Zundel, 2000), Visual MODflow (Waterloo Hydrogeologic, 2001), and Groundwater Vista (Rumbaugh and Rumbaugh, 2005). After application of the GIS tools for the various simulation of the input data, storage, and processing (pre and post) of the model is provided the more interest in groundwater flow simulation. Recently, many researchers (Adhikari, 2017; Pandey and Kazama, 2014; Shrestha et al., 2020; Zipper et al., 2017) used the numerical groundwater model for simulation of the real field flow with discretized problem in mathematical equation with associated boundary condition. A set of complex partial differential equations changed into the algebraic equation to easily solve the problem via a computer program/code (Loudyi, 2005).

2.6.2 Groundwater models

Groundwater models are broadly classified into three types; physical, analogue, and mathematical.

- Physical model: This model is physically built in the lab by incorporating the all hydrogeological phenomenon to achieve the groundwater problem. This method is simple and easy to set up for addressing the simple physical events but it cannot solve complicated problems that may be occurring at the catchment level.
- Analogue model: Analogue model is operated with the principle as the groundwater flow in a homogeneous, isotropic and porous soil medium with the Laplace's equation 2.25 like Darcy equation 2.27. Principle of Darcy law of groundwater movement can easily solve the simple analogue problem and the model can be easily set up for the study of the groundwater movement.
- Mathematical model: It is a conceptual model and it is formulated with a set of equations representing the physical phenomenon of the groundwater environment like initial conditions, boundary conditions, physical properties, etc. Mathematical model is commonly used and it solves the problem either analytical or numerical base. Finite difference and finite element method (Anderson et al., 2015) were used for solving the numerical problem and the selection of the suitable method depended upon the model outputs. The other factors like the initial condition of the model, time and space discretization, boundary conditions of the model, and quality of the data used also concerned with the quality of the model output.

Now, there are many computational computer codes available with its properties, capability, operational characteristics, and the limitations and the selection of the suitable code is not straight forward (Kumar, 2019). The basic principle, objectives of simulation, and performance of code are more important and the commonly used computational techniques are described below.

a) MODFLOW

MODFLOW (Harbaugh, 2005) is the conceptual and numerical groundwater hydrological model generated by the USGS. It can simulate the ground and surface water interaction, solute transport, various groundwater parameters estimation, aquifer composite system, land subsidence, and other features. Details of the MODFLOW have been already discussed in the above literature. The USGS has been released the six versions of MODFLOW version;

MODFLOW-84, MODFLOW-88, MODFLOW-96, MODFLOW-2000, MODFLOW-2005, and MODFLOW 6. The new version of the model was developed by adding the extra tools, computer language, interface, and supports system in the core MODFLOW but the main processing principle and the engine is remaining the same. The selection of the model version basically depends on the types of simulation outputs. The groundwater flow model has additional package and interactions have been generated as per Table 2.8 for controlling and advancing the model outputs.

Table 2-8 List of Versions of MODFLOW

S.N.	Software	Details
1	MODFLOW-NWT	Separate program for solving drying and rewetting of the unconfined GWF equation.
2	MODFLOW-LGR	A 3D local grid refinement finite-difference GWF model
3	MODFLOW-USG	An unstructured grid version of MODFLOW using control volume techniques for simulating GWF
4	GWM	Groundwater flow simulation with groundwater management capability.
5	FMP	Program used for the irrigation and agriculture by simulating dynamically integrated supply-and-demand component.
6	GSFLOW	Coupled program of surface and sub-surface flow by the USGS Precipitation-Runoff Modeling System (PRMS) and MODFLOW-2005.
7	OWHM	Integrated the water movement for human and natural within a supply demand framework
8	CFP	Model for turbulent groundwater-flow conditions.

S.N.	Software	Details
9	SEAWAT	A 3D computer program for variable density and transport groundwater flow.
10	Surface-Water Routing (SWR)	Model for surface-water and groundwater flow interactions.

b) PMWIN (Processing Modflow for WINdows)

It has simulated the aquifer (single confined, unconfined, and both) groundwater flow using the block centered approach of MODFLOW package. During the simulation, the interaction between the well, recharge, evapotranspiration, flow-through drain, the river bed, and aquifer system is also found (Chiang, 2005).

c) mflab (Modflow Laboratory)

This model is operated based on a MATLAB script. The all simulation, setup, run, and analysis are similar to the MODFLOW operating tools like; (+SWI), MODPATH6, MT3DMS and SEAWAT is used (Olsthoorn, 2011).

d) GMS (Groundwater Modeling System)

The system was building in model based on the supporting tools of the MODFLOW, MODPATH, RT3D, SEEP2D, MT3DMS, FEMWATER, and UTEXAS. The main features of this conceptual model was 2D and 3D geo-statistics, stratigraphic modeling (Liang et al., 2012).

e) Visual MODFLOW Flex (VMOD)

This software was developed by the Waterloo Hydro-geologic, Canada (Waterloo Hydrogeologic, 2001). It is the graphical interface of the MODFLOW engine and later new extension like MODFLOW-SURFACT, MT3DMS (mass-transport 3D multi-species) and a 3-D model explorer. Visual MODFLOW supports MODFLOW-2000, MODFLOW- 2005, MODFLOW-LGR, MODFLOW-NWT, MODFLOW-SURFACT, and SEAWAT is also added.

f) FEFLOW (Finite Element subsurface FLOW system)

It is also another computer program based model on the mass and heat transfer in porous and fractured media for obtaining the groundwater features. The saturated and unsaturated groundwater condition is simulated based on solving the finite element approach with the governing principle of mass and heat transport, fluid density effects and others (Kumar, 2019).

g) MODFLOW-SURFACT

This model analyzed the subsurface system in the three-dimensional finite-difference approach for flow and transport modeling. It is also used the core code of the MODFLOW with advancing the other tools for addressing the transport problem and modeling, rewetting of the drain cell, numerical dispersion and oscillation, etc. (Bedekar et al., 2012).

h) Groundwater Vistas (GV)

It is the advanced software package for simulating the 3D groundwater flow for transport modeling, calibration, and optimization of the parameters from the MODFLOW codes. It was either coupled with the graphical analytical tools or the independent operating graphical design system for the code of MODFLOW MODPATH (both steady-state and transient versions), MODFLOWT, MT3DMS, MODFLOW2000, MODFLOW-SURFACE, GFLOW, PATH3D, SEAWAT, RT3D, and PEST. The uncertainty analysis was also simulated through the GV by the Monte Carlo analysis with the different packages of MODFLOW and other GW models (Rumbaugh and Rumbaugh, 2005).

i) MODHMS

It is a popular code of the MODFLOW to simulate the hydrological groundwater flow system as a physical base, spatially distributed, and flow integration of surface and sub-surface based. It simulates the complex hydrological process to meet the demand of the basin as per available water. The advance code MODFLOW-SURFACE is also used for the subsurface simulation for overland flow, channel flow, and transport modeling (Donn et al., 2012).

2.6.3 MODFLOW-2005: Operating principles and packages

Basic governing principles in all the aforementioned literatures were taken from the MODFLOW but the operating modes, interface, and the software packages were varying. The MODFLOW-2005 model is widely used as it is easy to understand, easy to

modify/customize, and freely available. The main advantage of the model is that the input and output data of the model are easily generated or analyzed through the GIS tools and other computer applications. Also, it enhances the output from the groundwater simulation. In this model, similar program functions are used together for computing specific tasks and generating the groundwater environment either single or together. The model is now in the Fortran 90 (American Institute National Standards, 1992) programming language which is subdivided into the package for the groundwater flow process. The entire package of the model solves the groundwater flow process by using the 3-D finite-difference Equation 2.25.

The principle of mass balance movement is considered for the constant density through the porous material and operates through the partial differential equation, as given below.

$$\frac{\partial}{\partial x}\left[K_{xx}\frac{\partial h}{\partial x}\right]+\frac{\partial}{\partial y}\left[K_{yy}\frac{\partial h}{\partial y}\right]+\frac{\partial}{\partial z}\left[K_{zz}\frac{\partial h}{\partial z}\right]+W=S_S\frac{\partial h}{\partial t} \qquad 2.25$$

Where;

K represents the hydraulic conductivity and x, y, and z represents the corresponding axes parallel to the major axes of hydraulic conductivity (L/T)

"h" is hydraulic head (L),

W is a volumetric flux per unit volume corresponding sources/sinks of water, with W< 0.0 for flow out, and W > 0.0 for flow into the ground-water system (T^{-1}), S_S is the specific storage of the porous material (L^{-1}), t is time (T)

In general, Ss, Kxx, Kyy, and Kzz are the function of space and W is a function of space and time. Equation describes ground-water flow in a heterogeneous medium under non-equilibrium conditions (Harbaugh, 2005). The head and flow magnitudes from equation are varying in all three directions (x, y, and z). For solving equation with respect to space and time the initial and boundary condition mostly exists. The solution of equation is not simple. So, for solving such numerical problem, the finite difference method is used by a finite set of discrete points in space and time by assuming that each discrete block is rectangular in both horizontal and vertical. In the steady-state condition, there is no change in store within the basin than the right-hand side is zero.

Boundary Conditions: - There are three types of condition are exists

a) Specified head boundary (Dirichlet condition):- It is also called constant head boundary condition, where the hydraulic head of the basin is assumed a constant.

b) Specified flow boundary (Neumann condition):- In this condition, the gradient of the head is given across the boundary. If head or flux is stated zero means the no condition in the boundary.

c) Head-dependent flow boundary (Cauchy or mixed boundary):- Where the flux is calculated by head value and is also called a head boundary condition.

Initial Condition:- There are two types of initial condition occurs during the simulation.

a) Steady-state condition:- where the time is not variable and the change in storage is zero.

b) Unsteady state condition or transient condition:- head may be change with respect to time

The groundwater flow of the basin is obtained based on the continuity equation by using finite difference techniques; sum of the flow in and out within the cell must be equal to the rate of change in water storage in that cell value is given as Equation 2.26.

$$\sum Q_i = SS \frac{\Delta h}{\Delta t} \Delta V \qquad 2.26$$

Where Q_i, SS, Δh, Δt, and ΔV, is the flow rate in the cell I in (L^3T^{-1}), specific storage coefficient in the cell, change in head (L), change in time (T) and the change in volume (L^3) with corresponding time and head respectively.

In detail, equation gives the change in volume (change in head Δh in cell area) of water taken by each cell in the different surrounding cells with a change in the time Δt. The negative sign is a change in head represents the outflow or loss from the cell. The flow rate in each cell is found by Darcy's Equation 2.27 to use the central finite difference techniques in i, j, and z direction as per Figure 2-5.

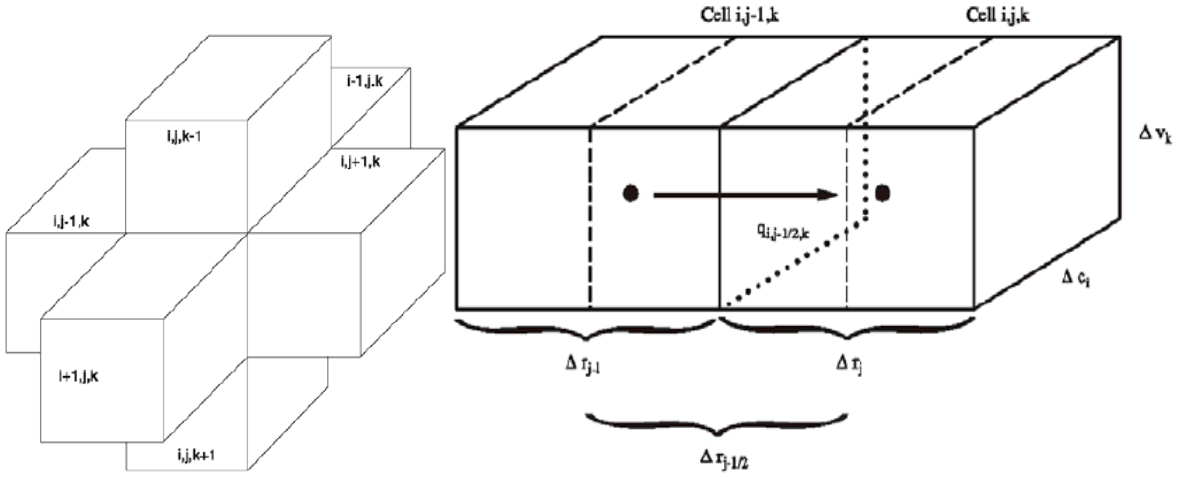

Figure 2-5 a) Indices for the six adjacent cells surrounding cell i, j, k b) Flow into cell i, j, k from cell i, j-1, k.

(Sources:- (Harbaugh, 2005)*)*

$$q_{i,j-1/2,k} = K_{i,j-1/2,k}\Delta c_i \Delta v_k \frac{(h_{i,j-1,k} - h_{i,j,k})}{\Delta r_{j-1/2}} \quad 2.27$$

Where,

$q_{i,j-1/2,k}$ is the flow rate through the cell i, j, k, and I, j-1, k (L^3T^{-1})

$K_{i,j-1/2,k}$ is the hydraulic conductivity along the corresponding nodes (LT^{-1})

$\Delta c_i \Delta v_k$ is the area of the cell normal to the flow direction (L^2)

$h_{i,j-1,k}$ is the head in corresponding node (L), and

$\Delta r_{j-1/2}$ is the distance between the node (L)

The output of above equation is a one-dimensional steady-state case in the cell aquifer and faces of similar others are also found by the change of the cell values. In homogeneous soil, the hydraulic conductivity of soil in any direction is same and the corresponding equation can be simplified with the introducing the hydraulic conductance properties as per Equation 2.28.

$$q_{i,j-1/2,k} = CR_{i,j-1/2,k}\,(h_{i,j-1,k} - h_{i,j,k}) \quad 2.28$$

Where $CR_{i,j-1/2,k}$ is the hydraulic conductance property between i row and k layer between the j and j-1 node and written as per Equation 2.29.

$$CR_{i,j-1/2,k} = \frac{(K_{i,j-1/2,k}\Delta c_i \Delta v_k)}{\Delta r_{j-1/2}} \quad 2.29$$

The flow rate in the six adjacent cells is calculated by the above equation and the external features affects the flow rate in each cell like river, well, recharge, evapotranspiration, drain, and other sources. The flow rate in the external sources may depend on the head only in receiving cell but not in other and aquifer flow from outside is calculated by Equation 2.30.

$$a_{i,j,k,n} = p_{i,j,k,n}\, h_{i,j,k} + q_{i,j,k,n} \quad 2.30$$

Where $a_{i,j,k,n}$ is the flow rate from the external n sources into cell i, j, k. and the $p_{i,j,k,n}$ is the constant flow through the external sources n in the cell i, j, k (L^2T^{-1}). The negative value indicates the discharge from the aquifer. For reducing the error during the simulation process, backward finite difference approach is adopted and equation is solved in each time steps simultaneously as per Equation 2.31.

$$CR_{i,j-1/2,k}\left(h^m_{i,j-1,k} - h^m_{i,j,k}\right) + CR_{i,j+1/2,k}\left(h^m_{i,j+1,k} - h^m_{i,j,k}\right) + CC_{i-1/2,j,k}\left(h^m_{i-1,j,k} - h^m_{i+1,j,k}\right) + CC_{i+1/2,j,k}\left(h^m_{i+1,j,k} - h^m_{i,j,k}\right) + CV_{i,j,k-1/2}\left(h^m_{i,j,k-1} - h^m_{i,j,k}\right) + V\left(h^m_{i,j,k+1} - h^m_{i,j,k}\right) + P_{i,j,k}h^m_{i,j,k} + Q_{i,j,k} = SS_{i,j,k}\left(\Delta r_j \Delta c_i\, \Delta v_k\right)\frac{h^m_{i,j,k} - h^{m-1}_{i,j,k}}{t^m - t^{m-1}}\ \text{z} \quad 2.31$$

Where, R, C, and V represent the row, column, and vertical grids of the central cell. $h^{m-1}_{i,j,k}$ is the head at the beginning time steps of t^{m-1}. During the simulation of equation, the main objective is to predict the head distribution in the time steps. So, initial head ($h^0_{i,j,k}$) of the each grid is assigned for solving.

Groundwater flow computer program is highly capable of solving to solve the hydrological problem by running the different codes as per the hydrological problems, and a number of these codes are called a package. The selection of packages is found by the modular problem and the outputs from the solver package gets the better result after simulation (Loudyi, 2005; Basnet, 2016; Shrestha et al., 2020). These are available for download as open-source software products in USGS web portal.

For the simulation of the hydrological stress in the groundwater flow process, certain concepts are required. These stresses (called package) are the boundary condition for solving

the groundwater inflow/outflow, the basic governing principle and the governing equation is described below.

Well Package;

The principle of the package is that the withdrawal and add water in the aquifer in the constant rate in the given stress periods, where recharge and pumping from the well are independent in the cell area and head. Q is the recharge or discharge from the aquifer and the negative sign is used for the pumping or discharge from the well and calculate as per Equation 2.32.

$$\frac{Q_n}{Q_W} = \frac{T_n}{\sum T} \qquad 2.32$$

Where, Q_n, Q_W, T_n, and $\sum T$ is the recharge (L^3T^{-1}) (negative for pumping) from the layer n in the well as per assigned stress period, Total recharge from well (L^3T^{-1}), Transitivity (L^2T^{-1}) of layer n, and sum of the transitivity of all layer respectively.

Recharge package

This package simulates the recharge in the distributed form spatial and temporal scale in the surface of the basin. The common phenomenon in the GWF system is the precipitation and recharge through the percolation. It is expressed as per Equation 2.33.

$$QR_{i,j} = I_{i,j}\, DELR_j\, DELC_i \qquad 2.33$$

Where, $QR_{i,j}$, $I_{i,j}$, $DELR_i$, and $DELC_j$ is the recharge flow in the horizontal cell (i, j) (L^3T^{-1}), recharge flux rate per unit area in the in the horizontal cell (i, j) (LT^{-1}), horizontal cell width of i, and j respectively. Artificial recharge is also used in the recharge terms but it is either inbuilt with precipitation outside the model or provide the recharge in each cell by other techniques.

General-Head Boundary Package

This package is used when the flow in and out through any cell from any external sources and the flow rate in the cell depends on the head difference between the cell and the external sources or head assigned to the source. This principle is applicable to the GWF system by managed aquifer system recharge or other surface sources. If the head difference is constant throughout the cell (like lake, sea, river, etc.) is called boundary conductance and cell flow is linearly depends upon the head difference as given below Equation 2.34.

$$QB_n = CB_n\,(HB_n - h_{i,j,k}) \quad 2.34$$

Where, QB_n, CB_n, and HB_n is the boundary flow into the cell i, j, k (L^3T^{-1}), boundary conductance in n number of boundary (L^2T^{-1}), and head of the external sources (L) respectively.

River Package

The river conductance value in the GWF in the basin is highly sensitive than the other for the variation of the water balance in the groundwater. The water contribution in the groundwater basin is mainly relies on the type of river or the level difference between the aquifer level and the flow surface of the river. In this package the simulation is conducted based on the seepage to or from the surface to the groundwater flow in each grid cell is linearly correlated with the head difference between the cell head and the source as per given Equation 2.35.

$$QRIV_n = CRIV_n\,(HRIV_n - h_{i,j,k}) \quad 2.35$$

Where, $QRIV_n$, $CRIV_n$, and $HRIV_n$ is the flow through river to aquifer (L^3T^{-1}), hydraulic conductance between the aquifer to river bed (L^2T^{-1}), and water level or head in the river reach (L) with the corresponding cell head ($h_{i,j,k}$). For the reverse flow from cell to the river reach the value of $QRIV_n$ is negative or the cell head is higher than the river surface. The assumption is taken that the measurable head difference has not occurred during the flow from the aquifer layer to the sources and vice versa and each cell in between the flow is in a saturated condition. The generation of the river conductance in the reach is more complicated and the average value is calculated by the following Equation 2.36 based on the average value of the river bed hydraulic conductivity.

$$CRIV_n = \frac{K_n\,L_n\,W_n}{M_n} \quad 2.36$$

Where, K_n, L_n, W_n, and M_n represents the hydraulic conductance of the riverbed material (LT^{-1}), length of the river within the block (L), width of the river reach (L), and thickness of the river bed material (L) with the n number river reach respectively.

Drain Package

This package is generated for the simulation of the effect of the agricultural drain during the irrigation of the basin, in the system the water withdrawal from the aquifer to the irrigation land in the proportional basis with the assumption that the elevation difference between the aquifer and the fixed head in the drainage system. It means the difference in the head is

always proportional. If the level of the drain is fall-down the aquifer there is no effect in the aquifer system. The mathematical equation of the package is represented by Equations 2.37 and 2.38.

$$Q_{out} = CD\left(h_{i,j,k} - HD\right) \quad \text{When } h_{i,j,k} > HD \quad 2.37$$

$$Q_{out} = 0 \quad \text{When } h_{i,j,k} \leq HD \quad 2.38$$

Where, Q_{out} represent the discharge through the aquifer to drain (L^3T^{-1}), CD means the hydraulalic conductance of the drain bed material, (L^2T^{-1}), HD is the drain elevation at the corresponding cell elevetion ($h_{i,j,k}$), and n denotes the number of the drain layer in the cell. If the simulation in the reverse flow and equation is re-write as per Equations 2.39 and 2.40

$$QD_n = CD_n\left(HD_n - h_{i,j,k}\right) \quad \text{When } h_{i,j,k} > HD_n \quad 2.39$$

$$QD_n = 0 \quad \text{When } h_{i,j,k} \leq HD_n \quad 2.40$$

The above equation is similar to the river and aquifer interaction.

Evapotranspiration Package

This package simulates the quantity of water leaving from the groundwater system by plant transpiration and evaporation. The quantity of the evapotranspiration is varies on the elevation difference between the aquifer water level and the evaporation cutoff depth in the cell. The evapotranspiration rate is simulating based on the level difference in cutoff depth and the cell head level. a) when the aquifer water table is the same or above the surface elevation (ET surface), b) when the aquifer water level in between the ET surface and the cutoff level, and c) aquifer water table is below the cutoff level. The concern Equations 2.41, 2.42, and 2.43 is written as

$$RET = EVTR \quad h_{i,j,k} > SURF \quad 2.41$$

$$RET = EVTR\ \frac{h_{i,j,k} - (SURF - EXDP)}{EXDP} \quad (SURF - EXDP) \leq h_{i,j,k} \leq SURF$$

2.42

$$RET = 0 \quad h_{i,j,k} < SURF - EXDP \quad 2.43$$

Where

RET is the rate of loss of water from water table per unit surface area (LT^{-1}) due to evapo-transpiration

$h_{i,j,k}$ is the water elevation of the cell i, j, k where evapotranspiration occurs

$EVTR$ is the maximum possible rate of evapotranspiration in the cell (LT^{-1}).

$SURF$ is the water level elevation in the cell in which depth the maximum evapotranspiration loss is occurred (L)

$EXDP$ is the cutoff depth (L) in which water level of the cell from that the evapotranspiration loss ceases

The volumetric rate of the loss from the surface area can be found in each cell by the product of horizontal surface area and the rate of evapotranspiration loss as per Equation 2.44.

$$QET = RET\ (DELR_j - DELC_i) \qquad 2.44$$

QET is the rate of volume of water loss through the evapotranspiration (L^3T^{-1}). It is the similar conceptualized as the recharge package.

2.6.4 Application of MODFLOW model

Dong et al. (2012) stated that the three-dimensional groundwater flow simulation performs a better output by using the MODFLOW-2000/2005 recharge and well package. The model has been used in simulation at the regional groundwater flow of the Pinggu basin (459 km^2), China. The distributed precipitation and irrigation infiltration considered as a recharge parameter and the irrigation pumping from the groundwater aquifer is considered as a well pumping or discharging through the aquifer. Total pumping discharge can be categorized into three demands (agriculture, industrial and domestic users) by Arial Recharge and Discharge (ARD) method. The demand and supply of groundwater are related to recharge by the external irrigation. The hydrogeological setting of the model was defined as the top unconfined layers followed by the three confine layers. The integration of the model input with the concerned output the required analysis was conducted after and before the simulation of MODFLOW. How much quantity of groundwater can be withdrawn from the aquifer without changing the groundwater hydrology or water balance is a challenging task for a researcher. Sustainable use of aquifer can be found without compromising limitation and constraint through groundwater modeling.

Van Camp et al. (2010) expressed that the sustainable use of the groundwater resources can be found by the groundwater depletion indicator. The indicators have been calculated based on the groundwater balance of the aquifer. Overexploitation of the Shahrekord Plain aquifer (645km^2) in Iran has occurred by the irrigation and others pumping with respect to the recharge capacity. Recharge is either irrigation in the agricultural field or natural precipitation. MODFLOW-2005 recharge package (used for the analysis of water balance) and drainage package (used for the river network analysis) were used for the simulation of groundwater aquifer having two layers with 14 years of simulation period (1989 to 2003). Assign parameters for the model were generated through the actual geological condition, hydrological characteristics of the basin, field test data, etc. From the computed model, groundwater depletion and change in storage rate of each year were obtained for the analysis of the six groundwater depletion indices (Filling index, Accumulated Filling Index, Recharge–Discharge Ratio, Accumulated Recharge–Discharge Ratio, Recharge–Discharge Difference, and Accumulated Recharge–Discharge Difference). From the results, overexploitation of the aquifer system causes a negative trend to show all indicators and that indicates the future sustainability is achieved for the consumptive use of groundwater in the irrigation system.

Narula and Gosain (2013) also explained the advantage of coupling of surface and sub-surface model by simulating the upper Yamuna watershed for finding the spatial and temporal impact in the water availability through the climate change and anthropogenic activity. The groundwater hydrology is not directly connected with climate change and anthropogenic activity but it is coupled with surface interaction through the recharge pattern change with the change precipitation, and LULC due to urbanization, excess of pumping by raising the population, etc. Lowering of the groundwater table reduces the head difference between river and groundwater has declined the base flow. SWAT and MODFLOW with the MT3DMS solver package were used for the analysis of contaminant transport and water balance. An aquifer is a large natural groundwater reservoir with easily recharge and withdrawal. The natural streams and the lakes have high interaction with the groundwater reservoir. Construction of recharge dam and Managed Aquifer Recharge (MAR) are proven practices for the recharge of groundwater reservoir (Abiye et al., 2009). The recharge through the riverine or lake relied on the properties of the interaction layer (texture, stratification, and isotropy of sediments) (Sanford, 2002).

Salem et al. (2020) showed that the restoration of natural reservoir or groundwater reservoir recharge through the floodplain is more effective and economical techniques. The study was carried out in the 15 km wide floodplain (500 km^2) of the Drava River in Hungary. The rise in water level in the lake, recharge through the lake bed, and its corresponding effect in the groundwater level was detected by the model. For the simulation, MODFLOW-2005 and NWT (Newton-Raphson Techniques) solver package were used with the Model-Muse graphical interface. This technique solved the problem of drying and wetting of cells in the model by the nonlinearity of unconfined groundwater flow. The groundwater reservoir and lake/river interaction were simulated through the LAK7 package and the required hydro-geological parameter is taken from the field test. Four vertical layers were formulated in the basin representing the soil heterogeneity. Three different recharge scenarios were applied for the fulfillment of the deficit capacity in the river/lake and the corresponding level rise in the groundwater table was simulated. The economic and social viability was also considered during the study. After the rise, two meter water surface elevation in the lake was increased by 0.8 m groundwater table at the surrounding of the basin. Regulate the recharge and groundwater interaction with sub-surface water balance was easily simulated by the groundwater flow model (MODFLOW-NWT) through the volumetric exchange between the reservoirs.

2.7 Groundwater assessment under climatic variability and LULC change.

For assessing the impacts of projected future changes on groundwater resources, numerous investigations have been conducted in the different locations (Aslam et al., 2018; Luoma, 2016; Pandey et al., 2019; Sener and Davraz, 2013). Aslam et al. (2018) has integrated the groundwater venerability with respect to the change of the climatic variability, climate change, and anthropogenic activities. The analysis was based on the analytical and reviews of the past literature by assuming the different GW venerable indicators and the impact is assessed by the individual or the combination of the indicator with changing the climatic variability. Key indicators were selected based on the previous literature like change in groundwater recharge, sea-level rise, change in rainfall, population growth, change in slope, change in transmissivity, aquifer media, soil media, impact of vadose zone, etc. the hierarchy and the weightage of the indicator are assigned by using the Modified-DRASTIC-AHP (Sener and Davraz, 2013) based on the experience and the export evaluation. In the conclusion of the study, the authors indicated that the climate change parameters were variable with the downscaling techniques and taken scenarios. The climatic variability creates

a negative impact on the key indicator with respect to groundwater vulnerability and the choice of the indicator is the key parameter for the evaluation. Climatic variability influencing parameters like urbanization, population increase, and the LULC change-related indicators and its composite impact has a significant role in the future groundwater change. The groundwater environment is overstressed due to the current ineffective management of the water resources (Foster and Macdonald, 2014). So, for effective groundwater management with acceptable limits, economic and social benefit can be achieved through past and present experience of the modular, performance of the groundwater system., and behavior of the users in that response (Cao et al., 2005).

LULC changes have adverse sway to the hydrological cycle through vegetation cover change, change in the runoff, groundwater recharge, and evapotranspiration (Bhaskar and Welty, 2015). Zipper et al. (2017) stated that surface hydrological changes and land-use change have been propagated the impact in groundwater flow and its surrounding ecosystem. The analysis is focused on the urbanization impact on groundwater recharge and its impacts on the crop yield with replenishing the water depth in the crop root zone. Three models are coupled for the analysis with the corresponding task and called MODFLOW-AgroIBIS (MAGI); a) AgroIBIS model (model based on the dynamic growth of vegetation in natural and managed ecosystems) (Kucharik, 2003), b) HYDRUS-1D (One-dimensional saturated flow model for heat and water transport) (Simunek et al., 2005), and c) MODFLOW-2005 (three-dimensional groundwater flow model) (Harbaugh, 2005). The outputs of the two scenarios (urbanization rate is less than 50% and greater than 50%) have been analyzed in three hydrological parameters (vertical water balance, water table depth, and agro-ecosystem yield) base and the individual and combined effects have been drawn. In the upland, the initial water table is already below from the surface and the water flow dynamics tend to flow in the lower land by the elevation difference. Similarly, groundwater flow in the midland is same and the magnitude is slow compared to the upland. But in low land has a tendency to accumulate the water in their groundwater system. The urbanization pattern of upland, the crop yield has no significant change due to unchanged of moisture deficiency after and before simulation (already deficit in base period). In low land, due to the rise in water level, the moisture content is higher than the required and it creates the oxygen deficiency in the plant and causes the reduction of crop yield. This study clearly states that the water table depletion rate in the sloppy topographical region has a greater tendency than flat. In the unconfined aquifer, flow rate and gradient are more supportive of flow towards the low land if

urbanization is concentrated in the low land and the effects were localized. For the sustainable use of groundwater resources due to the future urbanization, population and pumping rate increase and LULC change, proper groundwater recharge estimation has been essentially required and also incorporate the future LULC change impact in the declining of the recharge area and capacity of that area (Lamichhane and Shakya, 2019a).

The fossil groundwater resource is not the active part of the hydrological cycle but its impact in the stream flow and related ecosystem may be devastating due to over-abstraction in that resource (Foster et al., 2004). For water balance in the groundwater system, abstraction is always less than the recharge in the basin but the present urbanization, LULC change, population growth, increase in the demand of food, industrial and domestic water, and the change in climatic variability abstraction rate exceed rapidly than the recharge (Basnet, 2016; Foster et al., 2004; Shrestha et al., 2020; Wada, 2016). The conceptual relationship between the climate, groundwater, and pumping is shown in Figure 2.6. Reduction in the water balance in the aquifer system due to overexploitation has forced the secondary problems to decline the water table, land subsidence (Shrestha et al., 2017b), and contaminate the groundwater environment. The groundwater simulation was conducted with the MODFLOW and solute transport solver package of MT3D for the analysis of the groundwater hydraulics, land subsidence and solute transport in southwestern Kyushu, Japan (Cao et al., 2005). The simulated result showed that the land subsidence occurs rapidly and the shrinkage in the land surface would be detected in the near future and the head difference between sea level and the groundwater table would create the possibility to inject the seawater. In the Kathmandu Valley, the depletion rate of the groundwater table mainly varying at the rate of increase in withdrawal from the sources, where recharge is not more significant due to an increase in urban density (Lamichhane and Shakya, 2019a). S. Shrestha et al. (2017b) acknowledged that the supply water demand in the KV is approximately 31% (86 MLD) and 38% (105 MLD) in dry and wet seasons respectively and the remaining deficit has been fulfilled by the extraction from groundwater. Similarly, Thapa et al. (2018) specified that the KUKL has only 19% in dry seasons and 31% in wet season capacity to provide the required demand in the service area (core city of the valley) and the deficit quantity has fulfilled through the extraction from groundwater resources by different suppliers. Shrestha (2009) has reported that the groundwater pumping rate is six times greater than the recharge capacity and it has induced decline in the water table approximately 2.5 m/year. In the present and future, the scenario is more remarkable, demand is dramatically increasing and the recharge is declining due to

LULC change. Pandey et al. (2010) also reported the decline of the water table due to the number of driving forces by 1.38 to 7.5 m from 2000 to 2008. In that period the rate of groundwater extraction is quantified by 21.56 million cubes and the recharge is 9.6 million cubes. The analysis is analytically based but better results have been obtained by the numerical simulation of groundwater flow. If such unmanaged uses of the groundwater resource, it might result depletion and degradation in quantity and quality (Collin and Melloul, 2003).

The ground and surface water resources are similar resources and it is interlinked with the hydrological and physical parameters. Integrated simulation of surface and surface modeling affords the extra parameter calibration efforts have provided for the modeler by feedback loops between the models. Some parameters like rate of evapotranspiration, surface runoff, soil-zone flow, soil moisture content, infiltration, and other basin characteristics are interlinked with both models. Therefore, surface water and groundwater are inextricably connected. One cannot be considered or evaluated without considering the other. So a couple of surfaces and sub-surface models have given better performance during calibration and simulation (Kumar, 2019; Liang et al., 2012; Rumbaugh and Rumbaugh, 2005; Shrestha et al., 2020)

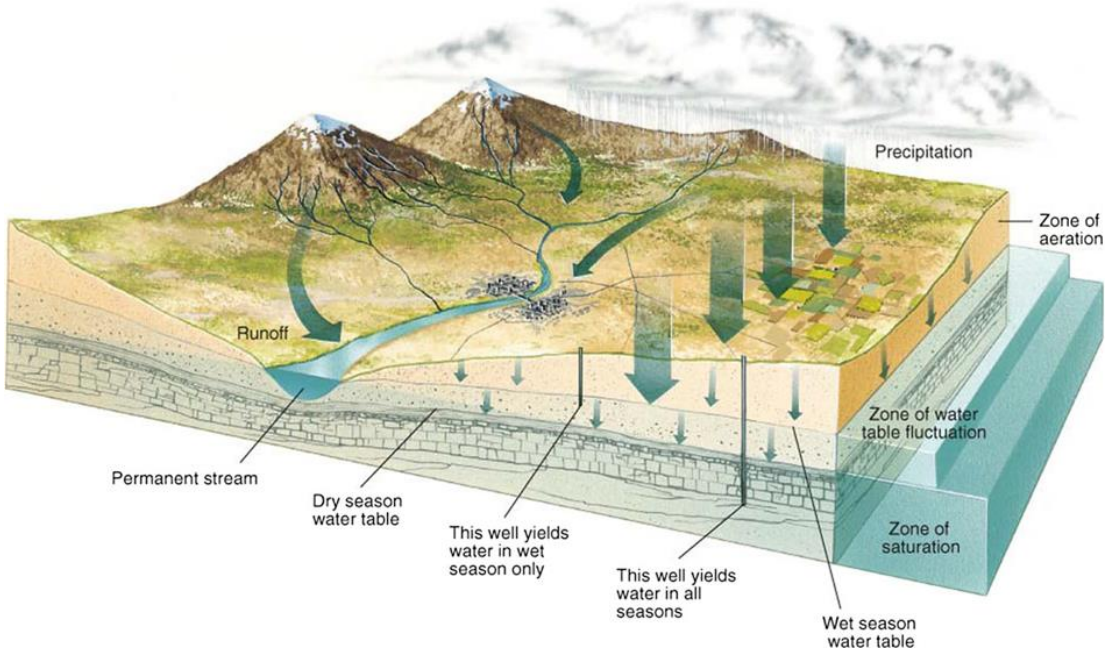

Figure 2-6 Conceptual representation of climate, groundwater, and pumping.

(Sources:- (Wada, 2016)*)*

2.8 Earlier studies in the Kathmandu Valley.

Numerous studies have been conducted in the KV with respect to the urbanization or LULC change (Lamichhane and Shakya, 2019a; Rimal et al., 2017; Thapa and Murayama, 2009), change in recharge dynamics (Dahal et al., 2019; Lamichhane and Shakya, 2019a), climate change impact in the river basin (Babel et al., 2014; Dhital et al., 2013; Mishra and Herath, 2014; Sharma and Shakya, 2006), LULC change impact in the river basin (Pokhrel, 2018), water demand and supply pattern (Gautam and Prajapati, 2014; Shrestha, 2009; Thapa et al., 2018; Udmale et al., 2016) and groundwater assessment (Adhikari, 2017; Basnet, 2016; Shrestha et al., 2020, 2017, 2016a). Some studies related to the set objectives have been described below.

Table 2-9 Selected earlier studies in the Kathmandu Valley

LULC change and urbanization				
S.N.	Methodology/approaches	Results	Gaps	Reference
1	Analysis based on three time series (1978, 1991, and 2000) land use/cover maps driven from satellite remote sensing data	From 1978 to 2000, the shrub, forest, agricultural, and built-up areas were changed by -7.38, -4.32, +8.17, and +3.54% of the total area (635 km^2) respectively. The expansion is mostly outward to the ring road area	The analysis is based on the historical information, future implication and projection of LULC is not considered	(Thapa and Murayama, 2011)

2	LULC change is analyzed based on the 1976 to 2015 LULC data. The LULC map was prepared by processing the satellite image with GIS environment. Comparative analysis was found through a conversion matrix	Urban built-up area was increased by +12.8% and reduction of the cultivated land by -6.79%, bush area by -3.4%, forest cover by -2.23%, open field by -0.16% and water body by -0.21%. The expansion of the valley is denser in the core part and scattered in the peri-urban and foothills	Field validation of the generated map and restricted zone is not considered for the analysis	(Rimal et al., 2017)
3	Analysis was based on the four decadal (1989, 1999, 2009, and 2016) land sat images of the core valley over an area of 422.84 km^2. A supervised classification technique in GIS tool was adopted for the classification of five LULC categories (built-up, forest, agriculture, bush, and river)	The urban extension in the core valley area was more haphazard compared to the peri-urban areas. Urban expansion in the valley was found to be 20.96% of total area, and fertile agricultural land was diminished by 25.24%. Urbanization can be observed in all the areas, particularly denser within the major road corridors.	Core urban area or similar to the groundwater basin or plan land is only considered for the analysis. Whole Bagmati watershed is not considered, most of the forest land in the valley is excluded.	(Ishtiaque et al., 2017)

4	Different driving forces (bio-physical, socio-economic, neighborhood properties, and transportation accessibility) were considered the projection of the future LULC change. Three projection scenarios (spontaneous, environment-protecting, and resource-saving) were taken for the growth projection upto 2050.	All the scenario analysis and growth rate projection showed that the conversion of non-built-up (agriculture and barren) to built-up will continue in the future and the projection through the spontaneous scenarios provided the better LULC change.	Only population growth is considered with the physical facilities but the actual demand and the other restricted condition is not mention.	(Thapa and Murayama, 2012)
5	LULC change projection based on population, migration, political, and socio-economic drivers from 2016 to 2032 by using the cellular-automation Markov model	The barren and agricultural land was reducing due to expansion of built-up area in future.	The scope is only within the future projection of the KV	(Rimal et al., 2018)

6	Future expansion (upto 2030) was done with the assumption of historical (1996 to 2011) LULC change with the application of land change model (LCM) and Markov Chain principles. Surface runoff of the KV was generated by the application of CN curve method.	The future urbanization has been increased in the northern and the southern peri-urban (foothills) part of the Kathmandu. Future built-up area was increased by 12.8% of the total area during 29 years period. Due to LULC change surface runoff and groundwater recharge will be increased and decrease in the future.	The projection is based on the historical change and the basin theoretical approach is adopted for the surface runoff. The climatic and physical characteristic is not considered during analysis.	(Dahal et al., 2019)

Climate change impact assessment in Bagmati Basin				
S.N.	Methodology/approaches	Results	Gaps	Reference
1	The stream flood flow frequency was generated with the application distributed daily GCM precipitation and temperature data bias corrected using quantile mapping method	The climate change effect in the flood events (magnitude and frequency) of the return period 2 to 100 years has been increased by the 24% to 40% due to change in the climatic drivers of the catchment area upto 2100s.	Simple rainfall runoff model and the only climatic variables are adopted for flood frequency analysis. The minimum, average, daily, monthly and annual flow sequence is undefined	(Mishra and Herath, 2014)
2	Hydrological response of the river flow due to climatic change by the application of the historical flow series.	The historical hydrological response sensed that the shifting flood magnitude, frequency, and duration with respect to climate change.	Climate change effect is quantify by the past river flow data but the future projection is not considered during analysis.	(Sharma and Shakya, 2006)
3	Multi model (HBV, BTOPMC, and SWAT) approach was adapted for the finding the suitable hydrological model.	From the outputs of the various models, SWAT model gave the better performance than others.	All the analysis is focused only the performance of the model.	(Thapa et al., 2017)

4	Effect of climatic variability in the stream flow by using the hydrological model with application of GCM data and projection with emission scenario A2 and B2.	The change in stream flow was increased by 10.82% and 12.84% at the end of the century with change in the climate scenarios.	Only focused on the climate change effect and the seasonal variation in the river flow	(Babel et al., 2014)

LULC change impact assessment Kathmandu Valley				
S.N.	Methodology/approaches	Results	Gaps	Reference
1	LULC change impact in the river basin hydrology and sediment transport has been assessed through the SWAT model with the application of past LULC changed. Historical (2000 to 2010) climatic, river flow, sediment flow and LULC map is used for the simulation.	The raised in built-up area (6.46%) change the model parameters and its corresponding effect increased the surface runoff by 27% and reduce the lateral and groundwater flow contribution in the river reach by 25% and 21% respectively due to the less recharge capacity of the basin. The hydrological imbalance was clearly seen in the model outputs due to LULC change in the catchment level through the model parameters.	The analysis is only focused the LULC change and the sediment transport capacity of the river reach. Effect of LULC change in the groundwater balance is overlooked during study.	(Pokhrel, 2018)

Groundwater-related studies				
S.N.	Methodology/approaches	Results	Gaps	Reference
1	The resiliency of groundwater system in the KV due to increase in climatic variability and the pumping rate was assessed by the coupling of surface (SWAT) hydrological model and the groundwater flow (MODFLOW-2005) model. The climatic analysis is based on the three RCMs data with two RCP4.5 and RCP8.5 projection scenarios.	The resiliency maps of the KV showed that the overexploitation of the groundwater resources has declined and the problem is more critical in the near future. The core area is more sensitive than the boundary because the pumping rate is quite high and the recharge tendency is less compare the peri-urban area.	Only focused on the climate change and the pumping rate increase scenario but the effect of LULC change and recharge dynamics is not considered during the study	(Shrestha et al., 2020)
2	Hydro-geological characteristics (Transmissivity (T), hydraulic conductivity (K) and Specific coefficient (SC)) of the shallow and deep aquifer in the Kathmandu valley by using the GIS tools.	The thickness of shallow and deep aquifer varies from 0 to 85m and 25 to 285 m respectively and similarly T, K, and SC estimates with the range of 163 to 1,056 m^2/day, 0.32 to 8.8 m/day, and 0.00023 to 0.07000 respectively.	This application is very useful for the basic input information for the groundwater modeling and it just provides the basic hydrogeological characteristics of the KV	(Pandey and Kazama, 2011)

3	Delineation of potential areas for the groundwater development by using the GIS based ARC(A means groundwater Availability, R means Release potentiality and C means Cost of groundwater development) model in the KV	Quantify the volume of storage in the shallow groundwater aquifer in the KV and the potential location for the groundwater development. Model showed that the future groundwater development is more viable for northern and southern parts for the shallow aquifer and north-east and north-west parts for deep aquifer.	Analysis is based on the observed data and only focused in the potentiality of the basin.	(Pandey et al., 2013)
4	Pumping capacity through the deep aquifer with maintaining the safe allowable drawdown of the KV by using the integrated GSFLOW model. The GSFLOW simulation is achieved by first developing the Precipitation Runoff Modeling System (PRMS) and the groundwater flow model (MODFLOW)	Within the allowable safe extraction of the basin, increase in pumping rate concluded that the northern and southern parts of the basin are more stable in the future pumping rate increase context. The central core part of the valley has the less capacity to extract the groundwater.	The study are only focused on the deep aquifer system, hypothetical pumping rate and location, assuming the same recharge tendency in the urban and open area.	(Basnet, 2016)

5	Assessment of the groundwater aquifer vulnerability and the associate risk due to the pollution of the KV by using the GIS based DRASTIC model for the vulnerability and Groundwater Risk Assessment Model (GRAM) for to assess the groundwater risk.	From the analysis, it was concluded that more than half of the groundwater are susceptible to pollution. Northern groundwater district is less contaminated compare to the central and southern groundwater district. Similarly nearby 87% of the groundwater basin area is moderate risk by the pollution.	This analysis is only focused in the nitrate concentration in the groundwater and the analysis is based on the weighted overlay of the data in the GIS environment	(Shrestha et al., 2016a)
6	Identify the potential extraction of shallow groundwater in the VDC level of the KV in the climatic variability and the pumping rate change. The simulation was conducted in the groundwater model (MODFLOW-2005) and the climate change scenario RCP 8.5 was taken for the future analysis.	The potential pumping rate increase was found as 1% to 3% from the surface hydrological model with respect to change in recharge depth in shallow aquifer system. The northern and southern VDCs having large open and potential recharge area have a high potential to extraction of shallow groundwater.	The study was concentrate with the climate and shallow pumping rate change in future but the change in the recharge volume due to urbanization process is not considered.	(Adhikari, 2017)

2.8.1 Historical urbanization/LULC change

Thapa and Murayama (2011) analyzed the past intricate urban growth pattern of the KV and suggested some suggestions for reducing the impact in the urban environment. The authors incorporated three time series (1978, 1991, and 2000) land use/cover maps for analysis. Past base maps were produced from remote sensing satellite driven data and processed in GIS environment. A total area of 685 m^2 of the KV (the major part of Kathmandu, Bhaktapur, and Lalitpur district) was considered in the study. The land use maps were prepared for five land use categories (shrubs, forest, water, built-up, and agriculture). The restricted area was not considered as a separate land category; rather they were considered as their land covers. From the base map, the land use/cover transition was analyzed using a conversion matrix from 1978 to 2000. The shrub, forest, agricultural, and built-up areas were changed by -7.38, -4.32, +8.17, and +3.54% of the total area respectively as shown in Figure 2-7. Fundamentally, agricultural and shrubs land have been changed into the built-up area. During this period, the built-up area was raised to 87 km^2 from 32 km^2. After the development of the ring-road and extension of radial feeder road from the ring-road, urbanization pattern has extensively increased in the core areas and road corridors since 1980s and this trend is continuing till date.

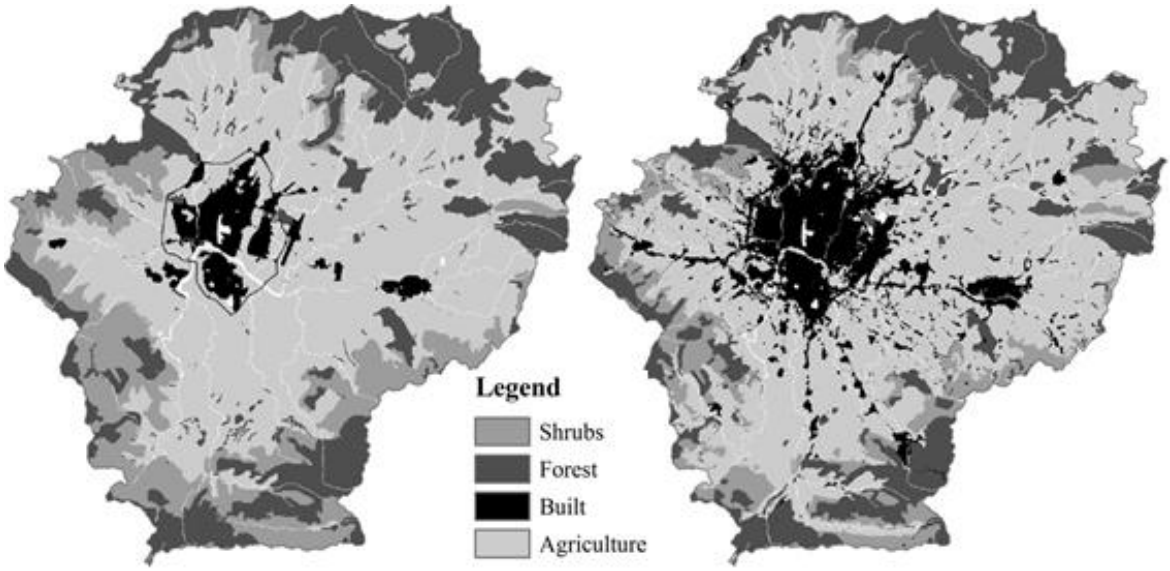

Figure 2-7 LULC map of Kathmandu Valley during 1978 and 2000

(source:- (Thapa and Murayama, 2011))

The land use change process has intensified since 1980s. The spatial distribution of urban/built-up areas has blowout outward from the core city area and laterally the major roadways. With expansion of the road network and easy access to the market, farmers

have been motivated for agricultural production, ultimately reducing the shrubs and forest land. These economic activities, business opportunities, urban facilities, and changing lifestyle, have encouraged people to move towards the urban area.

An increased rate of population migration with multi-culture, socioeconomic change, and haphazard urbanization creates an imbalance in the urban environmental health, use of natural resources, and change in land-use practices of the Kathmandu Valley. Rimal et al. (2017) presented the past historical urbanization pattern and compared the trend of the LULC change of the Kathmandu Valley (Kathmandu, Lalitpur, and Bhaktapur district) from 1976 to 2015. In this study, the land use map of the KV was generated through the land sat images with the GIS application tools. From the analysis of the CBoS (2011) data, between 1976 and 2011, the population was increased from 0.6 million to 2.5 million. The population growth and its implication in land-use change scenario from 1976 to 2015 was analyzed through a conversion matrix, which showed an increase of the urban built-up area by +12.8% and reduction of the cultivated land by -6.79%, bush area by -3.4%, forest cover by -2.23%, open field by -0.16%, and water body by -0.21% as shown in Figure 2-8. As shown in figure, as all the decreased area of the valley was open land, which creates the hydrological imbalance of the basin in terms of surface runoff and groundwater recharge. The past urban development trend of the KV indicates that open area (like agriculture, open, bush area) will be converted to built-up areas in near future. The expansion of the valley is denser in the core part and scattered in the peri-urban and foothills, which have more potential for groundwater recharge.

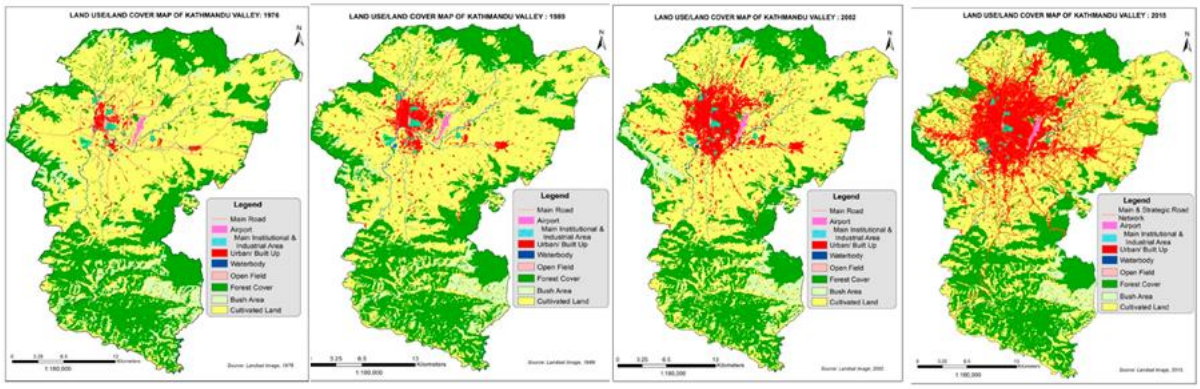

Figure 2-8 LULC map of Kathmandu Valley in 1976, 1989, 2002 and 2015

(source:- (Rimal et al., 2017)*)*

The study by Ishtiaque et al. (2017) performed for four decadal LULC change analysis of the Kathmandu Valley showed that the urban extension in the core valley area was more haphazard compared to the peri-urban areas. This analysis was based on the four decadal (1989, 1999, 2009, and 2016) land sat images of the core valley over an area of 422.84 km^2. A supervised classification technique in GIS tool was adopted for the classification of five LULC categories (built-up, forest, agriculture, bush, and river). Urban expansion in the valley was found to be 20.96% of total area, and fertile agricultural land was diminished by 25.24%. Meanwhile, there was an increase in partial forest coverage within the valley. The LULC change due to urbanization is shown in Figure 2-9. Urbanization can be observed in all the areas, particularly denser within the major road corridors.

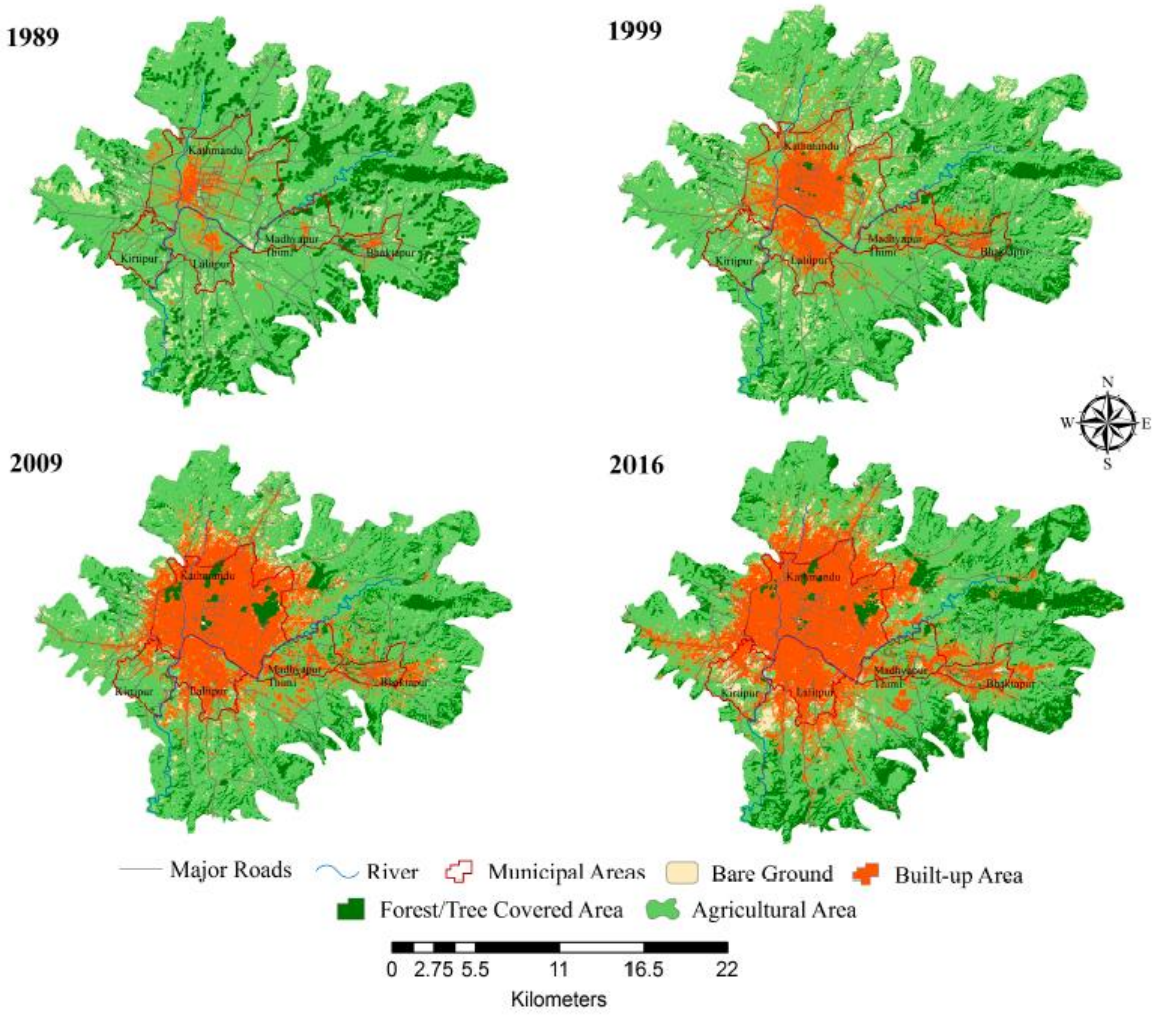

Figure 2-9 Land use/cover map of Kathmandu Valley

(source:- (Ishtiaque et al., 2017))

2.8.2 LULC projection and recharge area change

Thapa and Murayama (2012) studies concluded that up to 2050 urban and peri-urban area of the KV will have more stress to future land resources development and they deteriorate the natural river and forest ecosystem. Bio-physical, socio-economic, neighborhood properties, and transportation accessibility was used for the driving forces with the alternate three projection scenarios [spontaneous (normal growth), environment-protecting (restricted development), and resource-saving (less than normal growth)] using artificial neural network (ANN) model to assess the future growth. These entire scenarios have shown that the conversion of non-built-up to built-up will continue in the future. The spontaneous scenarios (Figure 2-10) show the realistic distribution of LULC change rather than the others.

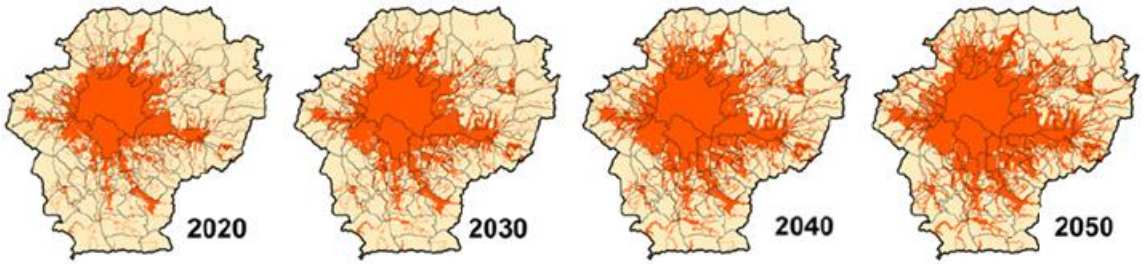

Figure 2-10 Projected land use/cover map of Kathmandu Valley

(source:- (Thapa and Murayama, 2012))

Rimal et al. (2017) also explored the continuous urbanization process in the KV highlighted that this creates the environmental disequilibrium in the all-natural resources. The LULC change study was conducted from 2016 to 2032 by using the cellular-automation Markov model with the change rate in population growth, migration, political scenarios, and socio-economic factors. The expansion of the built-up area and encroachment of the open space (barren and agricultural land) and land fragmentation due to anthropogenic activities have been dismantling the environmental equilibrium.

Dahal et al. (2019) demonstrated that the future urbanization has been increased in the northern and the southern peri-urban (foothills) part of the Kathmandu Valley and this increment mostly affect the potential recharge area of the basin. This study was conducted with the past data (over 1996 to 2011) and projected from 2011 to 2030. The future projection was done by the application of land change model (LCM) with the social-physical driving forces. The future projection has been generated with the suitability mapping of the changing area by using the Markov Chain principles and mostly the outputs have governed by the driving forces. From this analysis, it showed that the future built-up area was increased

by 12.8% of the total area and it reduced the open area of agriculture, vegetation and water body during 29 years period. The increase in the built-up area is directly coupled with the population rise, increase domestic water and food demand, the decline rate of infiltration, recharge and water table. From the map observation and theoretical runoff characteristics (CN) curve of the basin found that the LULC change increase the runoff and decrease the groundwater recharge potential. Mostly the northern and southern part of the peri urban or foot hill of the mountain are the more potential for the groundwater recharge as per other studies (JICA, 1990; K.C., 2011; Pandey and Kazama, 2011).

2.8.3 Climate change impact assessment

Mishra and Herath (2014) revealed that the climate change effect in the flood events (magnitude and frequency) of the return period 2 to 100 years has been increased by the 24% to 40% due to change in the climatic drivers of the catchment area upto 2100s. An analysis was conducted in the Bagmati River using precipitation and temperature data is downloaded from MRI-GCM. Quantile mapping technique was adopted for the biased correction and a distributed rainfall-runoff model, Afflussi-Deflussi (AFFDEF), was used for the flood analysis. The assessment of the hydrological process through the historical climate data of the KV of Bagmati basin has been assessed by the multi model (HBV, BTOPMC, and SWAT) approach (Thapa et al., 2017); from the outputs SWAT model gave the better performance than others. The historical hydrological response of the Bagmati basin has been sensed through the shifting flood magnitude, frequency, and duration with respect to climate change (Sharma and Shakya, 2006). The change in water availability of the Bagmati river is augmented by 10.82% and 12.84% by the end of the century with change in the climate scenarios under the A2 and B2 projection scenarios (Babel et al., 2014).

2.8.4 LULC change impact assessment

Pokhrel (2018) suggested that the continuous land-use change cause serious hydrological effect which may be causing a rise in the Bagmati River. The output was simulated by using LULC change (2000 to 2010) in the Kathmandu Valley with coupling the SWAT model. The accumulation of sediment in the river reach induced the numerous problems in river reach and flood plain. The increased built-up area (6.46%) was estimated by the processed land-sat images and LULC changed were coupled with the hydrological SWAT model. From the simulation, such hydrological parameters were more sensitive to the changing context; EPCO, ESCO, SOL_AWC, SURLAG, GW_REVAP, REVAPMN, ALPHA_BF,

GW_DELAY, RCHRG_DP, CN2 and CANMX. Reducing the greenery area, EPCO (means the water up-taking factor for the transpiration plant) and ESCO (soil evaporation compensation factor) was reduced and the effect was seen in the ET. GW_REVAP (water move from shallow aquifer to unsaturated overlying soil layer factor), REVAPMN (threshold water in the aquifer or release to deep aquifer), and SOL_AWC (soil parameter or allowable water content of the soil) were decreased by decreasing the recharge capacity of the basin (Burba and Verma, 2005). ALPHA_BF (base flow recession factor) was contributing the water for the base flow during lean season and reduced by reducing the recharge capacity of the ground. Also, it affects the lag time from surface to shallow aquifer GW_DELAY. CANMX means maximum canopy storage of moisture that influences the recharge and infiltration from the surface. The corresponding effect from that parameter was increased the surface runoff by 27% and reduce the lateral and groundwater flow contribution in the river reach by 25% and 21% respectively due to the less recharge capacity of the basin. The hydrological imbalance was clearly seen in the model outputs due to LULC change in the catchment level through the model parameters

2.8.5 Groundwater-related studies

a) Groundwater resiliency analysis

Shrestha et al. (2020) revealed that the overexploitation of the groundwater resources has declined and the problem is more critical in the near future. So the effective management is required for the groundwater resiliency of the Kathmandu Valley. In the study resiliency maps of the Kathmandu Valley were generated in the context of future climate change in the three RCMs data with two RCP4.5 and RCP8.5 projection scenarios. The future recharge rate of the basin was projected by the SWAT rainfall-runoff hydrological model outputs. The water balance in the basin generates monthly and annual recharge rates of each basin and used as input parameters of the groundwater model. Groundwater flow simulation in the basin was accomplished by the MODFLOW-2005 engine. GMS-MODFLOW (couple model of surface and groundwater flow simulation) was used for the estimate of the future groundwater change in the change context in climate and the pumping rate as per the population increase rate. The population growth in the Kathmandu Valley is projected (Shrestha et al., 2017) by the logistic curve method with the three projection scenarios (20%, 35%, 50% of demand must be fulfilled by the groundwater pumping and the per-capita demand is 270 lpcd). The steady-state groundwater flow simulation was conducted by assuming that the water basin is only the core flat Kathmandu Valley Area (327 km^2) and

outside the boundary, it is conducting as inactive cells. The sensitivity parameters were obtained by the calibration and validation of the model with the 258 and 18 numbers of pumping and observation well were used. In the climate projection scenarios, temperature and precipitation has an increasing trend. From the simulation result, the water level declination within the basin is unequal; the central core area has a more declination compared to the northern and southern part of the valley in all pumping scenarios. The northern and southern part of the valley is more resilient compared to the other part especially the central core area of the valley is more critical than others. In this study, the core area is more sensitive than the boundary because the pumping rate is quite high compared to the peri-urban area of the valley. Similarly, the recharge capacity in that area may be low due to the compact settlement and less recharge area. The dynamics of the groundwater flow is passing through the higher elevation (the boundary of the basin) to the lower elevation (core valley). Similarly, future LULC change projection in the Kathmandu Valley has been also changed.

The changing built-up area pattern is denser in the peri-urban than the core city area. Similarly, the growth of the urban area is more rapid in the peri-urban area of the valley (Lamichhane and Shakya, 2019a). In every decade the 6% of open land is converted into the impervious surface. In the future, the LULC change scenario is more sensitive to the groundwater environment. This model assumed 327 km^2 groundwater basin area and the boundary effects are null. But the shape of the Kathmandu Valley is in the bowel (Thapa et al., 2016) and the initial head of the basin is given by the corresponding ground surface elevation. The model iterates with this initial head boundary condition value and horizontal water flow in the subsurface from top elevation to the bottom. From the Kathmandu Valley geological map, northern and eastern part soil is more fragile and has high hydraulic conductivity. The recharge capacity of that area is high and recharged water flows towards the core basin area due to elevation difference. But the model assumed that the outer part of the basin (the most mountainous area is the rock outcrops and the recharge is negligible) having the less contribution and assumed that the outer cell is an inactive cell. In reality, those areas are open and moderate recharge capacity and it cannot be assumed the inactive in the model or avoid.

b) Allowable drawdown study

Basnet (2016) quantified the deep aquifer level drawdown for the safe withdrawal quantity and location in the Kathmandu Valley with the integrated GSFLOW model and the projected pumping scenario. The GSFLOW simulation is achieved by first developing the Precipitation

Runoff Modeling System (PRMS) and the groundwater flow model (MODFLOW). The both models are calibrated with the data of KV river basin. The model provides a better understanding of surface and groundwater interaction through the change in surface water scenario and its corresponding impact in groundwater variability, especially in the deep aquifer. The surface and the groundwater model parameters are calibrated and validated after simulation. The principle of simulation is that the allowable hydraulic drawn in the deep aquifer system should not be greater than 1m/year (Shrestha et al., 2017) and the pumping well is set in the grid pattern in the groundwater hydrological boundary. Altogether of 35 nos. pumping well is set up with a spacing of 3 km and it is assumed that pumping from one of these wells will not affect the others as per Figure 2-11 (a).

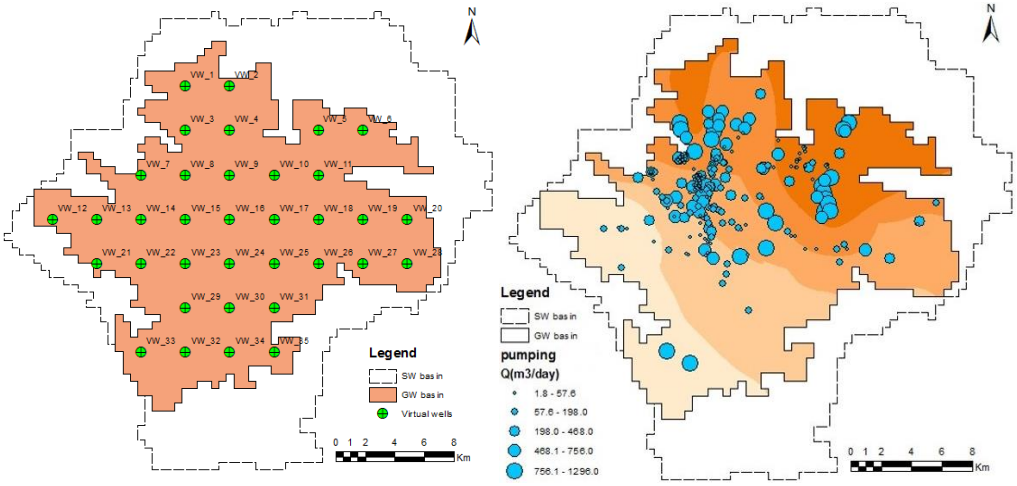

Figure 2-11 Virtual well setup for sensitivity analysis b) Pumping (1999) comparison with proposed extraction zone

(Sources:- (Basnet, 2016)*)*

The surface water balance data were generated from the calibrated PRMS model output and the precipitation factor in each grid cell assumed as a recharge in the cell. The average recharge was taken as 51% of the precipitation throughout the year. The year of 1999 pumping volume was assumed as a base pumping and the pumping rate of each virtual well is assigned by equally. 10% of the pumping rate was increased when allowable safe drawn was achieved during the simulation. The sensitivity was estimated by the change in the head with respect to the unit rise in pumping rate (m^3/s) and the analysis showed that the northern groundwater aquifer was more robust than the southern, central part shows the intermediate impact through it. The hypothetical extraction rate with respect to allowable safe drawdown output maps indicated that the extraction rate was decreased as we moved from the northern part of the groundwater basin to the southern part. Dharmasthali, Budhanilkantha, Nayapati,

and Mulpani side areas have high extraction rates and those areas had high potential to recharge and storage capacity. Geologically those areas covers Tokha, and Gokarna formation having the poorly graded gravel, sand, and silt layer with partial interaction with a clay layer. The layers have high storage and transmissivity capacity compare to the other. This study only pertain the vulnerability of the deep aquifer groundwater system but in the present context major extraction in the valley is from the shallow aquifers. Thus, it would not be justifiable to depict any approach or scenario for the sustainable development/management of the groundwater system with the present demand-supply gap and the change present recharge tendency due to LULC change for shallow aquifers.

c) Shallow aquifer analysis through pumping rate scenario

The abstraction of shallow aquifer groundwater at the household level is continuously used and it is increasing rapidly in day by day. There are no records of such abstraction and not much is known about its future due to the lack and difficulties of studies. In the context, Adhikari (2017) gave some picture of the shallow groundwater scenario with the change of climatic variability. In the study, Model-Muse graphical interface was used to create and run MODFLOW input files with Newton Solver (NWT) package to solve MODFLOW equations. For the input of the surface hydrological characteristics, the PRMS model is used to generate the shallow aquifer properties for the seasonal (wet and dry seasons) analysis. RCP8.5 scenario has been taken for the finding the climatic variability effects in the shallow aquifer due to a change in precipitation and pumping rate. The recharge pattern assumed that 43.18% of the precipitation in the wet seasons and 87.38% in the dry seasons as per the output of the PRMS model. The future pumping rate of each Village Development Committees (VDCs) was generated from the MODFLOW model with respect to climate change variability, the future population, and demand scenarios. Shallow water pumping rate was analyzed by the water balance in the surface hydrology of each grid cell from PRMS model outputs as per Equations 2.45, 2.46, and 2.47 and Figure 2-12.

$$\Delta H_w = H_{in} - H_{sink} - H_{lat\ flow} - H_{pump} \quad (2.45)$$

$$\Delta H_w = \Delta H \times Saturation\ index \times effective\ porosity \quad (2.46)$$

$$Pumping\ rate = \frac{H_{pump} \times cell\ area}{time\ interval} \quad (2.47)$$

Where, ΔH_w, H_{in}, H_{sink}, $H_{lat\ flow}$, and ΔH is the change in depth (L), total infiltration depth (L), depth of water for deep aquifer recharge (L), depth of water for lateral flow (L), shallow

water pumping depth (L), and change in groundwater table depth (L) in each cell respectively.

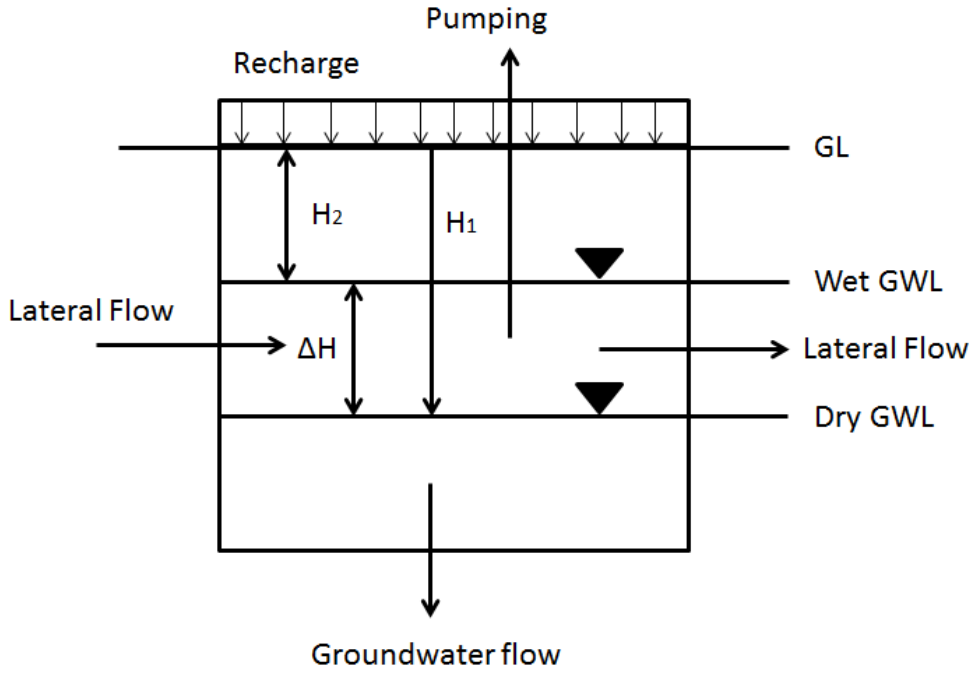

Figure 2-12 Graphical representation of pumping rate calculation principle

Similarly the rate of change of water demand was calculated by the product of the per capita demand and linear population growth rate with the base pumping. For future pumping scenario was taken by using different growth rates; 1.0% for already greater pumping rate (greater than 100 m^3/day) and those are already developed area, 1.5 % for newly developing areas (pumping rate is 50 to 100 m^3/day) and 3.0% (pumping rate less than the 50 m^3/day) for the areas in the outer peripheral part of the valley. From the results of the projected population and climate change, maximum extraction by pumping was estimated sustainably in each VDCs level to limit the drawdown on average to 2.40 meters as per Figure 2-13(a).

d) Artificial recharge techniques

The future pumping rate and the climate change effect are incorporate during pre and post-processing of the MODFLOW model but the enlargement of the built-up area due to population growth would not be considered. For the sustainability of the groundwater system and to predict future problems, a better understanding of its dynamics is required with the corresponding problem. Groundwater reservoirs are effective alternatives for the storing surplus monsoon runoff for dry periods and the capacity of storage mainly depends on the hydrogeological characteristics, climatic conditions, and LULC. In the present GW condition, enhance the magnitude of recharge dynamics and reduce the water scarcity in the basin,

artificial recharge techniques are the more convenient way forward (Thapa et al., 2018). Regmi (2017) suggested that artificial recharge techniques may reduce the water level depletion in the basin where overexploitation is happening. The same principle, limitation, and models are used as per Adhikari (2017) and the developed model has been employed to study the effects of artificial recharge on the restoration of the groundwater levels on the regional scale. For finding the viability of artificial recharge, a number of artificial recharge shaft virtually installed individually and combined form in five directions (north, south, east, west and central) in the model. Due to artificial recharge, the groundwater table was increased from 191 mm (minimum) up to 3687 mm (maximum). High increased in groundwater table was seen in North sector (Dhapasi, Tokha Swarswati, Tokha chandeshowri, Chunkhel, Bhudhanilkhantha, Mahankal, VDCs) and then East sector (Duwakot, Thaukhel, Chhalng VDCs) followed by North-East (Kapan, Jorpati, Mulpani, Gothatar, Gokenshwor VDCs) and then south part of Lalitpur as given Figure 2-13(b). These studies had clearly given that the location of potential storage capacity, recharge tendency and fluctuation of the groundwater table due to urbanization or increase of pumping rate in the Kathmandu Valley.

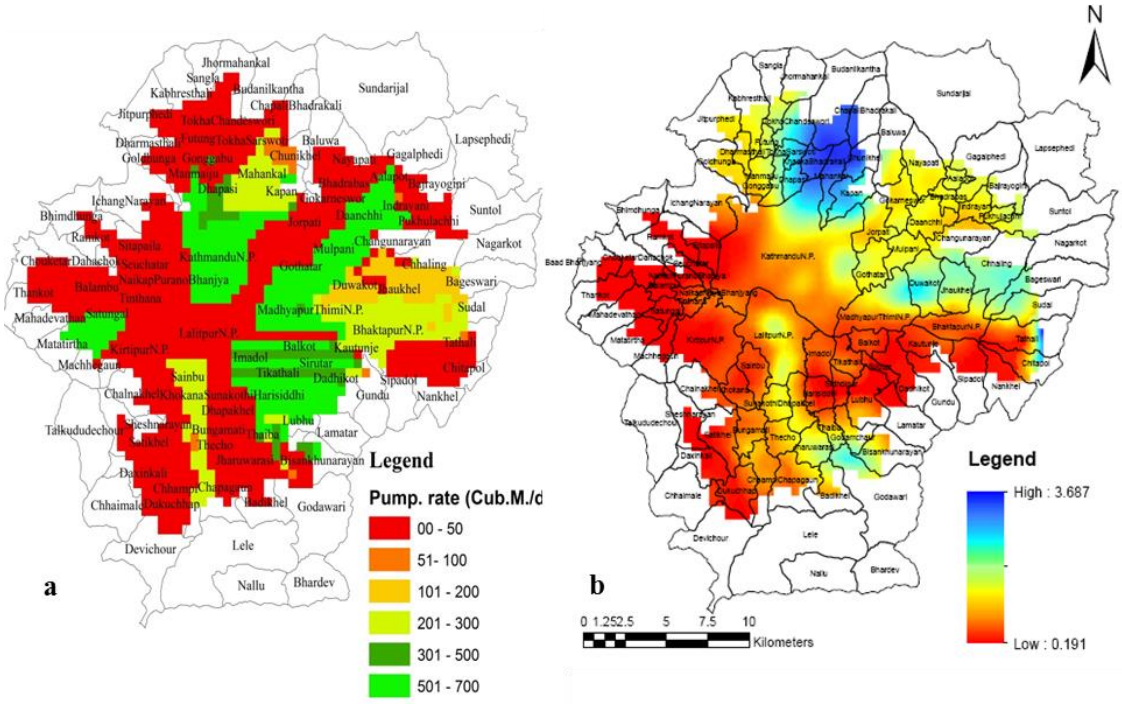

Figure 2-13 a) VDCs wise probable maximum pumping rate from Shallow aquiferb) Increase in the head due to recharge shafts within groundwater basin

(Source:- a) (Adhikari, 2017) b) (Regmi, 2017))

2.9 Summary of study in KV

In the present global or regional level, water security is major challenges due to the increase in population density as well as the urbanization of the area (Thapa et al., 2018). Declining the water availability in the surface as well as groundwater sources were created by the change of climatic variability and LULC (Aryal et al., 2017; Lamichhane and Shakya, 2019b).

Global as well as Kathmandu Valley urbanization pattern and LULC change increased the urban area that creates the LULC change more towards the impervious surface. Urbanization is not only a single factor for developing the hydrological imbalance in the river basin but it also plays the role of catalyst for climate change as well. Numerous studies have been conducted in the KV with respect to the urbanization or LULC change (Lamichhane and Shakya, 2019a; Rimal et al., 2017; Thapa and Murayama, 2009) and change in recharge dynamics (Dahal et al., 2019; Lamichhane and Shakya, 2019a). The above studies prevailed that the past and future urbanization more crucial for the river peak and base-flow, groundwater recharge dynamics, and urban land management. Overexploitation of the groundwater resources declines the water table and base flow of the river reach due to the increase in the population growth rate and encroachment of potential recharge areas (Dahal et al., 2019; Lamichhane and Shakya, 2019a). Similarly, Climate change effect hydrological cycles (temperature, precipitation, runoff, evapotranspiration, and other), and the LULC change plays a role of exciter in the hydrological change (Shrestha et al., 2018). Some studies in climate change and its implication in the river runoff has been conducted in the Bagmati Basin (Kathmandu Valley) (Babel et al., 2014; Dhital et al., 2013; Mishra and Herath, 2014; Sharma and Shakya, 2006), future change in the hydrological water balance has been seen through it. Historical LULC change pattern in the valley induced the river runoff, and sediment flow sequence has been detected by the Pokhrel (2018). Both climate and LULC change are major elements for changing the hydrological parameter on the regional and global scale, so its combined effect should not be overlooked in the future (Lamichhane and Shakya, 2019b). Therefore, there is still a gap in the variation of surface runoff or basin water balance due to future climate and LULC change. Change in climatic characteristics, LULC behavior, recharge dynamics, overexploitation of the groundwater resources also induced the declination of groundwater table and groundwater contribution to the river reach (Gautam and Prajapati, 2014; Shrestha, 2009; Thapa et al., 2018; Udmale et al., 2016). The study of

the groundwater basin in the valley indicated that the shallow and deep aquifer is not uniform in the geological formation, depth of aquifer, and other hydrogeological characteristics (Dongol, 1985; Gurung et al., 2007; JICA, 1990). Some studies have also conducted in the basin for the analysis of groundwater depletion rate, groundwater contribution, venerability in terms of the pollution in shallow and deep aquifer assessment (Adhikari, 2017; Basnet, 2016; Shrestha et al., 2020, 2017, 2016a).

The aforementioned studies basically focus on the individual impact in the surface and subsurface of the river basin as well as groundwater system but the integration of the all approach is still lagging in the case of KV. The summary of those literatures is described in Table 2-9. The haphazard urbanization pattern of the urban area creates a multi-scale change in the hydrological environment. Increase in the impermeable surface, encroach the recharge area, reduce the infiltration capacity, increase the runoff characteristics are the major effecting sector in the hydrological regime. Numerous studies have been conducted in the climate change impact on surface and subsurface hydrological water balance, only few studies are conducted on the LULC change impact in the river basin surface runoff and they avoid or overlook the impact of LULC change in the surface and sub-surface basin. The LULC change in the future, its consequence in the river runoff through surface and sub-surface environment is considered in this research. Encroachment of the potential recharge area and implication in the recharge dynamics is also considered through the groundwater simulation. Ultimately, the integrated impact through various scenarios is quantified in the basin surface hydrology and groundwater dynamics.

Chapter 3. Study Area

Kathmandu Valley (KV) is located at the headwater of the Bagmati river basin (Figure 3-1). The KV covers the Kathmandu, Lalitpur and Bhaktapur districts, which are urbanized highly in haphazard way. Urbanization, population growth, and subsequent increase in built-up areas are affecting river runoff, groundwater recharge, and water demand in the area.

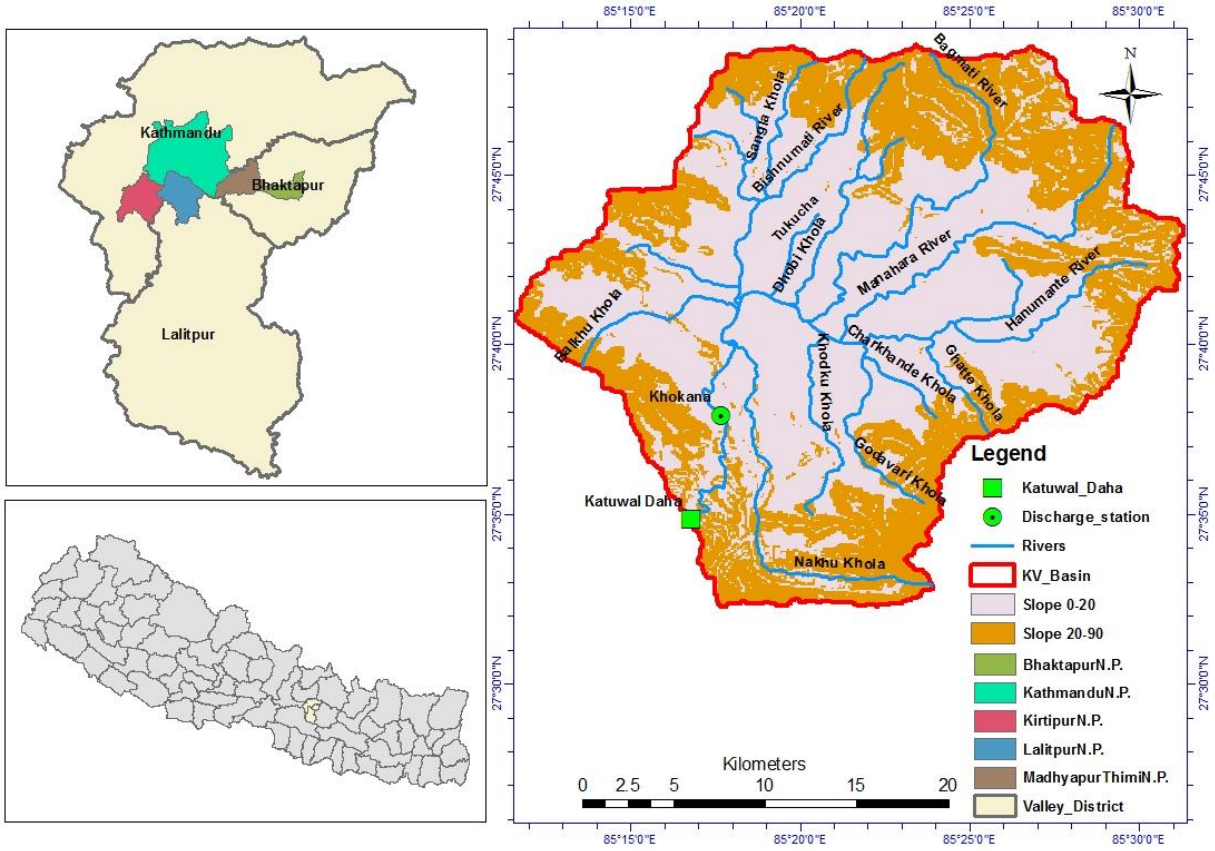

Figure 3-1 Location of the study area along with relevant details

3.1 Geography, topography, and drainage system

The KV watershed is located between $27^0$32'13" and $27^0$49'10"N latitudes and $85^0$11'31" and $85^0$31'38"E longitudes shown in Figure 3-1. It has watershed area of 613 km^2 delineated nearby (partially upstream) Katuwal Daha (85^0 16' 41.96" East and 27^0 34' 54.6" North). Kathmandu is the capital city and situated in the central part of the country Nepal, which is. The bowel shaped valley covers most urbanization parts of Kathmandu, Lalitpur and Bhaktapur districts. The elevation ranges from 1,212 to 2,722 m above the mean sea level (masl) according to the 30 m ASTER Global Digital Elevation Map (GDEM). Almost the terrain of the basin is mountainous having the average slope of 5 degree and the maximum is

nearby 60 degree. The outer periphery of the basin is mountainous and the central part is mostly plain area. The LULC is categorized in to the major five components; agriculture, forest, built-up, water body, and restricted area as per Figure 3-2(a).

Bagamati is the major river in the KV that originated from northern Shivapuri hill, flows towards the south, and drains out the KV. Bisnumati, Balkhu, Dhobi Khola, Manohara, Hanumante, and Nakhhu are the tributaries of the Bagmati River. The KV is enclosed by the Mahabharat mountain range associated with four hills namely Phulchowki (2762 m) in the southeast, Shivapuri (2762 m) in the northwest, Chandragiri/Champadevi in the southwest, and Nagarkot in the northeast, formerly known as the forts of the valley (Rimal et al., 2017). The drainage network of the KV and its geological formation is shown in Figure 3-2.

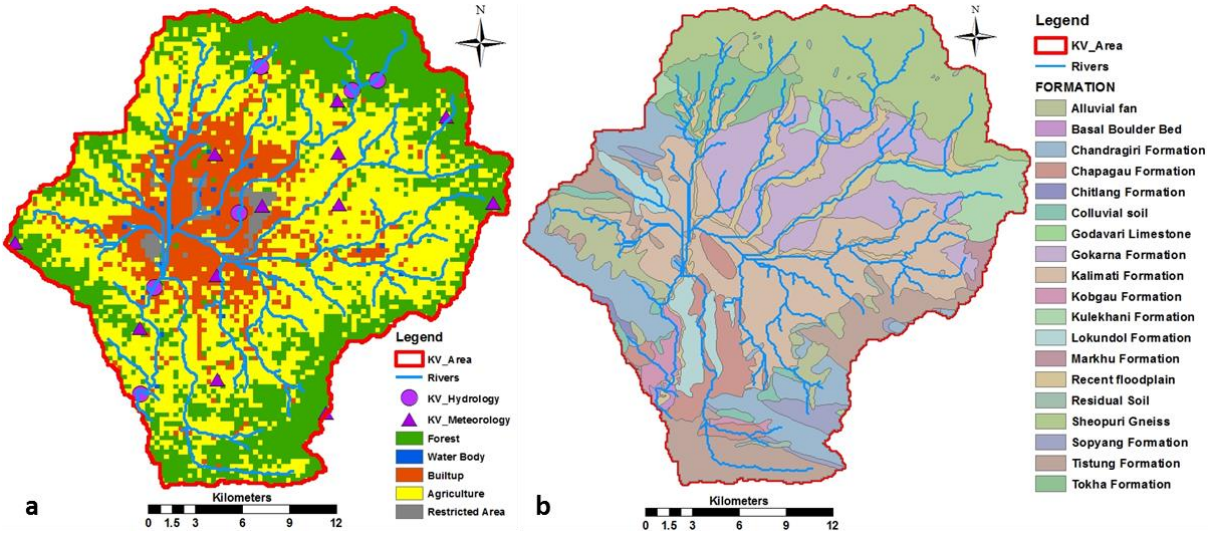

Figure 3-2 a) River, LULC and Hydro-meteorological station map b) Geological formation map of the study area

3.2 Climate

The Bagmati river basin's climate is mostly sub-tropical. Small variation of the horizontal varies the high elevation in the north to south in the KV, so it has diversified in topography, climatic character, and surface runoff pattern within the basin. The monthly average maximum and minimum temperatures vary from 29.8^{0}C to 3.4^{0}C and the average humidity of the basin is 75% (DHM, 2015). Weather of the KV is mainly considered into three stages 1) pre-monsoon (Mar-May), 2) monsoon (Jun-Sep), and 3) post-monsoon (Oct-Feb). Average mean monthly precipitation ranges from 4.2 mm in December to 402.1 mm in July and average annual rainfall is 1,533 mm/yr. There is strong seasonality in the rainfall, with more than 80% of the annual rainfall of the basin is received during the monsoon period (June -

September). The historical observed minimum and maximum temperature data at the Khumaltar station (St.No. 1029) showed that minimum temperature of the all seasons are in increasing trend, thus, indicating prospects for the warmer future and subsequent increase in evaporation from the basin. Similarly, the maximum temperature has rising trend in the monsoon season but decreasing in the pre-monsoon and post-monsoon seasons (Figure 3-3). The rising trend in the mean temperature indicates prospects for increasing water scarcity with in the basin.

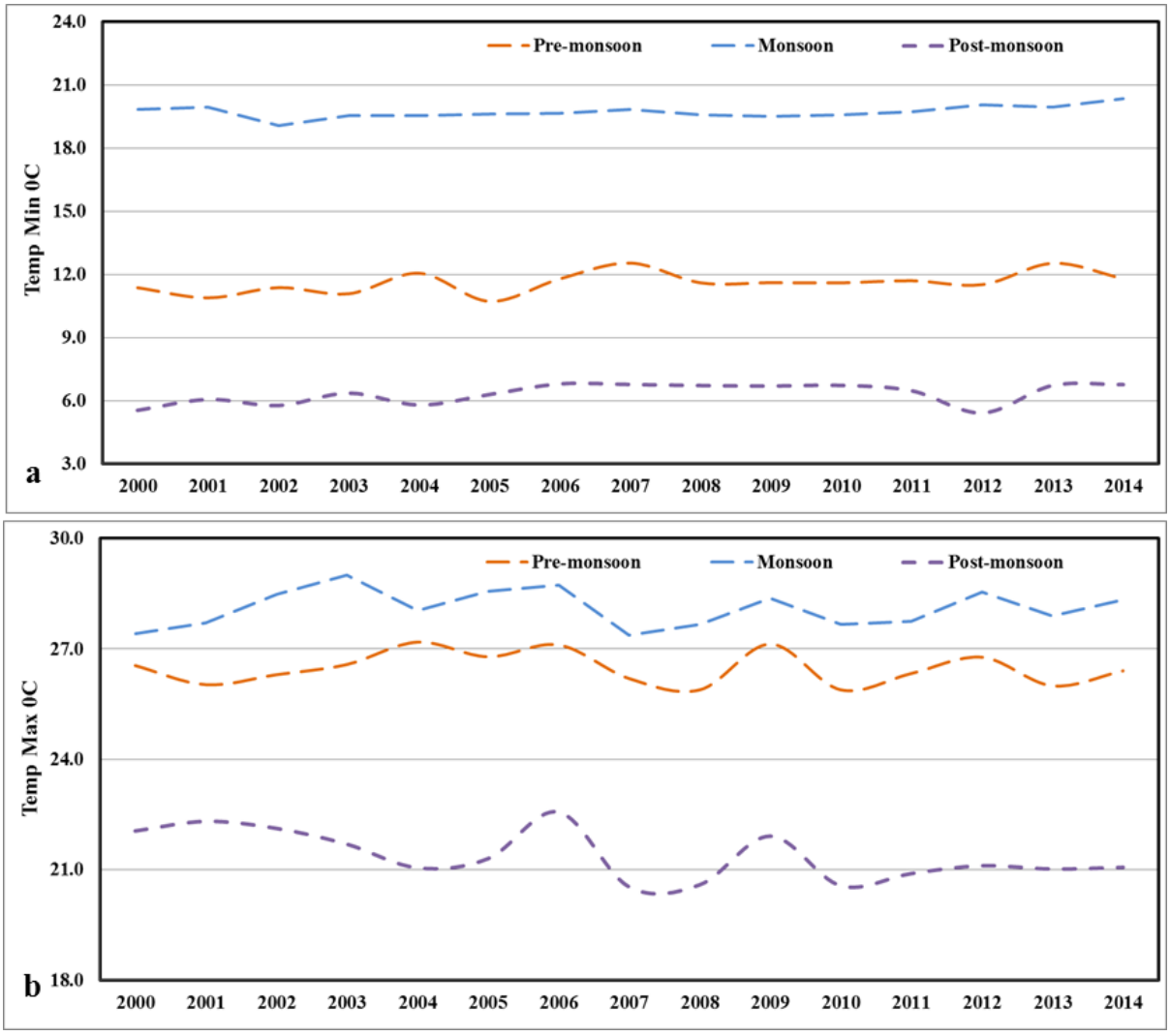

Figure 3-3 Average annual observed seasonal temperature a) Minimum temperature b) Maximum temperature.

3.3 Water resources

Both surface and groundwater resources are available in the KV watershed. Groundwater is available in unconfined and confined aquifers as well as springs in the foothills, and surface water is available through Bagmati River and its tributaries. Bagmati River is the spring-fed

runoff river and it shows the greater variation of the flow. Rivers discharge in the KV has a power relationship to rainfall. In the dry season due to minimum precipitation, there is minimum flow and high flow during monsoon by the excess of precipitation. The average annual river flow at Khokana station is 14.19 m^3/s (or 456.01 Million Cubic Meters (MCM) a year) (2000 to 2014 DHM data), which varies minimum to maximum flow from 8.48 m^3/s to 23.64 m^3/s.

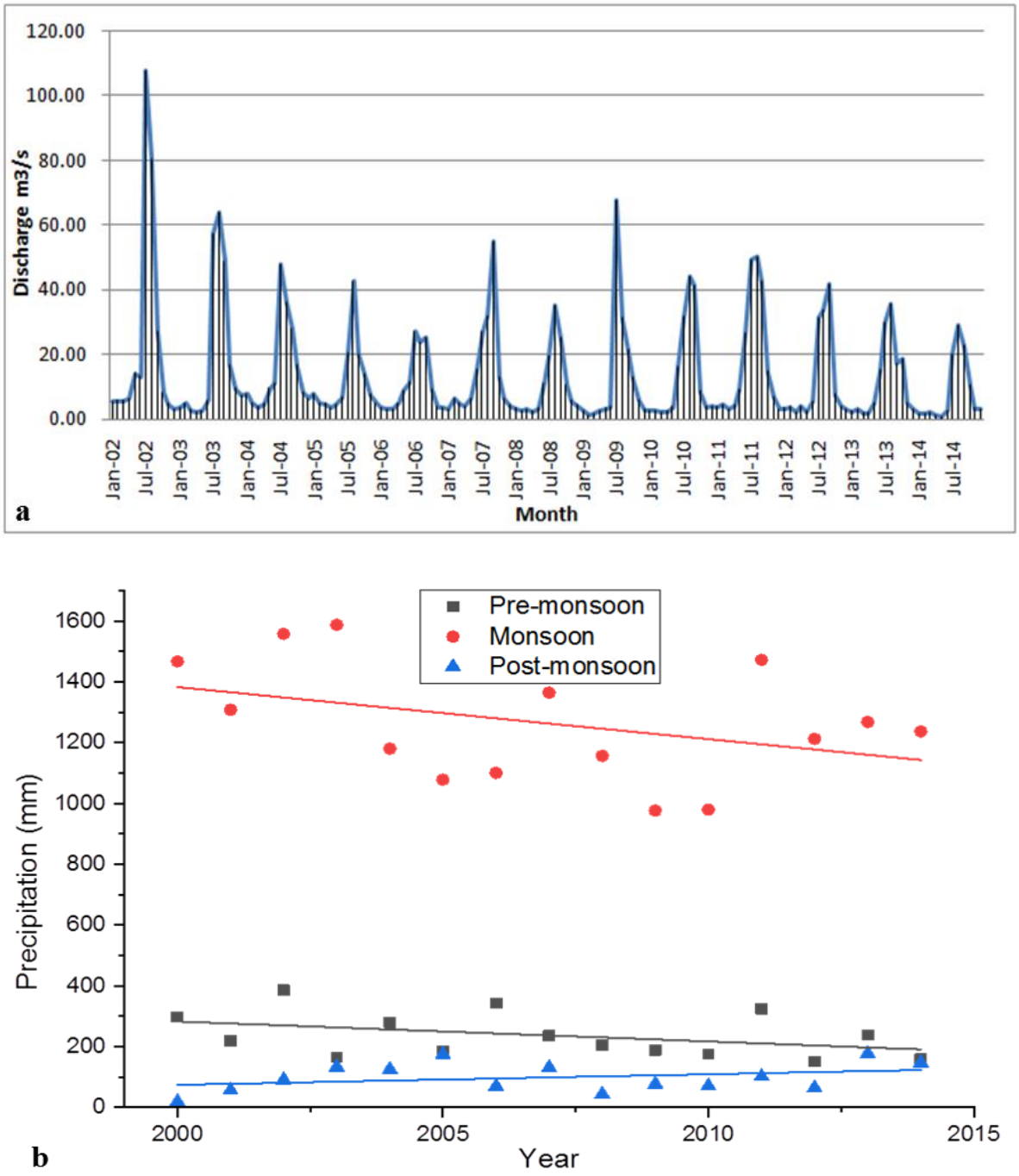

Figure 3-4 a) Observed monthly river flow at Khokana station b) Seasonal precipitation

The extreme minimum and maximum flows record during this period is 1.07 to 107.76 m^3/s in monthly and 0.03 to 814 m^3/s in daily flow, respectively. Monthly flow series of the river basin shown in Figure 3-4 (a) clearly indicate decreasing trend in the river flow. The seasonal (Pre-monsoon, Monsoon, and Post-monsoon) average rate of precipitation in the KV watershed is declining and it reduces the river runoff and groundwater recharge is shown in Figure 3.4(b).

3.4 Demography

As per the earlier administrative structure (CBS, 2012), KV represents the three districts Kathmandu (two Municipalities and 57 Village Development Committees (VDCs) now Rural Municipality), Lalitpur (one Municipality and 41 VDCs), and Bhaktapur (two Municipalities and 16 VDCs), and the details are given in Tables 3-1 and 3-2. Five major cities (Kathmandu, Lalitpur, Bhaktapur, Kritipur, and Madhayapur- Thimi) in the KV are mostly dense. Rather than this, other numerous developing markets are going to denser. The outer periphery (hilly area) of the Kathmandu valley is enclosed by mixed forest, peri-urban areas are open land of agricultural and built-up land, and the core central area of the valley is mostly covered by built-up area (Thapa et al., 2017).

Table 3-1 Population and associated details of the district in the KV

S.N	District	Area (km^2)	HH 2001	HH 2011	Population 2001 (nos)	Population 2011 (nos)
1	Kathmandu	395	235387	436344	1081845	1744240
2	Lalitpur	385	68922	109797	337785	468132
3	Bhaktapur	119	41253	68636	225461	304651

Table 3-2 Population and associated details of the Municipality in the KV

S.N	Municipality	Area (km^2)	HH 2001	HH 2011	Population 2001 (nos)	Population 2011 (nos)
1	Kathmandu Metropolitan City	49.49	152155	254292	671846	975453

2	Lalitpur Sub-Metropolitan City	15.15	34996	54581	162991	220802
3	Bhaktapur Municipality	6.56	12133	17639	72542	81748
4	Kritipur Municipality	14.76	9487	19441	40835	65602
5	Madhayapur Municipality	11.11	9551	20302	47751	83036

Source:- (CBS, 2011)

Increase in population of the KV will trigger the demand of the water resources. In near future, authorized agency KUKL will face more challenges to balance the demand and supply. The Government of Nepal aims to deliver 135 lpcd water to the residents of Kathmandu Valley by 2025 after the completion of Melamchi Water Supply Project. The projection for 2021 showed that 540 MLD water will be required to fulfill the demand (KUKL, 2015). On the other hand, the current supply is 69 MLD in dry season and 115 MLD in the wet season, meanwhile, the demand is 370 MLD (Udmale et al., 2016). The deficit as well as supply is being fulfilled by the extraction of groundwater through waterspouts, KUKL pumping stations (nearby 50% in wet and 60-70% in dry season), private pumping, private water tankers etc. This gap of supply and demand will create over stress into the shallow aquifer and its environment.

3.5 Kathmandu valley groundwater setting

In Kathmandu Valley, the basin is filled with the Quaternary fluvial-lacustrine sediments having the depth more than 600 m. The central part of the basin is with the lower Pleistocene lacustrine clays and gravels sediments called by the Lukundol Formation (Yoshida and Igarashi, 1984). The Lukundol formation is overlaid by a lignite member (Dongol, 1985), which is in turn succeeded by thick black lacustrine clay unit locally known as the Kalimati Clay (Sakai, 2001). The topmost layer of the groundwater basin is filled by the fluvial-lacustrine terraces and fan deposits (mostly sands and gravels) of the Patan, Gokarna, Itahiti, and Thimi formations (Sakai, 2001; Yoshida and Igarashi, 1984). In the northern mountain foothill part of the basin is formed by the delta deposits and it contains the course sediment see in figures 3-5 and 3-6.

Kathmandu Valley aquifer is divided into the shallow and the deep aquifer separated by the thick clay aquitard layer. The shallow aquifer is recharged directly by precipitation and the groundwater flow in the deep aquifer which is slow due to the presence of thick clay bed layers in between them (Gurung et al., 2007). The thickness of the clay layer in the central part is quite high (nearly 200 m) and it decreases towards the boundary of the basin. It is partially exposed in the north and southeastern side of the valley as per Figure 3-5 (Metcalf & Eddy, 2000). So in this region, it is considered that the northern and southern part of the valley has more potential to recharge in the deep aquifer compare to the other. Binnie & Partner (1988) suggested that the transmissivity capacity of the Kathmandu is varied from 120 to 1350 mm^2/day per meter, which means the thickness layer is quite variable and the soil is heterogeneous and it varies the hydraulic conductivity of the basin layer.

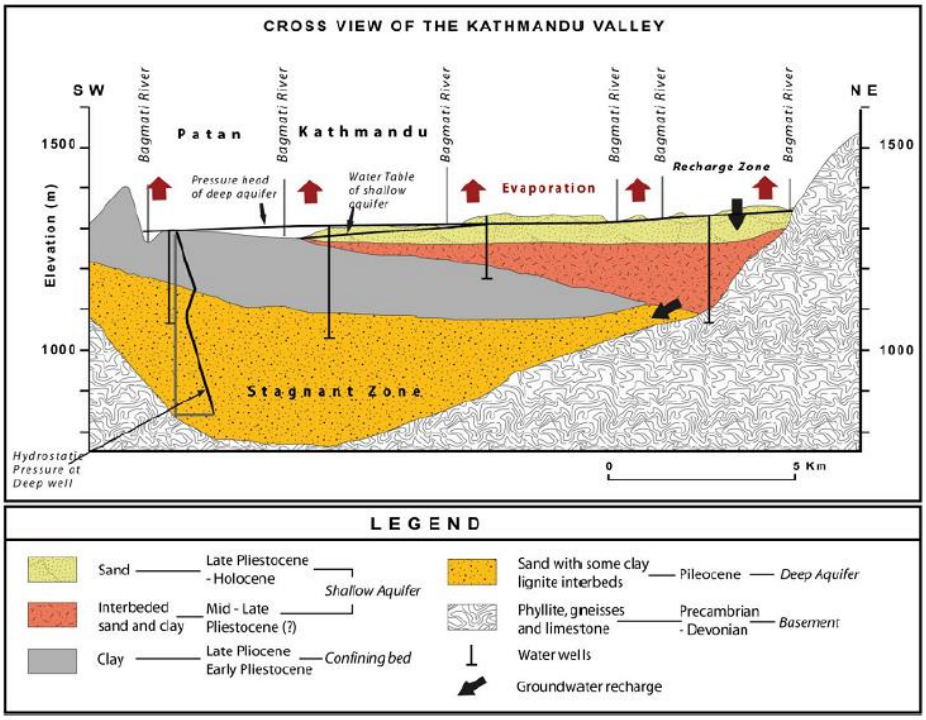

Figure 3-5 Sectional view of subsurface geological map of Kathmandu Valley

(extracted from Cresswell et al., (2001))

JICA (1990) report mentioned that the KV groundwater core area has a thick clay layer acting as aquitard in the basin. Groundwater basin of the valley is divided into the three parts; Northern basin formed by the Gokarna and Tokha geological formation having high recharge capacity, Central basin formed with the Kalimati formation having thick clay aquitard layer with less recharge capacity, and Southern part formed with the integrated combination of Chapagaun, Lukundol, alluvial fan deposit, and the colluvium soil formation having moderate

recharge capacity (Figure 3-6). This study marks the potential high recharge area in the northern and southern groundwater basin of the valley with the graded soil and gravel as per Figure 3-7.

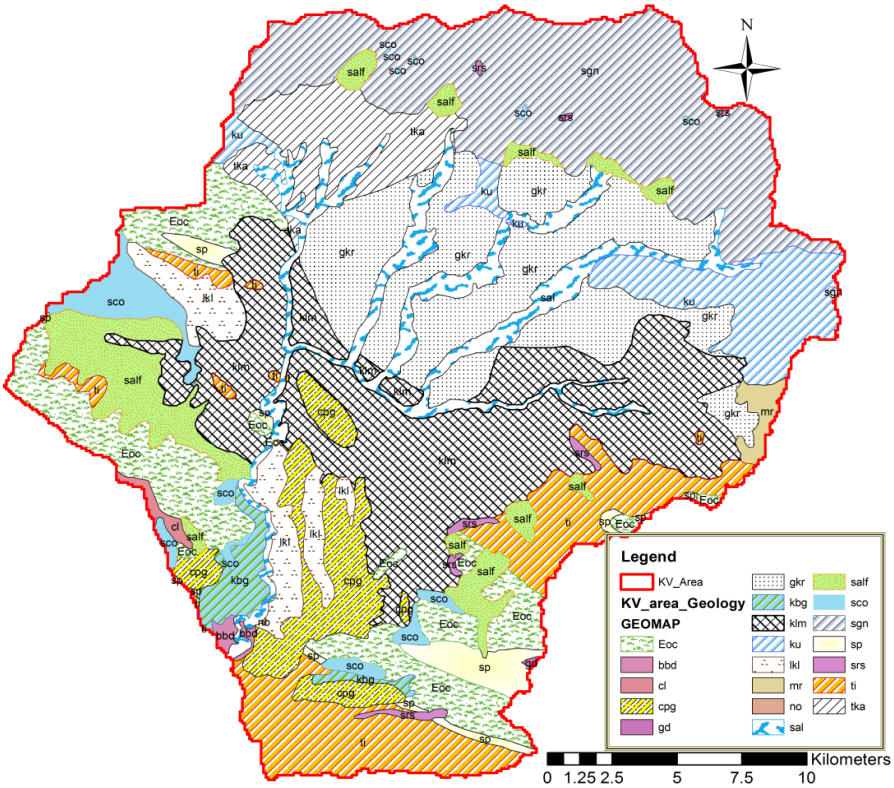

Figure 3-6 Geological map of the Kathmandu Basin.

(Sources:- GON, Departments of Mines and Geology)

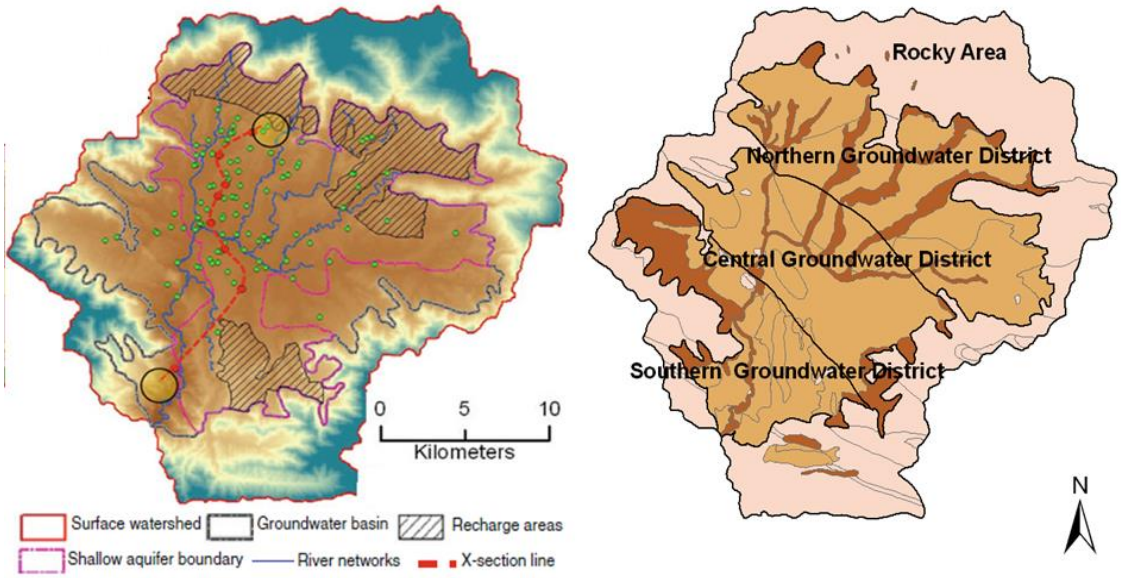

Figure 3-7 Kathmandu Valley groundwater basin Nepal.

(Sources:- (JICA, 1990; Pandey et al., 2013)*)*

Pandey et al. (2010) mentioned that the large precipitation (1755 mm/year) behavior of the basin may not recharge as per withdrawal tendency due to the major forms of the impermeable black clay layer. Most (86 km^2) of the area (Tokha, Sundarijal, Budhanilakantha, Tehecho, Dhobikhola, Gokarna, Manohara,Bansbari, Sunakothi, Sankhu, Chapagaon, Bungmati, Chunikhel, and Godavari) has a high potential recharge capacity and it is similar to the JICA (1990) report. Pandey and Kazama (2011) assigned the potential transmissivity of the aquifer system with corresponding storage capacity of the aquifer. The empirical relation has been developed through the various observed data and it quantifies the range in shallow and deep aquifer is 163 to 1056 m^2/day and 22.5 to 737 m^2/day respectively. From the vertical observational data, the thickness of the layer in the various ranges has been identified. Two aquifer layers have been separated by the thick aquitard layer varying from 10 to 200 m, while shallow and deep aquifer has the vertical depth 0 to 85 m and 25 to 285 m respectively. The shallow aquifer in the northern part is thicker and has high potential to recharge and somewhere deep aquifer expose location. In south-eastern and south-western parts the thickness of the shallow aquifer is nominal or exposed the aquitard in the surface. The southern part of the groundwater basin deep aquifer has a high tendency of vertical depth. The north-east part of the groundwater basin has a greater potentiality to store in the shallow aquifer and similarly in the southern part is more viable for the storage of water in the deep aquifer (Pandey et al., 2013). The shallow groundwater potentiality of the basin has been quantified as 1,452.25 MCM by using the ARC indicators (Availability, Release potentiality and Cost) approach and GIS tools in the basin and the author suggests that the estimation is proper if the groundwater flow dynamics and recharge pattern could be simulated through the groundwater model. The hydraulic properties of the groundwater system of the KV are presented in Table 3-3.

Table 3-3 Hydro-geological properties of the KV groundwater basin

(Sources:- Pandey and Kazama, (2011))

S.N.	Features	Units	Shallow Aquifer	Deep Aquifer
1	Surface area (A)	km^2	241	327
2	Transmissivity (T)	m^2/day	163.2-1056.6	22.6-737
3	Hydraulic Conductivity (K)	m/day	12.5-44.9	0.38-8.8

4	Storage Coefficient (s)	Unit less	0.2	0.00023-0.7
5	Total Aquifer Volume	MCM	7261.27	56813.7

Various studies in the KV showed that the recharge tendency of the basin was less than the abstraction and the increasing demand will be creating over stress in the groundwater resources (Dahal et al., 2019; Shrestha, 2009; Shrestha et al., 2020; Thapa et al., 2018). The annual report by KUKL (2015) showed that 22.5% of total demand of the valley was supplied from groundwater resources. The groundwater contribution in the valley in dry season, wet season, and average was reported as 35%, 11%, and 19% respectively. Pandey and Kazama (2014) also reported that the total abstraction of groundwater resources was increased from 21.26 MCM to 25.52 MCM during 2005 to 2009. From the aforementioned information and studies showed that the water security situation of the KV is more challenging in the current supply context.

Chapter 4. Methods

The overall methodological framework adopted in this study is shown in Figure 4-1. Three future scenarios were generated, namely, projected land use/cover (LULC), climate, and pumping rate induced from population growth. LULC was modeled and projected using CLUE-S model. Future climate was projected using multiple climate models under multiple Representative Concentration Pathways (RCPs) scenarios. Recharge areas were delineated using multiple layers and multi-criteria decision making (MCDM) tool. Current and future hydrology and water balance components were simulated by developing a hydrological model in Soil and Water Assessment Tool (SWAT). Current and future groundwater flow dynamics were simulated by developing a groundwater flow model using MODFLOW code. Impacts on surface water resources were assessed under climate change (CC) scenarios, LULC change scenario, and combined (or integrated CC and LULC change) scenarios. Impacts of urbanization on groundwater dynamics were simulated considering change in recharge areas (supply side) and change in pumping rates (demand side) as parameters of urbanization that affect groundwater resources. Following sub-sections describe the methods in detail.

4.1 Future LULC projection

4.1.1 Past LULC change and validation of LULC map

Land use/cover (LULC) maps of the study area for the period of 2010 to 2018 were prepared by processing of the Landsat image obtained from United States Geological Survey (USGS) web portal. Clear and less cloud effect image was used for the processing. The images were processed and analyzed using Geographic Information System (GIS) tools. A supervised classification technique was used for the generation of LULC map. Only five types of LULC category (agriculture, built up, forest, water body, and restricted area (like airport, park, administrative office area, cultural area, etc.) were used in the LULC map prepared in this study (Figure 4-2, a), which were selected based on potential for surface runoff generation, recharge capacity of the LULC, and intensity of urbanization (Dahal et al., 2019; Thapa and Murayama, 2012). ICIMOD also prepared the LULC map of Nepal in 2010 (Figure 4-2, b). In this map, nine LULC types were identified, viz. Agricultural, River, Barren, Built Up, Grass, Needle-leaved open forest, Needle-leaved close forest, Broad-leaved close forest, and Broad-leaved open forest. For the validation purpose, the nine LULC in the ICIMOD's LULC map was aggregated into five categories. Kappa statistics (K) was used as a measure

of agreement between the two maps. The Kappa values vary from zero to one. The maximum value (means one) represents the most perfect agreement between two raster maps and minimum value (zero means) no level of agreement (Cohen, 1960). The K value can be represented by Equation 4.1 as follows:

$$K = [\frac{Pr(a)-Pr(e)}{(1-Pr(e))}] \quad 4.1$$

Where, $\Pr(a)$ is the observed relative agreement among all rasters and $\Pr(e)$ is the hypothetical probability of a chance of an agreement.

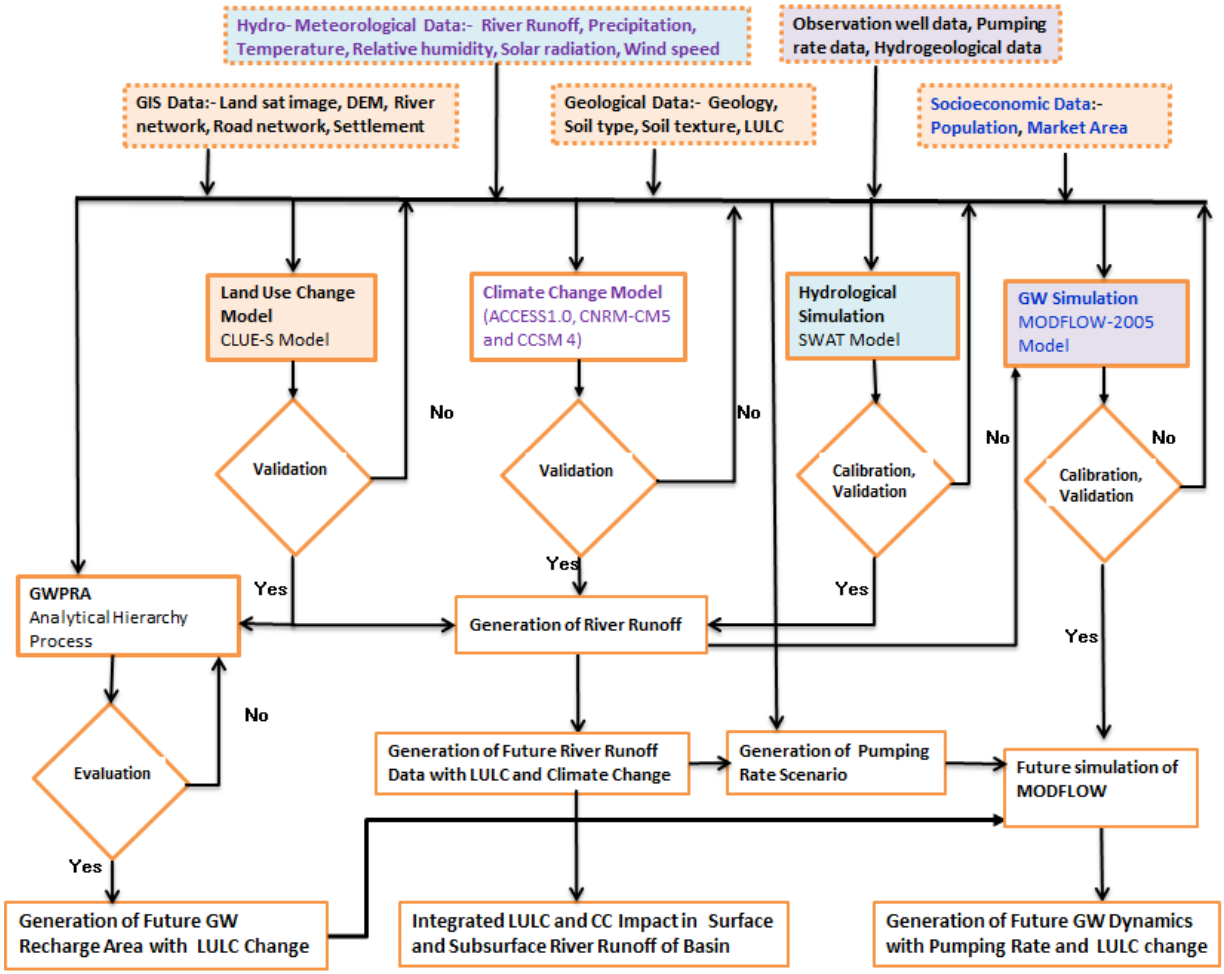

Figure 4-1 Methodological framework of the study

Note: LULC: Land Use/Cover, GW: Groundwater, DEM: Digital Elevation Model, GWPRA: Groundwater Potential Recharge Area, CC: Climate Change, SWAT: Soil and Water Assessment Tool, MODFLOW: MODular groundwater FLOW

Background and colour represents the corresponding inputs.

For finding the similar nature of LULC characteristics of the area, the signature file generated during the preparation of 2010 LULC was used for generating the LULC maps of 2012, 2014, 2016 and 2018 as well. Trend analysis of LULC for the period of 2010 – 2018 is shown in Figure 4-3. Urbanization pattern with conversion of open land into built-up area is clearly evident. Such changes affect surface runoff and recharge capacity of the basin (Dahal et al., 2019; Rimal et al., 2017; Shrestha et al., 2018; Thapa and Murayama, 2012). There is no notable change in the forest land because most of those areas in the KV are situated in the outer peripheral mountainous part and managed by Community Forest User Groups (CFUGs). Therefore, for future LULC scenarios, forest area was considered as the low conversion area. On the other hand, major government centers, Airport, Parks, and Religious areas were considered as restricted areas due to the government's restriction that those LULC cannot convert into the other LULC types. Due to encroachment of liner waterway of the river and water body, water way of the KV cannot pass peak runoff and therefore results in flooding in the urban area (Shrestha, 2015).

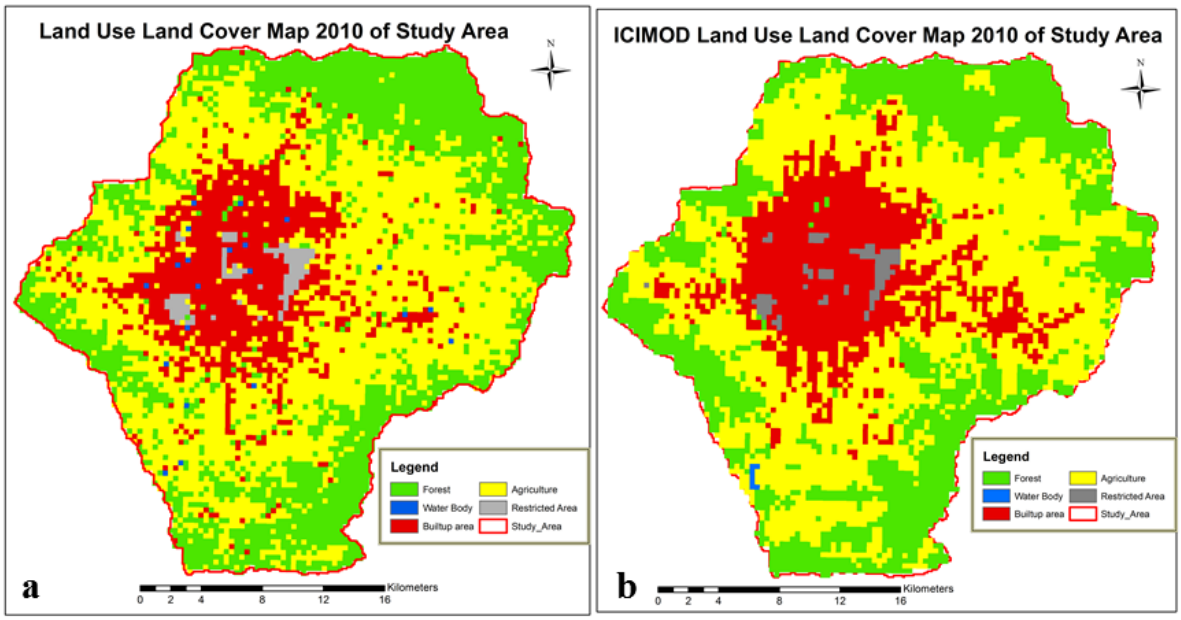

Figure 4-2 LULC map a) 2010 generated b) ICIMOD 2010

Currently, the Bagmati Integrated River Basin project and River Road Corridor project are also implemented for the management of the river corridor. After implementing this project, all river corridor of the Bagmati River is defined and there is not possibility to encroach the water body. In this study, it considered that the LULC of the water area is not changing. So, the land use demand projection scenario was basically assessed the change in built up and agricultural open land in map with respect to change in urban population in the KV.

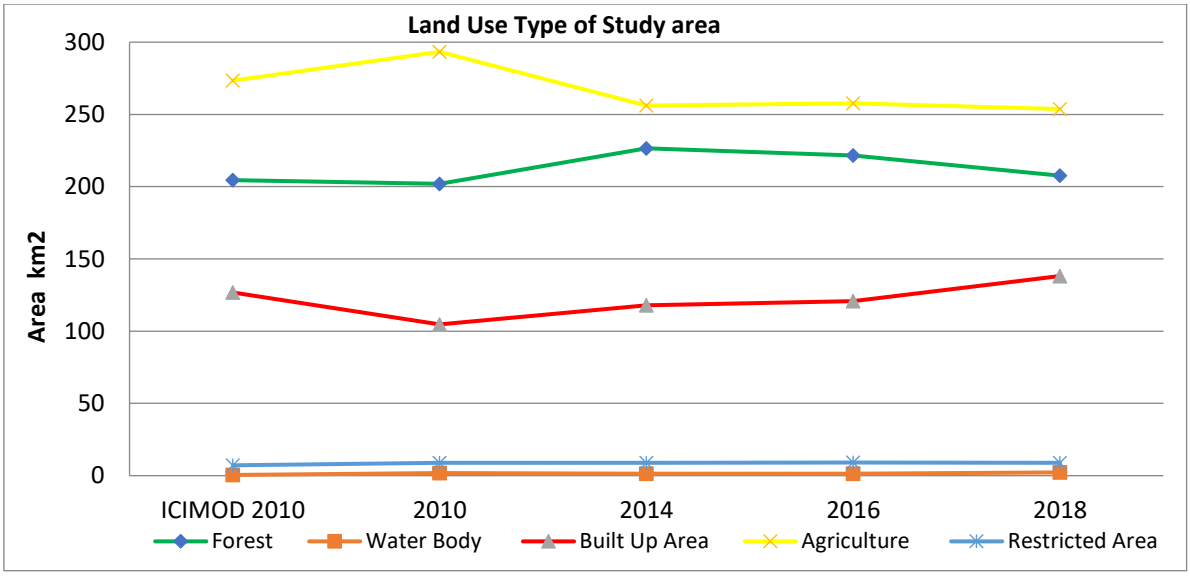

Figure 4-3 Land coverage in the study area in different year

From the generated map and obtained data set, it was clearly seen that the trend of encroachment of open land by urbanization (Figure 4-4). The area changes of restricted area and water body was not properly seen but the decreased the agricultural fertile and increase the more impervious built-up area. From the formation of CFUGs for the forest conversation, the overall area of the forest was not significantly change. If similar trend follow for the population growth, haphazard urbanization and encroachment of open land that affects the urban water environment of the KV.

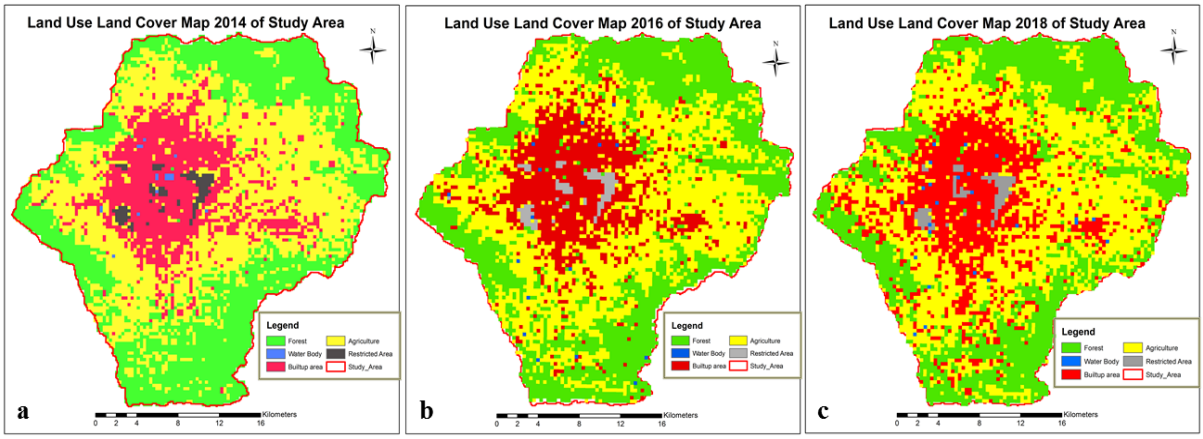

Figure 4-4 Historical LULC map of the study area a) 2014, b) 2016, and c) 2018

4.1.2 LULC projection scenario

Future LULC demand projection was basically done by two approaches one is economic scenario and other is conservation scenario. Economic scenario was based on the economic development of that area and historical LULC change as well as population change.

Conservation scenario was based on the restricted LULC change with respect to governmental requirements (Shrestha et al., 2018). Following five types of LULC demand scenarios were analyzed based on built area and population increase rate to project future LULC.

a) Normal LULC change scenario: - This analysis was based on the actual historical LULC change rate. The actual LULC change data was found from the generated historical LULC map or dataset. In this scenario, normal LULC change pattern of the study area was adopted and it is assumed that the all LULC change factors will have same trend in the future.

b) Double LULC change scenario: - In this scenario, the urban population and urbanization pattern of the study area will go up rapidly compared to the historical pattern. So, it was assumed that the LULC change trend is double than the historical.

c) Half of LULC change scenario: - It is the restricted scenario, in which, the trend of the LULC change is already controlled and future projection rate will be half of normal LULC change trend.

d) Population growth rate scenario: - The population growth rate of the urban area is much higher than the historical built-up area. In this scenario, the rate of increase in population is correlated with the household number. Then rate of change of the LULC pattern is determined based on the increase in the household number.

e) Half of population growth rate scenario: - It is also restricted scenario, in which the population and household growth rate are considered as half of the historical trend. It is also assumed that the other relative factors influencing population growth are controlled.

For the analysis, the relevant data was taken from the CBS (2011) and the detail of the process data was given in Annex-I

4.1.3 CLUE-S model application

The Conversion of Land Use and its Effects at Small regional extent (CLUE-S) model was selected for future LULC projection. The CLUE-S is updated version of CLUE, a dynamic model that can simulate the LULC conversion with the reference of driving forces (Veldkamp and Fresco, 1996), developed for the purpose of small extent analysis (Verburg, 2010; Verburg et al., 2002), which CLUE cannot do correctly. The CLUE-S analyzed LULC

change based on an empirical equation of location suitability and it combined with the dynamic simulation of spatial and temporal of LULC systems (Verburg et al., 2002).

The model is divided into two modules, non-spatial demand and spatially explicit allocation module. The demand module studies the various demand for LULC through past LULC change trends or assigned scenario-based LULC. Then it translates the demand of LULC for application by the spatial allocation module (Verburg, 2010). The allocation module distributes the suitable LULC change with respect to the demand-based output from the non-spatial module. The overall methodological process of the CLUE-S model is shown in Figure 4-5.

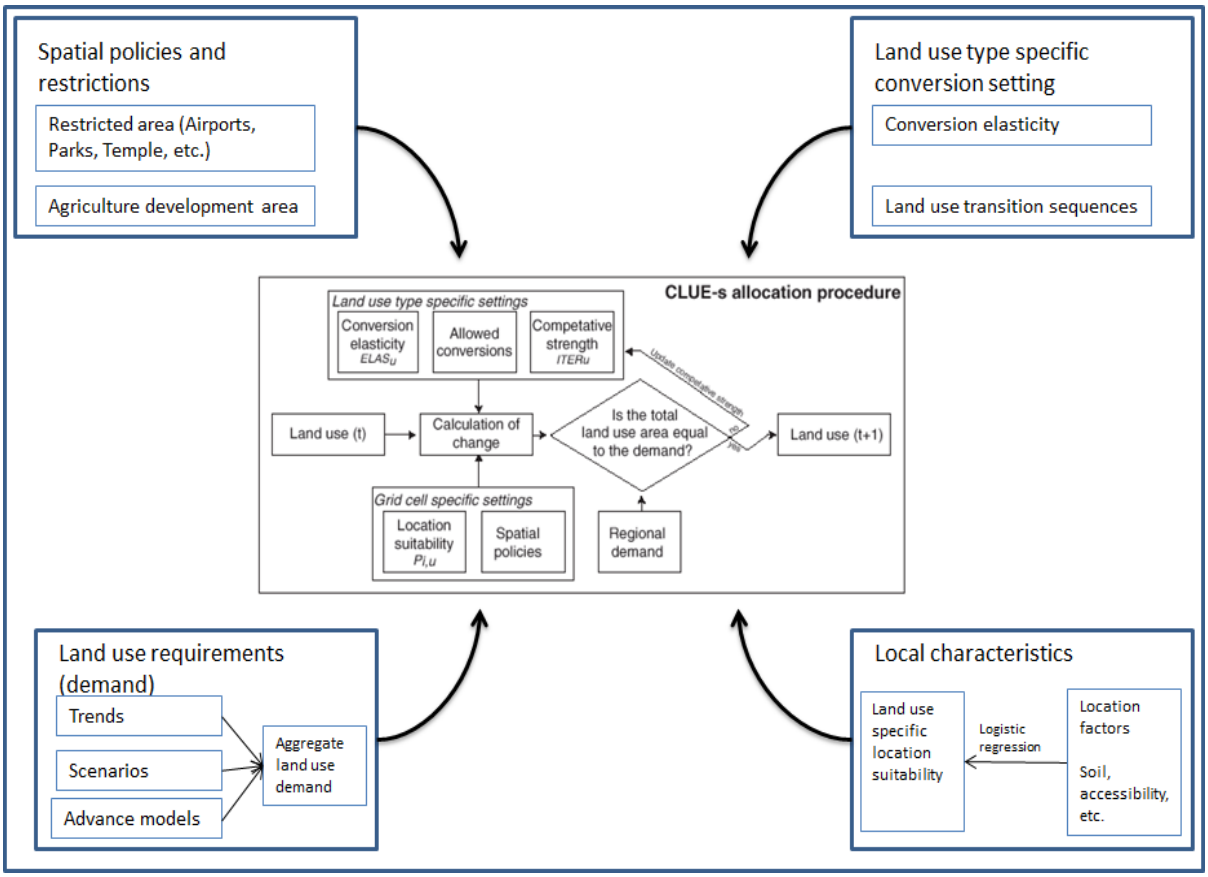

Figure 4-5 Work flow diagram of the CLUE-S model

The LULC type conversions of the area at analysis period were basically depends upon the highest suitability of the specific land use type. The suitability (preference) of the land use type was found by the empirically estimated from the different driving factors that are considered during the analysis of land use conversion as per Equation 4.2.

$$R_{ki} = a_k X_{1,i} + b_k X_{2,i} \qquad 4.2$$

Where R_{ki} is the weightage to devote location i to land use k,

$X_{1,i}.$, are characteristics of driving forces of location i and

a_k and b_k the relative weightage of these characteristics on the preference for land use k.

The preference of land use type R_{ki} cannot be directly observed and measured; it is the cumulative response of the observer. So, the value was quantified based on the probabilistic approach with the regression model.

Two types of regression analysis model were used for the analysis of land use change for the selection of driving forces and its corresponding probability of the LULC change. One is ordinary logistic regression model and it used in various studies (e.g. Chen et al., 2010; Shrestha et al., 2018; Verburg et al., 2002; Zhou et al., 2016), which is simply used for the normal analysis. The other is the auto-logistic regression model, which is used for the elimination of the spatial autocorrelation effect in the LULC model (Jiang et al., 2015). It is assumed that the effect of spatial dependence into the ordinary logistic regression model is insignificant.

Firstly, the study area was separated into 300m x 300m grid units and the response variable (LULC type) was in a binary number (1 showed the transition occur and 0 showed the non-transition) (Verburg et al., 2002). The ordinary logistic regression model was expressed in Equation 4.3.

$$log\left(\frac{P_i}{1-P_i}\right) = \beta_0 + \beta_1 x_{1,i} - - - - - - - + \beta_n x_{n,i} \qquad 4.3$$

Where P_i is the probability of specified land use type i transition in the grid, and, β_i is a coefficient to be estimated for each explanatory variable $x_{n,i}$.

The logistic regression model of the probability of the suitability of the land use was analyzed based on the Statistical Package for the Social Sciences (SPSS) (Rosner, 2010) tools and goodness of fit of the analysis is checked by the ROC value (Pointius and Schneider, 2001). The ROC value lies between 0.5 and 0.7 indicates the model is low accuracy, the value varies between 0.7 and 0.9 indicates the credible accuracy; and when the ROC value is larger than 0.9 provides the model for high precision (Stephanie et al., 2001). The probability of each grid was calculated based on driving forces and generate the suitability map of different land use and based on actual land use condition define a set of rules to control the difficulties of transitions between land use. Then combined the initial land use map, suitability map, and

land use transition rules. Total probability of each grid for each land use was calculated by Equation 4.4.

$$TPROP_{i,u} = P_{i,u} + ELAS_u + ITER_u \quad 4.4$$

Where, $TPROP_{i,u}$ is the total obtained probability of grid cell i for suitable land use type u. $P_{i,u}$ is the logistic regression value of spatial distribution probability; $ELAS_u$ is the transition elasticity probability of land use u and it varies from 0 (lesser stability) to 1 (higher stability), and $ITER_u$ is the probability of iteration variable in land use u. As per above empirical equation, CLUE-S model generates the probability map of each land use type and corresponding change. The outputs from the CLUE-S was found in the ASCII file and easily analyzed from ArcGIS tools. Soil type, existing land use type, distance from settlements, distance from road, distance from river, slope, aspect, and population density were assumed the driving forces for the analysis and the datasets are taken as per maintain in Annex-I. The sensitivity of the driving forces with respect to land use type was found by the ROC and the value of each land use type was calculated from the SPSS tools. From the transition elasticity or conversion demand elasticity, the projected LULC maps were prepared by using the CLUE-S model with various scenarios. The different scenario output maps are shown in Annex-I.

4.2 Groundwater recharge area delineation

The groundwater recharge tendency of the basin is basically quantify based on the properties of infiltration and the runoff within the surface of basin. There are many factors (like; physical characters, LULC, climatic characteristics, etc.) involved in the groundwater recharge, the major factors that were considered in the analysis is given in the Table 2.1

4.2.1 Data standardization

For analyzing the each thematic layer of the study, each thematic layer and its each grids had a unique value and the standardization process translates them into the dimensionless value of the layers. The standardization Equations 4.5 and 4.6 are given below to obtained the value of the study area was "larger the better" and "smaller the worst" of the alternative value of the grids in each thematic layer (Pei-Yue et al., 2010).

Standardization used for larger the better:

$$y_i = \frac{(x_i - x_i\,(min))}{(x_i(max) - x_i\,(min))} \quad 4.5$$

Standardization used for smaller the better:

$$y_i = \frac{(x_i(max) - x_i)}{(x_i(max) - x_i\,(min))} \quad 4.6$$

Where, y_i is the standardized value of the thematic grid and i is the index of thematic grid and x_i $x_i(\max)$, $x_i(\min)$ are the original, maximum and minimum values of the thematic grids, respectively.

4.2.2 Delineation of the groundwater potential recharge areas

All the thematic layers (three in first hierarchies and its corresponding second hierarchies) standardized value were then aggregated in GIS to get a single score of potential recharge area (Equation 4.7) (Malczewski, 1999). The product of each weights with its corresponding grid value and summation product gave the potential recharge value (Jhariya et al., 2016). The potential recharge value of each grid, layer computed the theoretical potential recharge areas. The higher value of the grid has higher potential and vice-versa.

$$\text{GWPRA} = \sum_{j=1}^{m} \sum_{i=1}^{n} \left(w_j \times x_i\right) \quad 4.7$$

Where, GWPRA is the sum of groundwater potential recharge area in the grid of the study area; x_i is the normalized weight of the i^{th} class of the thematic layer; w_j is the weight factor derived from AHP of the j^{th} thematic layer; and m is the number of assigned thematic layer and n is the number of class provided in thematic layer.

The obtained recharge value of each grid cell from the analysis was characterized in the six different zones. The dimensionless theoretical output value of the grid cell was analysis through the GIS environment. GWPRA was classified as per Table 4-1 (Singh et al., 2018).

Table 4-1. Potential groundwater recharge value

S.N.	Very Low	Low	Moderate low	Moderate high	High	Very High
Potential GW recharge value	2.1 - 3.0	3.1 - 4.0	4.1- 5.0	5.1 - 6.0	6.1 -7.0	7.1 - 8.0

The Analytical Hierarchy Process (AHP), a multi-criterion decision-making (MCDM) technique, was used to determine weights to the three primary hierarchies and its 10

corresponding secondary indicators. MCDM techniques are powerful tools for the analysis and optimization of the uncertainties associated with the decision objective. In these methods evaluate the decision variables by given rank basis evaluation criteria for each decision variables. Multi-objective or multi-attribute are the two methods are broadly used for combining several rank criteria for the decision performance (Chow and Sadler, 2010). Remote sensing (RS), GIS, and Multi-Criteria Decision Analysis (MCDA) techniques are the combine tools for the application of the data acquisition, storage, and analysis capability for the highly complex spatial data problem with considering socio-economic variables. Analytical Hierarchical Process (AHP) method is expert judgment-based approach, rank, and weight-age were given by a pairwise comparison between the various influencing or driving factors. AHP method was used for the decision-making process by dividing into the various parameter, assemble the parameters in hierarchical based and making the judgment on the relatively important of pair element (Saaty, 2004). With the combination of GIS and AHP is provided to integrate a large quantity of heterogeneous data for finding the complex analysis (Jhariya et al., 2016; Singh et al., 2018). Generation of suitability map for the potential groundwater recharge area by the first (primary) hierarchies (topography, climate, and socio-economic) and its corresponding secondary ten (Slope, River distance, Geology, Land use, Aspect, Elevation, Precipitation, Population density, Market distance, and Road distance) different thematic layers were compiled in GIS and given the pair compression value to evaluate the weight-age value in each thematic layer by AHP. All combination and conceptual flow diagram are shown in Figure 4-6.

The advantages of this method in MCDM techniques is that all type of information, judgments, and weight of each factor is structured with knowledge, skill, and experience of the expert (Chaudhary et al., 2016). The weight-age factor was obtained by pair comparison and inconsistency of the decision was detected by the consistency ratio (CR). If CR value is greater than 10%, the comparison matrix of each layer is inconsistent and it should be revised for consistent weight (Saaty, 2004). So, the main disadvantage of this method is that the weight-age factor of each decision criteria is varying with the expert by expert and the results of the process are not unique. Pair wise comparison of the layer was made by using a scale from 1 to 9 with the relationship of the layer and the inverse relation was made by the inverse value which is shown in the Table 4-2.

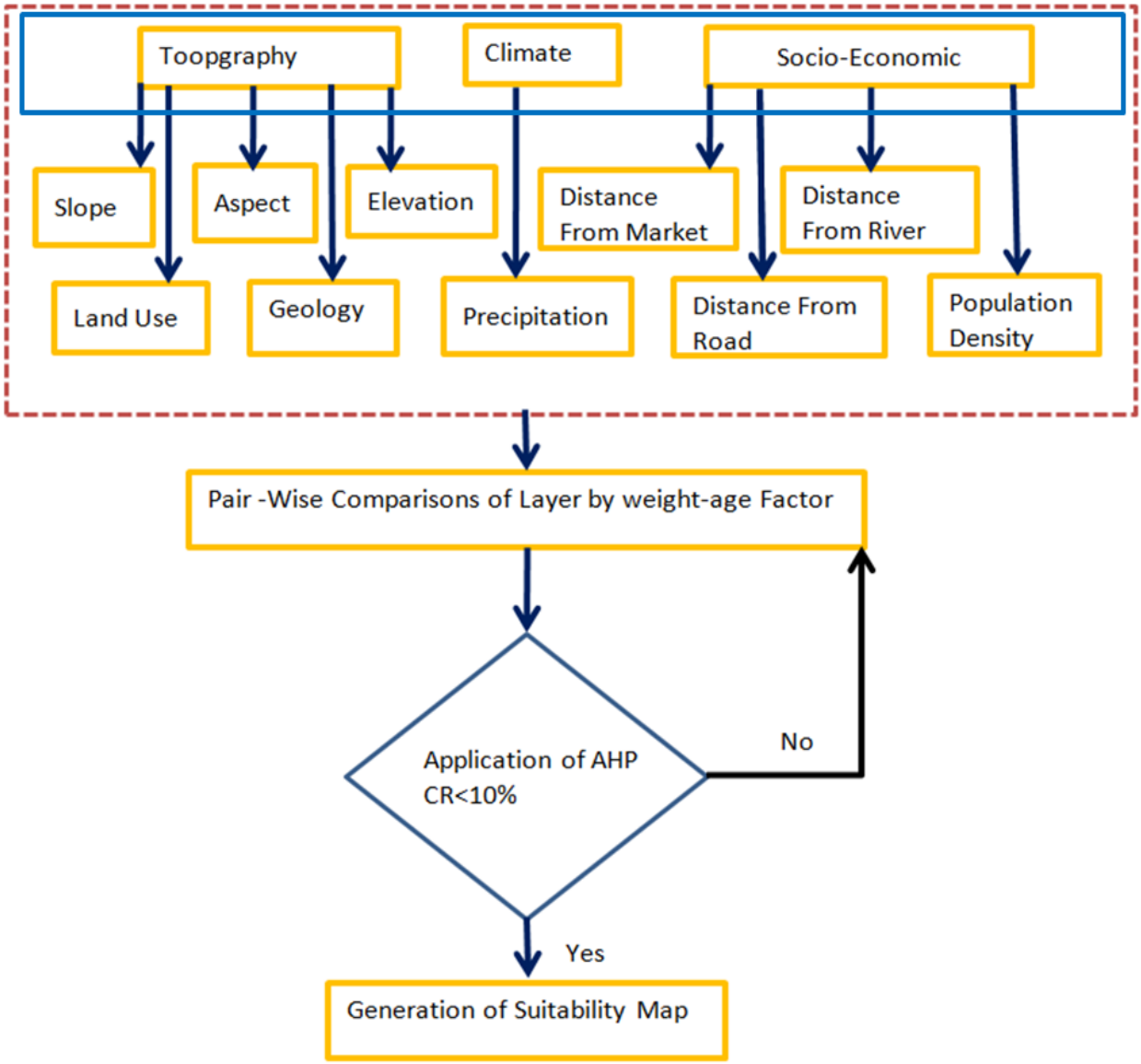

Figure 4-6 Flow diagram of the AHP method

Table 4-2 AHP scale and its interpretation

(Sources:- (Eastman, 2003))

Less Important				Equally Important	More Important			
Extremely	Very Strongly	Strongly	Moderately		Moderately	Strongly	Very Strongly	Extremely
1/9	1/7	1/5	1/3	1	3	5	7	9

Comparison matrix was made as shown below Equation 4.8 from the comparison factor and the diagonal element of the square matrix was always one because of the same factor comparison.

$$A = [aij] = \begin{bmatrix} a_{11} & \cdots & a_{1n} \\ \vdots & \ddots & \vdots \\ a_{n1} & \cdots & a_{nn} \end{bmatrix} \quad 4.8$$

Such that $[aij] > 0$.

Three major steps involved in the AHP analysis for computing consistency ratio (CR) value for the various thematic layer (Saaty, 2004),

1) Normalized pair wise comparison matrix is A_1 is built as Equation 4.9

$$A_1 = \begin{bmatrix} a'_{11} & a'_{12} & \cdots & a'_{1n} \\ \vdots & & \ddots & \vdots \\ a'_{n1} & a'_{n2} & \cdots & a'_{nn} \end{bmatrix}, \; a'_{ij} = \frac{a_{ij}}{\sum_1^n a_{ij}} \; for \; i, j = 1, 2, \ldots\ldots, n \quad 4.9$$

2) The eigenvalue and the eigen vectors are found as per Equations 4.10 and 4.11.

$$= \begin{bmatrix} W_1 \\ W_2 \\ . \\ . \\ . \\ W_n \end{bmatrix} and \; w_i = \frac{\sum_1^n a'_{ij}}{n} \quad for \; i = 1, 2, \ldots\ldots, n \; and \quad 4.10$$

$$w' = AW = \begin{bmatrix} w'_1 \\ w'_2 \\ . \\ . \\ . \\ w'_n \end{bmatrix}, and \; \lambda_{max} = \frac{1}{n}\left(\frac{w'_1}{w_1} + \frac{w'_2}{w_2} + \cdots + \frac{w'_n}{w_n}\right) \quad 4.11$$

Where, W is the Eigen vector; w_i is the Eigen value; λ_{max} is the average eigen value of the pair wise comparison matrix.

Consistency of the output from the pair wise comparison was found by the consistency ratio (CR) as per Equation 4.12.

$$CR = \frac{CI}{RI} \quad 4.12$$

Where, CI is the consistency index and it is calculated by the pair comparison value as per Equation 4.13. RI is the ratio index and found from the standard given table by Saaty 1988 (Saaty, 1988).

$$CI = \frac{\lambda max - n}{n-1} \quad 4.13$$

Where, n = number of thematic layers used in analysis. If the constancy ratio of the pairwise comparison is less than 10% is acceptable, otherwise, reevaluate the corresponding weights of each thematic layer.

4.2.3. Evaluation of groundwater recharge map

Theoretical recharge potentiality of KV estimated as described above was further evaluated based on collected field test infiltration data. Infiltration from the surface and the recharge of groundwater aquifer has a strong relationship and it is also verified by the using pressure sensors, single/double-ring infiltro-meters, soil sensors, and observation wells (Ganot et al., 2017) Single and double ring infiltration method is used for the in situ field test of the infiltration, and from these, the double ring infiltro-meter was given the better preference (Verbist et al., 2010). Double ring infiltro-meter in situ filed test was conducted for the estimation of infiltration information at various spatial location of the KV. Infiltration rate at 83 locations as shown in Figure 4-7, with wide spatial coverage of infiltration properties, was estimated from field test. The selection of the test point was based on the change location of geological, soil, slope, LULC, and open area etc. By spatial interpolation and application of GIS tools, a raster map of infiltration capacity was developed. Those two maps (theoretical and field test) were compared using Kappa statistical analysis (K) for the evaluation as per Equation 4.1 and Section 4.1.1.

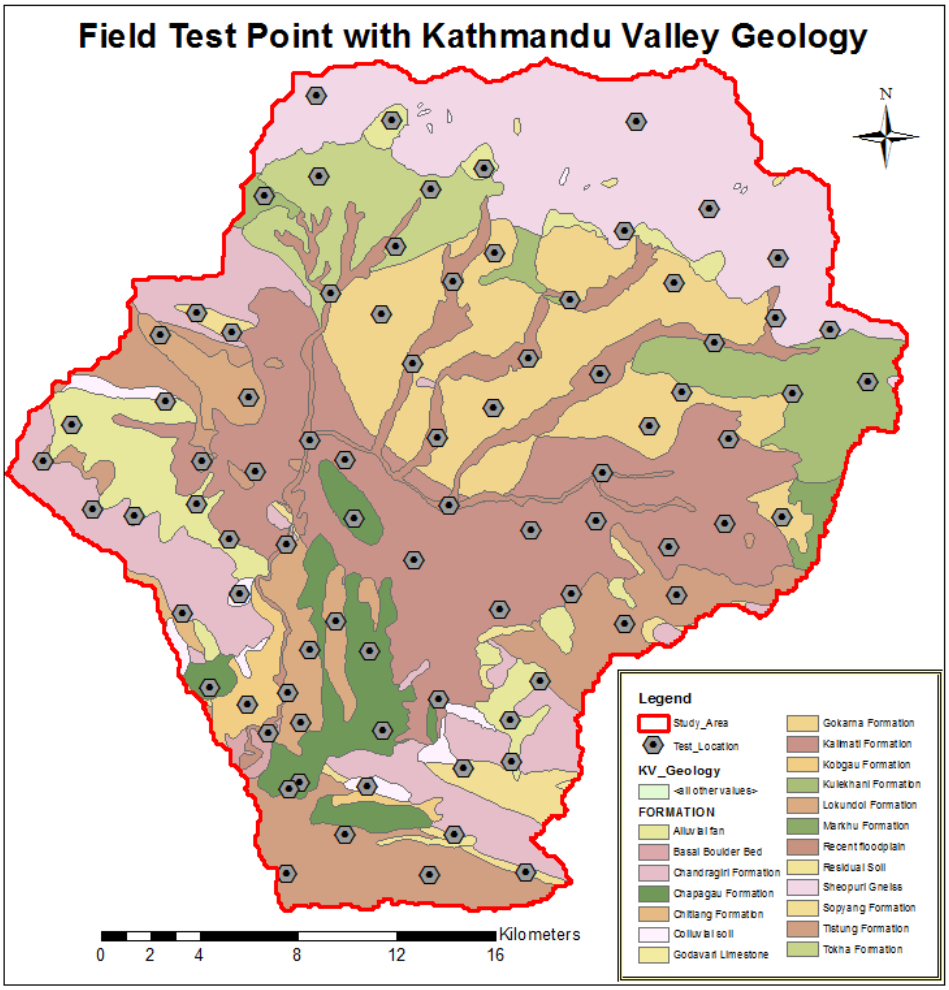

Figure 4-7 Infiltration test point in the Kathmandu Valley

4.2.4 Estimating future encroachment in groundwater potential areas

After evaluation of baseline potential groundwater recharge area, the weightage value of each factor (shown in Table 2-1) was remaining same except the land use type. The groundwater potential recharge areas (GWPRA) for each decade were prepared by the evaluated weightage factor and decadal LULC change. The generated potential theoretical recharge grid value of the map was the unit less factor, and the data were changed to mm/hr unit by correlating with the field test point value. The field test values were obtained by the double-ring infiltro-meter test in different basin points discussed in above section. The final dimensionless potential recharge map was produced. Then the future potential recharge areas were compared with baseline 2020 map to estimate encroachment value in recharge areas by using GIS environments.

4.3 Future climate projection

4.3.1 Climate models selection and use

The future climate was projected in the study area based on three regional climate models (RCMs), namely, ACCESS-CSIRO-CCAM, CNRM-CM5 and CCSM4. Those RCMs are recommended as reliable for alpine and sub-tropical climate (Aryal et al., 2017), which fits well to the context of this study area. Daily precipitation and temperature (maximum and minimum) data of the region were downloaded and analyzed from 2000 to 2005 under RCP4.5 and RCP8.5 scenarios. Daily and monthly average generated data of RCMs were evaluated through the observed historical data. The statistical indicators (Root mean square (RMS) and standard deviation (SD)) were analyzed for the statistical validation before and after bias correction. In the regional scale, the RCMs give a better preference and before the application of data some bias correction has been required while using it (Li et al., 2014).

4.3.2 Bias correction

For bias correction, linear scaling and quantile mapping techniques were used in the RCM projections. They are elaborated in the following sub-sections. Among the two bias-corrected time series, the one that suits most in the study area is taken for further analysis.

i) Linear scaling

Linear scaling technique is basically to match the daily and monthly climate value into the observed value with certain correction. This method is similar to the constant scaling. It is applied to the mean value and corrects with the generated value with the historically observed deviation of temperature and precipitation data. It is the easiest method for bias correction and it is also wildly used (Aryal et al., 2017; Bajracharya et al., 2018; Sangam. Shrestha et al., 2017). For linear scaling, the temperature is in an additive correction basis, and precipitation is in multiplier basis as pre below Equations 4.14-4.17

$$P_{his}(d)^* = P_{his}(d) \,.\, [\mu_m \{P_{obs}(d)\}/\mu_m \{P_{his}(d)\}] \quad 4.14$$

$$P_{sim}(d)^* = P_{sim}(d) \,.\, [\mu_m \{P_{obs}(d)\}/\mu_m \{P_{his}(d)\}] \quad 4.15$$

$$T_{his}(d)^* = T_{his}(d) \,.\, [\mu_m \{T_{obs}(d)\} - \mu_m \{T_{his}(d)\}] \quad 4.16$$

$$T_{sim}(d)^* = T_{sim}(d) \,.\, [\mu_m \{T_{obs}(d)\} - \mu_m \{T_{his}(d)\}] \quad 4.17$$

where, P, T, d, and μ_m indicates the precipitation, temperature, daily and long term mean monthly values, respectively, and the asterisk indicates the biased corrected RCMs data.

ii) Quantile mapping

In quantile mapping is done by the empirical cumulative distribution function which includes both dry and wet days of the daily data. This method is derived from empirical transformation function (Themeßl et al., 2012) and effetely used in the precipitation and temperature simulated RCM for bias correction. In this research, the QM method was done in R language (Venables and Smith, 2013) with the following governing Equations 4.18-4.21. It is successfully used in the different research (Aryal et al., 2017; Mishra and Herath, 2014; Shrestha et al., 2018) and efficiently correct in the bias data of standard deviation, mean, and as well as wet and dry day frequency.

$$P_{his}(d)^* = F_{obs,m}^{-1}\{F_{his,m}(P_{his,m})\} \quad 4.18$$

$$P_{sim}(d)^* = F_{obs,m}^{-1}\{F_{sim,m}(P_{sim,m})\} \quad 4.19$$

$$T_{his}(d)^* = F_{obs,m}^{-1}\{F_{his,m}(T_{his,m})\} \quad 4.20$$

$$T_{sim}(d)^* = F_{obs,m}^{-1}\{F_{sim,m}(T_{sim,m})\} \quad 4.21$$

Where F is the cumulative distribution function and F^{-1} is its inverse.

4.4 Hydrological modeling

Hydrological modeling was performed to assess spatio-temporal distribution of current water balance and evaluate projected impacts of climate change and LULC change. Following sub-sections describe the methodology in detail.

4.4.1 Model description

In this study, for the future analysis with both LULC and climate change scenario, SWAT (Arnold et al., 1998) model was simulated for past and future discharge of the Bagmati river basin. The analysis was based on the generated discharge from the SWAT hydrological model. The SWAT model is a semi-distributed, conceptual, and process-based river basin hydrological model. All model parameters were calibrated and then validated through observed river discharge at the Khokana station (station number 550.5) (DHM, 2015). Spatial data (like DEM, soil type, land use) and temporal data (temperature, wind speed, precipitation, solar radiation, relative humidity) are the input data during the simulation of the model and water balance equation is used for the analysis of the model as shown in Equation 4.22.

$$SW_t = SW_o + \sum R_{day} - Q_{surf} - E_a - W_{seep} - Q_{gw} \quad 4.22$$

where, SW_t is the final soil water content in mm, SW_o is the initial soil water content in mm, R_{day} is the amount of precipitation in a day in mm, Q_{surf} is the amount of surface runoff in a day in mm, E_a is the amount of evapo-transpiration in the day in mm, W_{seep} is the amount of water entering the vadose zone in a day in mm and Q_{gw} is the amount of return flow in the day in mm. The river basin of the study area was discretized into the sub-basin, and each basin has own outlets before joining the others. The each sub basins was generated by the various number of hydrological response units (HRU). HRU is the smallest component of the model and it formed by the combination of unique features of land use, soil, and slope class with its own identity. The model was simulated within the basin of all HRUs and the aggregate the outputs at the sub-basin to river reach. GIS-based SWAT model (ArcSWAT ver.10.2) is the composite assemble of the GIS tools with SWAT and it can easily model the spatial variation and hydrological response of the basin like river runoff, latter flow, evapo-transpiration, groundwater flow, percolation, etc

4.4.2 Model setup, calibration and validation

The reliability of the model output depends upon the accuracy of model parameters calibration and mostly correlates with the observed data used in the calibration and validation process. Manually or automatically outlet was generated above the junction of the river network based on the given threshold area. In this research, 149 numbers of sub-basins were generated and followed by 486 hydrological response units (HRUs). From the observed spatial and the temporal data, the obtained result was calibrated and validated.

In this study, Khokana hydrological station data was used for the calibration and validation. Overall river flow data from 2000 to 2014 was collected and used, where 2002 to 2010 flow data was used for the calibration of the model parameter and remaining data from 2011 to 2014 data was used for the validation the model. The list of the calibrated parameter is shown in the Table 4-3. For the better analysis and reduce the uncertainty of the river runoff, two-year warm-up period was given. All the calibration of the model parameter was done by the manual calibration and the base value of the parameter was taken from the previous study (Bajracharya et al., 2018; Pokhrel, 2018; M. Shrestha et al., 2017; Thapa et al., 2017).

Table 4-3 SWAT parameters initial range value

Parameter	File	Definitions	Range Value
ALPHA_BF	gw	Base flow recession coefficient	0–1 (0.048)
GW_DELAY	gw	Groundwater delay	0–500 (31)
GW_REVAP	gw	Groundwater re-evaporation coefficient	0.02–0.2 (0.02)
SHALLST	gw	Initial depth of water in the shallow aquifer	0–50000 (1000)
GWQMN	gw	Threshold water depth in shallow aquifer required for return flow to occur	0–5000 (1000)
RCHRG_DP	gw	Fraction of deep aquifer percolation	0–1 (0.05)
REVAPMN	gw	Threshold depth for water in the shallow aquifer for re-evaporation or percolation to occur	0–500 (750)
GWHT	gw	Initial groundwater height	0–25 (1)
CANMX	hru	Maximum canopy storage	0–100 (0)
EPCO	hru	Plant evaporation compensation factor	0–1 (1)
ESCO	hru	Soil evaporation compensation factor	0–1 (0.95)
sOV_N	hru	Manning's n value for overland flow	0.01–30 (vary)
HRU_SLP	hru	Average slope steepness for overland flow	0–1 (vary)
SLSUBBSN	hru	Average slope length	10–150 (vary)
SURLAG	hru	Surface runoff lag coefficient	0.05–24 (2)
LAT_TTIME	hru	Lateral flow travel time	0–180 (0)
SOL_AWC	sol	Available water capacity of the soil layer	0–1 (vary)

SOL_K	sol	Saturated soil conductivity	0–2000 (vary)
SOL_Z	sol	Depth from soil surface to bottom of layer	
CN2	mgt1	SCS runoff curve number for moisture condition II	35–98 (vary)
CH_K2	rte	Effective hydraulic conductivity in main channel alluvium	0–500 (0)
CH_N2	rte	Manning's "n" value for the main channel	0–1 (0.014)
ALPHA_BANK	rte	Base flow alpha factor for bank storage	0–1 (0)
TLAPS	sub	Temperature laps rate	-10 –10 (-5.6)
PLAPS	sub	Precipitation lapse rate	-1000–1000 (0)
CH_N1	sub	Manning coefficient in (tributary, main) channel alluvium	0.01–30 (0.014)
CH_K1	sub	Effective hydraulic conductivity in (tributary, main) channel alluvium	0–300 (0)
SFTMP	bsn	Snowfall temperature	-20–20 (1)
SMTMP	bsn	Snow melt base temperature	-20–20 (0.5)
SMFMN	bsn	Minimum melt rate for snow during the year	0–20 (4.5)
SMFMX	bsn	Maximum melt rate for snow during the year	0–20 (4.5)
SURLAG	bsn	Surface runoff lag coefficient	0.05–20 (4)

The evaluation of the model parameters output during calibration and validation periods was found by using statistical parameters which are used widely in various modeling-related. In this research, the statistical indicators such as; Nash–Sutcliffe simulation efficiency (NSE), Percentage Bias (PBIAS), the coefficient of determinants (R^2), and the ratio of RMSE to SD

(RSR) were calculated to evaluate model performance. As per NSE, the model performance is considered very good, good, acceptable and unsatisfactory if the values are greater than 0.75, in between 0.65 and 0.75, in between 0.5 and 0.65, and less than 0.5, respectively (Table 4-4). The NSE is computed using Equation 4-23 (Moriasi et al., 2007).

$$NSE = 1 - [\frac{\sum_{i=1}^{n}(Qi-Qi')2}{\sum_{i=1}^{n}(Qi-\overline{Qi})2}] \quad 4.23$$

Where, Qi, Qi' and $\overline{Qi}$ means the observed discharge, simulated discharge, and mean observed discharge of the basin in 'i' the observation respectively.

Similarly, R^2(-1 to 1) value represents the degree of linear correlation between the observed and simulated values. It is computed using Equation 2.15. If R^2 value is greater than 0.5, the model performance can generally be considered as acceptable (Santhi et al., 2001).

In case of PBIAS, it is calculated using Equation 2.14. The PBIAS values of positive, zero and negative indicate under estimation, exact estimation, and over estimation of flow volume, respectively. Lower the magnitude of the PBIAS value, better is considered as the model performance.

Table 4-4 SWAT parameters initial range value (Moriasi et al., 2007; Santhi et al., 2001).

Performance	PBIAS	NSE	RSR
Very good	<± 10	>0.75	0 to 0.5
Good	± 10 to <± 15	0.75 to 0.65	0.5 to 0.6
Acceptable	<± 15 to <± 25	0.65 to 0.5	0.6 to 0.7
Unsatisfactory	> ± 25	<0.5	> 0.7

4.4.3 LULC and climate change impact assessment

The individual impacts of the climate (Mishra et al., 2018; Pandey et al., 2019) and LULC change (Liu et al., 2014; Pokhrel, 2018) in various study areas have been simulated in earlier studies, however, integrated impacts of both climate and LULC changes are looked into in very limited studies, by none in this study area. An integration of climate and LULC change create a unique imbalance in the hydrological parameters of the model. They generate the both positive and negative changes in the model outputs but the integrated impact in the same

model has not considered yet for future period simulation. A calibrated and validated SWAT model was used for future analysis. Individual and combined forms of LULC and climate change analysis were done with the decadal LULC data and two RCP climate scenarios. Further, basin and river reach future water balance was analyzed (seasonal and annual) based on the baseline.

4.5 Groundwater modeling

The overall methodological framework of groundwater modeling is shown in Figure 4-8 and elaborated in the following sub-chapters.

4.5.1 Model description

Groundwater flow model was set-up in the MODular groundwater FLOW model (MODFLOW) 2005 environment to simulate groundwater flow in the KV watershed. Model-Muse was used as the user interface for data pre-processing, model run, and results post-processing. It is a finite-difference three-dimensional (3D) groundwater model and that was first published in 1984. It has a modular structure that allows it to be easily modified to adapt the code for a particular application. Many new codes and facilities have been coupled to the original model. In the USGS, MODFLOW-2005 is the most current release free version groundwater model.

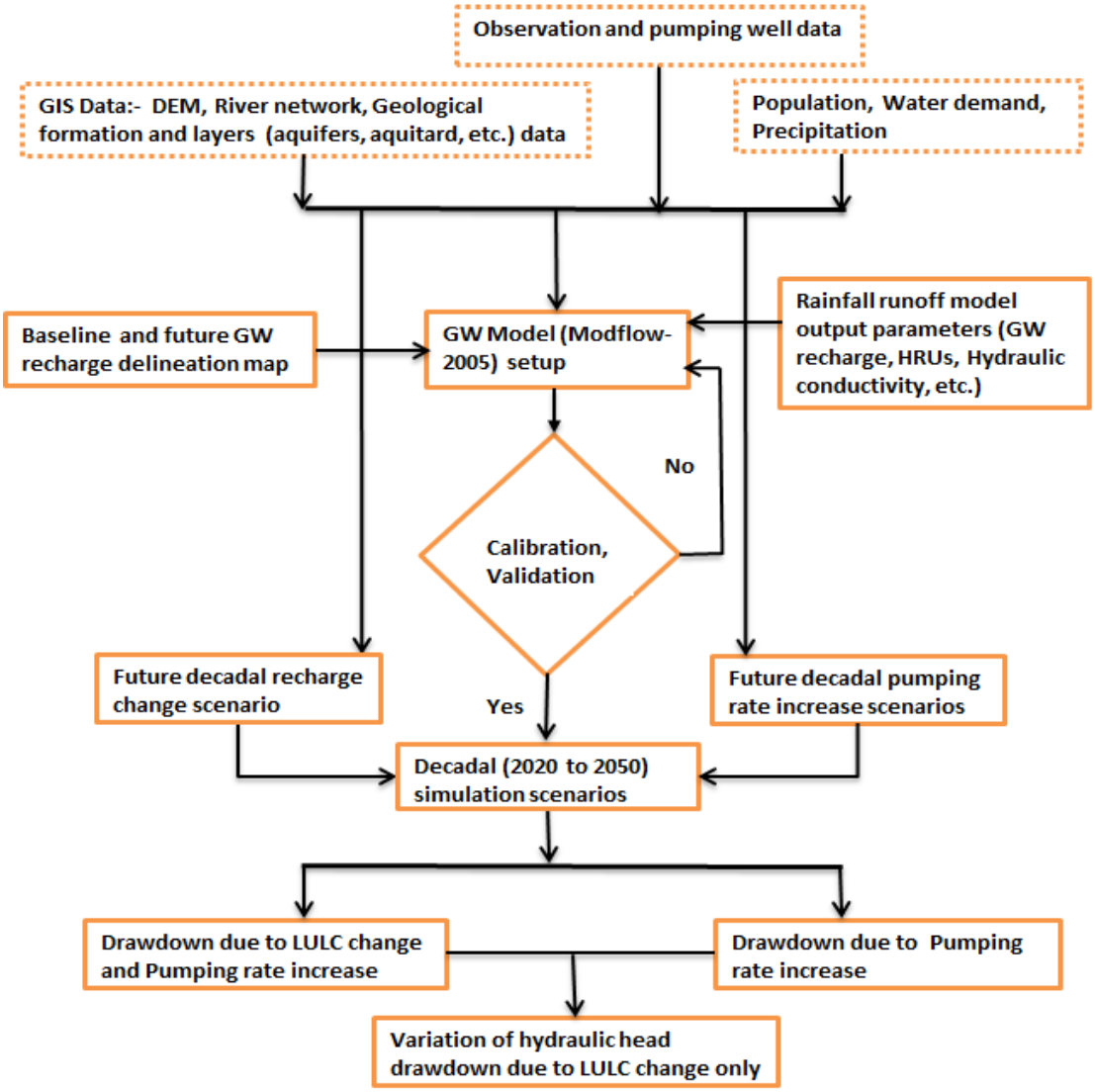

Figure 4-8 Methodological framework of the groundwater simulation

MODFLOW is written in the Fortran-90 programming language and the program code is divided into modules with a series of packages (Harbaugh, 2005). The concept of a model for the visual discretization is as shown in Figure 4-9. Other details of theoretical approach (section 2.6.3), governing Equations 2.25 to 2.31 and numerical schemes used for the groundwater flow simulation to solve the model in finite-difference equations are described as describe in the above section or guide manual (Harbaugh, 2005).

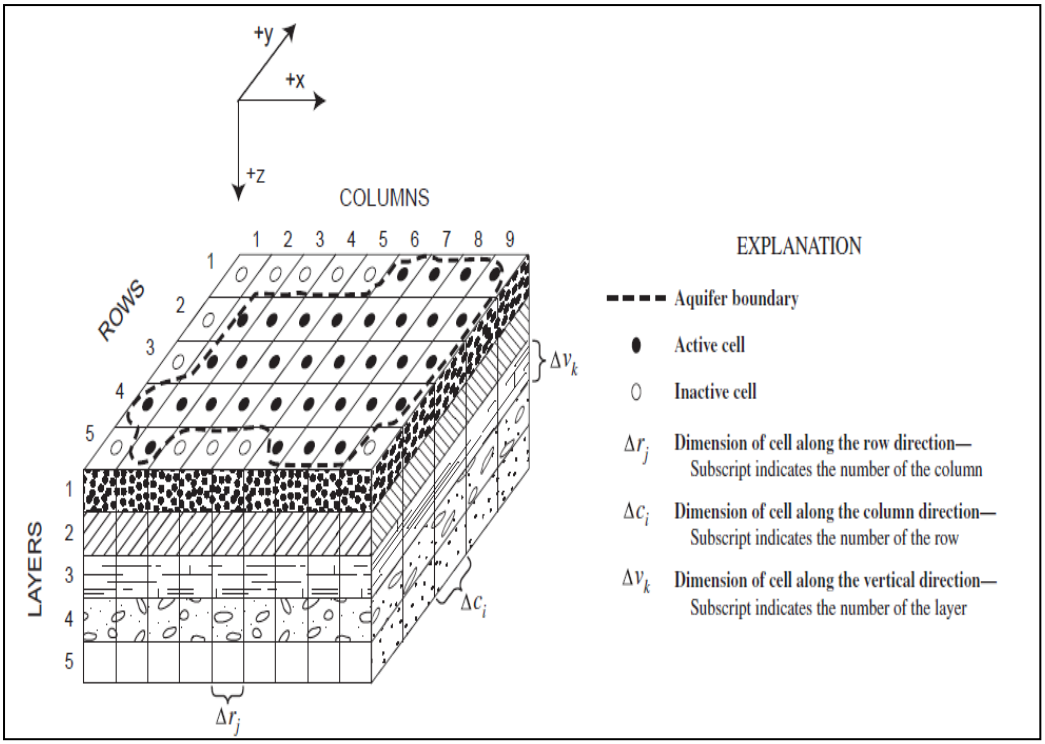

Figure 4-9 Hypothetical aquifer system used for the discretization

(Source:- (Harbaugh, 2005))

The head and flow magnitudes in the partial differential equation that describe the principle of mass balance in the groundwater movement vary in all three axes (x, y, and z). To solve the groundwater equation, the initial (steady state and unsteady state) and boundary condition (specific flow, specific head, recharge, and head-dependent flow) must exist and the solution is not simple. So, the finite difference method is used for solving such numerical problems by a finite set of discrete points in space and time with the assumption that each discrete block is rectangular in both horizontal and vertical directions. In the steady state condition, there is no change in storage within the basin which leads the right-hand side to zero. The details of the model are available in Harbaugh (2005).

4.5.2 Groundwater model setup

The watershed boundary (613 km^2) within the KV was used for the study, as shown in Figure 3-1, is considered as the modeling domain. Entire modeling domain is divided into three vertical layers, namely, shallow aquifer, aquitard, and deep aquifer, referring to earlier studies. Each layer is assumed as each vertical block in the model. Depth to each layers/blocks is assigned based on Pandey and Kazama (2011). The modeling domain in horizontal plane is discretized into the 500m × 500m grid cell having the unique surface

and subsurface characteristics, which results a total of 62 numbers of row and the 66 numbers of column to cover the entire modeling domain (as shown in Annex-III). The object layers (ground surface, initial water level, deep aquifer, aquitard, shallow aquifer layer, hydraulic conductivity, recharge, pumping well, river reach, observation well, etc.) are formatted for the initial input to the model. The active and passive grids in the model domain are assigned through the object layers. The recharge in the basin is assigned in terms of fraction of precipitation as well as LULC change. Pumping data was taken through the hydrological model and other input data were assigned as a input data features. The elevation and pumping rate are assigned at the Center of Gravity (CG) of grids. The graphical interface Model-Muse has been used in this study to create and run MODFLOW input files. Newton Solver (NWT) package has been used to solve MODFLOW equations. After selecting other desired MODFLOW packages, shape files, generated from GIS tools, were imported to Model-Muse. The inputs file in the form of object was generated through the GIS tools. They include grid file with active and inactive cells indicated, model layer elevations, stream segments and properties, shallow aquifer pumping rate, deep aquifer pumping rate, observation wells from shallow aquifer, and HRUs for applying HRU-wise hydrogeological properties. Detail maps are given in the Annex-III.

The 486 HRUs generated from the SWAT model were re-classified in 44 units (Figure 4-10) having similar properties to simplify set-up for model calibration. Initial hydraulic conductivity value of the each HRUs were assigned based on the previous hydrological model outputs and modified it during calibration of model. Similarly, in the hydraulic properties of aquifers, aquitard, rivers were also assigned in model. Nine river segments were used as drainage of the basin and the information of river conductance, river bed level, water level, and bank information with the DEM and field observation. 41 nos of observation well and 258 nos of pumping wells information were used in the model well package. For better analysis, shallow as well as deep aquifer pumping was used and the scenario was taken from the available data and the previous study (Adhikari, 2017; Basnet, 2016). All the layer data was taken from Pandey et al. (2010) and the previous study (Adhikari, 2017; Basnet, 2016; K.C., 2011; Regmi, 2017). The initial data, objects, and layers were prepared with the application of the GIS tools and import to the model. Water demand of each grid cells were calculated from the population density of the VDC, per capita water demand, and position of urban development in the LULC grid value.

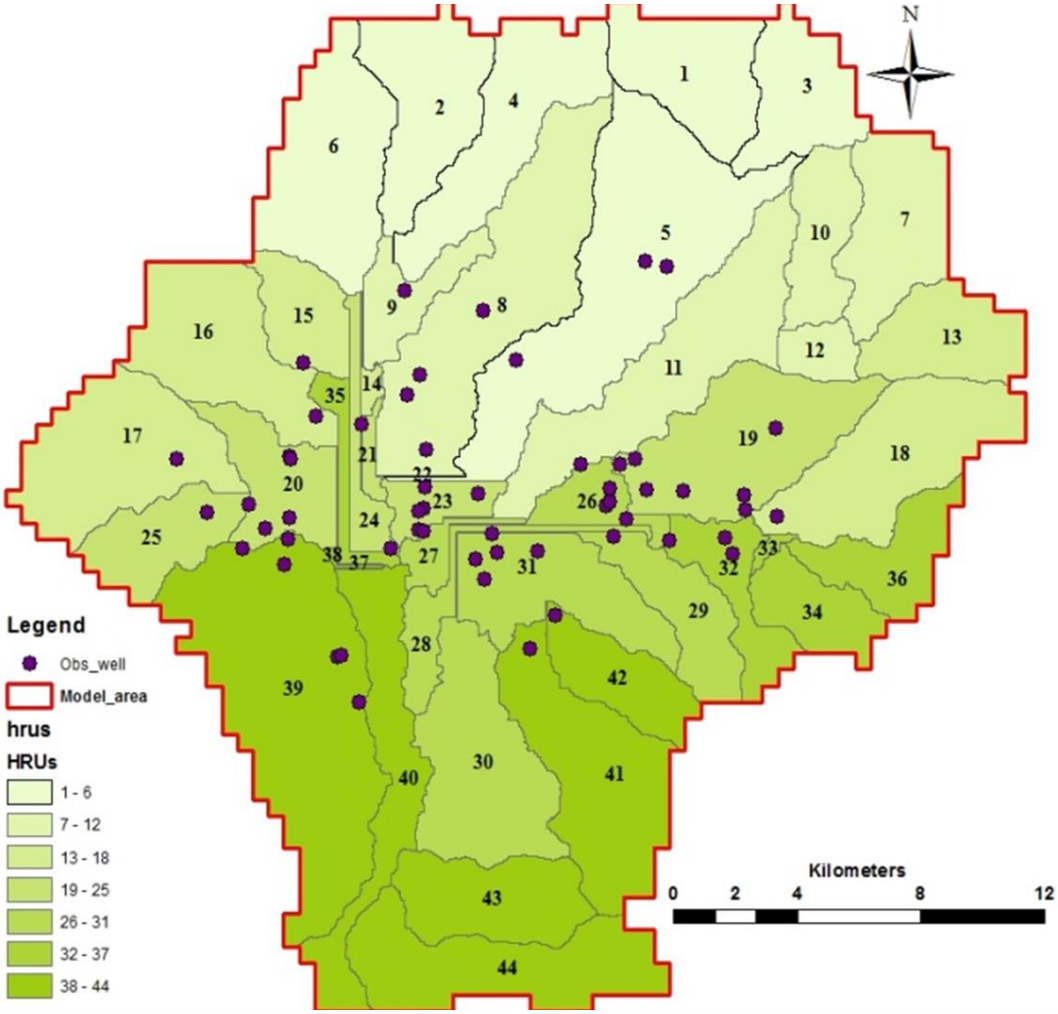

Figure 4-10 HRU map for Kathmandu valley

The KV groundwater system is assumed as a closed and isolated groundwater basin, with irregular and discontinuous aquifers. Sand beds are the principal aquifers with fluvial lacustrine sediment. They are predominant along with the northern and northern eastern part of the valley and occur along the alluvial fans and intercalated with clay and silts. In the core valley area (central part), sand and gravel layers are overlain by a thick (about 200 m) sequence of lacustrine clay. Similarly, gravel and sand units are inter-bedded with clay and silt layers in the south and southwestern part. Hills along the southwestern, southern, and south-eastern margins of the valley consisting of carbonate rocks have been classified as exposed aquitard (Cresswell et al., 2001; Metcalf & Eddy, 2000). The cross-sectional area and plan of subsurface geology are shown in Figures 3.5 and 3.6. The groundwater formation of KV is classified into shallow and deep aquifer separated by aquitard layer as per the pervious study (Cresswell et al., 2001; Metcalf & Eddy, 2000; Pandey et al., 2010).

Shallow aquifer

Shallow aquifer also known as unconfined zone lies north of Maharajgunj and Boudha and west of Gokarna extending to western and northern foothills of the valley. Medium to course-grained sand, gravelly sand and silty-sand compromises the major aquifer material. The shallow aquifer corresponds to Itaiti, Thimi, Patan and Gokarna Formation (Gurung et al., 2007; K.C., 2011; Metcalf & Eddy, 2000; Pandey and Kazama, 2011). It is up to 85 m thick in some places. The shallow aquifer is thicker towards the northern part of the basin. In the southern and some central parts of the Kathmandu Valley, the thickness of the aquifer is very small or null. In this aquifer, standing water levels are between 1 m to 20 m below ground level, increasing towards the southwest (K.C., 2011).

Aquitard

The aquitard layer is the separating hydrogeological units between shallow and deep aquifer. The aquitard layer varies from less than few meters to more than 200m. The thickness of clay aquitard is more at the center of the valley and decreasing slowly towards north and southern part. In the southern part of the valley clay aquitard is pinched out the shallow aquifer corresponding to Kalimati Formation and Lukondol formation. At the northern part of the valley (Gokarna and Manohara) and small southern part (Chapagaon), there is no evidence of the existence of the clay layers and these are the major recharge zones for the deep aquifer (Gurung et al., 2007; K.C., 2011; Metcalf & Eddy, 2000; Pandey and Kazama, 2011).

Deep Aquifer

Deep Aquifer also known as confined aquifer consists of coarse to very coarse sand, pebble, cobble and gravel. The deep aquifer corresponds to Bagmati and Tarebhir formation. The confined aquifer zone lies south of Maharajgunj and Boudha and extends to southern and western boundaries from Bode in the east. This aquifer thickens more than 300m beneath the Kathmandu and Patan cities in the center of the basin. It becomes thinner to the margins where it is in hydraulic contact with the upper aquifer (Gurung et al., 2007; K.C., 2011; Metcalf & Eddy, 2000; Pandey and Kazama, 2011).

Hydrogeological Districts

Based upon physical and chemical characteristics of the groundwater and geological conditions, JICA (1990) divided the deep part of Kathmandu basin into three groundwater districts; Northern Groundwater District (NGD) (156 km^2), Central Groundwater District (CGD) (114 km^2), and Southern Groundwater District (SGD) (56 km^2).

Hydraulic properties

Hydraulic properties including both horizontal and vertical hydraulic conductivities are key components for calibrating the groundwater model. The hydraulic property data for the Kathmandu aquifer system is derived from data published in previous studies (K.C., 2011; Pandey and Kazama, 2011). Hydraulic properties of the different geologic units have been reported by Pandey and Kazama (2011). The hydraulic conductivity of shallow aquifer ranges from 12.4 to 44.9 m/day with an average value of 23.7 m/day. The shallow aquifer has higher conductivity than deep aquifer. The hydraulic conductivity of the deep aquifer is reported to be 0.3 to 8.8 m/day with an average value of 4.5 m/day. The hydraulic conductivity of shallow aquifer is found to be 5 times higher than that of deep aquifer. The transmissivity of shallow aquifer varies from 163.2 to 1056.6 m^2/day with an average value of 609.9 m^2/day whereas that for deep aquifer varies from 22.6 to 737 m^2/day with an average value of 379.9 m^2/day. The transmissivity of shallow aquifer is found to be 1.6 times higher than deep aquifer. The storage coefficient of the shallow aquifer is almost constant through the study area with value 0.2. The storage coefficient of the deep aquifer varies from 0.00023 to 0.07.

4.5.3 Calibration and validation of MODFLOW model

The calibration and validation is an important component in the model simulation to ensure reliability of model for any further use such as scenario analysis. The groundwater flow model was calibrated against observed groundwater level data at 41 monitoring wells (see Figure 4-10 for their location) in 2016. The dry season (October to March) data was used for model calibration and wet season (April to September) data for validation. The model was calibrated by minimizing the error between observed and simulated heads at the observation wells in the steady-state condition. The calibration was performed manually and performance was evaluated based on following statistical indicators: Root Mean Square (RMS), PBIAS (Percent bias), Nash-Sutcliffe Efficiency (NSE), Mean Error (ME), and Mean Absolute Error (MAE). They are widely used for assessing goodness of fit of the model simulated data. Detail of PBIAS and the NSE process is already described in section 2.3.3 and 4.4.2, respectively. In the groundwater model NSE and PBIAS indicator always show the good performance even model outputs are not perfect. So, ME and MAE indices are showing a more reliable performance than others (Adhikari, 2017; Aghlmand and Abbasi, 2019). Mean error (ME) means the cumulative error between the observed and simulated outputs and it is expressed as per Equation 4.24.

$$ME = \frac{1}{n}\sum_{i=1}^{n}(h_0 - h_s) \quad 4.24$$

Where, h_0, h_c, and n is the observed head, simulated head and the number of observations well respectively. The zero value of ME gives the perfect evaluation, the positive value of the indices indicates the over pumping or the greater value of the parameters and negative value mean underestimation of the model outputs. Only single indicator is not perfect for judgment because some times greater error (positive and negative) value is also generating the better significant due to cumulative of positive and negative value. So, mean absolute error (MAE) gave the absolute cumulative error between observed and simulated value as per Equation 4.25.

$$MAE = \frac{1}{n}\sum_{i=1}^{n}|(h_0 - h_s)| \quad 4.25$$

MAE indicates the positive average error of the model, zero is the perfect goodness of fit and the higher value means the deviation through the mean value. Root mean square or the standard deviation is the same in the steady-state condition and it measures the mean of the square of the difference of the error as per Equation 4.26. It gives a higher error value than the MAE and if some outliers' value may generate the insignificant results from the indices.

$$RMS = \left[\frac{1}{n}\sum_{i=1}^{n}(h_0 - h_s)^2\right]^{0.5} \quad 4.26$$

The calibration and validation of the model were conducted in the steady-state condition in a seasonal variation. In the seasonal analysis, the observational data will be the change in the significant compare the daily, weekly, and even monthly (Aghlmand and Abbasi, 2019). Here only 2016 wet and dry season, 41 nos of observation well data was only available. The data was split in the dry season for the calibration and the wet season for the validation.

4.5.4 Developing spatially distributed recharge rates map

The spatial variation in LULC change and soil characteristics affect the present and future recharge capacities. The maximum recharge capacity in each grid cell can be obtained by the field test or the theoretical potential recharge technique. The theoretical potential recharge capacity, defined as the maximum recharge capacity of the soil without any obstruction, is the unit-less or non-dimensional value that can be updated with field data. Average deviation factor or Adjustment Factor (AF) between observed and simulated infiltration value from theoretical method is obtained by the simple mean deviation factor as per Equation 4.27.

$$A\,F = \frac{1}{n}\sum_{k=1}^{n}\left(\frac{Rf_k}{Rt_k}\right) \quad 4.27$$

Where, Rf_k, Rt_k, and n refer the field test recharge capacity value, theoretical recharge capacity, and number of field test, respectively. The unique value of the AF represents the perfect evaluation of recharge/infiltration capacity between the field and theoretical process. If the value of AF is greater than one, it signifies under-estimation from the theoretical method and less than one means over-estimation. Theoretically generated recharge map of the modeling domain was compared with the field test data map. The unit-less grid recharge was converted into the field recharge value by multiplying with the AF as depicted by Equation. 4.28.

$$R_i = Rt_i \times AF \quad 4.28$$

Where R_i and Rt_i represent the adjusted recharge capacity and theoretical recharge capacity of the soil in grid cell i respectively.

We developed an equation to express the groundwater recharge capacity as a fraction of precipitation, which depends up on the seasonal variability. The maximum recharge capacity of each grid value is standardized, based on normalization technique shown in Equation 4.29

$$Rv_{i,n} = P_{i,n} \times \left[\alpha_n^{min} + \left\{\frac{(R_{i,n} - Rmin_n)}{(Rmax_n - Rmin_n)}\right\} \times \left(\alpha_n^{max} - \alpha_n^{min}\right)\right] \quad 4.29$$

Where, $Rv_{i,n}$, $P_{i,n}$, α_n^{max}, α_n^{min}, $R_{i,n}$, $Rmin_n$, and $Rmax_n$ represent the actual recharge from the grid i in n year/seasons/months, precipitation, maximum permissible limit factor, minimum permissible limit factor, adjusted recharge capacity in the grid i in n year/seasons /months, minimum recharge capacity value in the n year/seasons /months, and minimum recharge capacity value in the n year/seasons /months respectively. The grid precipitation was calculated from the observed precipitation data and recharge capacity in each grid was calculated from Equation 4.29. The maximum and minimum recharge values (i.e., R_{max} and R_{min}) were taken from Lamichhane and Shakya (2019a).

The spatially distributed precipitation map is prepared based on station-based precipitation data in the study domain. The calibrated parameters of recharge, minimum and maximum factors, the recharge capacity, and the spatial distributed precipitation of each grid cell values are used to generate the actual recharge depth in spatial raster map or the object. The obtained object is used as the recharge input parameters during the simulation.

4.5.5 Evaluation of GW pumping rate

The available 258 deep well data was used in this study, but data from shallow well pumping are not available for Kathmandu Valley. In the Kathmandu valley, household level well, community level stone spouts, and common wells are being used traditionally, so, a lot of time and cost should be invested to collect all the shallow well data. To this end, theoretical water balance techniques are adopted to calculate the shallow pumping rate. Change in storage of the basin was considered for the shallow pumping value and the output was adopted from Adhikari (2017).

The change in groundwater storage within the basin HRUs was calculated for both wet and dry seasons. These pumping volume and rate were distributed in each grid value with reference to the population density of the VDCs. The pumping rate of each grid was then assigned. HRUs located on open land or lands without built-up area are assumed as no pumping area.

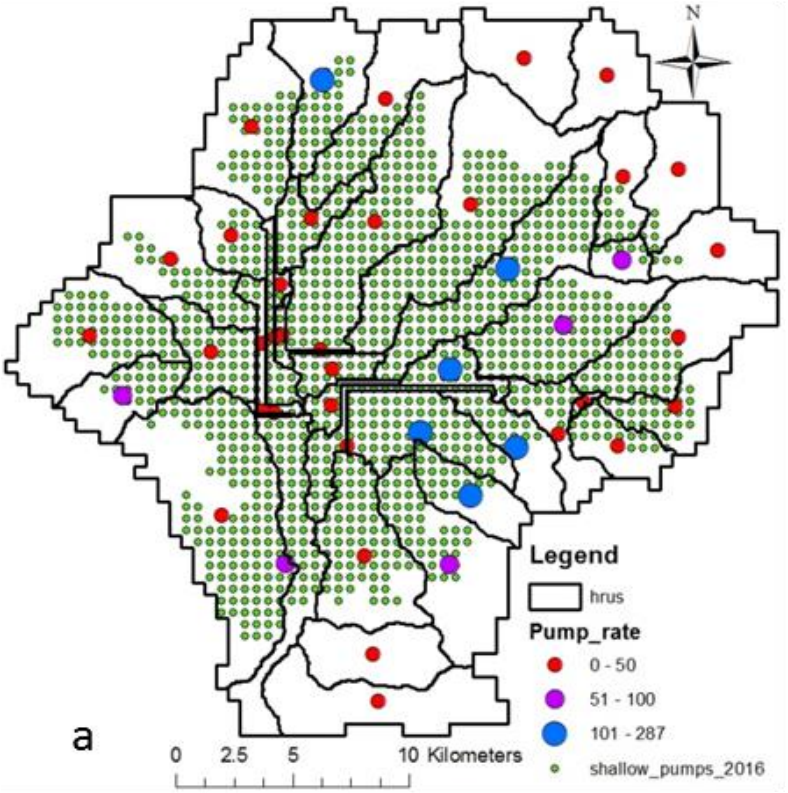

Figure 4-11 Calculated HRUs wise Pump rate in lpcd,

The assigned pump rates for each HRU are shown in Figure 4-11. The current change in storage due to the pumping rate calculation of the HRUs is shown in the Table 4-5.

Table 4-5 Pumping data for shallow aquifer in 2016

(Sources:- Adhikari (2017))

HRU_ID	x	y	Pumping rate per pump (2016) (m^3/day)	Remarks
2	630696	3075231	35	out of KUKL service area
6	627625	3073242	2.5	
7	645899	3071417		
8	632930	3069183	165	
9	630198	3069341	110	
10	643513	3071101		few well points, cannot estimate
11	638614	3067182	115	out of KUKL service area
12	643457	3067547	30	
13	647563	3067975		few well points, cannot estimate
14	628880	3066517	5	
18	645882	3064268	30	few well points, cannot estimate
19	640994	3064764	30	
20	625917	3063628		
21	628953	3064350	5	
22	630580	3063726		
23	631080	3062905	5	
24	628683	3064265	5	
25	622139	3061799	90	
26	636165	3062916	60	
27	631062	3061376	5	
28	631723	3059629	5	
29	638959	3059578	70	out of KUKL service area
30	632482	3054930	5	few well points, cannot estimate
31	634885	3060208	225	out of KUKL service area
32	640732	3060153	30	
33	641837	3061493		very small area with no wells
34	643298	3059649		
35	628098	3064000	5	
36	645772	3061304		
37	628581	3061029	5	
38	628103	3061152	5	
39	626369	3056690	30	few well points, cannot estimate
40	629107	3054644	30	
41	636091	3054577	110	few well points, cannot estimate
42	636994	3057527	210	out of KUKL service area

The value of the shallow pumping well was assigned to grid cell. It is assumed that the pumping well is in the center of gravity of the cell and effect is equally distributed throughout.

4.5.6 Development of future pumping scenarios

Groundwater pumping rate is one of the important data components for groundwater modeling with MODFLOW. But groundwater pumping data (i.e., location, rate or volume of pumping, and trends over the years) are not available for shallow aquifer in the KV. In fact, the pumping of groundwater from unconfined shallow aquifer is increasing rapidly at the household level. There are no actual records of such pumping and neither much is known about its future due to the lack of database. Shallow water pumping rate is analyzed by the water balance equation in surface hydrology from the rainfall runoff model as per Equations 2.45, 2.46, and 2.47 Figure 4-11 and Table 4-5 (Adhikari, 2017). The rate of change in the water demand is calculated as a product of linear population growth rate and the per capita demand with the base pumping. Future pumping scenario is taken by using three growth rates; 1% for the areas with greater pumping rate and developed areas (> 100 m^3/day), 1.5% for newly developing areas (pumping rate between 50 to 100 m^3/day), and 3 % (pumping rate less than the 50 m^3/day) for the areas in the peripheral parts of the valley.

The output of the pumping rate with corresponding water deficit was also checked with the SWAT model outputs and the result is comparable to the PRMS model developed by Adhikari (2017). Due to limited availability of well samples for groundwater table for dry and wet season of the year 2016 (sample conducted by working group-2 of SATREPS project) and well samplings not representing spatial distribution over the study area very well, the calculated pumping rate needs some adjustment while being used in MOFLOW model. Final HRUs wise pump rate in liter per person per day assigned in MODFLOW is shown in Figure 4-11.

Assumptions made while fixing shallow pumping wells are listed hereunder;

- Wells are fixed at the CG of (500mx500m) grids. Assumption is that such pumps will represent all shallow wells in that grid area and will give the same drawdown effect.
- Assigned pumping rate is based on pumping value found from water balance of calibrated/ validated from the hydrological model.
- The Pumping rate is found by equation (Pumping volume from HRU)/ No of pumps/ observation time in days).

- In some HRUs, there is observation well, but no pumping rate. In such HRUs, pumping rate is assigned based on neighbor similar HRUs given that area is not Kalimati formation area.
- All pumps (fitted at cg of grids) beyond the boundary of GW zone are of no significance, so removed.

4.5.7 Development of future LULC change scenario for groundwater model

Encroachments of the potential recharge areas and their impacts to the surface runoff and recharge is taken from previous studies (Lamichhane and Shakya, 2019a, 2019b). The studies highlighted that 6% (3.99 km^2) of the rechargeable areas would be converted to the impermeable surface due to growth of the physical infrastructures. The simulated annual average and minimum river runoff from the model including the LULC change resulted the average increment of 1.3% and decrement of 3.45% per year, respectively. The groundwater recharge is projected to decrease by 2% in every decade in the groundwater basin.

The study delineated the potential groundwater recharge area and the projection of the future scenario as per the urbanization pattern. The main principle of the scenario is that, the recharge tendency in each grid will vary with the LULC change. The surface recharge capacity will be decrease with the change context due to urbanization. So, recharge depth of the cell is the function of the precipitation and the potential groundwater recharge map of the basin. The minimum and maximum recharge capacity of the cell is estimated through model calibration process as describe above. The obtained spatially distributed raster or object outputs for spatially distributed recharge are assigned in the model for the future analysis.

4.5.8 Assessing impacts of future scenarios on drawdown

Due to projected changes in LULC and pumping rates, drawdown (or depth of groundwater table from ground surface) is also expected to change, both spatially and temporally. Increase in pumping rate and encroachment of potential recharge areas are likely to increase drawdown in future. Under both the scenarios considered, changes in drawdown and its spatial distribution are estimated by subtracting future drawdown from baseline drawdown. The outputs are presented in the form of geo-spatial maps and tables.

4.6 Data and sources

Both spatial and temporal data were collected from the concerned sources. Bio-physical, climatic (both observed and climate model outputs), socio-economic, hydrological,

hydrogeological, water supply and groundwater pumping data were collected from the concern agency and field. The pre and post processing for the results were performed by applying appropriate tools for the study. Details of data, their characteristics, and sources are presented in Table 4-6.

Table 4-6 List of data, characteristics, sources and processing tools

Type of Data	Sources	Resolution	Year/ Length	Processing tools
DEM	Advanced Spaceborne Thermal Emission and Reflection Radiometer (ASTER) Global Digital Elevation Model (GDEM) version 2 (USA)	30 m	2009	ArcGIS - 10.2
Geology	Department of Mines and Geology	1:50000	1998	ArcGIS - 10.2
Soil	Soil and Terrain Database (SOTER)	1:1000000	1998	ArcGIS - 10.2
Land use/ cover (LULC)	USGS (Land sat 5 to 8 image) and ICIMOD	30 (m)	2010 – 2018	ArcGIS - 10.2
Future climate (ACCESS-CSIRO-CCAM)	Collaboration for Australia Weather and Climate Research, Australian Government	1.25×1.40625°	1975–2099	ArcGIS10.2 (for processing netCdf files)
Future climate (CNRM-CM5)	Centre National de Recherches Me´te´orologiques (CNRM), France	1.4008×1.875°	1975–2099	ArcGIS10.2 (for processing netCdf files)
Future climate	National Center for Atmospheric Research	0.9424× 1.25°	1975–2099	ArcGIS10.2 (for

Type of Data	Sources	Resolution	Year/ Length	Processing tools
(CCSM4)	(NCAR), USA			processing netCdf files)
River runoff	DHM	Daily	2000-2014	Khokana (st no:-550.5)
Temperature	DHM	Daily	2000-2014	5 station
Precipitation	DHM	Daily	2000-2014	21 station
Relative Humidity	DHM	Daily	2000-2014	7 station
Solar Radiation	DHM	Daily	2000-2014	2 station
Wind Speed	DHM	Daily	2000-2014	2 station
Population	CBS, Nepal		1991,2001, 2011	
Settlements	Department of Survey	1:25000	2010	ArcGIS - 10.2
Market	Department of Survey	1:25000	2010	ArcGIS - 10.2
Road Network	Survey Department	1:25000	2010	ArcGIS - 10.2
Aquifer (latitude, longitude, elevation) data	Pandey and Kazama, (2011)	310 points	2011	
Pumping and Observation well	Working Group (WG-2) of WaSH-Mia/ SATREPS project	258 and 41 nos	2016	
Environment and geological	DMG,1998	GIS shape file	1998	

Type of Data	Sources	Resolution	Year/ Length	Processing tools
map				
Water supply data	KVWSMB, MWSP PID, KUKL		2016	

Note: USA: United States of America, USGS: United States of Geological Survey, ICIMOD: International Center for Integrated Mountain Development, CBS: Central Bureau of Statistics, DHM: Department of Hydrology and Meteorology, DMG: Department of Mining and Geology, MWSP PID: Melamchi Water Supply Project Implementation Directorate, GWRDB: Groundwater Resource Development Board, KVWSMB: Kathmandu Valley Water Supply Management Board, and KUKL: Kathmandu Upatyaka Khanepani Limited

Chapter 5. Results and Discussions

5.1 Projected change in land use/cover

Future land use/cover (LULC) was projected using CLUE-S model based on historical changes and bio-physical characteristics of the basin. Sensitivity analysis, validation, and evaluation were performed for reliable projection. Results are presented and discussed hereunder.

5.1.1 Validation of satellite driven data

Historical LULC data was retrieved from the USGS repository in the form of Landsat image and was processed in GIS. The images in Figures 4-2 (a) and 4-4 show the LULC maps between 2010 - 2018. For statistical validation, the observed map of 2010 was overlapped with the ICIMOD (2010) map (Figure 5-1, a). Overall, the LULC map generated in this study showed a good agreement with the map prepared by ICIMOD in 2010. After validation, the value of the Kappa coefficient (K) was obtained to be 0.68 from the analysis. This shows that the generated LULC change map of 2010 and the corresponding processes are considerably accurate. The same signature file and approach were used to generation the corresponding LULC maps from the data retrieved from the USGS repository. The output of the analysis is shown in Figure 5-1, a and the graphical representation of the historical LULC change is shown in Figure 5-1, b.

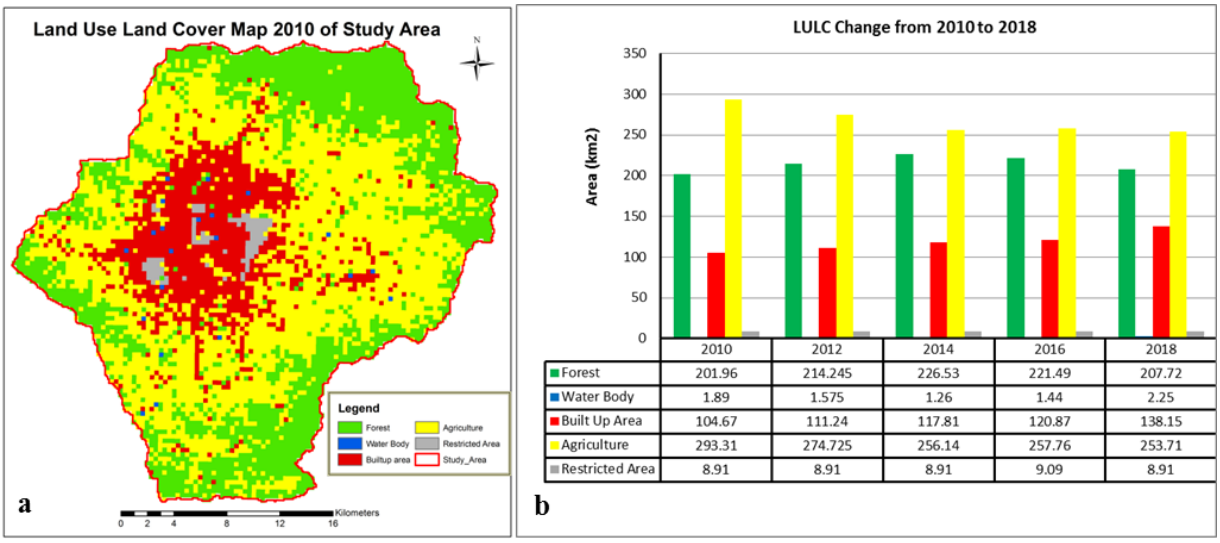

	2010	2012	2014	2016	2018
Forest	201.96	214.245	226.53	221.49	207.72
Water Body	1.89	1.575	1.26	1.44	2.25
Built Up Area	104.67	111.24	117.81	120.87	138.15
Agriculture	293.31	274.725	256.14	257.76	253.71
Restricted Area	8.91	8.91	8.91	9.09	8.91

Figure 5-1(**a**) 2010 LULC map of KV (**b**) Comparative bar diagram and respective LULC value.

Table 5-1 shows that the built-up areas increased by 4.96% and the agricultural area decreased by 6.51% between 2010 to 2018. It is worthy to note that due to the 2015 earthquake, the built-up area had decreased in 2016 but rapidly increased again in 2017 and 2018. Due to effective implementation of community forestry system in Nepal, encroachment of forest area has diminished considerably. As a result of rapid urbanization in the aftermath of 2015 earthquake, forest areas had decreased partially as highlighted by the decrement in the forest cover in 2016. The increase in built-up areas is reducing the agriculture and barren lands, thereby, adverse effects on groundwater are prominent. To assess the future dynamics, restricted areas and water body were considered to be constant.

Table 5-1 LULC conversion matrix during 2010 to 2018

LULC		**Land Use/Cover 2018 (%)**					
		Agriculture Land	Built-Up	Forest	Restricted Area	Water-Body	Grand Total
Land Use/Cover 2010 (%)	Agriculture Land	32.06	8.07	8.73	-	0.04	48.91
	Built-Up	4.00	12.50	0.34	0.11	0.02	16.97
	Forest	6.31	1.26	24.87	0.00	0.02	32.46
	Restricted Area	0.02	0.09	-	1.31	-	1.42
	Water Body	0.02	0.01	-	-	0.21	0.25
	Grand Total	42.40	21.93	33.94	1.42	0.30	100.00

Increase of the built-up area and decrease of the open land means that the surface of the basin will be impervious. It indicates that in future the groundwater recharge may be decreased and the peak runoff of the river basin may be increased in same precipitation nature.

5.1.2 Evaluation CLUE-S model

To assess the impacts of the LULC change, nine driving forces (Geology, soil type, settlements, road network, river, aspect, slope, population, soil type, and elevation.) were accounted as inputs as discussed in Section 4.1. The ROC value confirms that the logistic regression model can be used to delineate the driving forces. The ROC value equal to or greater than 0.9 shows high precision accuracy, whereas the values between 0.7 to 0.9 are considered as credible accuracy. Similarly, the ROC value below 0.7 is considered as low accuracy scenario (Pointius and Schneider, 2001). The ROC value of all LULC types was greater than 0.83, which shows a credible relationship between the driving forces and each LULC type. The analysis indicates that the regression results are credible and the regression coefficients from the driving forces were valid layers for each LULC change as depicted in Table 5-2.

Table 5-2 Receiver operating characteristic (ROC) curve value of each LULC

LULC Type	Forest	Water Body	Built up	Agriculture	Restricted Area
ROC	0.92	0.87	0.91	0.83	0.94

The sensitivity analysis of the LULC demand for the study area was performed using five demand scenarios as described in Section 4.1.2. The normal land use demand and population growth scenarios were respectively depicted based on the data between 2010-2018 and 1971-2011 for the KV. It is shown that the population projection was not realistic as it indicated that in 2045 all the agriculture land is projected to be converted into built up area and then encroachment of forest is likely to start (Figure 5-2).

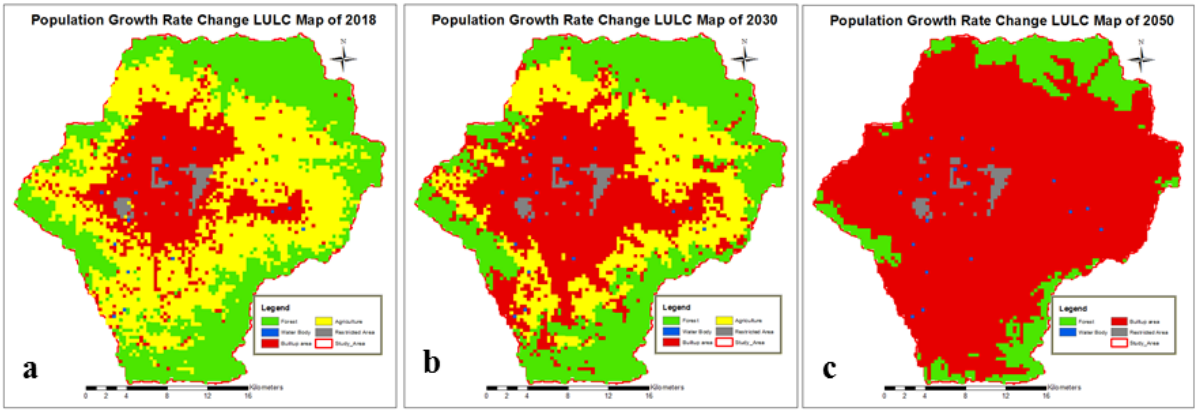

Figure 5-2 Future population growth rate scenario LULC map a) 2018 b) 2030, and c) 2050

It is shown that a half of the normal land use change growth was unrealistic. This scenario is more useful when the government implies the restriction to increase built-up area in the outer periphery of KV. However, the normal land use change seemed to be more pragmatic or credible compared to the other, it takes the historical LULC change pattern as shown in Figure 5-3. Similar type of consideration was also adapted in the study of Shrestha et al. (2018) and the historical data validation of LULC showed that the analysis is in considerable accuracy.

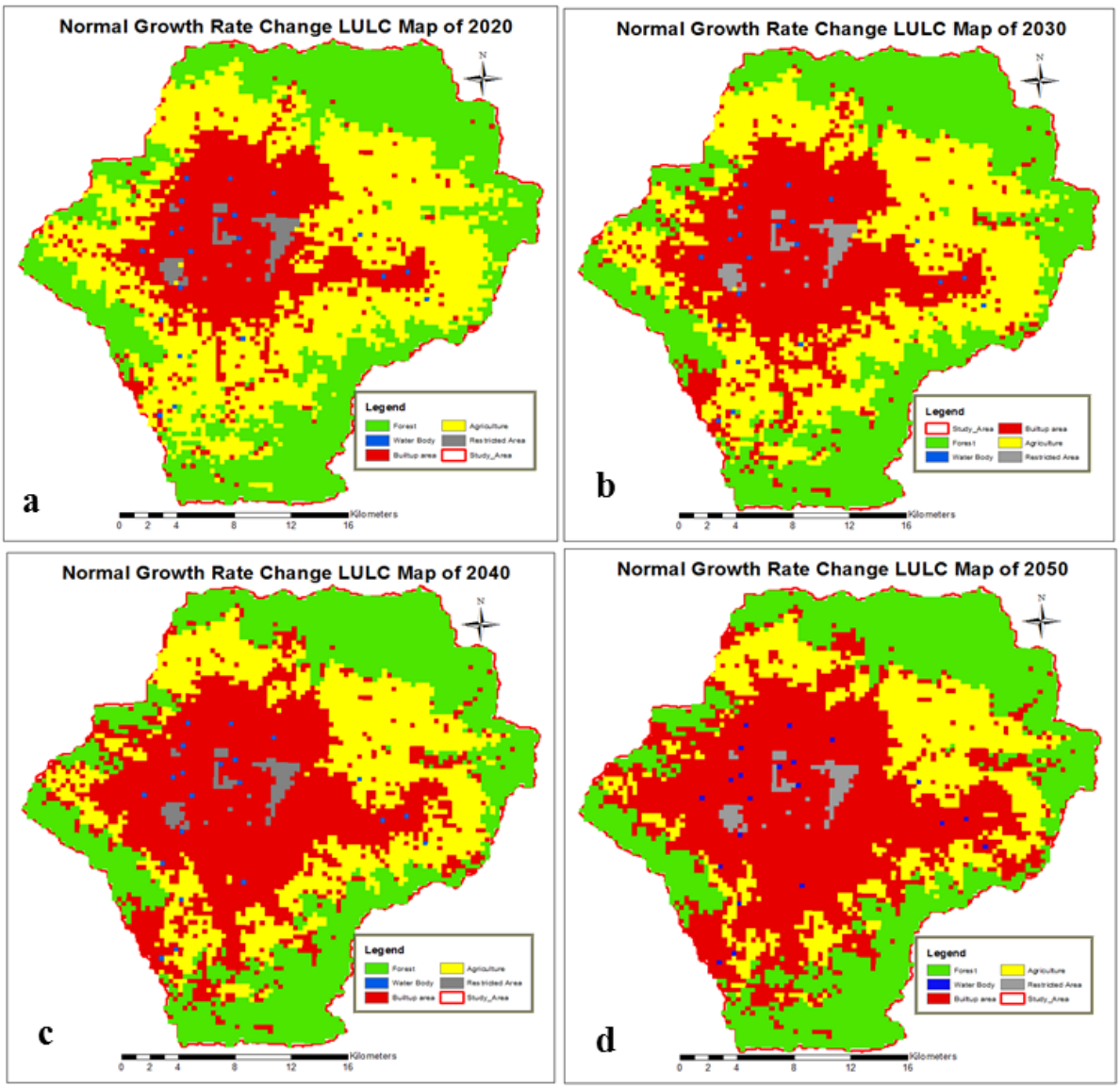

Figure 5-3 Future normal growth rate LULC map a) 2020 b) 2030 c) 2040, and d) 2050.

As per the LULC change scenarios of CLUE-S model, the normal land use change scenario was further considered for analysis. Whereas, water body and restricted areas are taken as the same for all scenarios. It should be noted that the LULC change was mainly due to changes in built-up and agricultural areas. For the validation purpose, the data between 2010-2018 was

used; meanwhile, the projected data between 2020 and 2050 was used for the analysis purpose. To validate the projected map from the CLUE-S model, the Kappa (K) coefficient was calculated for 2014, 2016 and 2018 and the values were obtained as 0.75, 0.64 and 0.62 respectively. The model assumed that urban development is concentrated into the existing core urban area and dense peri-urban neighborhoods; however, the development is fundamentally scattered due to expensive land and scarcity of open areas in the major core urban area.

5.1.3 Future LULC scenario

The CLUE-S model results show that there would be no change in water body, forest and restricted areas between 2020-2030. However, the agricultural area would decline from 40.1% to 33.4% between 2020-2030 (Table 5-3). The average annual decrement of the fertile land is estimated to be 0.67% (4.07 km^2) due to conversion into built-up areas. The built-up areas in the KV are estimated to increase by 6.8% between 2020-2030 as shown in the table appended to Figures 5-3, a and b.

Table 5-3 LULC conversion matrix during 2020 and 2030

LULC		Land Use/Cover 2030 (%)					
		Agriculture Land	Built-Up	Forest	Restricted Area	Water-Body	Grand Total
Land Use/Cover 2020 (%)	Agriculture Land	33.4	6.2	0.5	-	-	40.1
	Built-Up	-	23.4	-	-	-	23.4
	Forest	-	0.7	34.	-	-	34.7
	Restricted Area	-	-	-	1.5	-	1.5
	Water Body	-	-	-	-	0.3	0.3
	Grand Total	33.4	30.3	34.5	1.5	0.3	100.0

Similarly, agricultural areas between 2030 to 2040 is projected to decrease by 7.2% (Table 5-4) due to increase in built-up area as per. From the inspection of the two maps, most of the urbanization process is concentrated in the peri- urban areas of the KV (Figures 5-3, c and d). The model follows similar trend between 2040 to 2050 as well (Figure 5-3; Table 5-5).

Table 5-4 LULC conversion matrix during 2030 to 2040

LULC		Land Use/Cover 2040 (%)					
		Agriculture Land	Built-Up	Forest	Restricted Area	Water-Body	Grand Total
Land Use/Cover 2030 (%)	Agriculture Land	26.2	7.2	-	-	-	33.4
	Built-Up	-	30.3	-	-	-	30.3
	Forest	-	0.5	34.0	-	-	34.5
	Restricted Area	-	-	-	1.5	-	1.5
	Water Body	-	-	-	-	0.3	0.3
	Grand Total	26.2	38.0	34.0	1.5	0.3	100.0

Table 5-5 LULC conversion matrix during 2040 to 2050

LULC		Land Use/Cover 2050 (%)					
		Agriculture Land	Built-Up	Forest	Restricted Area	Water-Body	Grand Total
Land Use/Cover 2040 (%)	Agriculture Land	19.7	6.2	0.3	-	-	26.2
	Built-Up	-	38.0	-	-	-	38.0
	Forest	-	0.5	33.5	-	-	34.0

	Restricted Area	-	-	-	1.5	-	1.5
	Water Body	-	-	-	-	0.3	0.3
	Grand Total	19.7	44.7	33.8	1.5	0.3	100.0

The agricultural and forest areas are estimated to be decreased by 20.4% (125.05 km^2) and 0.9% (5.51 km^2) respectively between 2020-2050. The increase in built-up areas is estimated as 21.3% (130.57 km^2) (Table 5-6). In 30 years, 50% of the agricultural area will be changed to urban areas in the KV. In case of continuation of the same urbanization trend, more irrigable land would convert to built-up area, which may ultimate pressurize the open and restricted areas. Eventually, reduction in agricultural products, loss of soil fertility, and increment in food deficiency will be more prominent.

Table 5-6 LULC conversion matrix during 2020 to 2050

LULC		Land Use/Cover 2050 (%)					
		Agriculture Land	Built-Up	Forest	Restricted Area	Water-Body	Grand Total
Land Use/Cover 2020 (%)	Agriculture Land	19.7	19.6	0.8	-	-	40.1
	Built-Up	-	23.4	-	-	-	23.4
	Forest	-	1.7	33.00	-	-	34.7
	Restricted Area	-	-	-	1.5	-	1.5
	Water Body	-	-	-	-	0.3	0.3
	Grand Total	19.7	44.7	33.8	1.5	0.3	100.0

Reduction in groundwater recharge due to conversion of potential groundwater recharge areas into built-up areas would lead to drawdown in the groundwater table. The reduction in open areas due to urbanization from 2010 to 2018 was obtained as 10.4% (63.54 km^2) throughout the basin as shown in Figure 5-4, a. The LULC map for 2050 depicts that 21.4 % (130.68 km^2) of the open areas would be converted into built-up areas Figure 5-4, b. By increasing population and built-up area in the valley creates loss of production of agricultural food. In the near future, reducing the fertile land may create deficits of resources in the basin. The outputs of the LULC change model are also useful for the policymaker in the land resources planning, protection for the potential recharge area, and delineation of the probable urban growth area.

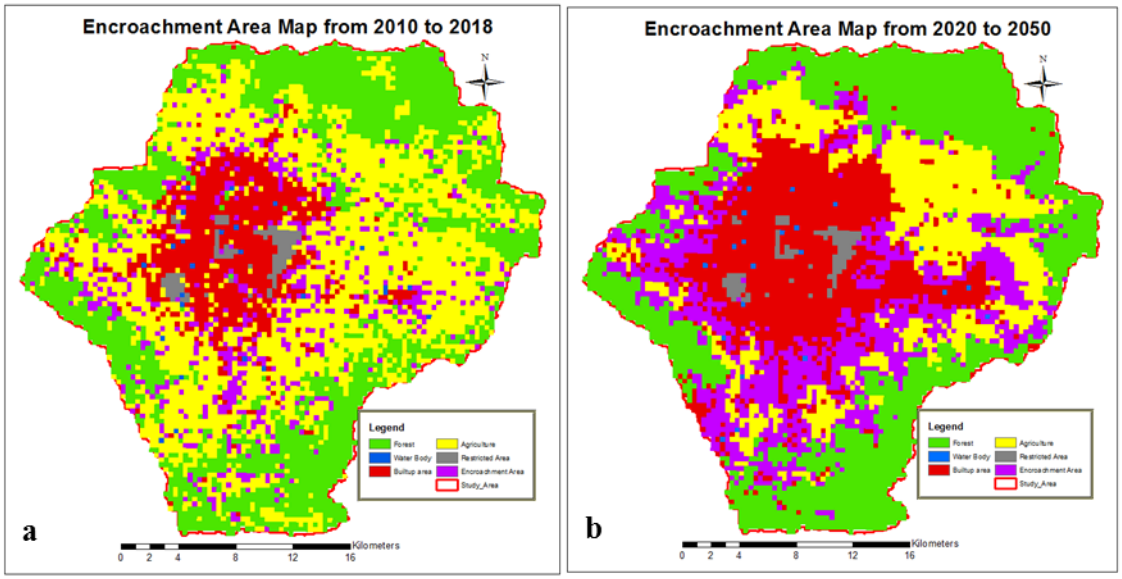

Figure 5-4 (a) Encroachment of open area map (Land conversion) of KV between 2010 to 2018; (b) Encroachment of open area map (Land conversion) of KV between 2020 to 2050.

5.2 Potential recharge areas for groundwater

Haphazard urbanization, LULC change, and encroachment open area are contributing to shrinking of the potential groundwater recharge areas in the KV. Such anthropogenic activities have increased the water demand and reduced the recharge tendency of the basin by declining the potential recharge area.

5.2.1 Delineation of theoretical potential areas for groundwater recharge

Potential areas for groundwater recharge were identified based on an index computed as a weightage overlay of overall ten thematic layers (three in primary ten in secondary hierarchies). Weights were assigned using AHP method. For the analysis, all required

thematic layer data was generated through the GIS tools and evaluated by the method. Each thematic layer was assigned to a grid value between 1-9 by pair-wise comparison. The weightage value of each layer was assigned as per previous literatures and expert knowledge (30 experts, mostly from the field of water resources, hydro-geology, and civil engineering) (Jhariya et al., 2016; Singh et al., 2018; Chaudhary et al., 2016). The consistency ratio (CR) obtained for each thematic layer was limited to 8% indicating the consistency of analysis. This highlights that the generated data from each layer was suitable for the future AHP analyses. The CR value of 9.7% highlights that the pair-wise comparison is more consistent (Saaty, 2004) leading to a more realistic output weightage. The comparison matrix and weightage factors for each layer are outlined in Table 5-7. The matrix was generated from the expert opinions considering that each layer influences the rate of groundwater recharge.

The analysis was performed that the topographical characteristics (63.92%) weightage of the study area is more predominant compare to the climate characteristics (28.91%) and socio-economic characteristics (7.17%). But the individual analysis showed precipitation (climate) as the most significant factor with 28.91% weightage for the groundwater recharge. Similarly, geology and land use were also found to be significant factors with weightages 18.52% and 17.16% respectively. Despite this, riverbank, which is formed due to deposition of river sediments, showed weightage of 12.89% as the bank area has high infiltration capacity. Slope modifies the contact time of runoff water and soil layer and higher slope leads to high velocity indicating less recharge and vice versa. By using GIS layers data of those ten factors and AHP weights factor the potential groundwater recharge area map was identified as shown in Figure 5-5, b. The output data by the combination of the layers are categorized with its value by using the quantile technique in GIS tools. The output map showed that the northern part of the valley had the high potential for the recharge compare to the other. Similarly, JICA, (1990) also gave some results about the recharge area of the valley, the north-eastern part of the valley had also high capability to recharge but after down the southern and western part the value was decreased. The geological formation in that area was more suitable for the recharge and storage of the groundwater (JICA, 1990; K.C., 2011; Pandey and Kazama, 2011; Shrestha et al., 2020).

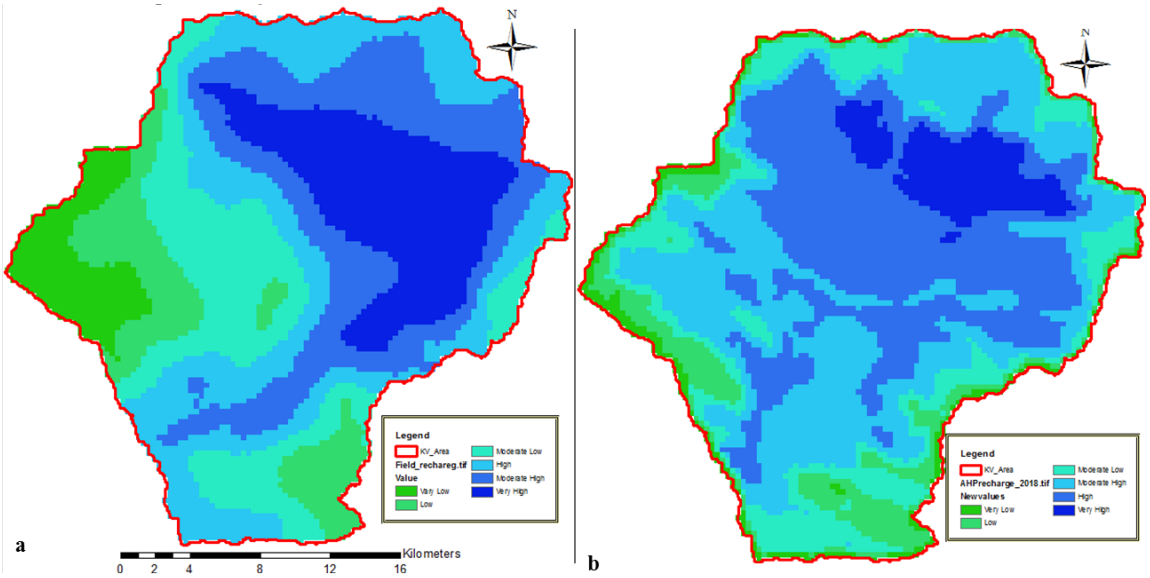

Figure 5-5 (a) Potential groundwater recharge area mapping by using field observation; (b) Potential groundwater recharge area mapping by using AHP method.

Table 5-7 Comparison matrix for delineation of GWPRA and weight factor of each layer

Type	Slope	RD	Geology	LU	PPT	Aspect	Elevation	PD	MD	RD	**%**
Slope	**1.00**	0.50	0.33	0.25	0.20	2.00	3.00	5.00	7.00	3.00	7.65 (T)
RD	2.00	**1.00**	0.50	0.50	0.33	4.00	6.00	9.00	9.00	3.00	12.89 (T)
Geology	3.00	2.00	**1.00**	0.50	0.50	6.00	7.00	9.00	9.00	9.00	18.52 (T)
LU	4.00	2.00	2.00	**1.00**	0.33	4.00	3.00	2.00	9.00	9.00	17.16 (T)
PPT	5.00	3.00	2.00	3.00	**1.00**	9.00	7.00	9.00	9.00	9.00	28.91 (C)
Aspect	0.50	0.25	0.17	0.25	0.11	**1.00**	2.00	2.00	4.00	2.00	4.32 (T)
Elevation	0.33	0.17	0.14	0.33	0.14	0.50	**1.00**	2.00	3.00	1.00	3.38 (T)
PD	0.20	0.11	0.11	0.50	0.11	0.50	0.50	**1.00**	2.00	0.50	2.62 (SE)
MD	0.14	0.11	0.11	0.11	0.11	0.25	0.33	0.50	**1.00**	0.33	1.51 (SE)
RD	0.33	0.33	0.11	0.11	0.11	0.50	1.00	2.00	3.00	**1.00**	3.06 (SE)

Note:- RD:- River Distance; LU:- Land Use; PPT:- Precipitation , PD:- Population Density; MD:- Market Distance; RD:- Road Distance, %:- Percentage; T:- Topographic characteristics , C:- Climatic characteristics; and SE:- Socio-economic characteristics.

5.2.2 Evaluation of theoretical recharge potential areas

To validate the generated potential groundwater recharge areas by AHP method, 83 spouts were identified on the basis of geology, hydrometeorology, and socio-economical changes. Tests were conducted in all locations where changes in land use, geology, and soil texture were identified. The test points were assured with no anthropogenic interventions and identified as open areas. The double ring infiltro-meter (Lucke et al., 2014) was conducted in 83 locations across the KV. The overall location of the field test point is shown in the map (Figure 4-7) and the detail of the study and the field information are presented in the section 4.2.3 and Annex-I respectively. The field infiltration rate (mm/hr) was used to prepare the raster map that was compared with the map generated using AHP to assess the quality of the output from theoretical dissemination. As limited information is available in terms of lithology, water table, soil density, moisture content, among others, the actual recharge rate would be affected considerably. The variation in the grid value the maps could not be exhaustively validated. However, the existing maps and literature (e.g. Adhikari et al., 2019; Pandey and Kazama, 2011; Thapa et al., 2017) highlight that the valley fringes with alluvial deposits and river corridors can be considered as the areas with the most recharge potential. The groundwater potential in the locations was computed using Equation 2.3 and the output of the study area was categorized into six parts as per the quantile mapping in GIS environment. The area covered by very low, low, moderately low, moderate high, high, and very high was respectively 4.29 %, 9.14% and 14.72 %, 32.59 %, 32.89 %, and 7.37 % of the total area as shown in Figure 5-5, a. The high and very high areas are still the open areas at the fringes of northern and eastern parts of the KV. The central valley also has the potential recharge area; however, most of such areas are now converted into built-up areas with no to very low recharge status. The northern and eastern parts of the valley have relatively higher recharge potential; meanwhile, the outskirts of the valley have less recharge potential because of the geological and terrain characteristics.

Through comparison of observed field data with existing literature and maps From the comparison of the observation of field test map, AHP generated map and previous literature and maps (Adhikari et al., 2019; JICA, 1990; K.C., 2011; Pandey and Kazama, 2011; Thapa et al., 2017), the likely recharge zones are found to be comparably consistent. The southern and northern foothills of the valley are the major recharge locations in the KV. If these areas could be preserved and well managed and additional artificial recharge systems be stored, the water security would be assured in the KV. It is found that the theoretically generated maps

from various layers using MCDM techniques are realistic and can be used in the areas with less groundwater recharge information such as Nepal.

5.2.3 Projected encroachments of potential recharge areas

Historical and projected LULC clearly indicate increase in impervious areas. The mushrooming urbanization gravely affects the groundwater recharge. This study depicts the future urban expansion considering the AHP weight factors and the LULC map created using CLUE-S model. Figure 5-6, a and b shows the potential recharge zones for the KV.

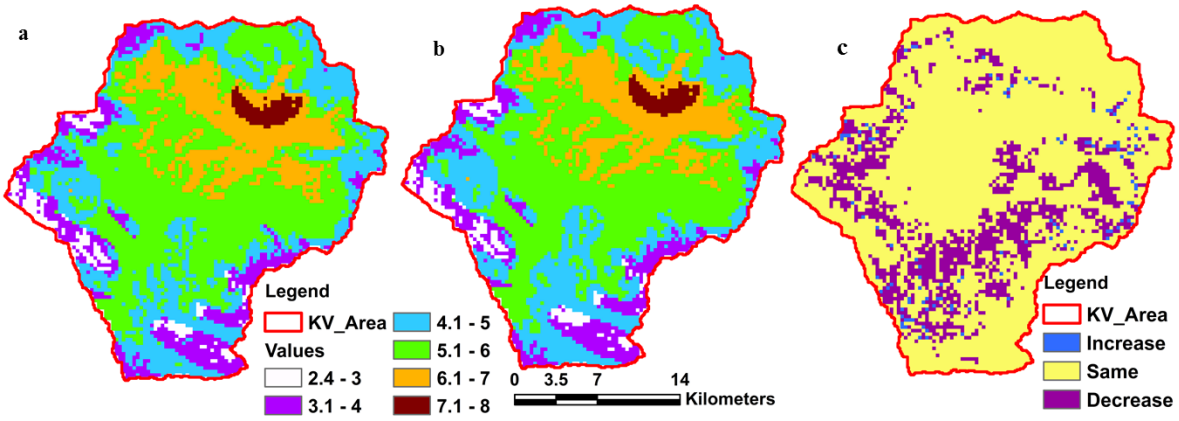

Figure 5-6 (a) Potential groundwater recharge map for 2020 (b) Potential groundwater recharge map for 2050 (c) Encroachment of recharge area potential urbanization during 2020 - 2050.

Figure 5-6 highlights that the open areas would decline by 6% in average in the KV as 3.66 km^2 lands would be converted into built-up area. The inconsistent trend as reported in Table 5-8 is probably due to the fact that this study considers LULC change as the only factor; however, LULC change is not solely the factor that controls recharge.

From the analysis of the maps, the northern and east-northern part has more potential for the groundwater recharge due to good geological formation as well as open forest and agricultural land. Similarly, the northern part of the basin has also greater depth of rainfall tendency compare to the other. So, larger precipitation and maximum infiltration capacity generates the more recharge compare the other. Most of the southern part, hard and less permeable geological formation, sloppy land, and less precipitation is occurred having less groundwater recharge tendency. Now, the urbanization (core and peri-urban area) is the key factor for reducing the recharge tendency of the KV due to rise in impervious surface of the basin.

Table 5-8 Decadal encroachment area and percentage of GWPRA

S.N.	Year	Increase recharge area (km^2)	Increase in percentage	Decrease recharge area (km^2)	Decrease in percentage	Actual Change percentage
1.	2020 - 2030	4.14	0.68	40.41	6.62	-5.94
2.	2030 - 2040	3.15	0.52	43.83	7.81	-6.66
3.	2040 - 2050	3.42	0.56	39.78	6.51	-5.95
4.	2020 - 2050	10.71	1.75	124.02	20.31	-18.55

Increasing and decreasing potential recharge area of the basin is also reported in the Table 5-8. This decrease will lower the groundwater recharge and subsequent reduction in the groundwater table and base flow contributions to the rivers. Basin hydrological parameter variation is not only the cause of climate change or the changing the precipitation pattern, LULC change is also playing a significant variation in the groundwater system. The rate of groundwater recharge is likely to decline in the future fundamentally due to increase in urban population and water demand. This will eventually affect the quality and quantity of the water in urban environments.

5.3 Performance of SWAT model

A large number of parameters were calibrated to develop a well calibrated and validated SWAT model for hydrological assessment. The model was calibrated and validated using daily and monthly discharge of the Bagmati River at Khokana station. For the calibration and validation of the model, manual technique was adapted with finding the model parameters. The initial and acceptable ranges of the parameters were taken from the previous study (Babel et al., 2014; Pokhrel, 2018; Thapa et al., 2017).

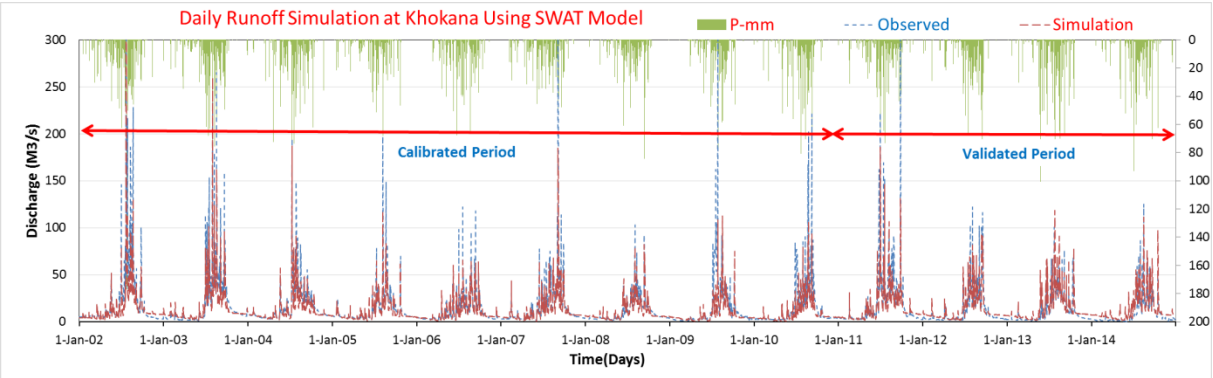

Figure 5-7 Daily observed and simulated discharge of river at Khokana station during calibration and validation.

The performance of the calibrated and validated model was evaluated by the graphical comparison and statistical parameters like NSE, R^2, and PBIAS. The calibrated and validated daily discharge of the river was shown in Figure 5-7 and the performance of the statistical parameter is presented in Table 5-9.

Table 5-9 Performance of model with daily and monthly discharge

Items	Calibration Daily (2002 - 2010)		Calibration Monthly		Validation Daily (2011 - 2014)		Validation Monthly	
	Obs	Sim	Obs	Sim	Obs	Sim	Obs	Sim
Mean Discharge (m3/s)	16.13	13.57	16.02	13.50	12.69	12.50	12.62	12.44
Minimum Discharge (m3/s)	1.20	0.91	2.39	3.01	0.03	0.69	1.07	1.39
Maximum Discharge (m3/s)	814.00	653.70	107.76	63.53	369.00	185.80	67.72	40.93
R^2	-	0.87	-	0.96	-	0.60	-	0.79
NSE	-	0.80	-	0.83	-	0.60	-	0.76
PBIAS	-	0.16	-	0.16	-	0.02	-	0.01

The values of statistical performance indicator NSE, PBIAS, R^2, and for daily simulation are 0.87, 0.16, and 0.80 respectively (Table 5-9), and monthly simulation are 0.96, 0.16, and 0.83 respectively. From the above result, the statistical parameter during calibration and validation was showed that the monthly values were better to perform than the daily value. During the calibration and the validation, the CN2 (mgt1), SOL_AWC (sol), SOL_K (sol), SOL_Z (sol), GWQMN (gw), and REVAPMN (gw) parameters were identified as more sensitive than the others. Details of the all parameters are presented in the Annex-II. In manual calibration, initially more sensitive parameters were adjusted. The initial value was taken from the previous study. During the sensitivity analysis, every parameter was identify and adjusted for providing the real scenario and the better preference of the model outputs. Initially, the model outputs were evaluated through visual inspection of runoff hydrograph (like, peak, shape, and base-flow), scattered plots, water balance comparison, and the flow duration curves. The uncertainty of the model represents the inconsistency between the simulated and measured variables. The source of uncertainty is produced from the different models (hydrological and climate model), inputs (like rainfall, temperature, etc), and the model parameters. P-factor and r-factor are the major tools for the uncertainty analysis for better calibration results. The most of the uncertainty associates with the quality, length, and the resolution of the data. Parameter uncertainty is relatively lesser than the input data uncertainty. In the case of KV, the observed inputs (meteorological and hydrological stations) are within acceptable quality (Pandey et al., 2019). Due to reasons such as the uncertainty of the model parameter, model formulation, error in observational data, and exact calibration of model parameters, the model may predict exact peak flow of the river but it gives the average flow pattern of the basin (Aryal et al., 2017; Pandey et al., 2019.; Mishra et al., 2018). The overall volume bias in the validation period was quite accurate in daily and monthly flow series and it showed that the calibrated SWAT model gave better preference in the river basin (Babel et al., 2014; Mishra et al., 2018; Pandey et al., 2019; Pokhrel, 2018; Shrestha et al., 2018; Thapa et al., 2017). From the optimized model parameters, the SWAT model was further simulated with LULC change and climate change scenarios with each decade (2020, 2030, 2040 and 2050).

5.4 Projected future climate

Two emission scenario viz. RCP4.5 (medium) and RCP8.5 (high) are used for the analysis of the future climate. Temperature and precipitation data are generated by using three RCMs (ACCESS-CSIRO-CCAM, CNRM-CM5-CSIRO-CCAM, and CCSM-4). As per the

recommendations by Aryal et al. (2017); they suggest that in alpine and sub-tropical climate these data are quite reliable. Daily maximum and minimum precipitation and temperature data of the study were downloaded from South Asia Cordex for the period of 2000 to 2005 under RCP4.5 and RCP8.5 scenarios and analyzed. To remove the uncertainty of the climate model generated data, biased correction was done by using the linear scaling method and quantile mapping.

All of the bias-corrected data were compared with the observed data (from 2006 to 2014) for better evaluation. Bias-corrected data with raw data from the climatic model is shown in Figure 5-8. From the observation, the climatic model gave the overestimation in the precipitation and the underestimation in the temperature to compare the observed data. For three RCMs, two RCPs, and two bias correction techniques, 12 scenarios were created. Overall comparison of the all climate model data to the observed data of the study area, the generated data from the ACCESS-1 model was more reliable than the other model. All the statistical parameters (NSE, R^2, and PBIAS) of the model are stronger than the other. Similarly, for the bias correction, the statistical indicator performance of the quantile mapping is better than the linear scaling, and that is shown in Figure 5-8 and Table 5-10. Another study has also prevailed that ACCESS-1 with quantile mapping bias correction gave a robust preference that climate and topographical region (Aryal et al., 2017; Babel et al., 2014; Bajracharya et al., 2018; Mishra et al., 2018).

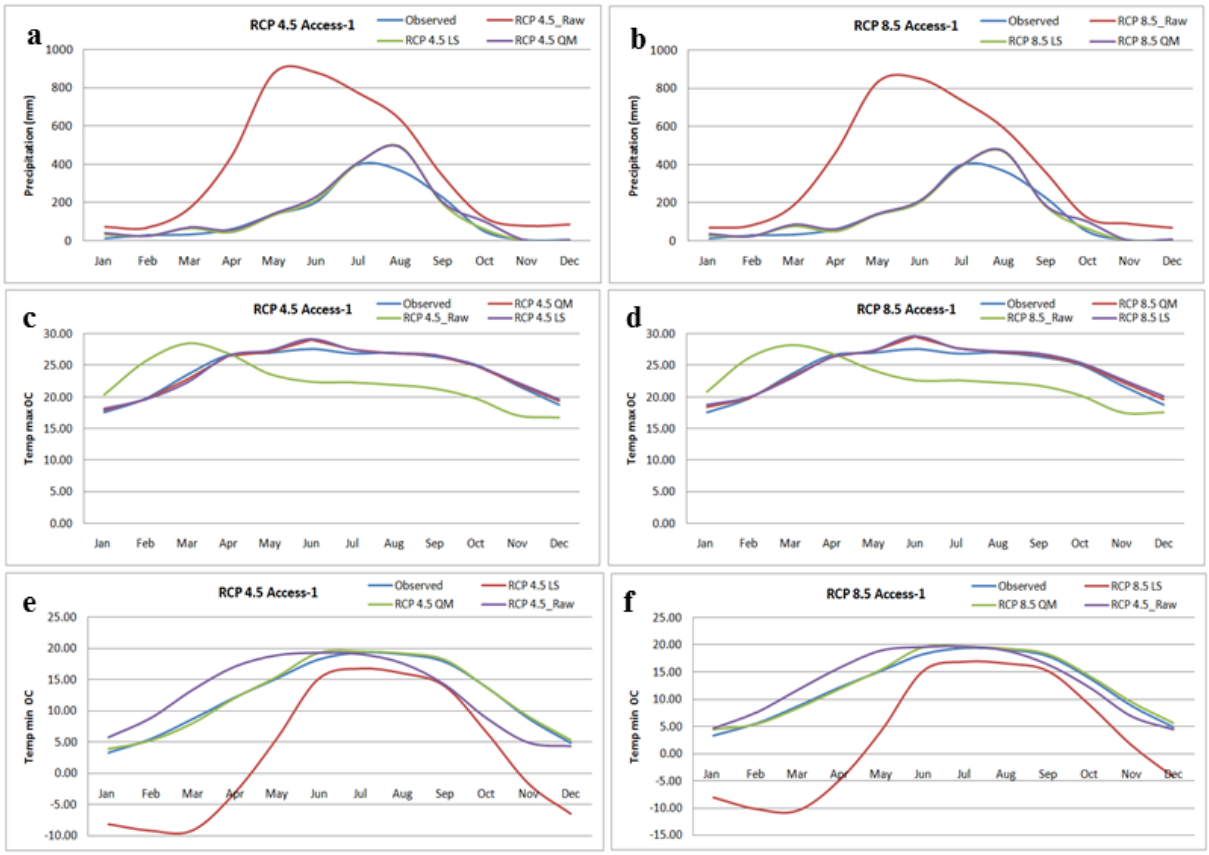

Figure 5-8 Compression graph of RCM ACCESS - 1 (a) Precipitation RCP4.5 (b) Precipitation RCP8.5 (c) Maximum temperature RCP4.5 (d) Maximum temperature RCP8.5 (e) Minimum Temperature RCP4.5 (f) Minimum Temperature RCP8.5.

The observed average annual precipitation (2000 to 2014), maximum and minimum temperature of the basin was 1535.4 mm, 24.2^{o}C, 12.3^{o}C respectively. Precipitation, temperature (max, min) of the study area was generated by the three RCMs for the analysis under RCP4.5 (medium) and RCP8.5 (high) scenario up to 2055. All the generated data is divided into each decade for the analysis. All the RCM projected data shows that each decade's precipitation, T_{max} and T_{min} is increased and its shows in Figure 5-8. The average annual precipitation up to 2050 will be raised 24% in RCP4.5 and 1% in RCP8.5 respectively by using quantile mapping bias correction. Similarly, in average annual T_{max} and T_{min} will be increased by 0.19°Cand 0.33°C in RCP4.5 and 0.89°C and 0.96°C in RCP8.5 respectively. In this study, data were used after bias correction and comparing with the baseline to assess the absolute changes in temperature and precipitation. Four decadal scenarios for 2020, 2030, 2040, and 2050 were accounted for analysis and RCM-based baseline was considered for analysis after bias correction to achieve realistic differences.

Table 5-10 Statistical performance indicator of a climate model with bias correction

Climate Model	RCP	Bias Correction	Precipitation			Temperature Maximum			Temperature Minimum		
			Nash	R^2	PBIAS	Nash	R^2	PBIAS	Nash	R^2	PBIAS
ACCESS - 1	4.5	LS	0.67	0.71	-0.02	0.80	0.86	0.02	-3.17	0.86	0.81
	8.5	LS	0.59	0.71	-0.09	0.80	0.82	0.01	-3.51	0.78	0.80
	4.5	**QM**	**0.56**	**0.64**	**-0.08**	**0.87**	**0.90**	**0.02**	**0.94**	**0.95**	**0.03**
	8.5	**QM**	**0.47**	**0.66**	**-0.16**	**0.88**	**0.95**	**0.01**	**0.95**	**0.95**	**0.01**
CNRM-CM5	4.5	LS	0.14	0.67	-0.23	0.74	0.80	0.01	0.91	0.92	0.01
	8.5	LS	0.31	0.68	-0.18	0.78	0.83	0.01	0.90	0.92	0.02
	4.5	QM	0.15	0.66	-0.28	0.83	0.87	0.02	0.95	0.95	0.02
	8.5	QM	0.32	0.67	-0.25	0.87	0.89	0.02	0.95	0.96	0.02
CCSM4	4.5	LS	0.24	0.61	-0.18	0.74	0.83	0.02	0.91	0.94	0.03
	8.5	LS	0.44	0.77	-0.27	0.84	0.89	0.02	0.87	0.90	0.03
	4.5	QM	-0.04	0.55	-0.26	0.84	0.89	0.02	0.95	0.96	0.03
	8.5	QM	0.20	0.72	-0.36	0.81	0.85	0.02	0.93	0.94	0.03

The baseline average maximum temperature, minimum temperature, and annual precipitation, for RCP4.5 are respectively 24.2°C, and 12.4°C and 1516 mm (2005-2014) (Table 5-11).

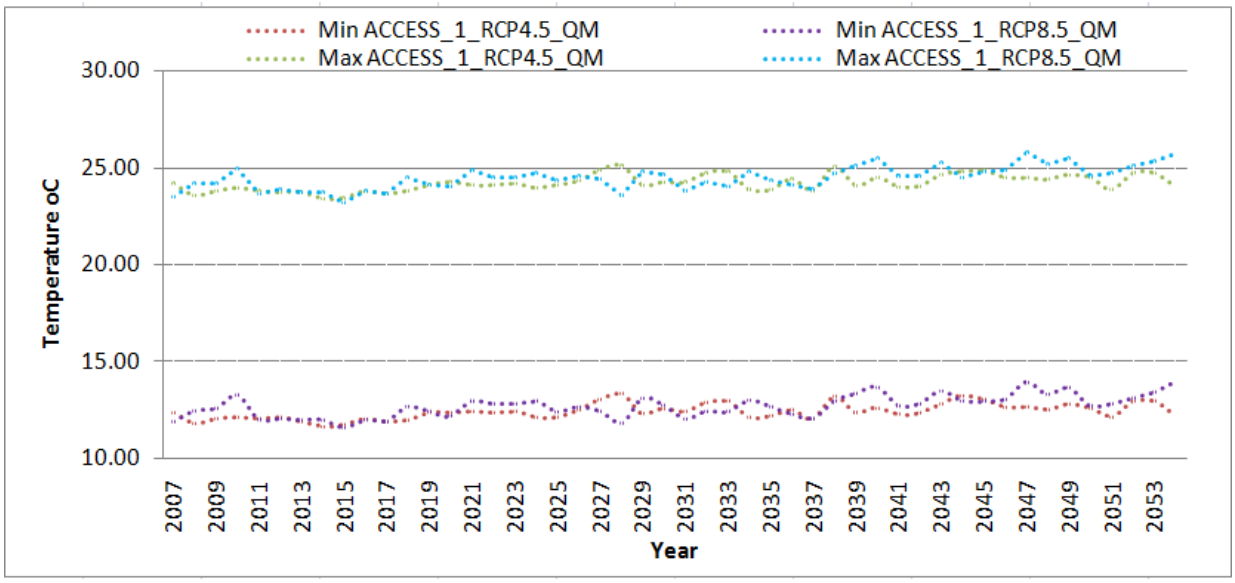

Figure 5-9 Future generated T_{max} and T_{min} by both RCP

For both scenarios, the average annual maximum and minimum temperatures are observed to be increased consistently. The absolute changes in the maximum average annual temperature are 0.15, 0.70, 0.53, and 0.66°C for RCP4.5 and 0.23, 0.32, 0.66, and 1.21°C for RCP8.5 in 2020s, 2030s, 2040s, and 2050s, respectively as shown in Table 5-11. The absolute changes in minimum average annual temperature are 0.15, 0.65, 0.54, and 0.60°C for RCP4.5 and 0.19, 0.24, 0.63 and 1.04°C for RCP8.5 in 2020s, 2030s, 2040s, and 2050s respectively. Figure 5-9 highlights that the increment in maximum temperature is more than the minimum temperature for both RCP scenarios. The RCP8.5 scenario highlights a greater increase when compared to RCP4.5. It is worthy to note that the pre-monsoon temperature (max.) is significantly higher when compared with the other season. The minimum temperature also follows the same trajectory. The variation of temperature are also widely reported in existing literature from Nepal and South Asia (e.g. Bajracharya et al., 2018; Guo-yu and Bhakta, 2017; Mishra and Herath, 2014; M. Shrestha et al., 2017). Similarly, the average annual precipitation is found to be increasing for all the considered decades expect the 2050s for RCP8.5. For instance, the precipitation is increased by 6%, 7%, 14% and 21% in 2020s, 2030s, 2040s, and 2050s for RCP4.5 scenario. It is to be noted that the percentage change is varying across the seasons. The RCP4.5 scenario depicts that the precipitation would increase during monsoon at the rate greater than the annual average.

Table 5-11 Change percentage in projected precipitation and temperature ACCESS-1 (base year 2007-2014)

Decade		RCP 4.5				RCP 8.5			
		S1	S2	S3	Annual	S1	S2	S3	Annual
Change in P (%) w.r.t. baseline	Baseline*	229	1,127	160	1,516	264	1,251	139	1,654
	2020	13	9	-25	6	-10	-2	46	1
	2030	-11	13	-8	7	5	-2	41	3
	2040	30	11	7	14	10	2	-15	2
	2050	32	13	66	21	29	-19	24	-8
Change in average Tmax (°C) w.r.t. baseline	Baseline$	25.10	27.20	20.25	24.18	25.22	27.17	20.72	24.37
	2020	0.11	0.00	0.34	0.15	0.38	0.29	0.02	0.23
	2030	0.91	0.51	0.67	0.70	0.14	0.56	0.26	0.32
	2040	0.52	0.39	0.69	0.53	0.64	0.56	0.77	0.66
	2050	0.45	0.66	0.87	0.66	1.33	1.44	0.85	1.21
Change in average Tmin (°C) w.r.t. baseline	Baseline$	11.40	18.89	6.85	12.38	11.40	18.89	7.50	12.6
	2020	0.11	-0.02	0.35	0.15	0.42	0.18	0.00	0.19
	2030	0.92	0.27	0.77	0.65	0.16	0.34	0.21	0.24
	2040	0.60	0.23	0.78	0.54	0.75	0.34	0.79	0.63
	2050	0.42	0.42	0.97	0.60	1.29	0.90	0.94	1.04

*Note: * is in mm; $ is in °C; S1 is pre-monsoon (Mar-May); S2 is monsoon (Jun-Sep); S3 is post-monsoon (Oct-Feb). W.r.t. in table stands for with respect to.*

After monsoon season highlights that the precipitation will decrease in the first two decades and increases in the latter decades. As the precipitation trend is not consistent as reported by several researchers (e.g. Aryal et al., 2017; Babel et al., 2014; Bajracharya et al., 2018; Karki

et al., 2017; Lutz et al., 2016; Mishra et al., 2018), the estimated change in precipitation may be erratic. For 2030, precipitation is expected to decrease by 11% and the variations of the maximum and minimum temperatures are +0.91 and +0.92 respectively. This highlights that 2030 would be drier than other decades. In both RCP Scenarios, the rate of increase in minimum temperature was greater than the max temperature. In summary, KV the summer days will be increased and winter might decrease in temperature. In the seasonal comparison, the rate of increase in winter maximum and minimum temperature is greater than the summer seasons that means the warmer day will be increased in the future. From the analysis of the dry (Oct to March) and wet (April to Sept) months in the study area showed that dry month precipitation was decline and in wet it was incline. From the analysis, the basin might be gone drier in dry and wet in the wet seasons.

5.5 Surface water resources under projected future scenarios

5.5.1 Impact of climate change

Climate change impacts on surface water resources were analyzed in terms of changes in average annual and seasonal discharge as well as water balance. Three seasons are considered for seasonal analysis, namely pre-monsoon (S1 or Mar-May); monsoon (S2 or Jun-Sep); post-monsoon (S3 or Oct-Feb). In addition, analysis is also carried out on decadal and annual scales. For climate change analysis on the river flow, it assumed that the land use is constant and 2010 LULC data is applied for the base period under both the climate scenarios. For the decadal analysis, after and before values are taken from the mid. Annual precipitation and temperature are increased in the future, which are contributing to create excess runoff. Increase in rainfall and river discharge in the future scenario is justified by the good correlation (0.67) between runoff and rainfall.

The model was simulated from 2006 to 2054 for daily and monthly scales under RCP4.5 and RCP8.5 scenarios. The results are summarized into a given Table 5-12 and Figure 5-10. The discharge of the river at the Khokana station is projected to increase significantly in the future in both the scenarios. The rate of increase in discharge in post monsoon is relatively higher than in other periods; such major rise was reported in other studies as well (Bajracharya et al., 2018; Sharma and Shakya, 2006).

Table 5-12 Summary of generated river discharge

Climate Model	Time	Discharge m^3/s		
		Maximum	Mean	Minimum
Observed (2000-2014)	Daily	814.00	14.28	0.03
	Monthly	107.76	14.19	1.07
ACCESS-1 RCP 4.5	Daily	1449.00	20.46	0.00
	Monthly	116.10	20.33	0.03
ACCESS-1 RCP 8.5	Daily	867.00	19.64	0.00
	Monthly	110.60	19.51	0.13

From the analysis, the RCP4.5 scenario created very high peak daily discharge compare to the RCP8.5 and observed data. But in the monthly simulation, the peak, average and minimum flow was more reliable. Thus the model gave better performance in monthly and seasonal variation.

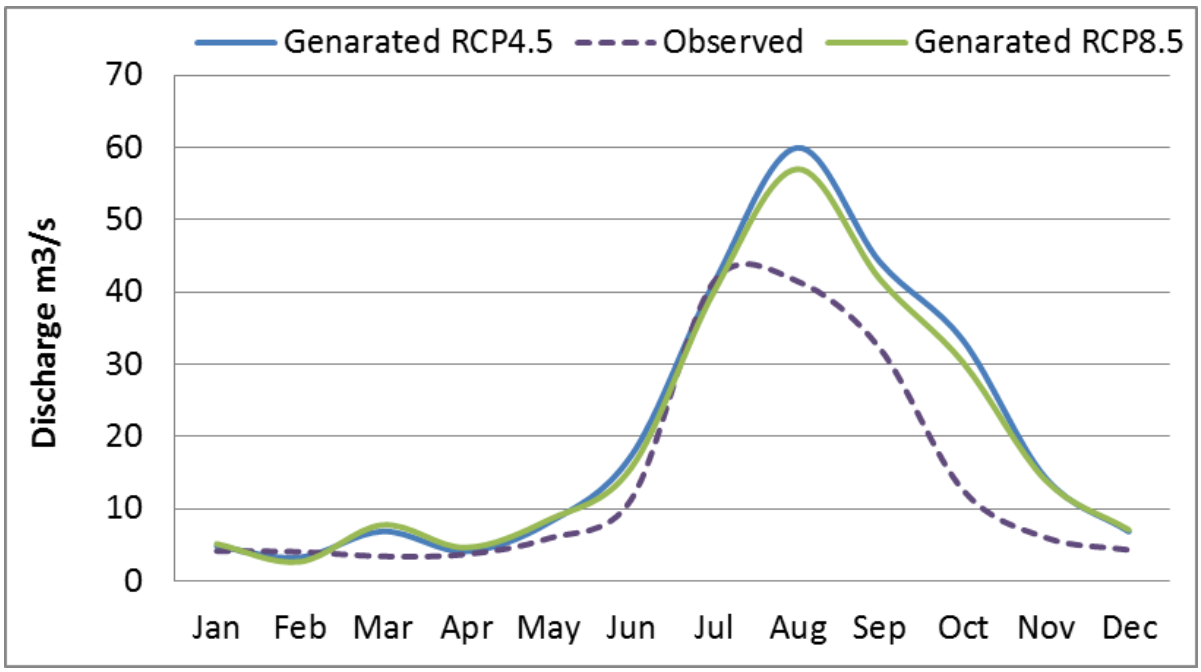

Figure 5-10 Average monthly flow by the CC scenario.

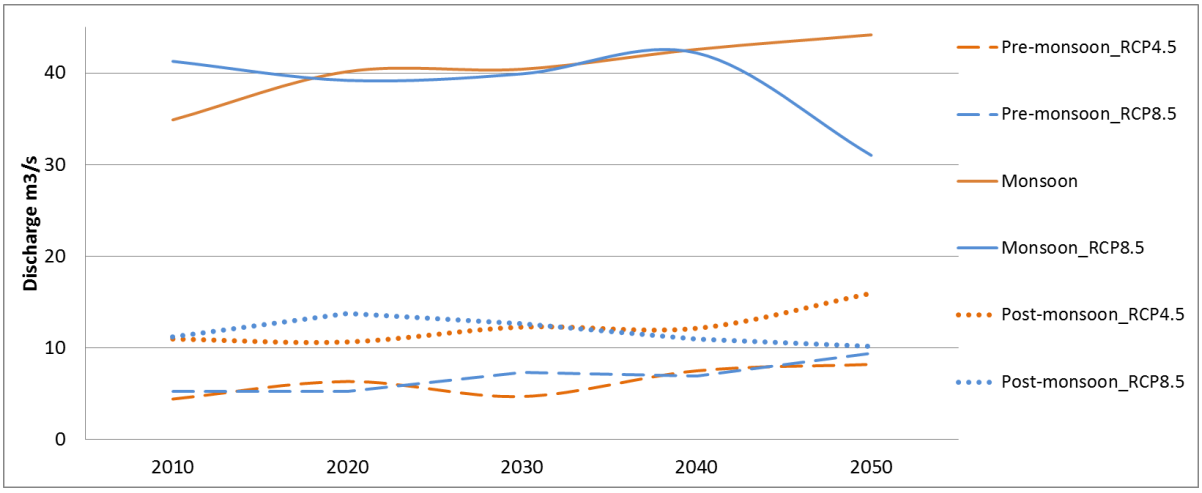

Figure 5-11 Generated seasonal flow of river in both scenarios.

In case of RCP8.5, it generated less quantity of precipitation and a high rate of increase in temperature that creates less runoff generation and high evaporation in the river basin. Except for pre-monsoon of RCP8.5, all the seasons the runoff generation from the basin will be decreased compared to the RCP4.5 (Figure 5-11). From the generated data, it is clearly seen that the peak of the hydrograph of the basin was shifted from August to September and the rate of increase in post-monsoon rainfall shift the river hydrograph in the left side (Sharma and Shakya, 2006). From this observation, due to climate change, seasonal runoff variation will occur in the future day.

The runoff of the basin basically depends upon the water balance component. Change in precipitation and temperature within the basin was clearly seen and that increase or decrease the runoff, evaporation, groundwater, lateral flow and other water balance component. Analysis of water balance components would lead to better characterization of the net water yield for the basin. The average baseline year parameters such rainfall, evapo-transpiration, precipitation, and runoff were 1516 mm, 573 mm, and 12.92 m^3/s respectively. The differences between the total inflow and outflow gives raise the change in storage. The percentage change in water balance components between baseline and other periods is presented in Table 5-13. Although runoff at the Khokana station is expected to increase; however, the rate of increment in terms of future periods considered, emission scenario, and season is not uniform.

In the case of the RCP4.5 scenarios, percentage increase in average annual runoff is increasing shows positive trend of 12% in 2020 to 37% in 2050 due to increase in precipitation by 7% and 23% respectively for 2020 and 2050. It is observed that the highest

percentage increase occurs in pre-monsoon season in the future. Due to small base value large variation was seen in the pre-monsoon compare to others. The increase in runoff has direct correlation with the increase in average annual precipitation. The rate of change of pre-monsoon water yield influences the monsoon and post-monsoon season scenarios. The post-monsoon groundwater recharge contributes the pre-monsoon base-flow to the river runoff hence percentage increase in the pre-monsoon water yield is found to be higher (Bajracharya et al., 2018; Sharma and Shakya, 2006). Furthermore, climate change impacts on water balance component would be varied spatially and temporally, which indicates drier winters (November, December, January, and February) and wetter summers (May, June, July, and August) in the future. The impact of such changes in the agriculture sector through, change the crop type, duration, showing and harvesting time will be changing in future day (Bhatt et al., 2014).

5.5.2 Impacts of LULC change

The impact of LULC analysis was based on CLUE-S projected LULC data (2010, 2020, 2030, 2040 and 2050) and 2010 LULC was considered for the base year. All hydro-metrological data for the future are assumed to be constant and the 2005 to 2014 data was used. The model simulated results with changed LULC shows that the average annual runoff of the basin is projected to increase according to the built-up area change within the basin and shown in Figure 5-12. Due to the LULC change in the current pattern, the mean and maximum discharge of the river basin is projected to have an increasing trend, but the minimum discharge is projected to decline. From the analysis of the model simulated results, the average rate of increase in peak discharge will be 5% per decade, and minimum discharge will be declining in each decade by 6%. Mostly in the dry period, the river basin water availability will be less, and that creates more water scarcity in the basin.

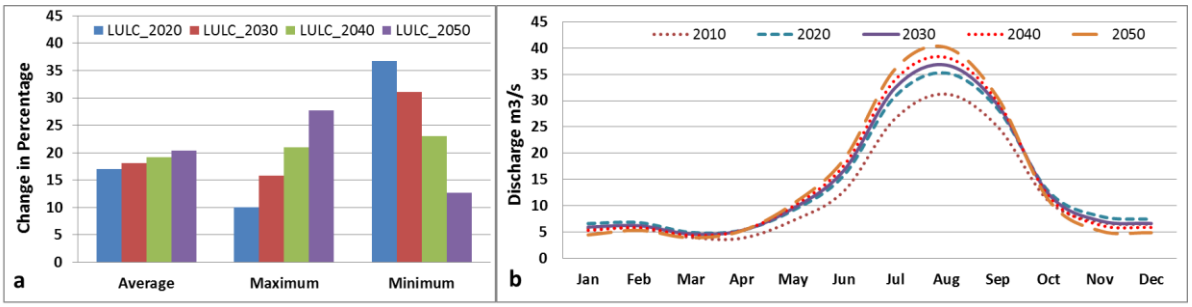

Figure 5-12 River discharge by LULC change: (a) Change in percentage of daily and monthly flow (b) Average monthly decadal flow of the river.

In the pre-monsoon period, the discharge within the basin is not significantly changing but in monsoon, the river runoff through the river has been increased by average 7% and the post-monsoon the discharge has been decreased with the average range of 9% is shown in Figure 5-13. From the result, the wet period of the basin has more water and creates a negative effect but in the dry period the availability of the resources will be in shortage in the coming days.

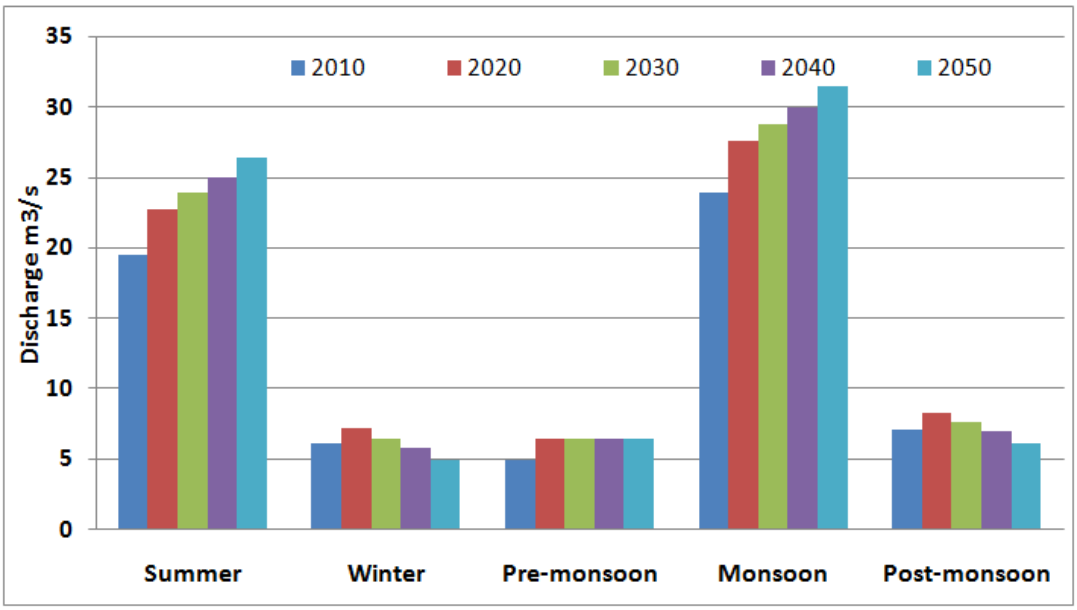

Figure 5-13 Seasonal discharge variation of river by LULC change.

In terms of water balance components, the rate of change of evapo-transpiration is mostly dependent on the rate of change of LULC pattern. After changing the urbanization pattern of the basin, it may be changed in response in the hydrological cycle. As shown in Table 5-14 the average annual evapo-transpiration is estimated to decline respectively by 13%, 14%, 15%, and 16% in 2020, 2030, 2040, and 2050, which shows a consistent change in evapo-transpiration for all seasons. Similarly, the average annual runoff is found to be increasing in a relatively similar way for pre-monsoon and monsoon seasons. It is important to note that the maximum runoff occurs in pre-monsoon season. The case of increment in runoff despite no significant changes in precipitation is conjectured with the decrease in evapotranspiration due to loss of vegetation cover and cultivated land. Lamichhane and Shakya (2019a) estimated that the changes in built-up, agricultural, and forest cover areas would be respectively+21.4%, -20.5%, and -0.9% between 2020-2050. These evidences provide strong foundation for increment in runoff and decrease in evapo-transpiration. The average monthly and seasonal peak flow variations are expected to increase in the future (see e.g. Figure 5-16).

The increment in built-up area would lead to a reduction in the lateral flow as well as groundwater recharge.

The agricultural water demand would increase in the future as a result of the LULC change because of the moisture deficiency in the agricultural field. This increased water demand for agriculture may lead the farmers to adjust the cropping pattern, type, and time schedule to familiarize the changing environment. The groundwater pumping would be elevated due to rapid urbanization that leads to a sharp decline in the groundwater and the contribution of groundwater in the basin would be reduced significantly. The analysis shows that it releases the excess of water in the wet period but scarce in the dry period which indicates the alternative water balance system will be introduced in the coming days to manage the water security in the basin.

Table 5-13 Impacts of climate change on hydrology. S1 is pre-monsoon (Mar-May); S2 is monsoon (Jun-Sep); S3 is post-monsoon (Oct-Feb).

		Precipitation (%)				Evapotranspiration (%)				Water yield (Runoff) (%)				Δ Storage (%)			
		S1	S2	S3	Annual	S1	S2	S3	Annual	S1	S2	S3	Annual	S1	S2	S3	Annual
RCP4.5	2020	17	9	-25	7	1	-2	-9	-2	49	15	-3	12	303	7	14	-15
	2030	-10	15	-9	9	1	-3	2	-1	7	17	11	15	-1264	38	25	7
	2040	31	12	8	14	8	-1	0	2	71	23	10	23	644	-2	7	-11
	2050	35	14	72	23	9	0	4	3	87	28	46	37	513	-4	2	2
RCP8.5	2020	-9	-3	56	1	-3	-1	3	-1	2	-5	24	3	-100	4	-6	6
	2030	6	-3	44	3	4	-1	3	1	40	-4	13	3	-100	-2	-12	11
	2040	12	2	-14	2	8	-2	-6	0	36	2	-3	3	-34	6	3	-1
	2050	31	-21	30	-8	10	-4	-1	1	80	-26	-8	-14	23	-32	-31	-2

Table 5-14 Impacts of land use/cover change on hydrology

	Precipitation (%)				Evapotranspiration (%)				Water yield (Runoff) (%)				Δ Storage (%)			
	S1	S2	S3	Annual	S1	S2	S3	Annual	S1	S2	S3	Annual	S1	S2	S3	Annual
2020	-	-	-	-	-9	-15	-10	-13	27	17	10	16	5	-5	1	-13
2030	-	-	-	-	-12	-16	-11	-14	28	23	0	18	-11	-11	-8	-15

2040	-	-	-	-	-15	-16	-12	-15	28	30	-11	19	-28	-18	-17	-17
2050	-	-	-	-	-17	-16	-13	-16	29	35	-21	21	-42	-24	-26	-19

Table 5-15 Combined impacts of climate change and land use/cover change on hydrology

		Precipitation (%)				Evapotranspiration (%)				Water yield (Runoff) (%)				Δ Storage (%)			
		S1	S2	S3	Annual	S1	S2	S3	Annual	S1	S2	S3	Annual	S1	S2	S3	Annual
RCP4.5	2020	17	9	-25	7	2	-1	-8	-1	69	24	-32	12	-307	-22	-26	-12
	2030	-10	15	-9	9	2	-2	2	-1	14	30	-22	15	-1686	-2	-22	1
	2040	31	12	8	14	9	-1	0	2	97	31	-18	22	-109	-29	-32	-11
	2050	35	14	72	23	10	1	5	4	112	36	18	36	-256	-30	-36	0
RCP8.5	2020	-9	-3	56	1	-2	-1	3	-1	17	2	-2	2	-170	-23	-39	3
	2030	6	-3	44	3	4	0	3	2	53	3	-11	3	-156	-27	-42	6
	2040	12	2	-14	2	4	0	1	1	65	10	-19	7	-101	-31	-40	-3
	2050	31	-21	30	-9	12	-3	-1	2	108	-22	-28	-14	-94	-48	-57	-9

In each decade the built-up area is projected to increase and the open infiltration ground is projected to decrease. This transformation of land use generates more runoff of the basin. The average rate of runoff CN value was increased by 0.43% each year that indicates the land use surface change through permeable to impermeable. From Figure 5-3 and the past urbanization pattern clearly indicate that the urbanization is horizontally expanding from the core area of the KV and denser day by day in the peri-urban area of the KV.

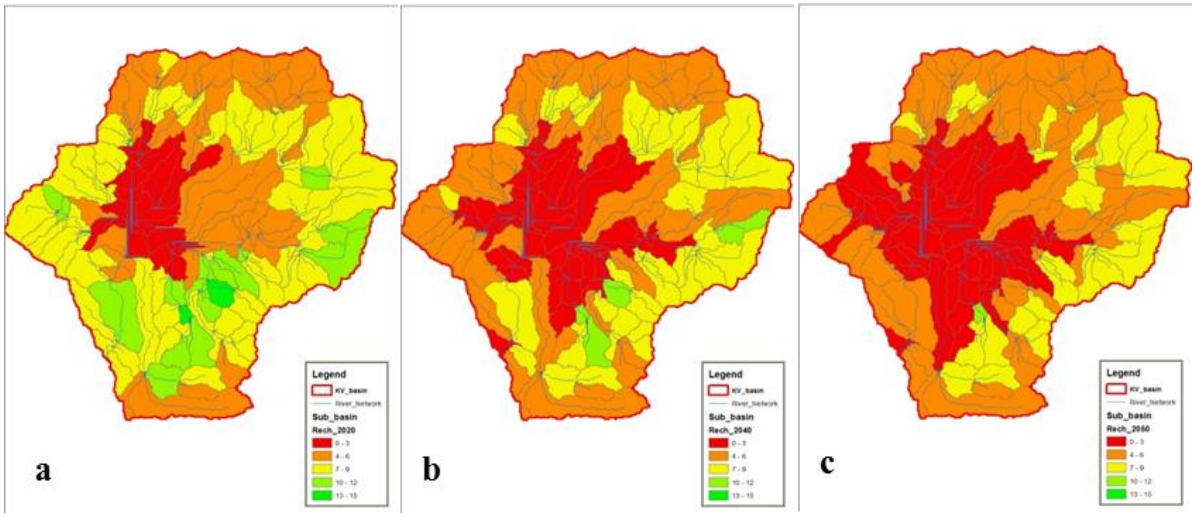

Figure 5-14 Groundwater contributions in the basin during a) 2020, b) 2040, c) 2050.

From these consequences and the above data clearly represent the runoff characteristic of the basin was rapidly increased due to the formation of concrete jungle in the valley. Similarly, the lateral flow and groundwater contribution of the river reach will decrease due to the increase in runoff and decrease in surface infiltration rate that was clearly shown in the given Figure 5-14. Increase the groundwater exploration and decrease the GW recharge declined the water table from the past few decades, and future it may be create excess of water scarcity in basin and river reach.

5.5.3 Integrated impacts of climate and LULC change

For the integrated impact assessment, 2010 was considered as base year and future simulated discharge under climate and LULC change scenarios were compared with respect to the baseline. The runoff volume and water balance of the basin are mostly depended upon the generated precipitation data of the climate model. The rate of change of volume of runoff or average flow will be increased and the lean flow of the basin will be decreased in the future year is shown in Table 5-16. In the RCP4.5 simulation, mostly all seasons runoff of the basin will be in rising trend and the RCP8.5 simulation the trend is decline is shown in Figure 5-15.

These values basically depends the rate of increase in precipitation varies with climatic scenarios. Due to maximum rise in minimum temperature in the post-monsoon creates the excessive evaporation in the basin and reduces the basin runoff characteristics.

Table 5-16 Daily and monthly simulation value by both changes

Climate Model	**Time**	**Discharge m3/s**		
		Maximum	**Mean**	**Minimum**
Observed (2000-2014)	Daily	814.0	14.28	0.03
	Monthly	107.76	14.19	1.07
LULC and CC ACCESS-1 RCP 4.5	Daily	1499.00	16.22	0.08
	Monthly	104.70	16.25	0.43
LULC and CC ACCESS-1 RCP 8.5	Daily	828.10	15.62	0.07
	Monthly	112.50	15.51	0.37

The changes in water balance elements are shown in Table 5-15. The average annual runoff for RCP4.5 scenario is estimated to increase by 12%, 15%, 22%, and 36% in 2020, 2030, 2040 and 2050 respectively; due to rise in precipitation rate. Both monsoon and pre-monsoon periods will have similar trend; meanwhile, the post-monsoon runoff is expected to increase for the future scenarios but in various extents, which indicates variation in the precipitation and evapotranspiration characteristics. The gradual estimated increments for the average annual evapo-transpiration are -1%, -1%, 2%, and 4% for 2020, 2030, 2040 and 2050 respectively. Notably, precipitation and temperature change affect the evapo-transpiration; the trend of variation does not adhere to the changes in LUCL and climate. The excessive surface runoff leads to a sharp decline in the groundwater and lateral flows. The groundwater contribution to the river discharge for the RCP 4.5 and RCP 8.5 scenarios are projected to decline with 40% and 68%, respectively at the end three decades. This will affect the volume of sub-surface water movement leading to the occurrence of moisture deficiency in agricultural areas.

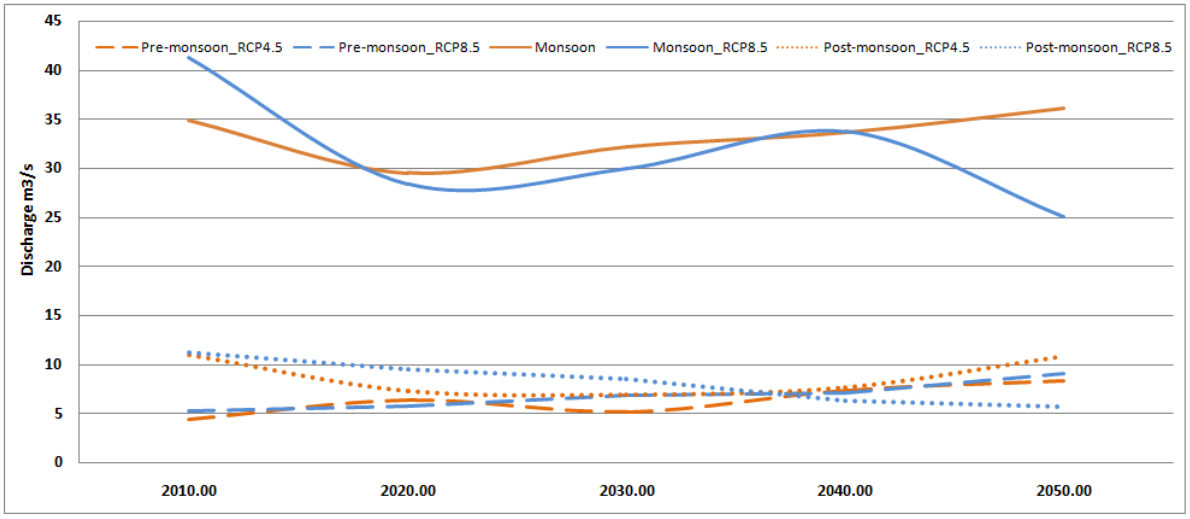

Figure 5-15 Seasonal discharge variation by combined scenario.

Table 5-17 and Figure 5-16 show the variation in runoff and water balance for LULC change only, climate change only (CC), and integrated changes for both aspects. In the case of CC only, the watershed runoff depends more on precipitation rather than temperature. As the minimum temperature more affects the evapo-transpiration from surface soil, moisture deficit during winter would be more prominent. This study does not incorporate the sensitivity due to basin size considering the RCM grids, this may also affect the future climate and hydrology. In the case of only LULC change, evapo-transpiration is found to be more sensitive towards runoff than precipitation due to urban expansion as it increases evapo-transpiration surfaces. But the rate of evapo-transpiration is partially decrease due to the constant climatic characteristics, and creates the more runoff in the basin. Similarly, only increases the maximum runoff and average flow; however, curtails base flow due to reduced recharge of groundwater.

While coupling the impacts of LULC and climate change, the total impact is found to be partially greater than the sum of individual impacts so superposition of the impacts would not be the actual scenario (Figure 5-17). In terms of peaks, the combined scenario leads to smooth the hydrograph of the basin and peak flow, whereas in the case of lean flow, there is slight increase in runoff (Figure 5-16). This is similar for both RCP scenarios. That indicates the water scarcity may be formed in post-monsoon seasons as per Table 5-17.

Table 5-17 Changes (%) in river discharge due to projected scenarios of CC only, LULC only, and integration in both changes in KV watershed

Scenario		Seasons	2020	2030	2040	2050
CC Only	RCP 4.5	S1	49	7	71	87
		S2	15	17	23	28
		S3	-3	11	10	46
		Annual	12	15	23	37
	RCP 8.5	S1	2	40	36	80
		S2	-5	-4	2	-26
		S3	24	13	-3	-9
		Annual	3	3	3	-14
LULC Only		S1	27	28	29	30
		S2	17	23	30	35
		S3	10	0	-11	-21
		Annual	16	18	19	21
Combined LULC+ CC	RCP 4.5	S1	69	14	97	112
		S2	24	30	31	36
		S3	32	-22	-18	18
		Annual	12	15	22	36
	RCP 8.5	S1	17	53	65	108
		S2	2	3	10	-22
		S3	-2	-11	-19	-28
		Annual	2	3	7	-14

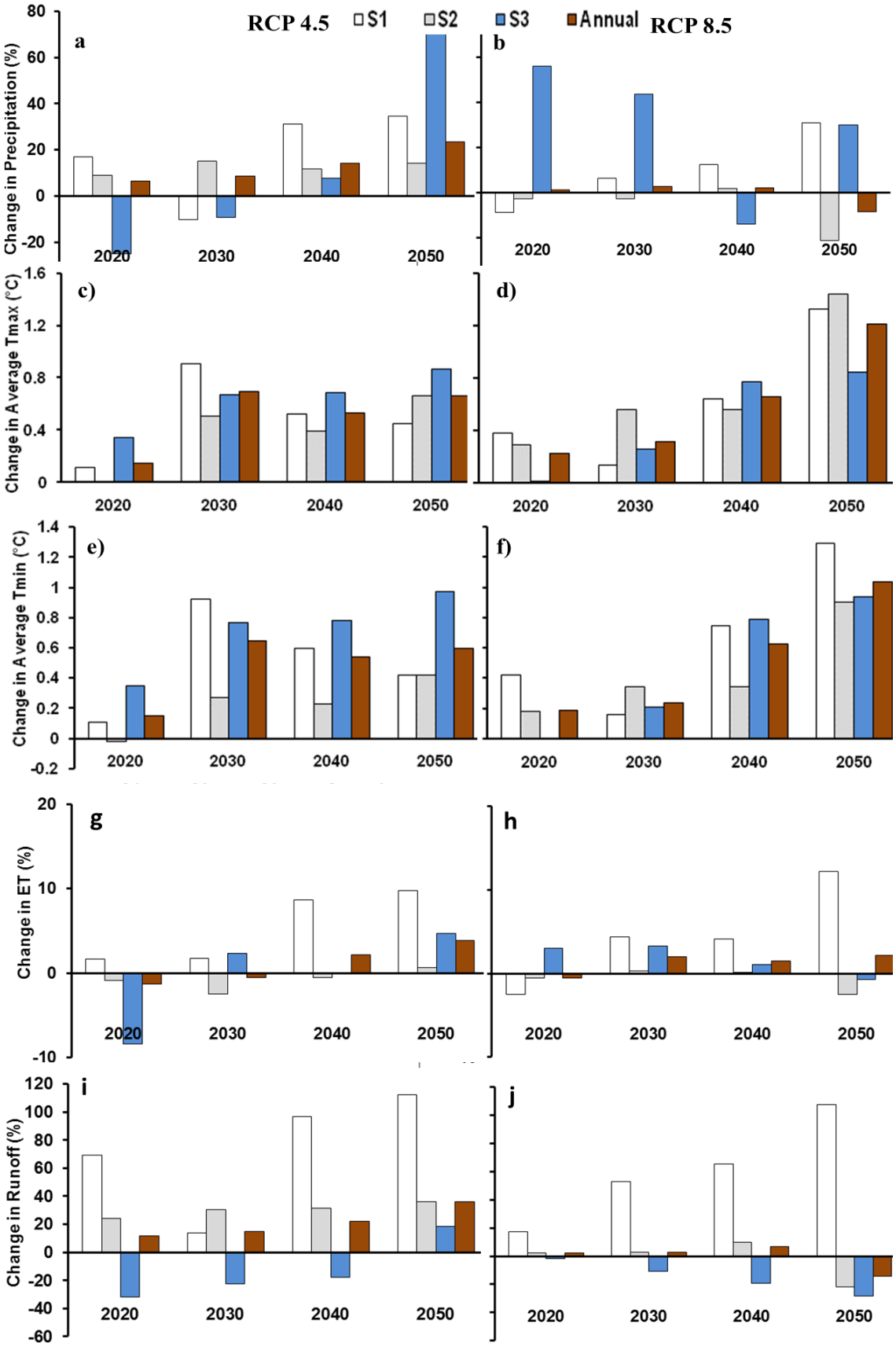

Figure 5-16 Changes in precipitation, temperature, evapotranspiration and runoff under projected changes in climate and LULC for RCP4.5 and 8.5 scenarios.

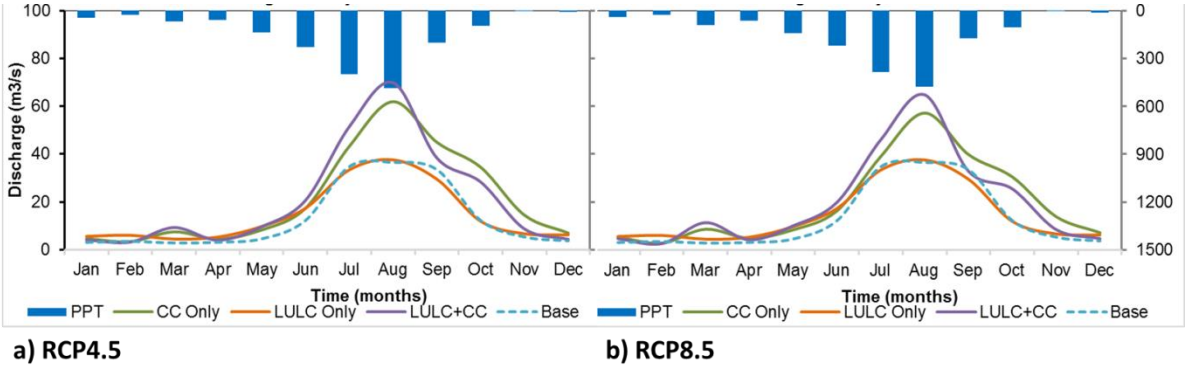

Figure 5-17 Simulated average monthly discharge under three scenarios.

From the simulation of the different model, previous study and analysis gave the clear picture that the climate change impact on water balance in river basin varies in temporal and spatial scales. In the dry season, the future days will be dryer and wet seasons will have excess of water availability. The LULC change is amplifying the natural water resources changes.

5.6 Performance of groundwater flow model

Seasonal field observation well data from the Working Group (WG-2) of WaSH-Mia/ SATREPS project was used for the calibration and validation of the groundwater flow model. Due to lack of historical observation groundwater level data, the one-year seasonal data was used. So, groundwater levels of dry and wet seasons were used for the calibration and validation. We used initial hydraulic conductivity of the sub-surface layers and the river reach as identified by previous studies (Adhikari, 2017; Basnet, 2016; Pandey and Kazama, 2011; Shrestha et al., 2020). Observation of groundwater levels at only 41 observation wells for 2016 and pumping rate data at 258 existing pumping wells were available for evaluating model performance. Root Mean Square Error (RMSE), Mean Absolute Error (MAE), and Mean Error (ME) were considered as the main statistical indicators for model performance evaluation. The model was calibrated at two stages. At the first stage, hydraulic conductance of sub-surface layers and rivers and the recharge factor was calibrated to the extent of reasonable performance. The recharge factors for the dry and wet seasons were obtained as 91% and 41% respectively. The recharge volumes for the dry and wet seasons were estimated as 1.07 and 1.191 MCM respectively. The second stage comprised the process in which the recharge volume was considered static for both seasons and the recharge depth was varied in every grid cell considering the recharge capacity from Equation 4.29. As recharge volume was kept static and other parameters were unchanged in the second stage, the model performance was similar to that of the first stage. The model performance statistics of the calibrated and validated model is shown in Table 5-18 and residuals and scatter plots are shown in Figure 5-18. The results of residual head plots highlight that except some wells (like dry (W39) and wet (W47 and W8)), almost all wells depicted a comparable head as that of the observed one. The zero values of the ME, MAE and RMSE highlight absolute performance of model; meanwhile, the minimum values depict better outputs. The nominal values of MAE and RMSE in Table 5-18 indicate that the model performance is significant and thus implemented for further analysis. The calibrated parameters are presented in Table 5-19. The hydraulic head and the drawdown due to pumping varies across the groundwater basin with the hydraulic properties of layers, riverbeds, and the recharge volume of the basin. The high value indicates higher recharge and lesser drawdown.

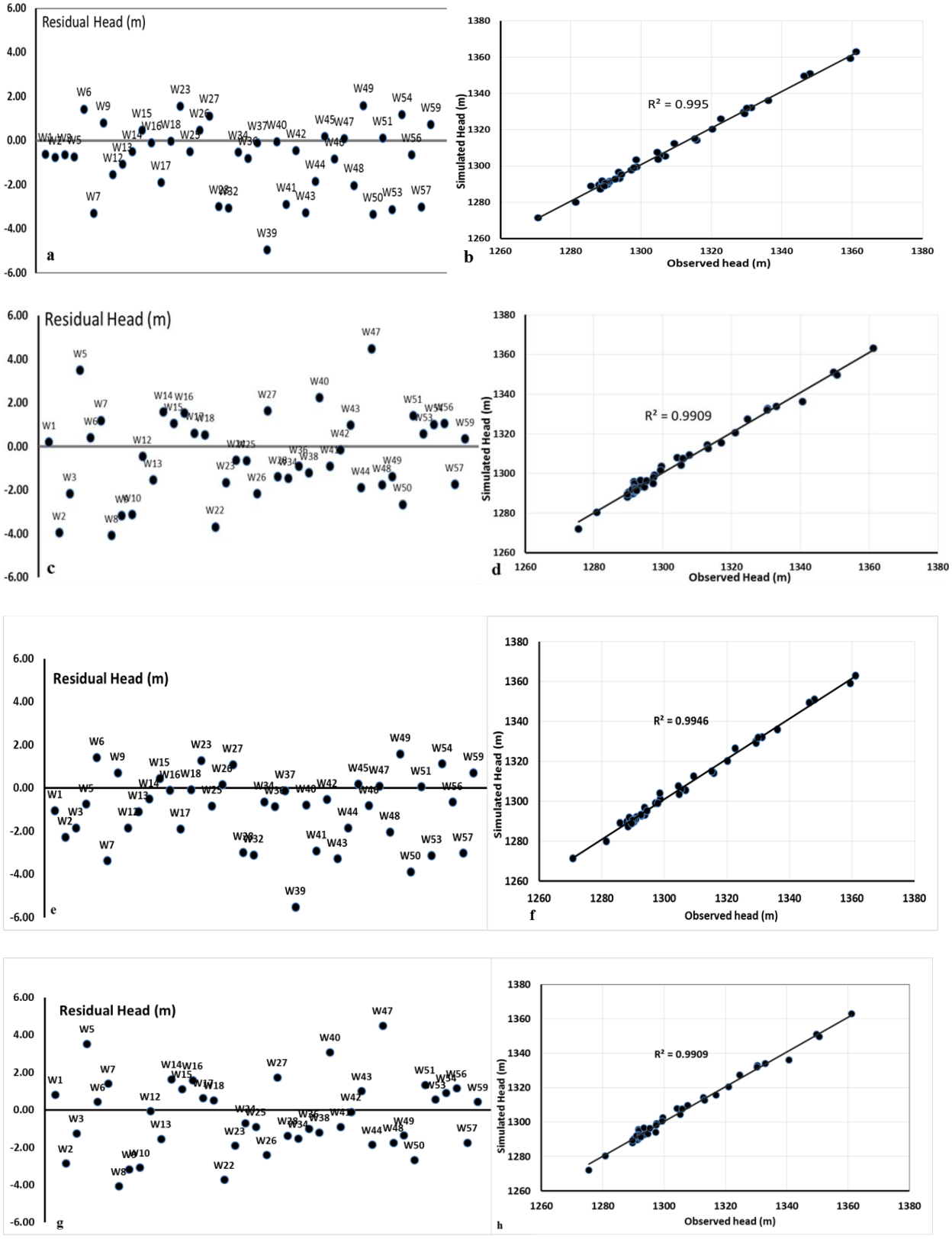

Figure 5-18 a) and b) Residual head and scattered plot of simulated and observed head during calibration in only pumping rate change scenario, c) and d) residual head and scattered plot of simulated and observed head during validation in only pumping rate change scenario, e) and f) residual head and scattered plot of simulated and observed head during calibration in both

Pumping rate and LULC change scenario, g) and h) residual head and scattered plot of simulated and observed head during validation in both Pumping rate and LULC change scenario.

Table 5-18 Preferment indicator of the Groundwater model during calibration and validation

Statistical indexes	Only pumping rate change		Both Pumping and LULC change	
	Dry (Calibration)	Wet (Validation)	Dry (Calibration)	Wet (Validation)
Mean error (ME)	-0.879	-0.44	-1.041	-0.35
Mean Absolute error (MAE)	1.34	1.63	1.476	1.646
Root mean square error (RMSE)	1.802	1.97	1.933	1.97
Nash efficiency	0.99	0.99	0.99	0.99
R^2	0.995	0.99	1.00	1.00

Table 5-19 Calibrated value of the groundwater model parameters

Parameters	**Symbol**	**Value Range**
Shallow Aquifer **(m/day)**	Kx	12 - 44
Aquitard **(m/day)**	Kx	0.01 to 0.001
Deep Aquifer **(m/day)**	Kx	0.1 - 8.8
Riverbed conductance(**(m/day)**	Kx	12
Groundwater recharge factor (Maximum) for dry and wet periods	α^{max}	95.38% to 48%
Groundwater recharge factor (Minimum) for dry and wet periods	α^{min}	85.34% to 38%

From the simulation, minimum and maximum head difference were 0.15m and 4.49m in well W42 and W47 respectively during calibration and 0.02m and 4.95m in well W18 and W39 respectively during validation. The model was calibrated, validated and the spatially simulated hydraulic head were used for the analysis and evaluation. Simulated model hydraulic head output during calibration (dry period) and validation (wet period) as shown

in Figure 5-19. Initially the hydraulic head of the cell value is simulated through model and the overall head of the dry period was less than the wet period. And the calibrated hydraulic conductivity parameters of the model in the river, aquifers, and aquitard was given in the Table 5-19

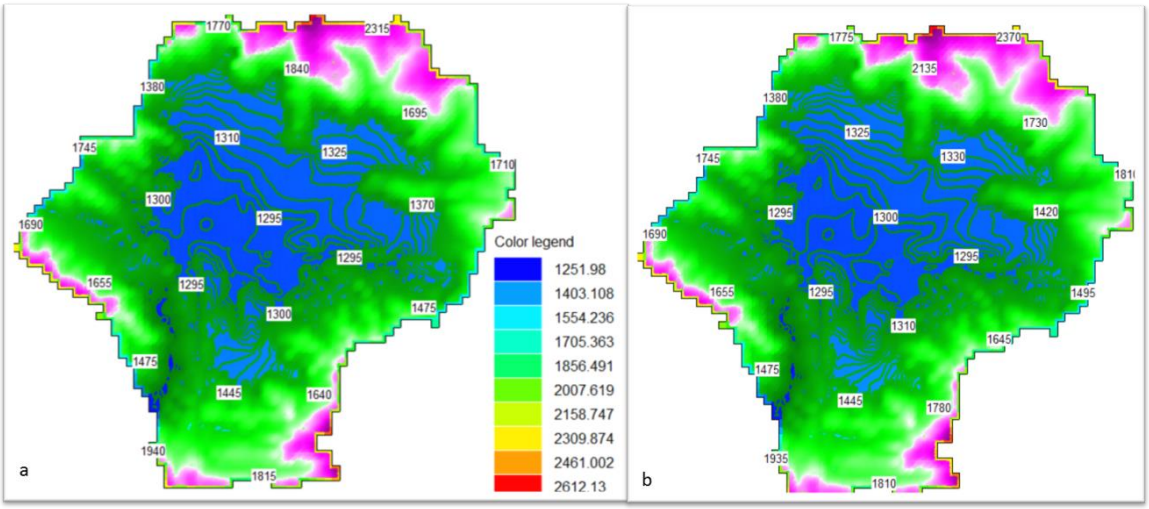

Figure 5-19 Generated groundwater level of Shallow aquifer for calibration period (Dry) and generated groundwater level of Shallow aquifer for Validation period (Wet)

The overall situation and the groundwater profile in the basin are given the Figures 5-20, 5-21 and 5-22. From figure and the results, the level difference between dry and wet seasons was clearly seen and the large difference was obtained in the central part of the KV.

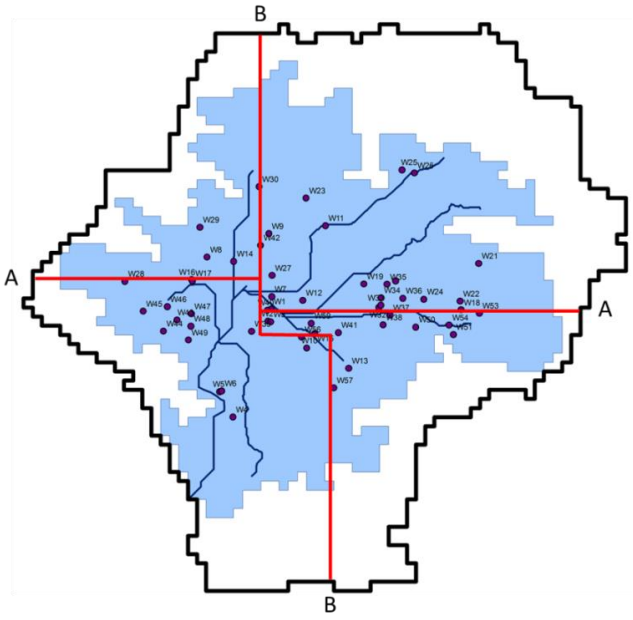

Figure 5-20 Figure showing well sections for which cross-section are plotted

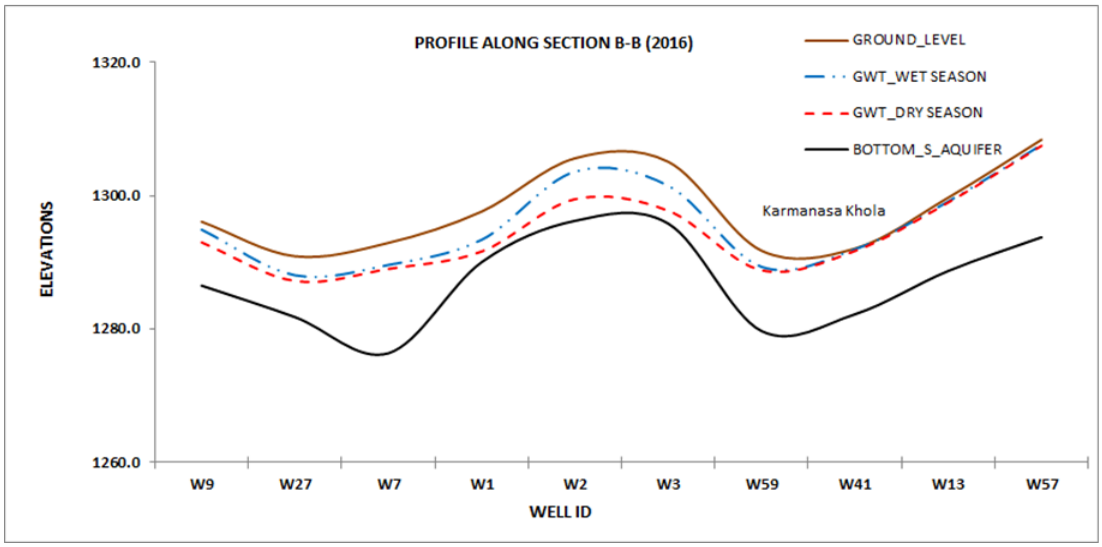

Figure 5-21 Simulated water tables along section B-B,

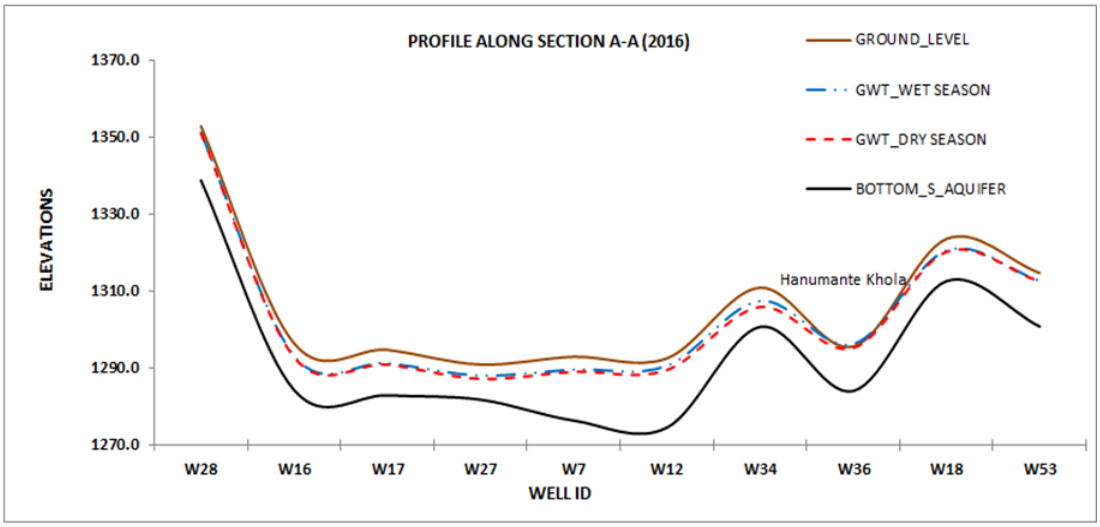

Figure 5-22 Simulated water tables along section A-A

5.7 Spatial distribution of groundwater recharge

The recharge rates and their spatial distribution are estimated through calibration of groundwater flow model. The calibration was performed at two stages. In the first stage, percentage of precipitation that goes as recharge in dry and wet seasons were estimated as 91% and 41%, respectively; equal to all the cells. Total volume of recharge corresponding to these recharge rates in dry and wet seasons are estimated as 1.07 Million-Cubic-Meters (MCM) and 1.91 MCM, respectively (Table 5-20) and recharge depths for dry period (Figure 5-23,a) and wet period (Figure 5-24, a) varies from 1.22 to 2.19 mm and 2.22 to 3.76 mm respectively. Notably, the spatial distribution adheres the distribution of precipitation and the

northern part of the model remains as the area having higher recharge depth when compared to the others.

Thereafter, the recharge depth was obtained for each grid cell distributing the recharge rate as per Equation 4.29. The model performance was appreciably significant and the recharge rates corresponding to the calibration were obtained as the recharge depths across the grid cells for both seasons. The recharge volume is the function of rainfall and recharge potential for each grid. The results for dry and wet seasons are depicted in Figures 5-24 and 5-25 respectively. The recharge depth in each grid cell was estimated with the help of spatially distributed precipitation and recharge factor as depicted by Equation 4.29. Figures 5-23, a and b highlight that the northern parts of the valley have greater tendency to precipitation whereas other parts have moderate only. Similarly, the northern and eastern part of the valley has high recharge potential. But the south eastern part has less precipitation; however, it has greater open and forest areas, so it contributes in recharge significantly. In 2020, recharge depth varies from 1.14 to 2.22 mm in dry season (Figure 5-24, a) and 2.25 to 4.09 mm in wet season (Figure 5-24, b). During this period, the total recharge volumes in dry and wet seasons are respectively found to be 1.052 and 1.949 MCM. Due to the unique precipitation characteristics of the basin in wet season as more than 75% of precipitation is occurred during this season, more volume was recharged when compared to the dry season. In dry season, the recharge tendency is high due to low precipitation intensity, frequency, duration, and dry surface condition.

In 2050, the recharge depth varies in the grid at the rate of 1.13 to 2.22 mm in the dry season (Figure 5-25, a) and 2.25 to 4.09 mm in wet season (Figure 5-25, b). The recharge volumes for the dry and wet seasons are estimated to be 1.048 and 1.947 MCM respectively. The maximum and average recharge depth variation from 2020 to 2050 across the grid cells are estimated as 0.033 and 0.006 mm respectively in dry season and 0.100 and 0.003 mm respectively in wet season. Such variation affects the recharge volume owing to the changed context. It is noted that at least 6% of the open area will be converted to built-up area every decade (Lamichhane and Shakya, 2019a). This paradigm highlights more significant impacts in the river runoff as well as recharge scenarios at various locations (Lamichhane and Shakya, 2019b). As shown in Figures 5-24 and 5-25, the northern and north-eastern parts of the valley show greater recharge potential and the same area would be affected by the future urbanization. This leads further reduction of the recharge depth in the future. Notably, the

variation in the recharge scenarios of dry and wet seasons would be relatively the same; however, the projected variation in the recharge volume would be affected due to the variation in precipitation that is associated with the climate change, which is not incorporated in this study.

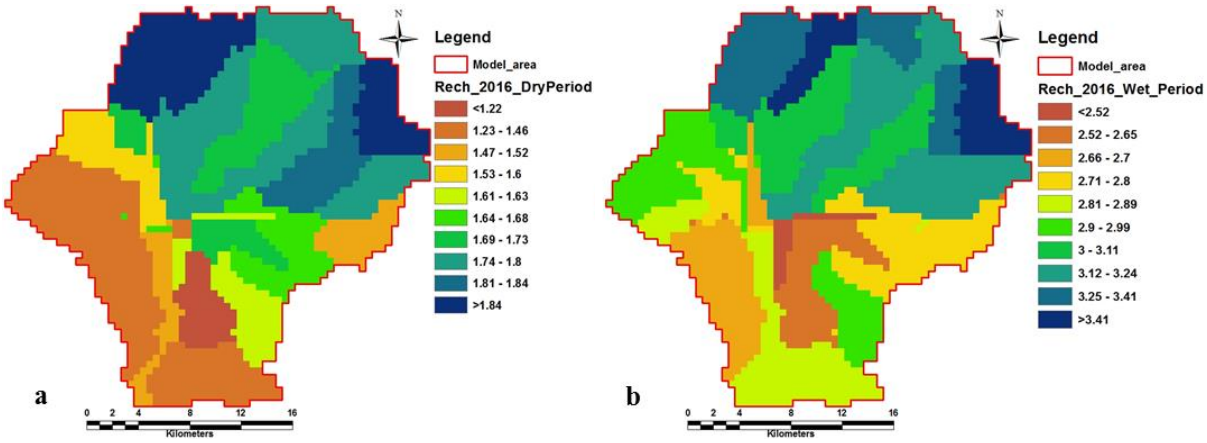

Figure 5-23 Recharge raster map only pumping rate change in: a) dry period and b) wet period

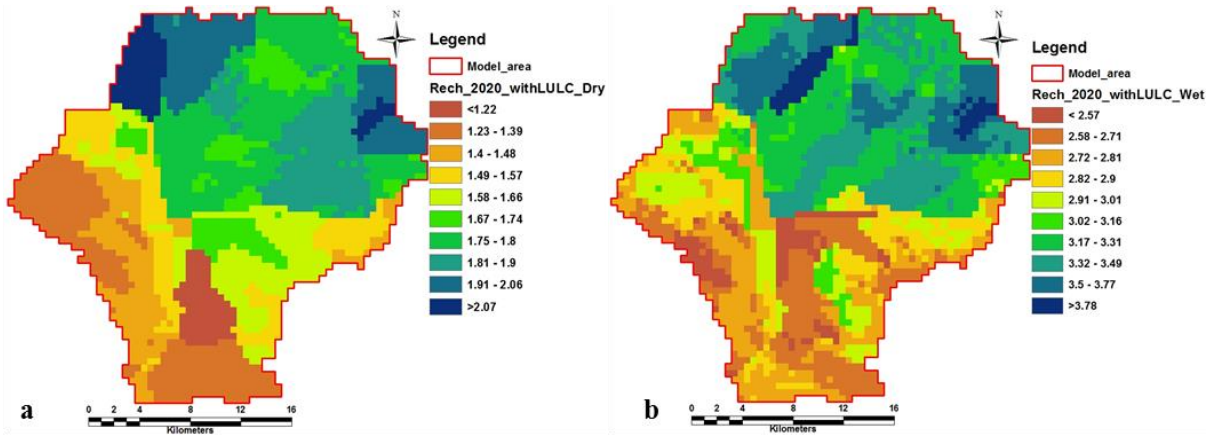

Figure 5-24 Recharge raster map both pumping rate and LULC change during 2020 in: a) dry period and b) wet period.

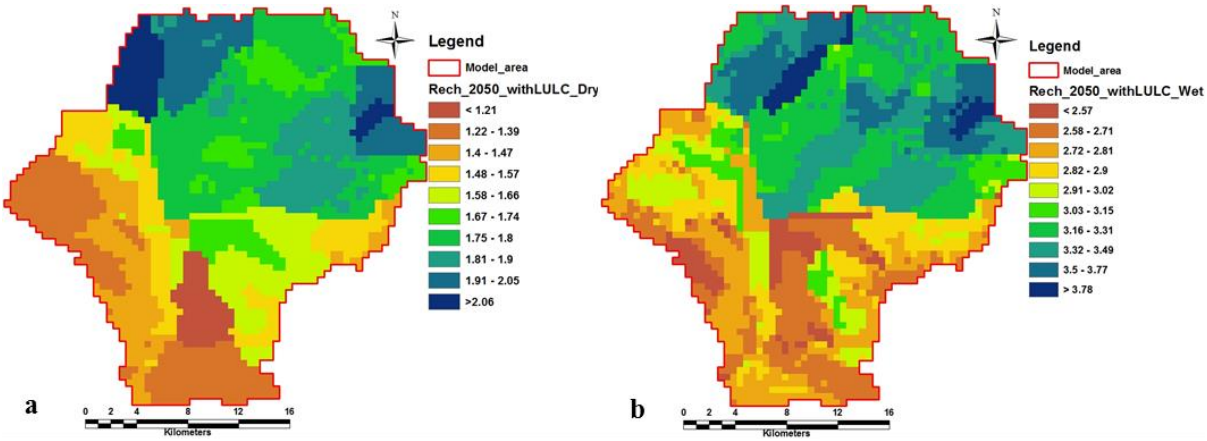

Figure 5-25 Recharge raster map both pumping rate and LULC change during 2050 in: a) dry period and b) wet period.

Note: Rech_2050_withLULC_Dry: Recharge 2050 with LULC and pumping change scenario at dry period; Rech_2050_withLULC_Wet:- Recharge 2050 with LULC and pumping change scenario at wet period

Table 5-20 Total recharge volume in various scenarios

Year	Season	Scenario	Volume (MCM)
2020	Dry	Only pumping rate change	1.065
2020	Wet	Only pumping rate change	1.911
2020	Dry	Both pumping rate and LULC change	1.052
2020	Wet	Both pumping rate and LULC change	1.949
2050	Dry	Both pumping rate and LULC change	1.048
2050	Wet	Both pumping rate and LULC change	1.947

5.8 Impacts of future scenarios on GW drawdown

5.8.1 Drawdown due to pumping dynamics

Though pumping rates for 258 deep wells in the valley were available and used in the model calibration, data of pumping from shallow aquifer are not available. Owing to this scarcity, theoretical water balance techniques were adopted to calculate the shallow pumping rate considering the storage dynamics in the basin, which is also adopted by Adhikari (2017). The rate and volume of pumping were distributed in each grid with reference to the population density as per Sections 2.8.5 and 4.5.6. The pumping well was considered as the center of gravity of the cell and the effects are homogenously distributed across the cell. The future

groundwater scenarios were developed at decadal scale (i.e., 2020, 2030, 2040, and 2050) taking into account the increase in pumping rate as per population growth rate and considering other conditions (climatic, geological, land use land cover etc.) as static.

Figure 5-26 highlights that the hydraulic head changes between 2020 to 2050 within the model domain for both seasons. For the observation wells, the hydraulic head in dry season declines due to high pumping and resettles the level during the wet season. For the simulation period, the wet season drawdown was obtained to be higher than the dry season. The drawdown was quite rapid in dry season in some pocket areas where the aquitard is exposed with high pumping rate or less hydraulic conductivity. The groundwater table is raised to the surface due to excess rainfall in the wet season; this leads to a wider seasonal variation in groundwater level becomes prominent in the pocket areas. The valley fringes have less pumping rate and moderate recharge capacity; however, the groundwater table seems not much affected. The major drawdown was observed in the semi-urban and urban areas of the valley, indicating a significant declination as shown in Figure 5-26. The observation wells from central and northern parts of the valley showed greater variation due to increased pumping rate, high potential recharge areas, and better transmissivity characteristics of the subsoil.

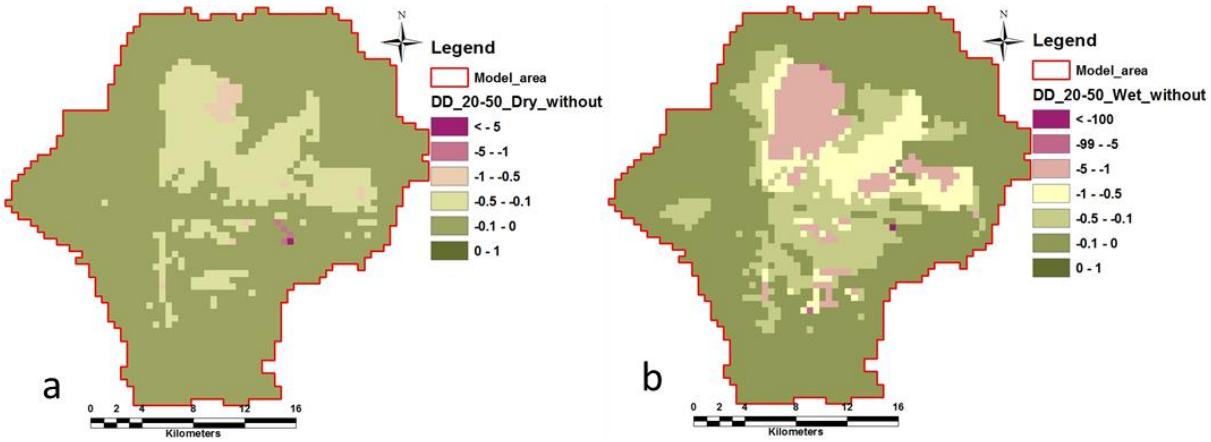

Figure 5-26 Drawdown change under only Pumping rate change scenario (during 2020 and 2050): a) dry period, b) wet period

Note: DD_20-50_Dry_without: Hydraulic head difference between 2020 - 2050 only pumping scenario

5.8.2 Drawdown due to both pumping rate and LULC change

Population growth and water demand play vital role in the pumping rate dynamics. Rapid urbanization will ultimately affect the recharge scenario and the conversion of open areas into built-up areas will affect the recharge volume of sub-surface. Recharge capacity of the surface was quantified as a product of rainfall, recharge areas map of respective decades (Figures 5-23 to 5-25), and recharge properties of that area with equation 4.26. The changes in drawdown between 2020 and 2050 for pumping rate increase and LULC change is shown in Figure 5-27. Figure 5-27 highlights that the valley fringes having forest cover and agricultural areas, less pumping rate, and open land cover lead to more stable water table for all seasons and scenarios. Both pumping scenarios showed grave decline in the groundwater table in the observation wells of central and peri-urban areas of the KV.

The dry pocket area from the grid cell was increased in the dry season compared to the wet. The rate of drawdown in the wet season was quite higher than the dry but the bottom level of elevation in dry season was low. Upper hilly part has forest cover thus the elevation of water table at its foothill is quite similar, but in the core areas and the northern foothills, the drawdown was quite high. Less recharge and high pumping rate may cause extensive drawdown in the future and may cause associated secondary effects. In the observation wells in the core and peri-urban areas, the groundwater level was rapidly declining for both pumping scenarios. The dry pocket area from the grid cell was increased in the dry season compared to the wet. The rate of drawdown in the wet season was quite higher than the dry but the bottom level of elevation in dry season was low. Upper hilly part has forest cover thus the elevation of water table at its foothill is quite similar, but in the core areas and the northern foothills, the drawdown was quite high. Less recharge and high pumping rate may cause extensive drawdown in the future and may cause associated secondary effects.

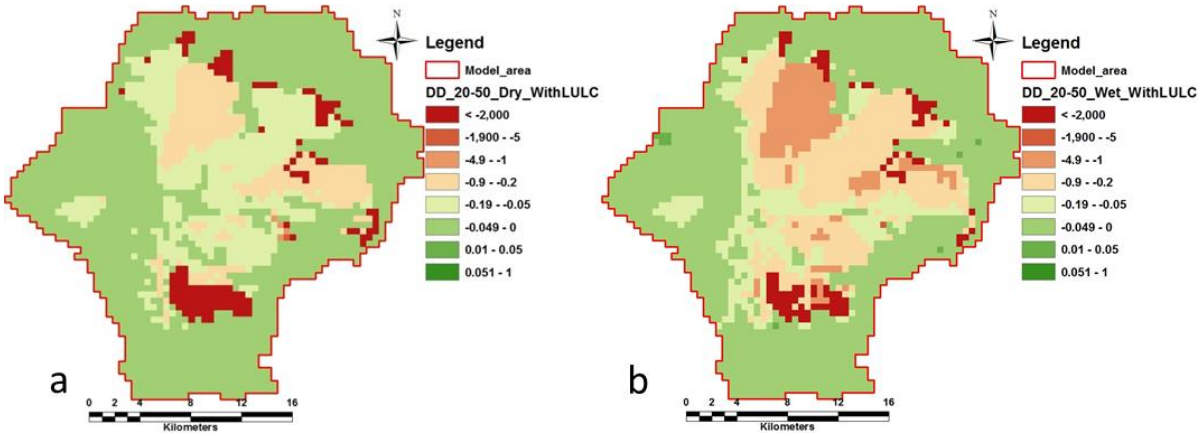

Figure 5-27 Drawdown change under the Pumping rate and LULC change scenarios (during 2020 and 2050): a) dry period, b) wet period

Note: DD_20-50_Dry_without: Hydraulic head difference between 2020 - 2050 both pumping and LULC change scenarios

5.8.3 Comparative drawdown due to scenarios

The haphazard urbanization in the KV is affecting groundwater basin through the increase in pumping rate and change in LULC pattern by single or combine. The differences between the two scenarios were assumed the only LULC change scenario. The variations of results in Figure 5-26 and Figure 5-27 are taken as the variations in drawdown due to LULC change only. The summary of the results is presented in Table 5-21.

Table 5-21 Head variation in various scenarios

Scenarios	Head difference (m)		
	Maximum	Average	Remarks
Dry season only pumping rate (2020-2050)	-4.87	-0.04	
Wet season only pumping rate (2020-2050)	-3.34	-0.16	
Dry season with LULC and pumping (2020-2050)	-5.25	-0.07	
Wet season with LULC and pumping (2020-2050)	-7.39	-0.26	
Dry season only LULC change	-1.09	-0.03	
Wet season only LULC change	-3.63	-0.11	

The data for the extreme dry pocket area was excluded in the analysis. The outcomes of this

study highlight that high drawdown locations are mostly concentrated in central and peri-urban areas. The maximum declination of the water head in the KV basin in dry season for three scenarios, viz. only pumping, both (pumping and LULC), and only LULC change were obtained as 162.33 mm/year, 175.00 mm/year, and 36.33 mm/year respectively. Similarly, for wet season, the maximum drawdowns were 111.33 mm/year, 246.33 mm/year and 86.83 mm/year respectively for only pumping, both, and only LULC change. The outputs outline that the drawdown level of the water table in dry season is more than the wet season. Similarly, the average variation of the water table throughout the basin during dry and wet periods for only pumping, both, and only LULC change were obtained as 1.33 mm/year and 5.50 mm/year, 2.50 mm/year and 8.82 mm/year, and 10.0 mm/year and 3.66 mm/year respectively. The sum of the observations highlights that the LUCL change is playing crucial role in the groundwater of the KV.

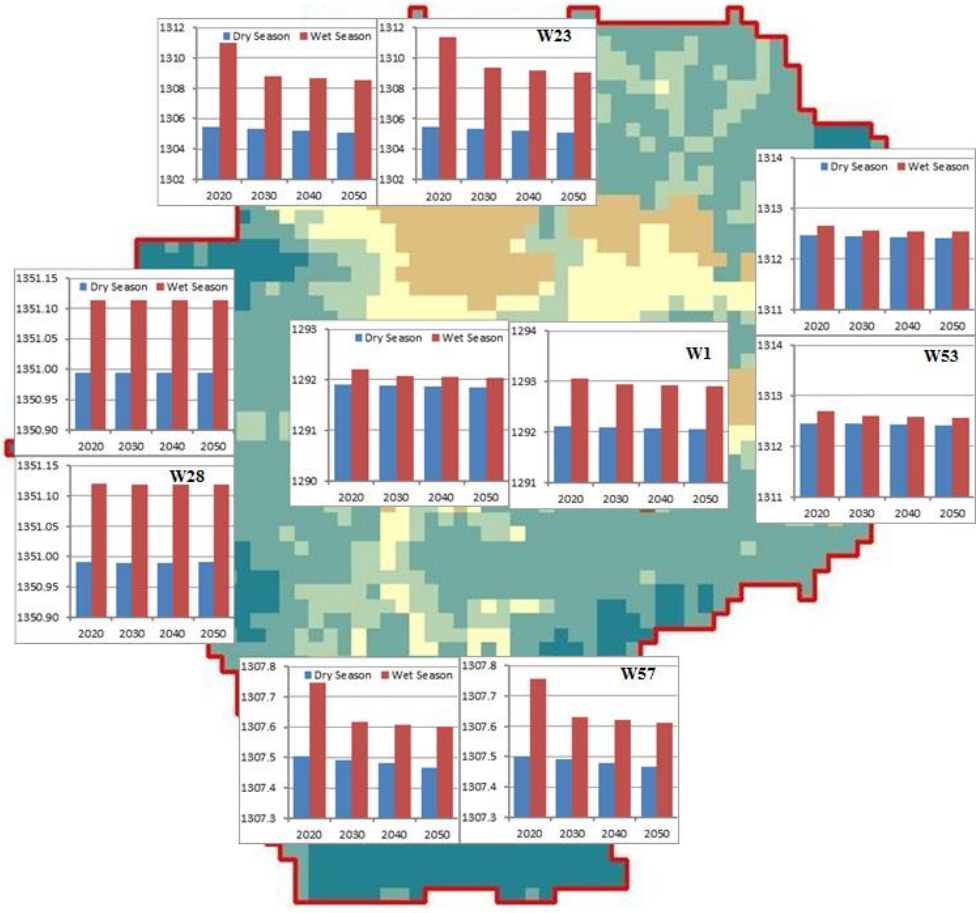

Figure 5-28 Water table drawdowns in observation wells for dry and wet periods

The gap created due to seasonal fluctuation in the water table may create land subsidence in the central valley too. Impact of increased pumping rate and LULC change on GWT is

shown in Figure 5-28 for wells W1, W23, W28, W53, and W57 for dry and wet seasons. In the two scenarios, the effect in pumping rate increment is higher compared to the LULC change in the outer area, but in the central and peri-urban areas both effects are quite similar. Due to the haphazard urbanization in the KV, synergetic effects of population growth and reduction in recharge areas are felt in the groundwater resources.

Chapter 6. Conclusion and Recommendation

This study aimed to evaluate impacts of future scenarios such as population growth and subsequent increase in pumping, land use/cover (LULC) change, and climate change (CC) on water resources (both surface and groundwater) in the Kathmandu Valley (KV) watershed located in the headwaters of the Bagmati River Basin in central Nepal. Multiple models and future scenarios are used to evaluate the impacts. CLUE-S model is used for developing LULC scenarios, multiple regional climate models (RCMs) for projecting future climate, and spatially varied multiple population growth scenarios to account for water demand scenarios. The results are presented in the form of current and future water balances, groundwater levels, and groundwater volumes under different scenarios. Key conclusions as well as recommendations from the study are highlighted in the following sub-sections.

6.1 Conclusions

The future LULC change scenarios considering five different cases in a CLUE-S model highlighted that the normal LULC change context showed better performance. To this end, normal scenario was incorporated for the assessment of LULC change led impacts. The depicted model highlights that the agricultural land would be decline at the rate of 6.5% due to increment of 4.96% of built-up areas. Notably, the forest area is obtained to be increased by 1.48% from 2010 to 2018 due to effective forest management initiatives in the Kathmandu Valley. Potential current and future groundwater recharge areas were delineated using various parameters and converting the parameter into an index using differential weights assigned based on analytical hierarchy process (AHP), a multi-criteria decision making (MCDM) technique. Currently, areas under high, moderately high, moderately low, low and very low are 7.37%, 32.89%, 32.59%, 14.72%, 9.14%, and 4.29%, respectively. The areas having high or moderately high recharge scenarios primarily fall in the urban continuously urbanizing and already highly urbanized areas. Therefore, the areas with high recharge potential would be under immense pressure due to urban expansion leading to a notable decrease in the recharge volume. This will eventually put pressure on the groundwater resources. In case of future, CLUE-S model projects increase in built-up areas by 21.4% and decrease in agricultural and forest areas by 20.5% and 0.9%, respectively, during 2020-2050. Six percentage (3.99 km^2) of the rechargeable area is estimated to become impervious as built-up areas encroach over a decade. The expanding urbanization would further aggravate the water security issues in the KV.

Future climate (temperature and precipitation) estimated using three Regional Climate Models (RCMs) (i.e., ACCESS-CSIRO-CCAM, CNRM-CM5 and CCSM4), and two representative concentration pathways (RCP) scenarios (i.e., RCP4.5 and RCP8.5) are used in this study after bias correction using quantile mapping technique. The maximum and minimum increment in temperature (T_{max} and T_{min}) and precipitation in the KV are projected to increase by 0.19^{o}C, 0.33^{o}C, and 24% respectively between 2010 to 2050 for RCP4.5 scenario and 0.89^{o}C, 0.96^{o}C and 1% respectively, for RCP 8.5 scenarios. In the same period, 21.4% (or 130.7 km^2) of the agricultural and forest areas within the KV watershed are projected to convert into the built-up areas. It is concluded that the temperature, summer, pre-monsoon, and monsoon runoff volume are estimated to increase; meanwhile, winter runoff is estimated to decrease. Thus, the dry season would be drier, and the wet season would be wetter in the future.

Current and future hydrology and water balance were characterized by developing a well calibrated and validated hydrological model using Soil and Water Assessment Tool (SWAT). An exhaustive performance evaluation of the SWAT model considering annual, seasonal, and monthly data led to conclude that the adopted method can replicate the hydrological regime considerably well. Three scenarios considering the effect of climate change only (CC), effect of land use land cover change (LULC), and integrated changes of CC and LULC are adopted for analysis in this study. Simulated future mean annual river discharge under RCP4.5 scenario showed projected increase by 37%, 21%, and 36%, due to climate change (CC) alone, LULC change alone, and combined (both LULC and CC) scenarios, respectively, at the Khokana station for 2050. Similarly, under the RCP8.5 scenario, projected changes in future runoff are -14%, +21%, and -14% for the same period and under same simulation scenarios. The groundwater contribution to the river discharge for the RCP 4.5 and RCP 8.5 scenarios are projected to decline with 40% and 68%, respectively at the end three decades, for the combined change due to CC and LULC because of the reduced infiltration.

Further to surface water, urbanization impacts on groundwater dynamics were also evaluated to generate evidence for informed planning for groundwater management. Urbanization is represented in the model in the form of LULC change and increasing pumping rate (due to population growth) scenarios to account for both supply side and demand side of groundwater resources. A groundwater flow model was developed using MODFLOW code to characterize current groundwater dynamics as well as alteration on the dynamics under various scenarios. The recharge rate was varied spatially using recharge factor. The average

recharge factors of the basin were obtained as 91% in dry and 41% in wet seasons after calibration and validation without LULC change consideration. For the LULC change, the maximum and minimum recharge factor was obtained as 95.35% to 85.34% and 48% to 38% for dry and wet seasons, respectively. Three scenarios (pumping rate increase, land use change, and combine) were simulated for the decadal (2020, 2030, 2040, and 2050) analyses. Except the dry pocket areas, the maximum drawdowns in the basin during 2020-2050 under combined and only pumping scenarios are estimated as -5.25 m and -4.87 m for the dry season and -7.39 m and -4.87 m for the wet season. The simulated results indicate that the future water table drawdown may create the secondary land subsidence effect within the basin. In the same period, the encroachment through LULC change led the drawdown of -1.09 m, -3.63 m for dry and wet seasons, respectively. From the obtained data, change in recharge dynamics through the LULC change eager to increase the drawdown and near future the rate will be increased rapidly. Similarly, in the dry season case of only pumping rate increase, both, and only LULC change scenarios, the maximum of 162.33, 175.00 and 36.33 mm/year drawdown are obtained respectively and for wet season the drawdowns for only pumping rate increase, both, and only LULC change scenario 111.33, 246.33, and 86.833 mm/year respectively. The average rate of groundwater drawdown in the basin for two seasons (dry and wet) respectively in the case of only pumping, both, and only LULC change are 1.33 mm/yr and 5.5 mm/year, 2.5 mm/yr and 8.82 mm/year, and 10.0 m/yr and 3.66 mm/year. All these findings clearly reveal that the effect of urbanization in groundwater recharge and pumping rate is remarkable in the KV.

It is worthy to note that the water balance and hydrological changes are fundamentally governed by climate change and LULC change. The increase in river discharge due to the estimated changes in CC and LULC depicts an opportunity for exploring potentials for storing excess runoff to use during the dry period. Reduction of groundwater flow tendency, encroachment of recharge area, decrease recharge water depth, and decline the groundwater table creates the integrated effects in the river basin hydrology and its corresponding effects (e. g., shrinkage of land, land-subsidence, water quality, etc.).

The highly potential recharge areas (northern foothill of mountains) need protection, and alternative recharge techniques are required for the region. Restricted open areas, parks, gardens as well as the individual open space of the basin should be used for the pocket recharge locations with suitable techniques. The research results will be useful in planning and management of water resources-related projects such as water supply and river basin

management in the study area, as well as the downstream projects like irrigation and hydropower analysis. Similarly, the variation of the flow characteristics in different scenarios is more valuable for future runoff scenarios in existing downstream projects such as Bagmati hydropower and Bagmati irrigation projects in the Bagmati River. The output from the research in groundwater dynamics will contribute in managing the future extraction scenario and recharge characteristics of the basin. It provides the information for the decision of the alternate groundwater recharge techniques. This study adds some insights in studies related to the impacts of urbanization on hydrology, especially in terms of integrated assessment of LULC change and hydrological changes.

6.2 Recommendations

The KV is rapidly developed and urbanized with built-up area expanding to decrease the agricultural land, open recharge area. The fragment of land parcels is more critical. So, the governments need to develop strategies to regulate urbanization patterns. A wide group of stakeholders is responsible for urban planning and groundwater management in Nepal; however, due to involvement of diverse line agencies, due coordination is still lacking, and the policy implementation has become yet challenging. An efficacious coordination between the line agencies is required at planning as well as operation levels are crucial. During the process of this study, some of the limitations had surfaced, which could be addressed in future studies. Some recommendations are as follows:

- Field level inventory should be done for the restricted area in the basin, and the rechargeable open areas will be delineated in such an area and should be verified the model outputs.
- For a better understanding of future urbanization in the basin, field-level information of road network, road width, hospital facilities, water supply facilities, and other livelihood facilities should be considered.
- Field level test data (moisture content, depth of water level, specific gravity, degree of saturation, etc.) should be monitored at regular interval for updating delineation of the potential groundwater recharge area.
- For a better understanding of the model parameters, overall performance of the model in base, peak, and average flow, more numbers of outlet points will be used for calibration and validation. Groundwater parameters of the model are more sensitive than the other for better estimation.

- Probability of occurrence (certainty) of the output from the various model (LULC, MCDM, SWAT, Groundwater) scenarios should be conducted to realize the outcome.
- All climate model data and LULC scenario (normal development and economic development scenario) should be simulated for a better understanding and reducing the uncertainty level of the hydrological model output.
- Multi-model approaches may be used for the better estimation of outputs of LULC change, MCDM techniques for delineation of groundwater recharge area, and hydrological model.
- Shallow groundwater pumping data can be generated from the inventory in the KV and the real pumping scenario can be simulated through the model.
- For the understanding, the actual scenario of the groundwater basin, the shallow, as well as the deep aquifer system, will be stimulated through the model.
- For generating the actual groundwater hydraulic conductivity characteristics in the basin, numerous field tests and bore log details in the shallow and deep aquifer should be conducted for better results.
- The observation well should be installed in the scattered form, and the measurement should be taken with proper temporal variation.
- Future impact of CC and the LULC change scenarios may be useful for the water and land resources management in the Kathmandu Valley. Similarly, the LULC change model is also used for urban planning as well as the demarcation of urban growth area in the KV and such type of analysis should be done in the other urban growth area.
- For the sustainable use of the resources, identify the possible shallow and deep aquifer recharge techniques (like, rainwater harvesting, managed aquifer recharge technique, sponge city techniques, etc.) in the valley.
- The outcomes of this research can be encapsulated to achieve the sustainable development and management of the surface and subsurface water resources.

References

Abbott, M.B., Bathurst, J.C., Cunge, J.A., O'Connell, P.E., Rasmussen, J., 1986. An introduction to the European Hydrological System - Systeme Hydrologique Europeen, "SHE", 1: History and philosophy of a physically-based, distributed modelling system. J. Hydrol. 87, 45–59. https://doi.org/10.1016/0022-1694(86)90114-9

Abiye, T.A., Sulieman, H., Ayalew, M., 2009. Use of treated wastewater for managed aquifer recharge in highly populated urban centers: A case study in Addis Ababa, Ethiopia. Environ. Geol. 58, 55–59. https://doi.org/10.1007/s00254-008-1490-y

ADB, 2015. Nepal: Kathmandu Valley Water Supply Improvement Project (South Asia Project Brief). sented AAG Annu. Meet. Washington, DC.

Adhikari, B., 2017. Study of Shallow groundwater hydrology of Kathmandu Valley. TU, IOE, Central Campus Pulchowk.

Adhikari, B.R., Shrestha, S. Das, Shakya, N.M., 2019. Future Urban Water Crisis in Mountain Regions: Example of Kathmandu Valley, Nepal, in: Urban Drought. Springer, pp. 169–182.

Aeschbach-Hertig, W., Gleeson, T., 2012. Regional strategies for the accelerating global problem of groundwater depletion. Nat. Geosci. 5, 853–861. https://doi.org/10.1038/ngeo1617

Aghlmand, R., Abbasi, A., 2019. Application of MODFLOW with boundary conditions analyses based on limited available observations: A case study of Birjand plain in East Iran. Water (Switzerland) 11. https://doi.org/10.3390/w11091904

Aher, P.D., Adinarayana, J., Gorantiwar, S.D., 2013. Prioritization of watersheds using multi-criteria evaluation through fuzzy analytical hierarchy process. Agric. Eng. Int. CIGR J. 15, 11–18.

Aich, V., Liersch, S., Vetter, T., Fournet, S., Andersson, J.C.M., Calmanti, S., van Weert, F.H.A., Hattermann, F.F., Paton, E.N. %J S. of the T.E., 2016. Flood projections within the Niger River Basin under future land use and climate change 562, 666–677.

Almeida, C.M., Gleriani, J.M., Castejon, E.F., Soares-Filho, B.S., 2008. Using neural networks and cellular automata for modelling intra-urban land-use dynamics. Int. J. Geogr. Inf. Sci. 22, 943–963. https://doi.org/10.1080/13658810701731168

American Institute National Standards, A., 1992. American National Standards Institute. Hemodialysis systems. ANSI/AAMI RD5-1992. Arlington, VA .

Anderson, P.M., Woessner, W.W., Hunt, J.R., 2015. Applied Groundwater Modeling. Elsevier.

Andersson, J.C.M., Arheimer, B., Traoré, F., Gustafsson, D., Ali, A., 2017. Process refinements improve a hydrological model concept applied to the Niger River basin. Hydrol. Process. 31, 4540–4554. https://doi.org/10.1002/hyp.11376

Arnold, J.G., Srinivasan, R., Muttiah, R.S., Williams, J.R., 1998. Large Area Hydrological Modeling and Assessment Part I: Model Development. 34, 73–89.

Aryal, A., Shrestha, S., Babel, M.S., 2017. Quantifying the sources of uncertainty in an ensemble of hydrological climate-impact projections. Theor. Appl. Climatol. 135, 193–209.

Aslam, R.A., Shrestha, S., Pandey, V.P., 2018. Groundwater vulnerability to climate change: A review of the assessment methodology. Sci. Total Environ. 612, 853–875. https://doi.org/10.1016/j.scitotenv.2017.08.237

Babel, M.S., Bhusal, S.P., Wahid, S.M., Agarwal, A., 2014. Climate change and water resources in the Bagmati River Basin, Nepal. Theor. Appl. Climatol. 115, 639–654. https://doi.org/10.1007/s00704-013-0910-4

Bajracharya, A.R., Bajracharya, S.R., Shrestha, A.B., Maharjan, S.B., 2018. Climate change impact assessment on the hydrological regime of the Kaligandaki Basin, Nepal. Sci. Total Environ. 625, 837–848.

Barlow, P.M., Harbaugh, A.W., 2006. USGS directions in MODFLOW development. Ground Water 44, 771–774. https://doi.org/10.1111/j.1745-6584.2006.00260.x

Bashir, A.M., Fakhry, A.A., Philip, E.L., James, W.L., Mostafa, M.S., 2008. Environmental Hydrogeology. Taylor & Francis Group, USA.

Basnet, S., 2016. Simulation of Kathmandu Valley River Basin Hydrologic Process Using Coupled Ground and Surface Water Model. by. IoE, Pulchowk Campus. TRIBHUVAN UNIVERSITY. https://doi.org/10.5151/cidi2017-060

Bedekar, V., Niswonger, R.G., Kipp, K., Panday, S., Tonkin, M., 2012. Approaches to the Simulation of Unconfined Flow and Perched Groundwater Flow in MODFLOW.

Ground Water 50, 187–198. https://doi.org/10.1111/j.1745-6584.2011.00829.x

Behzadian, M., Kazemzadeh, R.B., Albadvi, A., Aghdasi, M., 2010. PROMETHEE: A comprehensive literature review on methodologies and applications. Eur. J. Oper. Res. 200, 198–215. https://doi.org/10.1016/j.ejor.2009.01.021

Belhassan, K., 2011. Relationship between River Flow , Rainfall and Groundwater pumpage in Mikkes Basin (Morocco). Iran. J. Earth Sci. 3, 98–107.

Bergström, S., 2006. Experience from applications of the HBV hydrological model from the perspective of prediction in ungauged basins. IAHS-AISH Publ. 97–107.

Beskow, S., Norton, L.D., Mello, C.R., 2013. Hydrological prediction in a tropical watershed dominated by oxisols using a distributed hydrological model. Water Resour. Manag. 27, 341–363.

Beven, K.J., Kirkby, M.J., Schofield, N., Tagg, A.F., 1984. Testing a Physically-Based Flood Forecasting Model (Topmodel) for Three U. K. Catchments. J. Hydrol. 69, 119–143.

Bhaskar, A.S., Welty, C., 2015. Analysis of subsurface storage and streamflow generation in urban watersheds. Water Resour. Res. 51, 1493–1513. https://doi.org/10.1002/2014WR015607.Received

Bhatt, D., Maskey, S., Babel, M.S., Uhlenbrook, S., Prasad, K.C., 2014. Climate trends and impacts on crop production in the Koshi River basin of Nepal. Reg. Environ. Chang. 14, 1291–1301.

Binley, A., Elgy, J., Beven, K., 1989. A physically based model of heterogeneous hillslopes: 1. Runoff production. Water Resour. Res. 25, 1219–1226. https://doi.org/10.1029/WR025i006p01219

Binnie & Partner, 1988. Water supply for kathmandu and Lalitpur from outside the Valley, final report on feasibility study, Appendix-L (groundwater resources within the valley).

Biondi, D., Freni, G., Iacobellis, V., Mascaro, G., Montanari, A., 2012. Validation of hydrological models: Conceptual basis, methodological approaches and a proposal for a code of practice. Phys. Chem. Earth 42–44, 70–76. https://doi.org/10.1016/j.pce.2011.07.037

Bolch, T., Kulkarni, A., Kääb, A., Huggel, C., Paul, F., Cogley, J.G., Frey, H., Kargel, J.S., Fujita, K., Scheel, M., Bajracharya, S., Stoffel, M., 2012. The state and fate of

himalayan glaciers. Science (80-.). 336, 310–314. https://doi.org/10.1126/science.1215828

Boretti, A., Rosa, L., 2019. Reassessing the projections of the World Water Development Report. npj Clean Water 2. https://doi.org/10.1038/s41545-019-0039-9

Bormann, H., Breuer, L., Gräff, T., Huisman, J.A., Croke, B., 2009. Assessing the impact of land use change on hydrology by ensemble modelling (LUCHEM) IV: Model sensitivity to data aggregation and spatial (re-)distribution. Adv. Water Resour. https://doi.org/10.1016/j.advwatres.2008.01.002

Bosch, J.M., Hewlett, J.D., 1982. A Review of Catchment Experiments to Determine the effect of Vegetation changes on Water Yield and Evapotranspiration. J. Hydrol. 55, 3–23. https://doi.org/10.1017/CBO9781107415324.004

Bosznay, M., 1989. Generalization of SCS Curve Number Method. 115, 139–144.

Brown, C., Boltz, F., Freeman, S., Tront, J., Rodriguez, D., 2020. Resilience by design: A deep uncertainty approach for water systems in a changing world. Water Secur. 9, 100051. https://doi.org/10.1016/j.wasec.2019.100051

Burba, G.G., Verma, S.B., 2005. Seasonal and interannual variability in evapotranspiration of native tallgrass prairie and cultivated wheat ecosystems. Agric. For. Meteorol. 135, 190–201. https://doi.org/10.1016/j.agrformet.2005.11.017

Burnash, R.J.C., Ferral, R.L., McGuire, R.A., 1973. A generalized streamflow simulation system - Conceptual modeling for digital computers.

Cao, N., Hiroyuki, D.Æ., Hiroyuki, A.Æ., Kenichi, Y.Æ., 2005. Simulation of groundwater flow and environmental effects resulting from pumping 361–374. https://doi.org/10.1007/s00254-004-1158-1

Castaneda-Gonzalez, M., Poulin, A., Romero-Lopez, R., Arsenault, R., Brissette, F., Chaumont, D., Paquin, D., 2018. Impacts of Regional Climate Model Spatial Resolution on Summer Flood Simulation 3, 372–362. https://doi.org/10.29007/hd8l

CBS, 2011. Nepal Census 2011.

CBS, N., 2012. National population and housing census 2011, National Report.

Chaudhary, P., Chhetri, S.K., Joshi, K.M., Shrestha, B.M., Kayastha, P., 2016. Application of an Analytic Hierarchy Process (AHP) in the GIS interface for suitable fire site selection:

A case study from Kathmandu Metropolitan City, Nepal. J. Socio-Economic Plan. Sci. 53, 60–71.

Chen, F., Hu, Y., Peng, X., Wang, L., 2010. Simulation of land use/cover change based on the CLUE-S model, in: 2010 18th International Conference on Geoinformatics. IEEE, pp. 1–5.

Chen, S., Li, W.B., Du, Y.D., Mao, C.Y., Zhang, L., 2015. Urbanization effect on precipitation over the Pearl River Delta based on CMORPH data. Adv. Clim. Chang. Res. 6, 16–22. https://doi.org/10.1016/j.accre.2015.08.002

Chen, Y., Okudan, G.E., Riley, D.R., 2010. Decision support for construction method selection in concrete buildings: Prefabrication adoption and optimization. Autom. Constr. 19, 665–675. https://doi.org/10.1016/j.autcon.2010.02.011

Chiang, W.H., 2005. W.-H. Chiang 3D-Groundwater Modeling with PMWIN, New York.

Chow, T.E., Sadler, R., 2010. The consensus of local stakeholders and outside experts in suitability modeling for future camp development. Landsc. Urban Plan. 94, 9–19. https://doi.org/10.1016/j.landurbplan.2009.07.013

Chow, T.E., Sadler, R. %J L., Planning, U., 2010. The consensus of local stakeholders and outside experts in suitability modeling for future camp development 94, 9–19.

Chow, V.T., 1988. Applied hydrology. Tata McGraw-Hill Education.

Cohen, J., 1960. A coefficient of agreement for nominal scales. Educ. Psychol. Meas. 20, 37–46.

Collin, M.L., Melloul, A.J., 2003. Assessing groundwater vulnerability to pollution to promote sustainable urban and rural development. J. Clean. Prod. 11, 727–736. https://doi.org/10.1016/S0959-6526(02)00131-2

Crawford, N.H., Linsley, R.K., 1966. Digital simulation in hydrology: Stanford Watershed Model IV. Contemp. Hydrol.

Cresswell, G.R., Bauld, J., Jacobson, G., Khadka, M.S., Jha, M.G., Shrestha, M.P., Regmi, S., 2001. Estimation of groundwater quality in kathmandu valley. Ground Water 39, 449–457.

D€oll, P., Schmied, H.M., C., S., Portmann, F.T., Eicker, A., 2014. Global-scale assessment of groundwater depletion and related groundwater abstractions: Combining hydrological

modeling with information from well observations and GRACE satellites. Water Resour. Res. 5698–5720. https://doi.org/doi:10.1002/ 2014WR015595. Received

Dahal, A., Khanal, R., Mishra, B.K., 2019. Identification of critical location for enhancing groundwater recharge in Kathmandu Valley, Nepal. Groundw. Sustain. Dev. 9, 100253. https://doi.org/10.1016/j.gsd.2019.100253

Darcy, H., 1856. De`termination des lois d'e` coulement de l'eau a` travers le sable, in: Les Fontaines Publiques de La Ville de Dijon. pp. 590–594.

Dhital, Y.P., Tang, Q., Shi, J. %J J. of G.S., 2013. Hydroclimatological changes in the Bagmati River basin, Nepal 23, 612–626.

DHM, 2015. Hydrological records of Nepal, streamflow summary, updated version. Department of Hydrology and Meteorology: Goverment of Nepal, Ministry of Water Resources, Kathmandu.

Dingman, 2002. Physical Hydrology, Logn Grove. IL. Logn Grove. IL, Washington, DC.

Dong, Y., Li, G., Xu, H., 2012. An areal recharge and discharge simulating method for MODFLOW. Comput. Geosci. 42, 203–205. https://doi.org/10.1016/j.cageo.2011.10.005

Dongol, G.M., 1985. Geology of the Kathmandu fluvial lacustrine sediments in the light of new vertebrate fossil occurrences. J. Nepal Geol. Soc. 3, 43–57.

Donn, M.J., Barron, O. V., Barr, A.D., 2012. Identification of phosphorus export from low-runoff yielding areas using combined application of high frequency water quality data and MODHMS modelling. Sci. Total Environ. 426, 264–271. https://doi.org/10.1016/j.scitotenv.2012.03.021

Dwarakish, G.S., Ganasri, B.P., 2015. Impact of land use change on hydrological systems: A review of current modeling approaches. Cogent Geosci. 1. https://doi.org/10.1080/23312041.2015.1115691

Eastman, J.R., 2003. IDRISI Kilimanjaro, guide to GIS and image processing, user's guide (Ver. 14).

Engen-Skaugen, T., 2007. Refinement of dynamically downscaled precipitation and temperature scenarios. Clim. Change 84, 365–382. https://doi.org/10.1007/s10584-007-9251-6

Fishburn, P.C., 1967. Conjoint measurement in utility theory with incomplete product sets. J. Math. Psychol. 4, 104–119. https://doi.org/10.1016/0022-2496(67)90043-0

Fonseca, A., Botelho, C., Boaventura, R.A.R., Vilar, V.J.P., 2014. Integrated hydrological and water quality model for river management: A case study on Lena River. Sci. Total Environ. 485–486, 474–489. https://doi.org/10.1016/j.scitotenv.2014.03.111

Foster, S., Garduno, H., Evans, R., Olson, D., Tian, Y., Zhang, W., Han, Z., 2004. Quaternary aquifer of the North China Plain - Assessing and achieving groundwater resource sustainability. Hydrogeol. J. 12, 81–93. https://doi.org/10.1007/s10040-003-0300-6

Foster, S., Macdonald, A., 2014. The ‘ water security ’ dialogue : why it needs to be better informed about groundwater 1489–1492. https://doi.org/10.1007/s10040-014-1157-6

Freeze, R.A., 1971. Three-Dimensional, Transient, Saturated-Unsaturated Flow in a Groundwater Basin. Water Resour. Res. 7, 347–366. https://doi.org/10.1029/WR007i002p00347

Freeze, R.A., Witherspoon, P.A., 1966. Theoretical analysis of regional groundwater flow: 1. Analytical and numerical solutions to the mathematical model. Water Resour. Res. 2, 641–656. https://doi.org/10.1029/WR002i004p00641

Ganot, Y., Holtzman, R., Weisbrod, N., Nitzan, I., Katz, Y., Kurtzman, D. %J H., Sciences, E.S., 2017. Monitoring and modeling infiltration-recharge dynamics of managed aquifer recharge with desalinated seawater 21.

Gautam, D., Prajapati, R.N., 2014. Drawdown and dynamics of groundwater table in Kathmandu Valley, Nepal. Open Hydrol. J. 8.

Gautam, M.R., Acharya, K., Tuladhar, M.K., 2010. Upward trend of streamflow and precipitation in a small, non-snow-fed, mountainous watershed in Nepal. J. Hydrol. 387, 304–311. https://doi.org/10.1016/j.jhydrol.2010.04.022

Gonzalez-Aparicio, I., Zucker, A., 2015. Meteorological data for RES-E integration studies. https://doi.org/10.2790/349276

Gorelick, S.M. and Zhen, C., 2016. Global change and the groundwater management challenge Steven. Water Resour. Res. 3031–3051. https://doi.org/10.1002/2014WR016825.Received

Gudmundsson, L., Bremnes, J.B., Haugen, J.E., Engen-Skaugen, T., 2012. Technical Note:

Downscaling RCM precipitation to the station scale using statistical transformations – A comparison of methods. Hydrol. Earth Syst. Sci. 16, 3383–3390. https://doi.org/10.5194/hess-16-3383-2012

Guo-yu, R.E.N., Bhakta, A., 2017. Climate change in the Hindu Kush Himalaya ScienceDirect Climate change in the Hindu Kush Himalaya. Adv. Clim. Chang. Res. https://doi.org/10.1016/j.accre.2017.09.001

Gupta, H. V., Kling, H., Yilmaz, K.K., Martinez, G.F., 2009. Decomposition of the mean squared error and NSE performance criteria: Implications for improving hydrological modelling. J. Hydrol. 377, 80–91. https://doi.org/10.1016/j.jhydrol.2009.08.003

Gurung, J.K., Ishiga, H., Khadka, M.S., Shrestha, N.R., 2007. The geochemical study of fluvio-lacustrine aquifers in the Kathmandu Basin (Nepal) and the implications for the mobilization of arsenic. Environ. Geol. 52, 503–517. https://doi.org/10.1007/s00254-006-0483-y

Gyawali, R., Watkins, D.W., 2013. Continuous hydrologic modeling of snow-affected watersheds in the great lakes basin using HEC-HMS. J. Hydrol. Eng. 18, 29–39. https://doi.org/10.1061/(ASCE)HE.1943-5584.0000591

Hagen, G.H.L., 1839. Movement of water in a narrow cylindrical tub: Leipzig. Annalen Physik und Chemie 46, 423–442.

Han, D., Currell, M.J., Cao, G., Hall, B., 2017. Alterations to groundwater recharge due to anthropogenic landscape change. J. Hydrol. 554, 545–557. https://doi.org/10.1016/j.jhydrol.2017.09.018

Harbaugh, A.W., 2005. MODFLOW-2005 , The U . S . Geological Survey Modular Ground-Water Model — the Ground-Water Flow Process. U.S. Geol. Surv. Tech. Methods 253.

Hermans, E., Brijs, T., Wets, G., Vanhoof, K., 2009. Benchmarking road safety: Lessons to learn from a data envelopment analysis. Accid. Anal. Prev. 41, 174–182. https://doi.org/10.1016/j.aap.2008.10.010

Hydrologic Engineering Center (US), 1981. HEC-1 flood hydrograph package: Users manual . US Army Corps of Engineers, Water Resources Support Center, Hydrologic Engineering Center.

ICIMOD, 2010. Land Cover of Nepal 2010 [Dataset]. International Center for Integrated Mountain Development (ICIMOD): Kathmandu, Nepal. Available online at:

http://rds.icimod.org/Home/DataDetail?metadataId=9224. [WWW Document].

Iizumi, T., Yokozawa, M., Nishimori, M., 2009. Parameter estimation and uncertainty analysis of a large-scale crop model for paddy rice: Application of a Bayesian approach. Agric. For. Meteorol. 149, 333–348. https://doi.org/10.1016/j.agrformet.2008.08.015

IPCC, 2018. Intergovernmental Panel on Climate Change (IPCC), An IPCC Special Report on the Impacts of Global Warming of 1.5 °C Above Pre-Industrial Levels and Related Global Greenhouse Gas Emission Pathways, in the Context of Strengthening the Global Response to the.

IPCC, 2014. Climate Change 2014: Synthesis Report. Contribution of Working Groups I, II and III to the Fifth Assessment Report of the Intergovernmental Panel on Climate Change [Core Writing Team, R.K. Pachauri and L.A. Meyer (eds.)], IPCC, Geneva, Switzerland. https://doi.org/10.1177/0002716295541001010

IPCC, 2007. Intergovernmental Panel on Climate Change, "Summary for policymakers, climate change 2007: The physical science basis." Contribution of Working Group I to the Fourth Assessment Rep. of the Intergovernmental Panel on Climate Change . Cambridge University Press, Cambridge, U.K.

Ishtiaque, A., Shrestha, M., Chhetri, N., 2017. Rapid urban growth in the Kathmandu Valley, Nepal: Monitoring land use land cover dynamics of a himalayan city with landsat imageries. Environments 4, 72.

Jajarmizadeh, M., Harun, S., Salarpour, M., 2012. A review on theoretical consideration and types of models in hydrology. J. Environ. Sci. Technol. 5, 249–261. https://doi.org/10.3923/jest.2012.249.261

Jennings, D.B., Jarnagin, S.T., 2002. Changes in anthropogenic impervious surfaces, precipitation and daily streamflow discharge: A historical perspective in a mid-atlantic subwatershed. Landsc. Ecol. 17, 471–489. https://doi.org/10.1023/A:1021211114125

Jhariya, D.C., Kumar, T., Gobinath, M., Diwan, P., Kishore, N., 2016. Assessment of groundwater potential zone using remote sensing, GIS and multi criteria decision analysis techniques. J. Geol. Soc. India 88, 481–492.

Jiang, W., Chen, Z., Lei, X., Jia, K., Wu, Y., 2015. Simulating urban land use change by incorporating an autologistic regression model into a CLUE-S model. J. Geogr. Sci. 25, 836–850. https://doi.org/10.1007/s11442-015-1205-8

JICA, 1990. Groundwater Management Project in Kathmandu Valley. Nepal Water Supply Corporation, Kathmandu, Nepal.

K.C., G., 2011. Numerical Modeling of Groundwater in Kathmandu Valley, Nepal 85.

Kaliraj, S., Chandrasekar, N., Magesh, N.S., 2014. Identification of potential groundwater recharge zones in Vaigai upper basin, Tamil Nadu, using GIS-based analytical hierarchical process (AHP) technique. Arab. J. Geosci. 7, 1385–1401.

Karki, R., Hasson, S., Schickhoff, U., Scholten, T., 2017. Rising Precipitation Extremes across Nepal 1–25. https://doi.org/10.3390/cli5010004

Kharin, V. V., Zwiers, F.W., Zhang, X., Wehner, M., 2013. Changes in temperature and precipitation extremes in the CMIP5 ensemble. Clim. Change 119, 345–357. https://doi.org/10.1007/s10584-013-0705-8

Kim, O., 2010. Comparison of Two GIS based Land Change Modules for Constructing REDD Baselines in Bolivia., in: Paper Presented at the AAG Annual Meeting, Washington, DC. Washington, DC.

Kirkby, M.J., 1976. Hydrological slope models: the influence of climate, in: Geomorphology and Climate. Department of Geography, University of Leeds, pp. 245–267.

Knisel, W.G., 1980. {Creams} - a Field Scale Model for Chemicals, Runoff, and Erosion From Agricultural Management Systems. Science and Education Administration, Congressional Research Report 26. Department of Agriculture, Science and Education Adminstration.

Konidari, P., Mavrakis, D., 2007. A multi-criteria evaluation method for climate change mitigation policy instruments. Energy Policy 35, 6235–6257. https://doi.org/10.1016/j.enpol.2007.07.007

Krause, P., Boyle, D.P., Bäse, F., 2005. Comparison of different efficiency criteria for hydrological model assessment. Adv. Geosci. 5, 89–97. https://doi.org/10.5194/adgeo-5-89-2005

Kucharik, C.J., 2003. Evaluation of a Process-Based Agro-Ecosystem Model (Agro-IBIS) across the U.S. Corn Belt: Simulations of the Interannual Variability in Maize Yield. Earth Interact. 7, 1–33. https://doi.org/10.1175/1087-3562(2003)007<0001:eoapam>2.0.co;2

KUKL, 2015. Kathmandu Upatyaka Khanepani Limited Annual Report; Kathmandu Upatyka Khanepani Limited: Kathmandu, Nepal. Kathmandu Upatyka Khanepani Limited (KUKL), Kathmandu, Nepal.

Kumar, C.P., 2019. An Overview of Commonly Used Groundwater Modelling Software. Int. J. Adv. Sci. Eng. Technol. 6, 7854–7865.

Lamichhane, S., Shakya, N.M., 2019a. Alteration of groundwater recharge areas due to land use/cover change in Kathmandu Valley, Nepal. J. Hydrol. Reg. Stud. 26, 100635. https://doi.org/10.1016/j.ejrh.2019.100635

Lamichhane, S., Shakya, N.M., 2019b. Integrated Assessment of Climate Change and Land Use Change Impacts on Hydrology in the Kathmandu Valley Watershed, Central Nepal. Water (Switzerland) 11, 1–17. https://doi.org/10.3390/w11102059

Laurenson, E.M., Mein, R.G., RORB, V., 1983. 3: Runoff Routing Program-User Manual. Dep. of Civil Eng., RORB-vers ion , 3 .

Legates, D.R., McCabe, G.J., 1999. Evaluating the use of "goodness-of-fit" measures in hydrologic and hydroclimatic model validation. Water Resour. Res. 35, 233–241. https://doi.org/10.1029/1998WR900018

Lewarne, M., 2009. Setting up ArcSWAT hydrological model for the Verlorenvlei catchment 1–95.

Li, C., Sinha, E., Horton, D.E., Diffenbaugh, N.S., Michalak, A.M., 2014. Joint bias correction of temperature and precipitation in climate model simulations. J. Geophys. Res. Atmos. 119, 13,113-153,162.

Li, H., Sun, J., 2008. Ranking-order case-based reasoning for financial distress prediction. Knowledge-Based Syst. 21, 868–878. https://doi.org/10.1016/j.knosys.2008.03.047

Li, X., Yeh, A.G.O., 2002. Neural-network-based cellular automata for simulating multiple land use changes using GIS. Int. J. Geogr. Inf. Sci. 16, 323–343. https://doi.org/10.1080/13658810210137004

Liang, S., Zhao, X., Li, S., Feng, L., Liu, X., Qin, X., 2012. The application of GMS in numerical simulation of groundwater and faults disposing in Gaizi River Source. Adv. Mater. Res. 518–523, 4047–4056. https://doi.org/10.4028/www.scientific.net/AMR.518-523.4047

Liu, M., Hu, Y., Zhang, W., Zhu, J., Chen, H., Xi, F., 2011. Application of land-use change model in guiding regional planning: A case study in Hun-Taizi River watershed, Northeast China. Chinese Geogr. Sci. 21, 609.

Liu, M., Li, C., Hu, Y., Sun, F., Xu, Y., Chen, T., 2014. Combining CLUE-S and SWAT models to forecast land use change and non-point source pollution impact at a watershed scale in Liaoning Province, China. Chinese Geogr. Sci. 24, 540–550. https://doi.org/10.1007/s11769-014-0661-x

Loudyi, D., 2005. 2D finite volume model for groundwater flow simulations : integrating non-orthogonal grid capability into modflow. PQDT - Glob.

Lucke, T., Boogaard, F., van de Ven, F., 2014. Evaluation of a new experimental test procedure to more accurately determine the surface infiltration rate of permeable pavement systems. J. Urban Plan. Transp. Res. 2, 22–35.

Luoma, S., 2016. Groundwater vulnerability of a shallow low-lying coastal aquifer in southern Finland under climate change. University of Helsinki.

Lutz, A.F., ter Maat, H.W., Biemans, H., Shrestha, A.B., Wester, P., Immerzeel, W.W., 2016. Selecting representative climate models for climate change impact studies: an advanced envelope-based selection approach. Int. J. Climatol. 36, 3988–4005.

Malczewski, J., 2004. GIS-based land-use suitability analysis: A critical overview. Prog. Plann. 62, 3–65. https://doi.org/10.1016/j.progress.2003.09.002

Malczewski, J., 1999. GIS and multicriteria decision analysis. John Wiley & Sons.

McColl, C., Aggett, G., 2007. Land-use forecasting and hydrologic model integration for improved land-use decision support. J. Environ. Manage. 84, 494–512. https://doi.org/10.1016/j.jenvman.2006.06.023

McDonald, M.G., Harbaugh, A.W., 1984. U.S. Geological Survey (USGS). Open File Rep.

Metcalf & Eddy, 2000. Urban water supply reforms in the Kathmandu Valley (ADB TA Number 2998-NEP). Complet. report, vols I, II. Exec. Summ. main Rep. Annex 1 to 7. Metcalf Eddy, Inc. with CEMAT Consult. Ltd., 18 Febr. 2000.

Mishra, B.K., Herath, S., 2014. Assessment of future floods in the Bagmati River Basin of Nepal using bias-corrected daily GCM precipitation data. J. Hydrol. Eng. 20, 5014027.

Mishra, Y., Nakamura, T., Babel, M.S., Ninsawat, S., Ochi, S., 2018. Impact of climate

change on water resources of the Bheri River Basin, Nepal. Water (Switzerland) 10, 1–21. https://doi.org/10.3390/w10020220

MoFE, 2019. MoFE, Climate Change Scenarios for Nepal National Adaptation Plan.

Mohammady, M., Moradi, H.R., Zeinivand, H., Temme, A., Yazdani, M.R., Pourghasemi, H.R. %J T., climatology, applied, 2017. Modeling and assessing the effects of land use changes on runoff generation with the CLUE-s and WetSpa models 1–13.

Mohammady, M., Moradi, H.R., Zeinivand, H., Temme, A.J.A.M., Yazdani, M.R., Pourghasemi, H.R., 2018. Modeling and assessing the effects of land use changes on runoff generation with the CLUE-s and WetSpa models. Theor. Appl. Climatol. 133, 459–471. https://doi.org/10.1007/s00704-017-2190-x

Moriasi, D.N., Arnold, J.G., Liew, M.W. Van, Bingner, R.L., Harmel, R.D., Veith, T.L., 2007. Model Evaluation Guidelines for Systematic Quantification of Accuracy in Watershed Simulations. Am. Soc. Agric. Biol. Eng. ISSN 0001−2351 885 50, 885–900.

MoUD, 2017. National Urban Development Strategy, National Urban Development Strategy. https://doi.org/10.1017/CBO9781107415324.004

Nambiar, R., Shroff, R., Handy, S., 2018. Smart cities: Challenges and opportunities. 2018 10th Int. Conf. Commun. Syst. Networks, COMSNETS 2018 2018-Janua, 243–250. https://doi.org/10.1109/COMSNETS.2018.8328204

Narula, K.K., Gosain, A.K., 2013. Modeling hydrology, groundwater recharge and non-point nitrate loadings in the Himalayan Upper Yamuna basin. Sci. Total Environ. 468–469, S102–S116. https://doi.org/10.1016/j.scitotenv.2013.01.022

Nash, J.E., Sutcliffe, J. V., 1970. River flow forecasting through conceptual models part I - A discussion of principles. J. Hydrol. 10, 282–290. https://doi.org/10.1016/0022-1694(70)90255-6

Nasseri, M., Zahraie, B., Ajami, N.K., Solomatine, D.P., 2014. Monthly water balance modeling: Probabilistic, possibilistic and hybrid methods for model combination and ensemble simulation. J. Hydrol. 511, 675–691. https://doi.org/10.1016/j.jhydrol.2014.01.065

Neitsch, S.., Arnold, J.., Kiniry, J.., Williams, J.., 2011. Soil & Water Assessment Tool Theoretical Documentation Version 2009. Texas Water Resour. Inst. 1–647. https://doi.org/10.1016/j.scitotenv.2015.11.063

Nyeko, M., 2015. Hydrologic Modelling of Data Scarce Basin with SWAT Model: Capabilities and Limitations. Water Resour. Manag. 29, 81–94. https://doi.org/10.1007/s11269-014-0828-3

O'Neill, B.C., Kriegler, E., Riahi, K., Ebi, K.L., Hallegatte, S., Carter, T.R., Mathur, R., van Vuuren, D.P., 2014. A new scenario framework for climate change research: The concept of shared socioeconomic pathways. Clim. Change 122, 387–400. https://doi.org/10.1007/s10584-013-0905-2

Olsthoorn, T.N., 2011. User guide for mfLab 5678.

Oogathoo, S., 2006. Runoff Simulation in the Canagagiue Creek watershed using the MIKE SHE Model. McGill University Montreal, Canada.

Pandey, V.P., Chapagain, S.K., Kazama, F., 2010. Evaluation of groundwater environment of Kathmandu valley. Environ. Earth Sci. 60, 1329–1342. https://doi.org/10.1007/s12665-009-0263-6

Pandey, V.P., Dhaubanjar, S., Bharati, L., Thapa, B.R., 2019. Hydrological response of Chamelia watershed in Mahakali Basin to climate change. Sci. Total Environ. 650, 365–383. https://doi.org/10.1016/j.scitotenv.2018.09.053

Pandey, V.P., Kazama, F., 2014. From an open-access to a state-controlled resource: the case of groundwater in the Kathmandu Valley, Nepal. Water Int. 39, 97–112. https://doi.org/10.1080/02508060.2014.863687

Pandey, V.P., Kazama, F., 2011. Hydrogeologic characteristics of groundwater aquifers in Kathmandu Valley, Nepal. Environ. Earth Sci. 62, 1723–1732. https://doi.org/10.1007/s12665-010-0667-3

Pandey, V.P., Shrestha, S., Kazama, F., 2013. A GIS-based methodology to delineate potential areas for groundwater development: a case study from Kathmandu Valley, Nepal. Appl. Water Sci. 3, 453–465.

Paudel, B., Zhang, Y. li, Li, S. cheng, Liu, L. shan, Wu, X., Khanal, N.R., 2016. Review of studies on land use and land cover change in Nepal. J. Mt. Sci. 13, 643–660. https://doi.org/10.1007/s11629-015-3604-9

Pei-Yue, L., Hui, Q., Jian-Hua, W.U., 2010. Groundwater quality assessment based on improved water quality index in Pengyang County, Ningxia, Northwest China. J. Chem. 7, S209–S216.

Pointius, R.G., Schneider, L.C., 2001. Land-cover change model validation by an ROC method for the Ipswich watershed, Massachusetts, USA. Agric. Ecosyst. Environ. 85, 239–248. https://doi.org/10.4018/978-1-61692-871-1.ch003

Poiseuille, J., 1840. Recherches expérimentales sur le mouvement des liquides dans les tubes de très petits diamètres [Experimental research on the movement of liquids in capillary of very small diameters]. Comptes rendus Hebd. des séances l'Académie des Sci. 11, 1041–1048.

Pokhrel, B., 2018. Impact of Land Use Change on Flow and Sediment Yields in the Khokana Outlet of the Bagmati River, Kathmandu, Nepal. Hydrology 5, 22.

Praskievicz, S., Chang, H., 2011. Impacts of climate change and urban development on water resources in the Tualatin River Basin, Oregon. Ann. Assoc. Am. Geogr. 101, 249–271.

Pratomoatmojo, N.A., 2018. LanduseSim Algorithm: Land use change modelling by means of Cellular Automata and Geographic Information System. IOP Conf. Ser. Earth Environ. Sci. 202. https://doi.org/10.1088/1755-1315/202/1/012020

Qin, X.S., Huang, G.H., Chakma, A., Nie, X.H., Lin, Q.G., 2008. A MCDM-based expert system for climate-change impact assessment and adaptation planning - A case study for the Georgia Basin, Canada. Expert Syst. Appl. 34, 2164–2179. https://doi.org/10.1016/j.eswa.2007.02.024

Refsgaard, J.C., Højberg, A.L., Møller, I., Hansen, M., Søndergaard, V., 2010. Groundwater modeling in integrated water resources management - visions for 2020. Ground Water 48, 633–648. https://doi.org/10.1111/j.1745-6584.2009.00634.x

Regmi, J., 2017. Prospects of Arificial Recharge of Shallow Groundwater of Kathmandu Valley. M.Sc. Thesis. TU, Institute of Engineering.

Riahi, K., van Vuuren, D.P., Kriegler, E., Edmonds, J., O'Neill, B.C., Fujimori, S., Bauer, N., Calvin, K., Dellink, R., Fricko, O., Lutz, W., Popp, A., Cuaresma, J.C., KC, S., Leimbach, M., Jiang, L., Kram, T., Rao, S., Emmerling, J., Ebi, K., Hasegawa, T., Havlik, P., Humpenöder, F., Da Silva, L.A., Smith, S., Stehfest, E., Bosetti, V., Eom, J., Gernaat, D., Masui, T., Rogelj, J., Strefler, J., Drouet, L., Krey, V., Luderer, G., Harmsen, M., Takahashi, K., Baumstark, L., Doelman, J.C., Kainuma, M., Klimont, Z., Marangoni, G., Lotze-Campen, H., Obersteiner, M., Tabeau, A., Tavoni, M., 2017. The Shared Socioeconomic Pathways and their energy, land use, and greenhouse gas

emissions implications: An overview. Glob. Environ. Chang. 42, 153–168. https://doi.org/10.1016/j.gloenvcha.2016.05.009

Rimal, B., Zhang, L., Fu, D., Kunwar, R., Zhai, Y., 2017. Monitoring urban growth and the nepal earthquake 2015 for sustainability of Kathmandu Valley, Nepal. Land 6, 42.

Rimal, B., Zhang, L., Keshtkar, H., Haack, B.N., Rijal, S., Zhang, P., 2018. Land use/land cover dynamics and modeling of urban land expansion by the integration of cellular automata and markov chain. ISPRS Int. J. Geo-Information 7. https://doi.org/10.3390/ijgi7040154

Ritter, A., Muñoz-Carpena, R., 2013. Performance evaluation of hydrological models: Statistical significance for reducing subjectivity in goodness-of-fit assessments. J. Hydrol. 480, 33–45. https://doi.org/10.1016/j.jhydrol.2012.12.004

Rockwood, D.M., Davis, E.M., Anderson, J.A., 1972. User manual for COSSARR model . US Army Engineer Division, North Pacific.

Rogelis, M.C., Werner, M., Obregón, N., Wright, N., 2016. Hydrological model assessment for flood early warning in a tropical high mountain basin. Hydrol. Earth Syst. Sci. Discuss. 1–36. https://doi.org/10.5194/hess-2016-30

Romero, C., 1997. Goal Programming and Multiple Criteria Decision Making: Some Reflections 192–198. https://doi.org/10.1007/978-3-642-59132-7_22

Rosner, B., 2010. Fundamentals of Biostatistics (Seventh Edition), Fundamentals of Biostatistics. Harvard University. https://doi.org/10.5005/jp/books/10313

Rukundo, E., Doğan, A., 2019. Dominant influencing factors of groundwater recharge spatial patterns in Ergene river catchment, Turkey. Water (Switzerland) 11. https://doi.org/10.3390/w11040653

Rumbaugh, J., Rumbaugh, D., 2005. Groundwater Vistas 5.0.

Saaty, T.L., 2004. Fundamentals of the analytic network process—multiple networks with benefits, costs, opportunities and risks. J. Syst. Eng. Syst. 13, 348–379.

Saaty, T.L., 1988. What is the analytic hierarchy process?, in: Mathematical Models for Decision Support. Springer, pp. 109–121.

Sahin, V., Hall, J.M., 1996. The effects of afforestation and deforestation on water yields. J. Hydrol. 178, 293–309. https://doi.org/10.1109/IGARSS.2005.1525425

Sakai, H., 2001. (2001a) Stratigraphic division and sedimentary facies of the Kathmandu Basin Group. J. Nepal Geol. Soc. 25 (Specia, 19–32.

Salem, A., Dezso, J., El-Rawy, M., Lóczy, D., 2020. Hydrological modeling to assess the efficiency of groundwater replenishment through natural reservoirs in the Hungarian drava river floodplain. Water (Switzerland) 12. https://doi.org/10.3390/w12010250

Sanford, W., 2002. Recharge and groundwater models: An overview. Hydrogeol. J. 10, 110–120. https://doi.org/10.1007/s10040-001-0173-5

Santhi, C., J.G., A., Williams, J.R., Dugas, W.A., Srinivasan, R., Hauck, L.M., ABSTRACT:, 2001. Validation of the SWAT Model on a Large River Tributing Point and Nonpoint Sources so that the River Watershed in North Central Texas. J. Am. WATER Resour. Assoc. 37, 1169–1188.

Sardoii, E.R., Rostami, N., Sigaroudi, S.K., Taheri, S., 2012. Calibration of loss estimation methods in HEC-HMS for simulation of surface runoff (case study: Amirkabir dam watershed, Iran). Adv. Environ. Biol. 6, 343–348.

Scharffenberg, W.A., Fleming, M.J., Feldman, A.D., 2003. The Hydrologic Modeling System (HEC-HMS): Toward a Complete Framework for Hydrologic Engineering. World Water Environ. Resour. Congr. 1197–1204. https://doi.org/10.1061/40685(2003)172

Schilling, K.E., Chan, K., Liu, H., Zhang, Y., 2010. Quantifying the effect of land use land cover change on increasing discharge in the Upper Mississippi River. J. Hydrol. 387, 343–345. https://doi.org/10.1016/j.jhydrol.2010.04.019

Schönfelder, L.H., Bakken, T.H., Alfredsen, K., Adera, A.G., 2017. Application of HYPE in Norway.

Sener, E., Davraz, A., 2013. Evaluation de la vulnérabilité de l'eau souterraine basée sur un modèle DRASTIC modifié, sur un SIG et une procédure analytique hiérarchisée (AHP): Le cas du bassin du Lac Egirdir (Isparta, Turquie). Hydrogeol. J. 21, 701–714. https://doi.org/10.1007/s10040-012-0947-y

Sharma, R.H., Shakya, N.M., 2006. Hydrological changes and its impact on water resources of Bagmati watershed, Nepal. J. Hydrol. 327, 315–322.

Shaw, E.M., Beven, K.J., Chappell, N.A., Lamb, R., 2010. Hydrology in practice. CRC press.

Shi, T., Huang, Y., Wang, H., Shi, C.E., Yang, Y.J., 2015. Influence of urbanization on the

thermal environment of meteorological station: Satellite-observed evidence. Adv. Clim. Chang. Res. 6, 7–15. https://doi.org/10.1016/j.accre.2015.07.001

Shrestha, M., Acharya, S.C., Shrestha, P.K., 2017. Bias correction of climate models for hydrological modelling–are simple methods still useful? Meteorol. Appl. 24, 531–539.

Shrestha, P.K., Shakya, N.M., Pandey, V.P., Birkinshaw, S.J., Shrestha, S., 2017. Model-based estimation of land subsidence in Kathmandu Valley, Nepal. Geomatics, Nat. Hazards Risk 8, 974–996. https://doi.org/10.1080/19475705.2017.1289985

Shrestha, R.R., 2009. Water Storage "Rainwater Harvesting and Groundwater Recharge for Water Stoarage in the Kathmandu Valley." ICMIOD.

Shrestha, S., 2015. Assessment of Bagmati River Encroachment through Application of GIS and Remote Sensing. https://doi.org/10.13140/RG.2.2.26874.18884

Shrestha, S., Bhatta, B., Shrestha, M., Shrestha, P.K., 2018. Integrated assessment of the climate and landuse change impact on hydrology and water quality in the Songkhram River Basin, Thailand. Sci. Total Environ. 643, 1610–1622.

Shrestha, Sangam, Kafle, R., Pandey, V.P., 2017. Evaluation of index-overlay methods for groundwater vulnerability and risk assessment in Kathmandu Valley, Nepal. Sci. Total Environ. 575, 779–790. https://doi.org/10.1016/j.scitotenv.2016.09.141

Shrestha, S., Neupane, S., Mohanasundaram, S., Pandey, V.P., 2020. Mapping groundwater resiliency under climate change scenarios: A case study of Kathmandu Valley, Nepal. Environ. Res. 183, 109149. https://doi.org/10.1016/j.envres.2020.109149

Shrestha, S., Semkuyu, D.J., Pandey, V.P., 2016a. Science of the Total Environment Assessment of groundwater vulnerability and risk to pollution in Kathmandu Valley, Nepal. Sci. Total Environ. 556, 23–35. https://doi.org/10.1016/j.scitotenv.2016.03.021

Shrestha, Sangam., Shrestha, M., Babel, M.S., 2017. Assessment of climate change impact on water diversion strategies of Melamchi Water Supply Project in Nepal. Theor. Appl. Climatol. 128, 311–323. https://doi.org/10.1007/s00704-015-1713-6

Shrestha, S., Shrestha, M., Babel, M.S., 2016b. Modelling the potential impacts of climate change on hydrology and water resources in the Indrawati River Basin, Nepal. Environ. Earth Sci. 75, 280.

Simunek, J., Van Genuchten, M., Sejna, M., 2005. The HYDRUS-1D: Software Package for

Simulating the One-Dimensional Movement of Water, Heat, and Multiple Solutes in Variably Saturated Media. Univ. California-Riverside Res. Reports PP. 240.

Singh, L.K., Jha, M.K., Chowdary, V.M., 2018. Assessing the accuracy of GIS-based Multi-Criteria Decision Analysis approaches for mapping groundwater potential. Ecol. Indic. 91, 24–37. https://doi.org/10.1016/j.ecolind.2018.03.070

Singh, R.P., Nachtnebel, H.P., 2016. Analytical hierarchy process (AHP) application for reinforcement of hydropower strategy in Nepal. Renew. Sustain. Energy Rev. 55, 43–58. https://doi.org/10.1016/j.rser.2015.10.138

Singh, V.P., Woolhiser, D.A., 2003. Mathematical Modeling of Watershed Hydrology. Perspect. Civ. Eng. Commem. 150th Anniv. Am. Soc. Civ. Eng. 7, 345–367.

Snyder, B.R.L., 1993. Journal of Irrigation and Drainage Engineering 118, 977–980.

Soares-Filho, Rodrigues, H., Costa, W., 2009. Modeling environmental dynamics with Dinamica EGO. Inst. Geociências - Cent. Sensoriamento Remoto 114. https://doi.org/10.13140/RG.2.1.5179.4641

Spruill, C.A., Workman, S.R., Taraba, J.L., 2000. Simulation of daily and monthly stream discharge from small watersheds using the SWAT model. Trans. Am. Soc. Agric. Eng. 43, 1431–1439. https://doi.org/10.13031/2013.3041

Stephanie, M., Ceri, W.H., S.J., O., 2001. Evaluating presence – absence models in ecology : the need to account for prevalence. J. Appl. Ecol. 38, 921–931. https://doi.org/10.1080/09613210110101185

Sugawara, M., 1976. On a method of forecasting the daily discharge of Mae Nam Chao Phraya and its tributaries at several points by means of Tank model. Research notes of the National Research Center for Disaster Prevention , 24 .

Takeuchi, K., Hapuarachchi, P., Zhou, M., Ishidaira, H., Magome, J., 2007. A BTOP model to extend TOPMODEL for distributed hydrological simulation of large basins. Hydrol. Process 22, 3236–3251. https://doi.org/10.1002/hyp.6910

Tang, J., Wang, L., Yao, Z., 2007. Spatio-temporal urban landscape change analysis using the Markov chain model and a modified genetic algorithm. Int. J. Remote Sens. 28, 3255–3271. https://doi.org/10.1080/01431160600962749

Terink, W., Hurkmans, R.T.W.L., Torfs, P.J.J.F., Uijlenhoet, R., 2009. Bias correction of

temperature and precipitation data for regional climate model application to the Rhine basin. Hydrol. Earth Syst. Sci. Discuss. 6, 5377–5413. https://doi.org/10.5194/hessd-6-5377-2009

Thapa, B., Ishidaira, H., Pandey, V., Bhandari, T., Shakya, N., 2018. Evaluation of water security in Kathmandu valley before and after water transfer from another basin. Water 10, 224.

Thapa, B.R., Ishidaira, H., Pandey, V.P., Shakya, N.M., 2017. A multi-model approach for analyzing water balance dynamics in Kathmandu Valley, Nepal. J. Hydrol. Reg. Stud. 9, 149–162. https://doi.org/10.1016/j.ejrh.2016.12.080

Thapa, B.R., Ishidaira, H., Pandey, V.P., Shakya, N.M., 2016. Impact Assessment of Gorkha Earthquake 2015 on Portable Water Supply in Kathmandu Valley: Preliminary Analysis. J. Japan Soc. Civ. Eng. Ser. B1 (Hydraulic Eng. 72, I_61-I_66. https://doi.org/10.2208/jscejhe.72.i_61

Thapa, R.B., Murayama, Y., 2012. Scenario based urban growth allocation in Kathmandu Valley, Nepal. Landsc. Urban Plan. 105, 140–148. https://doi.org/10.1016/j.landurbplan.2011.12.007

Thapa, R.B., Murayama, Y., 2011. Urban growth modeling of Kathmandu metropolitan region, Nepal. Comput. Environ. Urban Syst. 35, 25–34. https://doi.org/10.1016/j.compenvurbsys.2010.07.005

Thapa, R.B., Murayama, Y., 2009. Examining spatiotemporal urbanization patterns in Kathmandu Valley, Nepal: Remote sensing and spatial metrics approaches. Remote Sens. 1, 534–556. https://doi.org/10.3390/rs1030534

Themeßl, M.J., Gobiet, A., Heinrich, G., 2012. Empirical-statistical downscaling and error correction of regional climate models and its impact on the climate change signal. Clim. Change 112, 449–468.

Tiwari, A., Ahuja, A., Vishwakarma, B.D., Jain, K., 2019. Groundwater Potential Zone (GWPZ) for Urban Development Site Suitability Analysis in Bhopal , India. J. Indian Soc. Remote Sens. 47, 1793–1815. https://doi.org/10.1007/s12524-019-01027-0

Tran, D.X., Pla, F., Latorre-Carmona, P., Myint, S.W., Caetano, M., Kieu, H. V., 2017. Characterizing the relationship between land use land cover change and land surface temperature. ISPRS J. Photogramm. Remote Sens. 124, 119–132.

https://doi.org/10.1016/j.isprsjprs.2017.01.001

Trescott, B.P.C., Larson, S.P., 1976. Finite-Difference Model for Simulation of Three-Dimensional Ground-Water Flow.

Udmale, P., Ishidaira, H., Thapa, B., Shakya, N. %J W., 2016. The status of domestic water demand: Supply deficit in the Kathmandu Valley, Nepal. Water (Switzerland) 8, 196.

UN, 2010. United Nations, The Right to Water, Fact Sheet no. 35, UN Office of the High Commissioner for Human Rights (OHCHR). UN Office of the High Commissioner for Human Rights (OHCHR), Geneva, Switzerland. https://doi.org/10.1080/00050326.1947.10436971

UN DESA, 2018. World Urbanization Prospects, Demographic Research. https://doi.org/10.4054/demres.2005.12.9

Van Camp, M., Radfar, M., Walraevens, K., 2010. Assessment of groundwater storage depletion by overexploitation using simple indicators in an irrigated closed aquifer basin in Iran. Agric. Water Manag. 97, 1876–1886. https://doi.org/10.1016/j.agwat.2010.02.006

Van Hear, N., Bakewell, O., Long, K., 2018. Push-pull plus: reconsidering the drivers of migration. J. Ethn. Migr. Stud. 44, 927–944. https://doi.org/10.1080/1369183X.2017.1384135

Velasquez, M., Hester, P., 2013. An analysis of multi-criteria decision making methods. Int. J. Oper. Res. 10, 56–66.

Veldkamp, A., Fresco, L.O., 1996. CLUE-CR: An integrated multi-scale model to simulate land use change scenarios in Costa Rica. Ecol. Modell. 91, 231–248. https://doi.org/10.1016/0304-3800(95)00158-1

Venables, W.N., Smith, D.M., 2013. An Introduction to R, Quantitative Geography: The Basics. https://doi.org/10.4135/9781473920446.n12

Verbist, K., Torfs, S., Cornelis, W.M., Oyarzún, R., Soto, G., Gabriels, D., 2010. Comparison of single-and double-ring infiltrometer methods on stony soils. Vadose Zo. J. 9, 462–475.

Verburg, P., 2010. The CLUE model. Hands-on Exercises. Course Material, in: The CLUE Model. Hands-on Exercises. Course Material. Institute for Environmental Studies,

University of Amsterdam.

Verburg, P.H., Soepboer, W., Veldkamp, A., Limpiada, R., Espaldon, V., Mastura, S.S.A., 2002. Modeling the spatial dynamics of regional land use: The CLUE-S model. Environ. Manage. 30, 391–405. https://doi.org/10.1007/s00267-002-2630-x

Wada, Y., 2016. Modeling Groundwater Depletion at Regional and Global Scales: Present State and Future Prospects. Surv. Geophys. 37, 419–451. https://doi.org/10.1007/s10712-015-9347-x

Wagener, T., Wheater, H., Gupta, H. V., 2004. Rainfall-runoff modelling in gauged and ungauged catchments . World Scientific.

Wakode, H.B., Baier, K., Jha, R., Azzam, R., 2018. Impact of urbanization on groundwater recharge and urban water balance for the city of Hyderabad, India. Int. Soil Res. Water Conserv. 6, 51–62.

Wang, Q., Xu, Youpeng, Xu, Yu, Wu, L., Wang, Y., Han, L., 2018. Spatial hydrological responses to land use and land cover changes in a typical catchment of the Yangtze River Delta region. Catena 170, 305–315.

Waterloo Hydrogeologic, 2001. Visual MODFLOW Pro, 3D groundwater flow and contaminant transport modeling. Waterloo Hydrogeol. 695.

Williams, J.R., Hann, R.W., 1973. HYMO: Problem-orientated computer language for hydrologic modeling Users Manual. Rep. (USDA ARS) 43.

Willmott, C.J., 1984. On the Evaluation of Model Performance in Physical Geography. Spat. Stat. Model. 443–460. https://doi.org/10.1007/978-94-017-3048-8_23

Yang, L., Feng, Q., Yin, Z., Wen, X., Si, J., Li, C., Deo, R.C., 2017. Identifying separate impacts of climate and land use/cover change on hydrological processes in upper stream of Heihe River, Northwest China. Hydrol. Process. 31, 1100–1112.

Yang, S., Cui, X., 2019. Building regional sustainable development scenarios with the SSP framework. Sustain. 11, 1–13. https://doi.org/10.3390/su11205712

Ye, X., Zhang, Q., Liu, J., Li, X., Xu, C.Y., 2013. Distinguishing the relative impacts of climate change and human activities on variation of streamflow in the poyang lake catchment, china. J. Hydrol. 494, 83–95. https://doi.org/10.1016/j.jhydrol.2013.04.036

Yin, J., Yin, Z., Zhong, H., Xu, S., Hu, X., Wang, J., Wu, J., 2011. Monitoring urban

expansion and land use/land cover changes of Shanghai metropolitan area during the transitional economy (1979-2009) in China. Environ. Monit. Assess. 177, 609–621. https://doi.org/10.1007/s10661-010-1660-8

Yoshida, Igarashi, M., 1984. Neogene to Quaternary Lacustrine Sediment in the Kathmandu valley. Nepal. J. Nepal Geol. Soc. 4, 73–100.

Zadesh, L.A., 1965. Fuzzy Sets. Inf. Control 8, 338–353.

Zhou, F., Xu, Y., Chen, Y., Xu, C.-Y., Gao, Y., Du, J., 2013. Hydrological response to urbanization at different spatio-temporal scales simulated by coupling of CLUE-S and the SWAT model in the Yangtze River Delta region. J. Hydrol. 485, 113–125.

Zhou, R., Zhang, H., Ye, X.-Y., Wang, X.-J., Su, H.-L., 2016. The delimitation of urban growth boundaries using the CLUE-S land-use change model: Study on Xinzhuang Town, Changshu City, China. Sustainability 8, 1182.

Zipper, S.C., Evren, M., Kucharik, C.J., Loheide, S.P., 2017. Quantifying indirect groundwater-mediated effects of urbanization on agroecosystem productivity using MODFLOW-AgroIBIS (MAGI), a complete critical zone model. Ecol. Modell. 359, 201–219. https://doi.org/10.1016/j.ecolmodel.2017.06.002

Zundel, A.K., 2000. Surface-water modeling system reference manual. Brigham Young University, Environmental Modeling Research Laboratory, Provo, UT..pdf.

ANNEXES

Annex – I: - LULC change and groundwater potential recharge area information

Annex – II: - Climate change, surface and sub-surface hydrological model information

Annex – III: - Groundwater flow model information

Annex – IV: - Publication

Annex – I

Population Data (1971 to 2011) (Source:- CBS, 2012) and projected upto 2051

Years	BHAKTAPUR	KTHMANDU	LALITPUR	Total
1971	110157.00	353756.00	154998.00	618911.00
1981	159767.00	422237.00	184341.00	766345.00
1991	172952.00	675341.00	257086.00	1105379.00
2001	225451.00	1081845.00	337785.00	1645081.00
2011	304651.00	1744240.00	468132.00	2517023.00
2021	340066.00	2011978.00	525211.00	2877255.00
2031	377660.00	2300890.00	585982.00	3264532.00
2041	408472.00	2522103.00	635151.00	3565726.00
2051	436553.00	2729056.00	680157.00	3845766.00

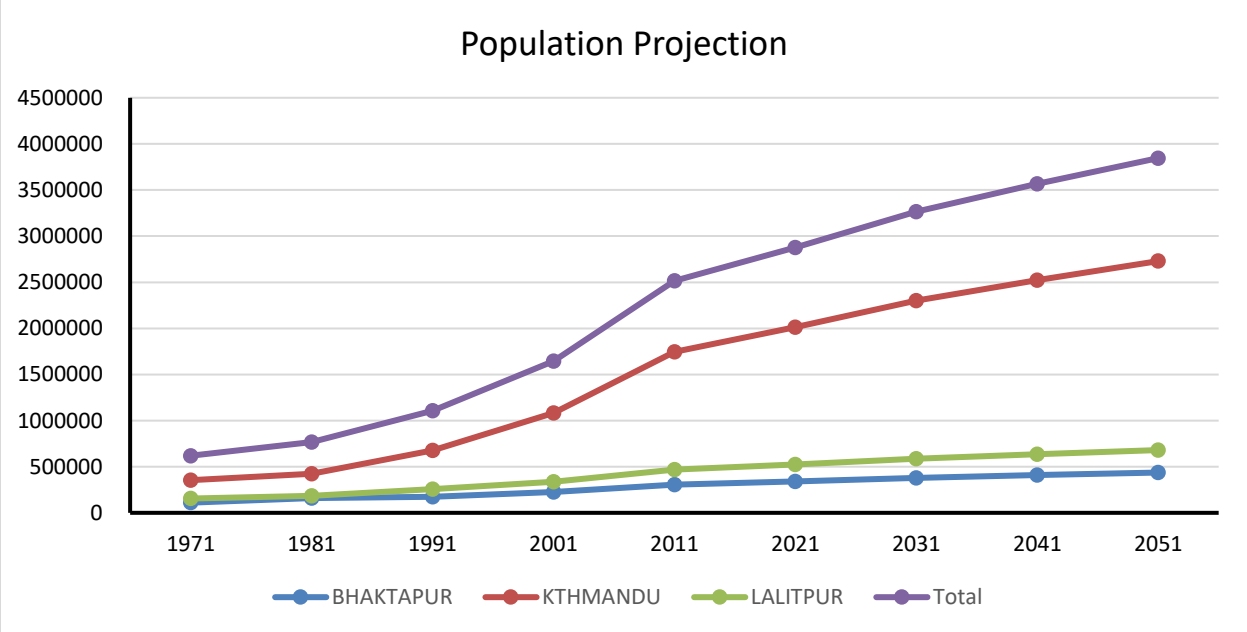

LULC table data of 2010, 2012, 2014, 2016, 2018

S.N.	Land Use Type	2010	2012	2014	2016	2018
1	Forest	201.96	214.245	226.53	221.49	207.72
2	Water Body	1.89	1.575	1.26	1.44	2.25
3	Built Up Area	104.67	111.24	117.81	120.87	138.15
4	Agriculture	293.31	274.725	256.14	257.76	253.71
5	Restricted Area	8.91	8.91	8.91	9.09	8.91

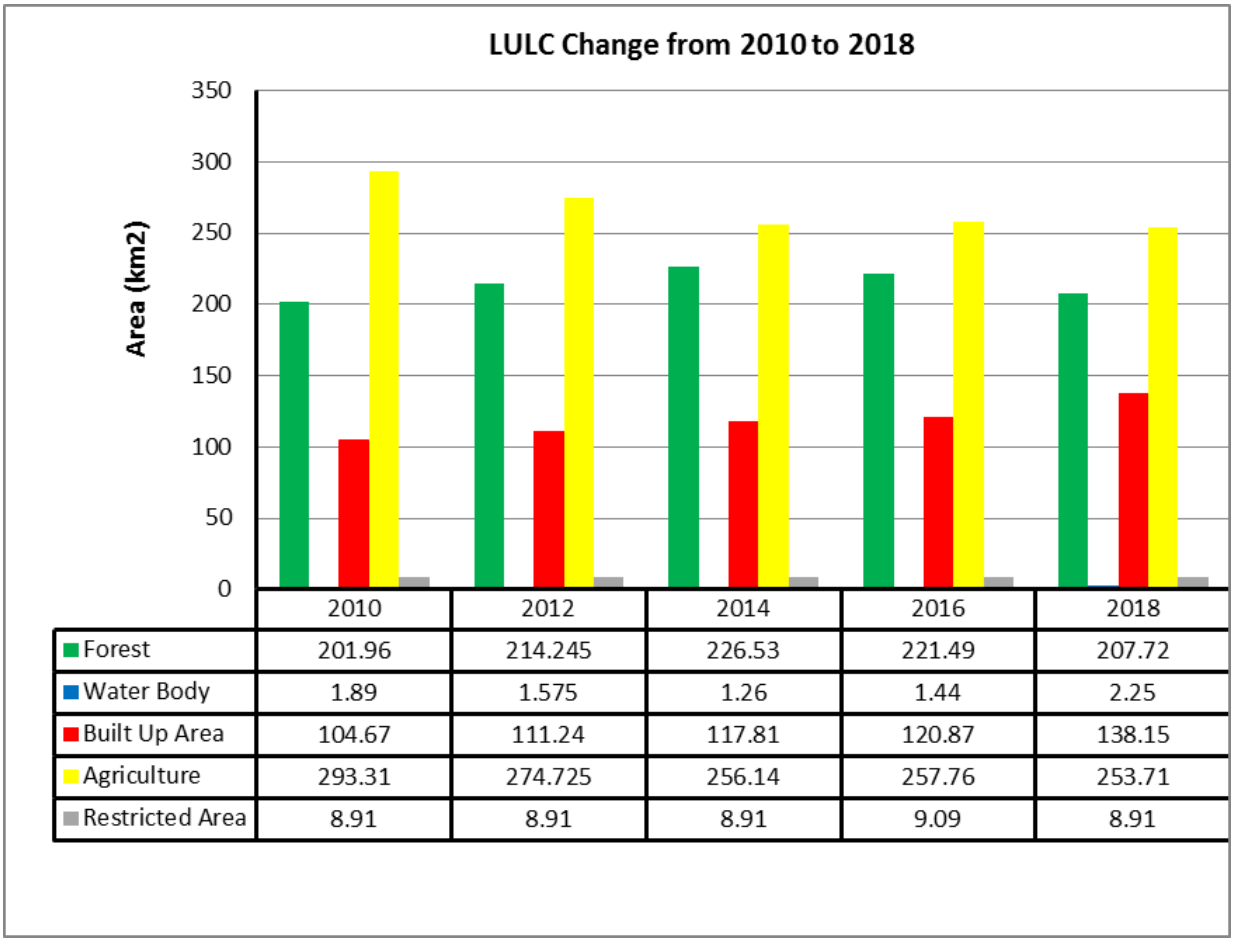

	2010	2012	2014	2016	2018
Forest	201.96	214.245	226.53	221.49	207.72
Water Body	1.89	1.575	1.26	1.44	2.25
Built Up Area	104.67	111.24	117.81	120.87	138.15
Agriculture	293.31	274.725	256.14	257.76	253.71
Restricted Area	8.91	8.91	8.91	9.09	8.91

CLUE-S allocation matrix

```
0
        -11.50648157
5
        -0.00698526 0
        0.39119996 1
        0.00591105 4
        0.10796518 5
        0.00371945 6

1
        35.08742779
1
       -0.0304047683244293 4

2
        3.47114127
7
          0.01302888 0
          -1.00830231 2
          -0.51379241 3
          -0.00247975 4
          -0.16399575 5
          -0.00033664 8
          -0.00024857 9

3
         9.77221254
7
           -0.01988859 0
           0.47766990 2
           -0.00608312 4
           -0.05385503 5
           -0.00162674 6
           0.00008101 8
           0.00015728 9

4
          21.27123774
4
             0.00869330 0
             -14.21695499 1
             -0.01886283 4
             -0.00036965 8
```

CLUE Run input features

5

1

7

10

102

108

9

617645.8066

3047331.7748

0 1 2 3 4

0.6 1 0.7 0.5 1

0 1 5

2010 2018

0

1

0

1 5

0

0

0.04

Layers relation matrix

Land use/Layers	Forest Area	Water Body	Built-up	Agriculture	Restricted Area
Constant	-21.061	1	0.289584	10.29	1
Population density	-0.007	0	0.013151	-0.02	0
Geology (Rocky)	0.431	0	0	0	0
Geology (Sediment)	0	0	-0.97384	0.497	0
Geology (Alluvium)	0	0	-0.45643	0	0
Elevation	0.00643	0	0	-0.007	0
Slope	0.106	0	-0.18061	-0.053	0
Aspects	0.004	0	0	-0.002	0
Distance from road	-0.00015	0	-0.00039	0.00015	0
Distance from market	0	0	-0.00034	0.0001	0
Distance from river	0	0	-0.0003	0.00017	0

LULC map of five different scenarios

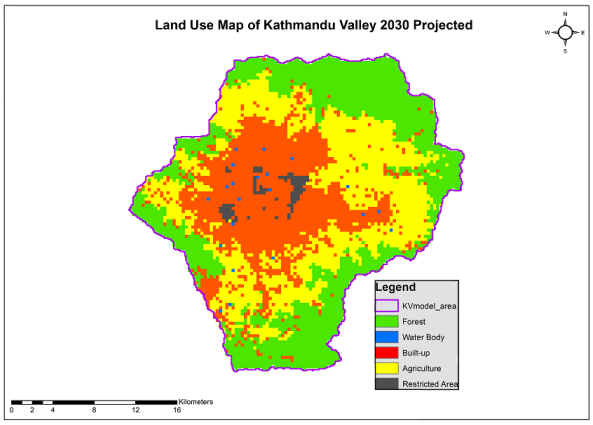

Normal growth rate 2030

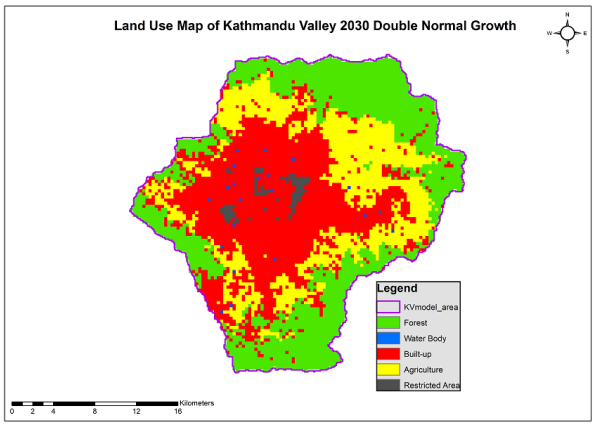

Double normal growth rate 2030

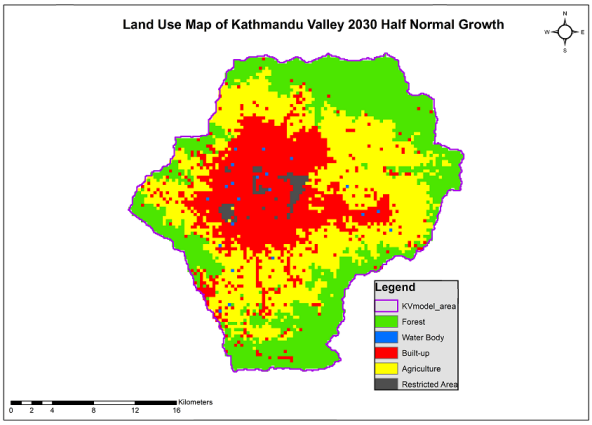

Half of normal growth rate 2030

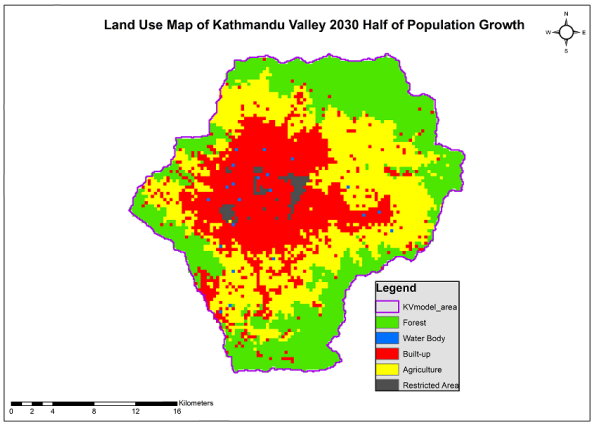

Half of population growth rate 2030

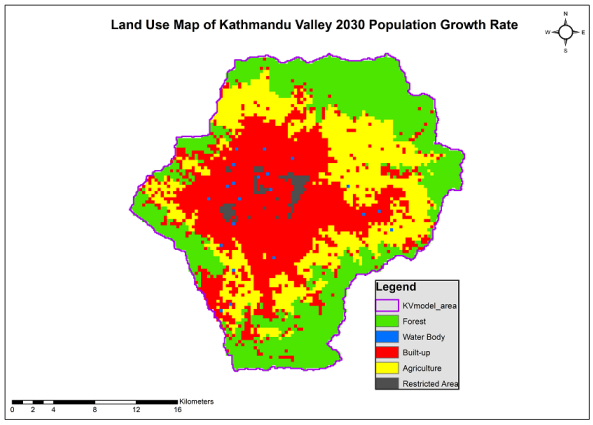

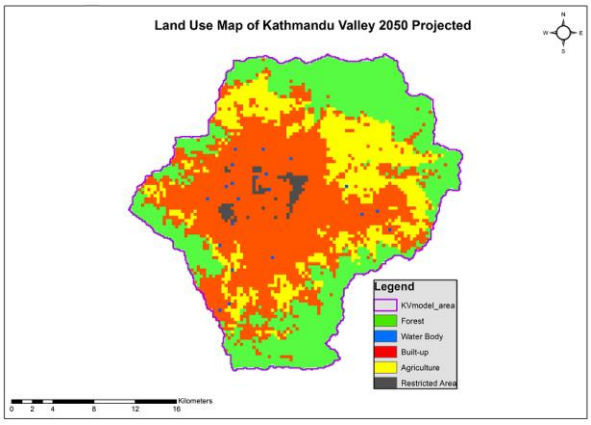

Population growth rate 2030	Normal growth rate 2050
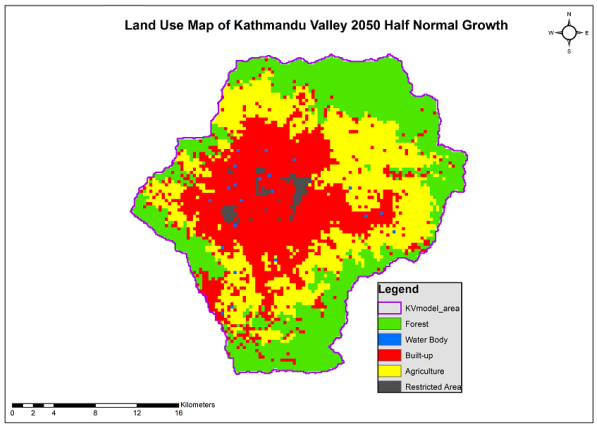	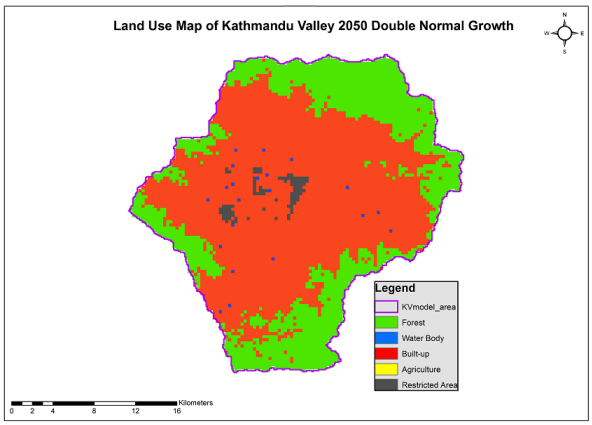
Half of normal growth rate 2050	Double of normal growth rate 2050
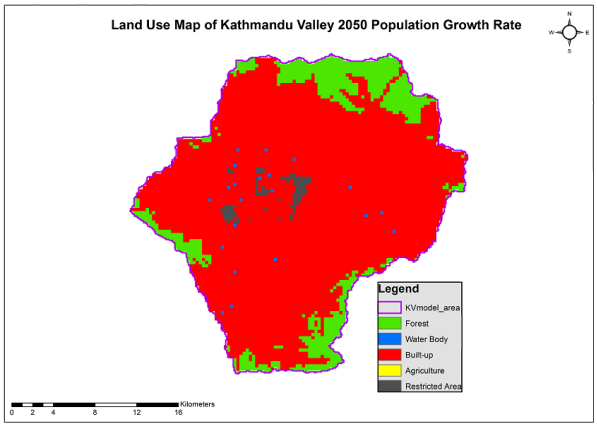	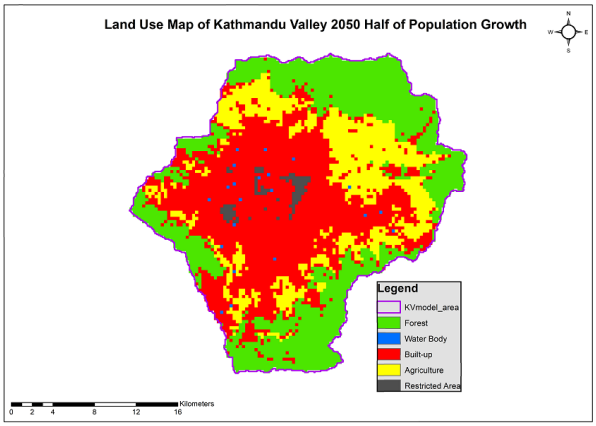
Population growth rate 2050	Half of population growth rate 2050

Field test data

S.N.	X	Y	Infiltration (mm/hr)	Location	Remarks
1	631442	3075726	7.1	Jaigaun	
2	631636	3071186	8.7	Dhapasi	
3	628846	3073683	8.57	Devisthan	
4	634810	3074003	6.6	Budanilkantha	

S.N.	X	Y	Infiltration (mm/hr)	Location	Remarks
5	629323	3069481	6.5	Sidditol	
6	641669	3069981	8.4	Bhadrabas	
7	639054	3066685	9.09	Dumkal	
8	635201	3065452	7.62	Kadaghari	
9	640833	3064868	8.82	Jhawkhel	
10	633235	3064345	5.39	Sinamangal	
11	636613	3061071	7.5	Balkot	
12	632414	3059943	4.6	Manoratha Church	
13	645659	3061664	5.11	Bindhabasini Tathali	
14	641608	3060541	8.82	Sipadol	
15	643723	3064397	9.64	Kharipati	
16	639193	3063163	7.22	Milli	
17	620040	3064653	3.8	Thankot	
18	623171	3067921	3.44	Nagarjun Hasantar	
19	626407	3065738	5.1	Kalanki	
20	624574	3061883	3.6	Gamcha Kritipur	
21	635973	3054260	6	Khare Tample Godabari	
22	635554	3058188	8.03	Tripingeshwor Tample Mahalaxmi	
23	633360	3054963	8.11	Dhaneshwor Tample Godabari	
24	631378	3053828	7.6	Chapagaun	
25	630878	3056653	6	Thecho	
26	629620	3057717	6.5	Sunakhothi	
27	628694	3056694	7.5	Bungmati	
28	628422	3054056	7.53	Karyabinayak	
29	627910	3055134	6.5	Farshidol	
30	628371	3051946	4.5	Tikabhairab	
31	633685	3061916	4.6	Narephat Manohara	
32	625121	3055299	6.67	Manamohn Dakshinkali	

S.N.	X	Y	Infiltration (mm/hr)	Location	Remarks
33	626465	3054720	6	Banganesh Dakshinkali	
34	626679	3063073	4.83	TU Kritipur	
35	629883	3063535	5.7	Bakhundol Lalitpur	
36	627242	3053662	7.7	Dukuchhap	
37	627827	3060438	3.75	Chobhar	
38	628609	3064205	5.5	Gusingal	
39	636488	3067205	8.7	Jorpati	
40	637926	3069348	8.9	Gokarneshwor	
41	633714	3069936	8.37	Mahankal	
42	632281	3066980	5.75	Sifal	
43	631154	3068748	6.81	Maharajgung	
44	626888	3072949	4.61	Golddhunga	
45	628720	3076555	5.31	Thali	
46	632886	3073251	7.69	Tokha	
47	640263	3075760	7.12	Sundarijal	
48	635201	3071013	9.09	Chunnikhel	
49	639865	3071819	7.69	Nayapati	
50	642923	3072676	6.8	GagalPhedi	
51	645433	3070931	7.18	Ghumarithok	
52	645378	3068756	8.68	Lapshiphedi	
53	647322	3068362	8.1	Garsinghpauwa	
54	643168	3067875	8.41	Changunarayan	
55	648692	3066531	5.89	Bisambhar	
56	646018	3066058	7.62	Telkot	
57	642016	3066086	8.67	Duwakot	
58	643603	3061407	8.75	Near Tathali	
59	638989	3061437	8.11	Katunje	
60	641904	3058784	6.5	Suryabinayak	

S.N.	X	Y	Infiltration (mm/hr)	Location	Remarks
61	638113	3058816	8.5	Anatalingeshwor	
62	640027	3057742	7.71	Gundu	
63	637001	3055649	4.33	Bisankhunarayan Godabari	
64	636561	3048797	4.5	Bhardev	
65	633092	3048650	6.51	Nallu Riverside	
66	633968	3050132	4.9	Sarashoti Kunda	
67	636007	3052746	4.41	Bairab Tample Godawari	
68	634307	3052489	4.37	Badikhel	
69	630817	3051787	5.1	Lele	
70	627961	3048650	6.31	Indra John Resort Lele	
71	630046	3050065	5.83	Shikharpa	
72	628024	3051674	7.14	Tikabhairab organicfarm	
73	630267	3061398	5.97	Mahalaxmisthan	
74	624747	3063429	3.87	Tinthana	
75	626135	3058668	5.21	Chalnakhel	
76	625729	3060648	3.88	Kritipur	
77	623417	3065546	4.6	Balambu	
78	618995	3063360	3.7	Chandagiri	
79	620833	3061643	3.46	Matatirtha	
80	624082	3057943	3.75	Seshnarayan	
81	622305	3061430	4.1	Machhayanarayan	
82	625749	3068022	5.5	Halchowk	
83	624477	3068720	3.3	Setogumba	

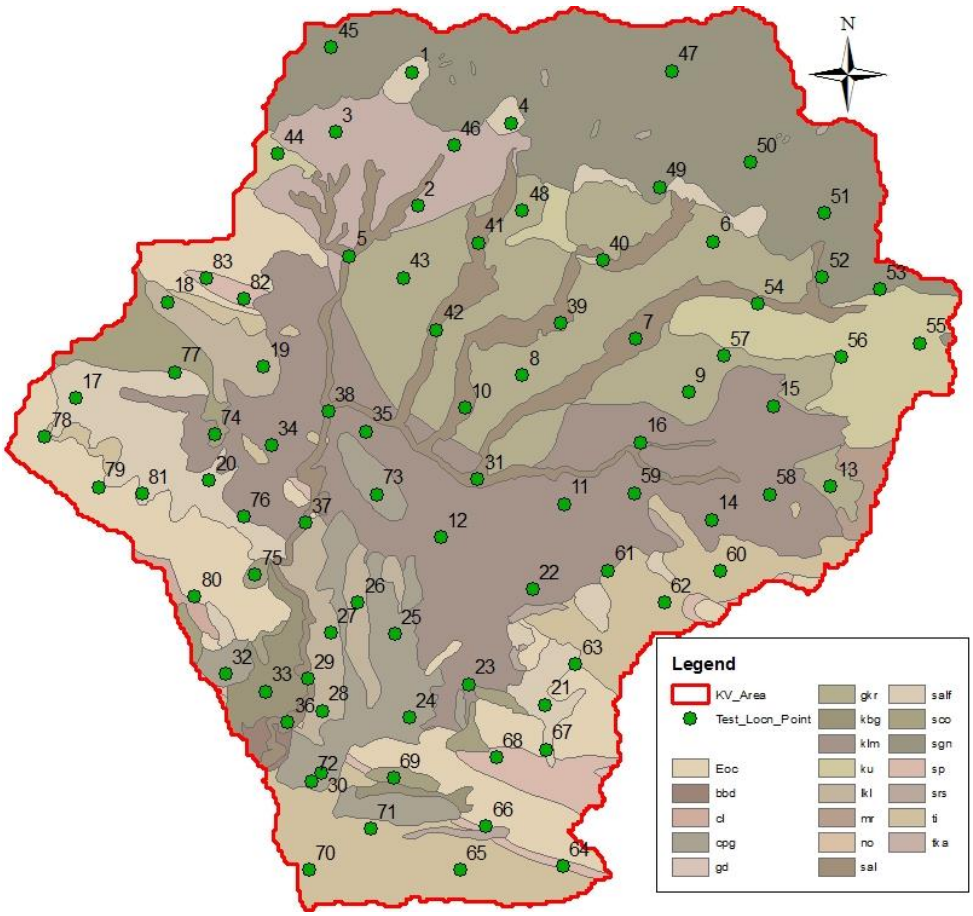

Field test location point

Field test photo and sample data

	
Insert the ring during test	Photograph during field test

	
Double ring during field test	Photograph during field test

Infiltration Record Sheet Using Double ring Infiltro-meter

Project : Bagmati Basin, Kathmandu

Date : 2075/09/26

Test Location : Bungmati

Start Time : 09:53am

SN	Time	Reading (cm)	Time Duration (s)	Depth In-filtered (mm)	Cumulative depth (mm)	Infiltration rate (mm/hr)
1	9:53	15	0	0	0	0.00
2	9:56	14	3	10	10	200.00
3	10:03	13	7	10	20	85.71
4	10:25	12	22	10	30	27.27
5	10:50	11.5	25	5	35	12.00
6	11:12	11	22	5	40	13.64
7	11:45	10.5	33	5	45	9.09
8	12:24	10	40	5	50	7.50
9	13:04	9.5	40	5	55	7.50

Infiltration Record Sheet Using Double ring Infiltro-meter

Project :-Bagmati Basin, Kathmandu

Date : 2075/09/28

Test Location: Thecho

Start Time : 10:24

SN	Time	Reading (cm)	Time Duration	Depth In-filtered (mm)	Cumulative depth (mm)	Infiltration rate (mm/hr)
1	10:24	15	0	0	0	
2	10:29	14	5	10	10	120.00
3	10:50	13	31	10	20	19.35
4	11:29	12.5	39	10	30	15.38
5	12:19	12	50	5	35	6.00
6	13:09	11.5	50	5	40	6.00

Normalized matrix

S.N	Land Use Type	1	2	3	4	5	6	7	8	9	10	Total	Average	Consistency Measure
1	Slope	0.06	0.05	0.05	0.04	0.07	0.07	0.10	0.12	0.13	0.08	0.76	0.08	10.71
2	River Distance	0.12	0.11	0.08	0.08	0.11	0.14	0.19	0.22	0.16	0.08	1.29	0.13	10.83
3	Geology	0.18	0.21	0.15	0.08	0.17	0.22	0.23	0.22	0.16	0.24	1.85	0.19	11.04
4	Land Use	0.24	0.21	0.31	0.15	0.11	0.14	0.10	0.05	0.16	0.24	1.72	0.17	11.30
5	Precipitation	0.30	0.32	0.31	0.46	0.34	0.32	0.23	0.22	0.16	0.24	2.89	0.29	11.12
6	Aspect	0.03	0.03	0.03	0.04	0.04	0.04	0.06	0.05	0.07	0.05	0.43	0.04	10.68
7	Elevation	0.02	0.02	0.02	0.05	0.05	0.02	0.03	0.05	0.05	0.03	0.34	0.03	10.53
8	Population Density	0.01	0.01	0.02	0.08	0.04	0.02	0.02	0.02	0.04	0.01	0.26	0.03	10.61
9	Market Distance	0.01	0.01	0.02	0.02	0.04	0.01	0.01	0.01	0.02	0.01	0.15	0.02	10.45
10	Road Distance	0.02	0.04	0.02	0.02	0.04	0.02	0.03	0.05	0.05	0.03	0.31	0.03	10.59

CI 0.14 RI 1.49 Consistency Ratio 0.10

Annex - II

River discharge (observed and simulated) (2000 to 2014) (Source:- DHM, 2015)

Date	Observed (m3/s)	Simulation (m3/s)	PPT (mm)
Jan-02	5.65	5.06	33.80
Feb-02	5.87	4.91	29.90
Mar-02	5.97	5.66	93.01
Apr-02	6.66	5.65	93.95
May-02	14.45	12.28	158.82
Jun-02	13.38	9.28	227.47
Jul-02	107.76	63.53	544.84
Aug-02	80.39	47.95	499.93
Sep-02	27.21	22.03	148.05
Oct-02	8.52	10.11	15.03
Nov-02	5.00	8.74	26.50
Dec-02	3.18	7.98	0.00
Jan-03	3.83	7.79	19.50
Feb-03	5.22	9.01	68.41
Mar-03	3.16	6.24	85.95
Apr-03	2.39	4.04	38.04
May-03	2.71	3.66	37.74
Jun-03	6.06	10.32	222.35
Jul-03	57.47	47.25	591.51
Aug-03	64.12	47.78	347.02
Sep-03	48.79	33.03	293.42
Oct-03	17.07	10.73	17.71
Nov-03	9.73	8.90	0.01
Dec-03	7.60	8.84	18.60
Jan-04	7.93	8.34	26.91

Date	Observed (m3/s)	Simulation (m3/s)	PPT (mm)
Feb-04	5.28	5.96	0.01
Mar-04	3.97	4.55	32.31
Apr-04	5.02	5.69	164.14
May-04	9.57	11.02	168.80
Jun-04	11.38	8.23	183.05
Jul-04	48.08	40.32	459.53
Aug-04	36.20	24.57	219.44
Sep-04	28.08	19.61	199.16
Oct-04	16.68	12.37	120.51
Nov-04	8.55	7.99	36.00
Dec-04	6.63	6.88	0.00
Jan-05	8.01	8.04	55.13
Feb-05	5.19	5.00	17.02
Mar-05	5.05	5.34	50.12
Apr-05	3.74	3.45	34.82
May-05	4.65	6.44	40.62
Jun-05	6.75	10.71	222.92
Jul-05	20.58	20.50	253.54
Aug-05	42.67	32.93	309.31
Sep-05	20.15	14.73	126.54
Oct-05	14.22	11.66	126.13
Nov-05	7.83	5.78	0.00
Dec-05	5.17	5.39	0.00
Jan-06	3.88	4.33	0.00
Feb-06	3.22	3.62	0.00
Mar-06	3.34	3.01	30.91
Apr-06	5.23	5.87	132.84
May-06	8.86	9.89	145.58
Jun-06	11.47	12.58	216.25

Date	Observed (m3/s)	Simulation (m3/s)	PPT (mm)
Jul-06	27.38	20.88	337.03
Aug-06	23.96	25.55	248.47
Sep-06	25.52	21.95	217.51
Oct-06	9.40	8.11	43.91
Nov-06	4.08	5.73	1.50
Dec-06	3.82	6.13	0.00
Jan-07	3.21	4.61	0.00
Feb-07	6.56	8.31	72.83
Mar-07	4.87	3.81	36.31
Apr-07	4.34	4.16	77.94
May-07	6.70	5.33	90.74
Jun-07	15.54	14.58	263.02
Jul-07	27.23	22.24	227.32
Aug-07	32.00	27.01	223.70
Sep-07	55.23	42.50	332.53
Oct-07	13.09	11.29	18.51
Nov-07	6.55	7.49	3.24
Dec-07	4.57	6.85	0.00
Jan-08	3.48	5.99	6.82
Feb-08	2.85	5.15	15.73
Mar-08	3.31	5.08	8.42
Apr-08	2.59	3.26	34.65
May-08	3.63	4.96	179.97
Jun-08	11.20	16.36	250.44
Jul-08	19.76	18.68	498.84
Aug-08	35.15	26.90	460.32
Sep-08	25.21	21.09	145.56
Oct-08	10.81	7.83	20.50
Nov-08	5.81	5.93	0.01

Date	Observed (m3/s)	Simulation (m3/s)	PPT (mm)
Dec-08	4.37	5.73	0.00
Jan-09	2.78	4.75	33.80
Feb-09	1.50	3.65	29.90
Mar-09	1.79	2.76	93.01
Apr-09	2.94	1.39	93.95
May-09	3.64	5.62	158.82
Jun-09	3.95	3.27	227.47
Jul-09	67.72	24.08	544.84
Aug-09	31.37	27.56	499.93
Sep-09	21.41	14.95	148.05
Oct-09	12.88	9.77	15.03
Nov-09	6.02	4.45	26.50
Dec-09	3.14	4.31	0.00
Jan-10	2.90	3.89	19.50
Feb-10	2.74	4.13	68.41
Mar-10	2.44	2.29	85.95
Apr-10	2.48	2.31	38.04
May-10	4.03	5.31	37.74
Jun-10	16.31	7.34	222.35
Jul-10	31.75	20.67	591.51
Aug-10	44.18	33.63	347.02
Sep-10	41.33	19.15	293.42
Oct-10	8.63	7.13	17.71
Nov-10	4.07	5.41	0.01
Dec-10	4.22	5.07	18.60
Jan-11	3.91	4.45	26.91
Feb-11	4.63	5.55	0.01
Mar-11	3.31	2.82	32.31
Apr-11	4.46	4.16	164.14

Date	Observed (m3/s)	Simulation (m3/s)	PPT (mm)
May-11	9.35	13.46	168.80
Jun-11	26.56	21.77	183.05
Jul-11	49.63	40.93	459.53
Aug-11	50.36	33.74	219.44
Sep-11	42.59	32.12	199.16
Oct-11	14.80	11.97	120.51
Nov-11	6.99	10.26	36.00
Dec-11	3.27	8.09	0.00
Jan-12	3.53	7.62	55.13
Feb-12	4.08	7.47	17.02
Mar-12	2.26	4.64	50.12
Apr-12	4.27	6.46	34.82
May-12	2.53	3.59	40.62
Jun-12	5.78	10.31	222.92
Jul-12	31.68	31.32	253.54
Aug-12	33.98	32.44	309.31
Sep-12	41.93	33.12	126.54
Oct-12	7.81	8.20	126.13
Nov-12	4.34	7.50	0.00
Dec-12	3.24	7.06	0.00
Jan-13	2.57	6.50	0.00
Feb-13	3.37	6.74	0.00
Mar-13	2.11	4.06	30.91
Apr-13	2.05	3.82	132.84
May-13	5.16	11.79	145.58
Jun-13	15.31	22.66	216.25
Jul-13	29.93	35.91	337.03
Aug-13	35.73	38.81	248.47
Sep-13	17.49	20.77	217.51

Date	Observed (m3/s)	Simulation (m3/s)	PPT (mm)
Oct-13	18.70	16.65	43.91
Nov-13	5.06	8.60	1.50
Dec-13	3.36	7.93	0.00
Jan-14	1.97	6.99	0.00
Feb-14	1.80	6.33	72.83
Mar-14	2.46	6.00	36.31
Apr-14	1.52	3.15	77.94
May-14	1.07	5.25	90.74
Jun-14	2.88	8.47	263.02
Jul-14	20.22	31.02	227.32
Aug-14	29.24	33.83	223.70
Sep-14	22.90	29.86	332.53
Oct-14	10.90	15.57	18.51
Nov-14	3.56	7.58	3.24
Dec-14	3.20	7.82	0.00

Data Summary (Source:- DHM, 2015)

S.N.	Station No.	Data type	Start Date	End Date	Remarks
1	1007	Precipitation, Relative humidity, Temperature	1/1/2000	12/31/2014	Complete
2	1015	Precipitation	1/1/2000	12/31/2014	Complete
3	1022	Precipitation, Relative humidity, Temperature	1/1/2000	12/31/2014	Complete
4	1029	Precipitation, Relative humidity, Temperature, Solar radiation, Wind speed	1/1/2000	12/31/2014	Complete
5	1030	Precipitation, Relative humidity, Temperature, Solar radiation, Wind speed	1/1/2000	12/31/2014	Complete
6	1035	Precipitation	1/1/2000	12/31/2014	Complete
7	1039	Precipitation, Relative humidity, Temperature	1/1/2000	12/31/2014	Complete
8	1043	Precipitation, Relative humidity	1/1/2000	12/31/2014	Complete
9	1049	Precipitation	1/1/2000	12/31/2014	Complete
10	1052	Precipitation	1/1/2000	12/31/2014	Complete

S.N.	Station No.	Data type	Start Date	End Date	Remarks
11	1059	Precipitation	1/1/2000	12/31/2014	Complete
12	1060	Precipitation	1/1/2000	12/31/2014	Complete
13	1073	Precipitation, Relative humidity	1/1/2000	12/31/2014	Complete
14	1074	Precipitation	1/1/2000	12/31/2014	Complete
15	1075	Precipitation	1/1/2000	12/31/2014	Complete
16	1076	Precipitation	1/1/2000	12/31/2014	Complete
17	1077	Precipitation	1/1/2000	12/31/2014	Complete
18	1079	Precipitation	1/1/2000	12/31/2014	Complete
19	1080	Precipitation	1/1/2000	12/31/2014	Complete
20	1081	Precipitation	1/1/2000	12/31/2014	Complete
21	1082	Precipitation	1/1/2000	12/31/2014	Complete

Summary of parameters

Parameter (file)	**Parameter Range**	**Calibrated Value**
ALPHA_BF (gw)	0-1 (0.048)	ALL = 0.01
GW_DELAY (gw)	0-500 (31)	FRST,BARR, AGRL, URRD, & WATR = 31
GW_REVAP (gw)	0.02-0.2 (0.02)	ALL = 0.02
SHALLST (gw)	0-50000 (1000)	ALL= 1000
GWQMN (gw)	0-5000 (1000)	FRST=1000, BARR, AGRL=1500 & URRD, WATR = 3000
RCHRG_DP (gw)	0-1 (0.05)	AGRL, BARR, URRD, & FRST = 0.05
REVAPMN (gw)	0-500 (750)	AGRL, BARR,URRD,WATR, & FRST = 750
GWHT (gw)	0-25 (1)	All = 1
CANMX (hru)	0-100(0)	ALL = 0
EPCO (hru)	0-1 (1)	ALL =1.0
ESCO (hru)	0-1 (0.95)	ALL = 0.95
OV_N (hru)	0.01-30(vary)	ALL = 0.14
HRU_SLP (hru)	0-1(vary)	
SLSUBBSN (hru)	10-150(vary)	
SURLAG (hru)	0.05-24(2)	ALL = 2
LAT_TTIME (hru)	0-180(0)	ALL = 0
SOL_AWC (sol)	0-1(vary)	Bd34-2bc AWC1, AWC2 = 0.117 & Bd35-1/2b AWC1,AWC2 =0.157

Parameter (file)	Parameter Range	Calibrated Value
SOL_K (sol)	0-2000(vary)	Bd34-2bc K1=35.65, K2 = 21.84 & Bd35-1/2b K1=28.52, K2=10.18
SOL_Z (sol)		Z1 =300, Z2 = 1000
CN2 (mgt1)	35-98(vary)	FRST, BARR = 73, AGRL=83, URRD = 72, & WATR = 91
CH_K2 (rte)	0-500 (0)	ALL = 0
CH_N2 (rte)	0-1 (0.014)	ALL = 0.014
ALPHA_BANK (rte)	0-1 (0)	ALL = 0.00
TLAPS (sub)	-10 –10(-5.6)	ALL = 0
PLAPS (sub)	-1000-1000 (0)	ALL = 0
CH_N1 (sub)	0.01-30(0.014)	ALL =0.014
CH_K1 (sub)	0-300 (0)	ALL = 10
SFTMP (bsn)	-20-20 (1)	ALL = 1
SMTMP (bsn)	-20-20(0.5)	ALL = 0.5

Annex -III

Initial input features in MODFLOW

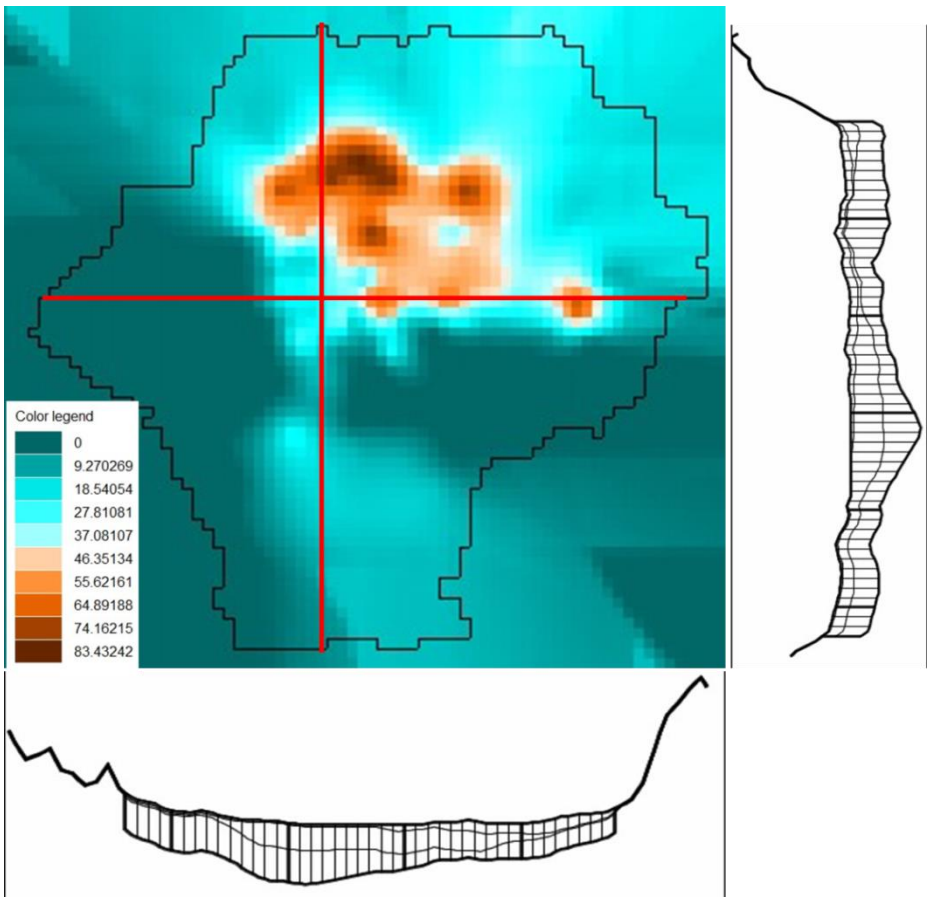

Shallow aquifer thickness and cross section map

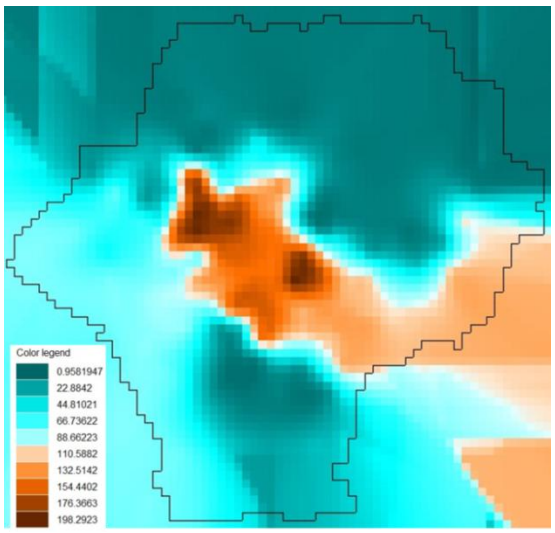

Depth of aquitard

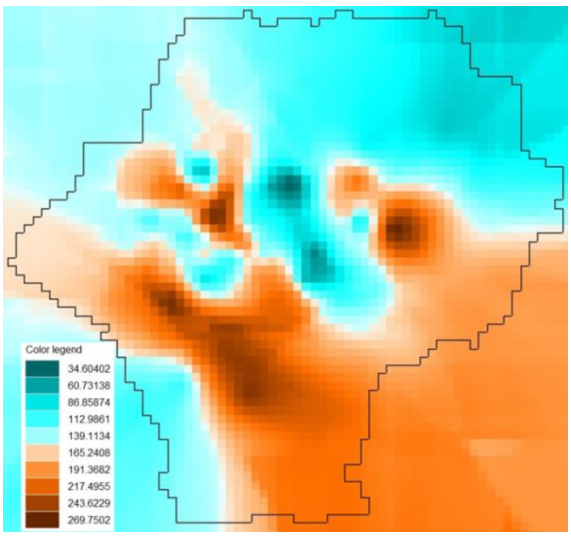

Depth of deep aquifer

Observational well Information in dry and wet (2016) (Source: SATREPS PROJECT)

WID	Location	Observation date	N (Y)	E (X)	GL	MB GL	GWT
W1	Talache tole	2/15/2016	3062717.62	630675.47	1297.6	6.6	1291.04
W2	Machhindra Bahal	2/15/2016	3062050.94	630512.71	1305.6	6.9	1298.72
W3	Minnath bahal	2/15/2016	3062012.33	630644.68	1305.1	7.99	1297.11
W5	Khokana, Rudrayanee School	2/16/2016	3058190.19	627856.49	1276.6	5.91	1270.69
W6	Khokana, Rudrayanee Mandir	2/16/2016	3058227.47	627976.73	1282.8	1.5	1281.37
W7	IOE-TU Pulchok Shallow	2/16/2016	3063392.21	630714.81	1292.9	7.2	1285.75
W9	Nagpokhari	2/17/2016	3066844.48	630557.14	1296.1	2.3	1293.80
W12	Koteshwor	2/19/2016	3063182.72	632407.87	1292.5	4.6	1287.94
W13	Lubhu, Machagot-7	3/18/2016	3059467.07	634931.86	1299.7	1.8	1297.92
W14	Hyumat	2/19/2016	3065323.54	628632.02	1292.1	3.4	1288.74
W15	Boje Pokhari, Imadol	2/19/2016	3061364.31	633058.04	1292.7	2.4	1290.36
W16	Kalanki, Shantidoot galli	2/20/2016	3064326.56	626323.93	1296.3	3.69	1292.69
W17	Kirtipur, Amritnagar	2/20/2016	3064251.24	626362.52	1294.7	5.7	1289.03
W18	Byasi-9, Bhaktapur	2/20/2016	3062673.72	641076.33	1323.5	3.37	1320.18
W23	Sukedhara	2/23/2016	3068784.44	632596.10	1308.0	1.19	1306.83
W25	Sandal, Gokarna	2/23/2016	3070329.96	637854.17	1336.8	7.65	1329.17
W26	Nayanadi, Sundarijal	2/23/2016	3070159.07	638527.14	1333.4	4.05	1329.37
W27	GWRDB, Babarmahal	2/23/2016	3064549.85	630729.76	1290.9	2.6	1288.33
W28	Balambu-6	2/23/2016	3064225.75	622671.95	1352.8	4.8	1348.01
W32	Madhyapur	3/6/2016	3062800.99	636583.07	1298.5	4.95	1293.64
W34	Chapacho-8	3/6/2016	3063325.68	636703.24	1310.8	5.55	1305.34
W36	Nikosera	3/6/2016	3063305.27	637895.55	1295.6	1.2	1294.40
W37	College Marga	3/6/2016	3062383.12	637201.66	1293.3	2.55	1290.79
W39	Voldhoka	3/6/2016	3061488.70	629608.54	1310.1	11.6	1298.52
W40	Nukabahal,Lalitpur	3/6/2016	3062650.58	630481.61	1298.4	5.9	1292.52
W41	Tikathali	3/18/2016	3061421.74	634362.04	1292.0	3.25	1288.83
W42	Kamaladi Ganeshthan	3/6/2016	3066199.96	630107.09	1294.3	4.1	1290.26
W43	Futsal	3/7/2016	3062115.40	625521.45	1351.8	5.62	1346.27
W44	Bhatkepati	3/7/2016	3061504.47	624785.03	1365.2	4.14	1361.12
W45	Taukhel	3/7/2016	3062588.96	623669.52	1366.1	6.7	1359.45
W46	Salyansthan	3/7/2016	3062839.49	624990.57	1334.3	3.06	1331.24
W47	Panga Dobato	3/7/2016	3062447.75	626314.40	1342.0	5.85	1336.17
W48	Samal Panga	3/7/2016	3061778.22	626285.45	1330.7	0.74	1329.97
W49	Charghare	3/7/2016	3061017.16	626157.12	1317.8	2.05	1315.77
W50	Katunje	3/12/2016	3061727.97	638609.60	1326.6	3.95	1322.67
W51	Survabinayak	3/12/2016	3061320.49	640658.95	1317.9	2.8	1315.18
W53	Liwali	3/12/2016	3062479.25	642089.90	1314.6	5.35	1309.34
W54	Barahisthan	3/12/2016	3061835.08	640433.74	1305.8	1.1	1304.79
W56	Imadol	3/18/2016	3061187.25	632347.36	1294.0	4.18	1289.83

WID	Location	Observation date	N (Y)	E (X)	GL	MB GL	GWT
W57	Sanogaun	3/18/2016	3058402.13	634112.98	1306.4	1.91	1304.49
W59	Imadol river bank	3/18/2016	3061931.89	632881.92	1291.7	2.2	1289.56
W1	Talache tole	8/23/2016	3062717.62	630675.47	1297.64	4.02	1293.62
W2	Machhindra Bahal	8/23/2016	3062050.94	630512.71	1305.62	5.93	1299.69
W3	Minnath Bahal	8/23/2016	3062012.33	630644.68	1305.10	5.75	1299.35
W5	Khokana, Rudrayanee School	8/25/2016	3058190.19	627856.49	1276.60	1.10	1275.50
W6	Khokana, Rudrayanee Mandir	8/25/2016	3058227.47	627976.73	1282.87	2.02	1280.85
W7	IoE	8/14/2016	3063392.21	630714.81	1292.95	2.11	1290.84
W8	Bafal	8/12/2016	3065549.50	627170.96	1293.08	1.40	1291.68
W9	Nagpokhari	8/27/2016	3066844.48	630557.14	1296.10	4.35	1291.75
W10	Ochu, Imadol	8/14/2016	3060574.62	632628.12	1298.58	5.10	1293.48
W12	Koteshwor	8/15/2016	3063182.72	632407.87	1292.54	2.40	1290.14
W13	Lubhu, Machagot-7	8/14/2016	3059467.07	634931.86	1299.72	2.11	1297.61
W14	Hyumat	8/12/2016	3065323.54	628632.02	1292.14	0.78	1291.36
W15	Boje Pokhari	8/22/2016	3061364.31	633058.04	1292.76	1.00	1291.76
W16	Kalanki, Shantidoot galli	8/19/2016	3064326.56	626323.93	1296.38	1.68	1294.70
W17	Kirtipur, Amritnagar	8/19/2016	3064251.24	626362.52	1294.73	2.81	1291.92
W18	Byasi-9, Bhaktapur	8/25/2016	3062673.72	641076.33	1323.55	2.45	1321.10
W22	Kasan-5	8/16/2016	3063142.02	641028.15	1306.62	2.38	1304.24
W23	Sukedhara	8/12/2016	3068784.44	632596.10	1308.02	0.30	1307.72
W24	Duwakot	8/16/2016	3063248.85	639050.47	1298.21	0.81	1297.40
W25	Sandal, Gokarna	8/17/2016	3070329.96	637854.17	1336.82	3.75	1333.07
W26	Nayanadi, Sundarijal	8/17/2016	3070159.07	638527.14	1333.42	2.95	1330.47
W27	Babarmahal	8/17/2016	3064549.85	630729.76	1290.93	1.20	1289.73
W28	Balambu-6	8/19/2016	3064225.75	622671.95	1352.81	3.07	1349.74
W34	Chapacho-8	8/19/2016	3063325.68	636703.24	1310.89	4.90	1305.99
W36	Nikosera	8/19/2016	3063305.27	637895.55	1295.60	0.25	1295.35
W38	Dakshin Barahi	8/19/2016	3061849.24	636813.01	1293.32	1.80	1291.52

WID	Location	Observation date	N (Y)	E (X)	GL	MBGL	GWT
W40	Nukabahal	8/23/2016	3062650.58	630481.61	1298.42	1.15	1297.27
W41	Tikathali	8/22/2016	3061421.74	634362.04	1292.08	1.02	1291.06
W42	Kamaladi Ganeshthan	8/27/2016	3066199.96	630107.09	1294.36	2.17	1292.19
W43	Futsal	8/26/2016	3062115.40	625521.45	1351.89	1.24	1350.65
W44	Bhatkepati	8/26/2016	3061504.47	624785.03	1365.26	4.05	1361.21
W47	Panga Dobato	8/26/2016	3062447.75	626314.40	1342.02	1.34	1340.68
W48	Samal Panga	8/26/2016	3061778.22	626285.45	1330.71	0.37	1330.34
W49	Charghare	8/26/2016	3061017.16	626157.12	1317.82	4.90	1312.92
W50	Katunje	8/25/2016	3061727.97	638609.60	1326.62	1.90	1324.72
W51	Suryabinayak	8/25/2016	3061320.49	640658.95	1317.98	1.00	1316.98
W53	Liwali	8/25/2016	3062479.25	642089.90	1314.69	1.49	1313.20
W54	Barahisthan	8/25/2016	3061835.08	640433.74	1305.89	0.55	1305.34
W56	Imadol	8/14/2016	3061187.25	632347.36	1294.01	1.63	1292.38
W57	Sanogaun	8/14/2016	3058402.13	634112.98	1306.40	0.50	1305.90
W59	Imadol River Bank	8/22/2016	3061931.89	632881.92	1291.76	2.06	1289.70

Shallow pumping information (Source:- Adhikari, 2017)

HRU ID	x	y	Pumping rate (m^3/day) at center of 500m X 500m grid	Remarks
2	630695.67	3075231.03	35.00	out of KUKL service area
6	627625.29	3073242.48	2.50	
7	645899.40	3071416.87		
8	632930.42	3069183.06	165.00	
9	630198.27	3069341.10	110.00	
10	643513.09	3071101.32		few well points, cant estimate
11	638614.03	3067181.99	115.00	out of KUKL service area
12	643456.96	3067546.56	30.00	
13	647562.98	3067975.03		few well points, cant estimate

14	628880.03	3066516.96	5.00	
18	645882.41	3064268.25	30.00	few well points, cant estimate
19	640994.08	3064764.44	30.00	
20	625916.94	3063628.13		
21	628953.35	3064350.06	5.00	
22	630580.33	3063726.30		
23	631080.19	3062904.50	5.00	
24	628682.90	3064264.60	5.00	
25	622139.42	3061799.36	90.00	
26	636164.71	3062915.97	60.00	
27	631062.40	3061375.92	5.00	
28	631723.06	3059629.13	5.00	
29	638959.26	3059577.67	70.00	out of KUKL service area
30	632482.43	3054929.71	5.00	few well points, cant estimate
31	634885.15	3060208.36	225.00	out of KUKL service area
32	640731.90	3060153.11	30.00	
33	641836.86	3061493.22		very small area with no wells
34	643297.74	3059648.84		
35	628097.72	3063999.54	5.00	
36	645772.19	3061303.87		
37	628580.97	3061029.16	5.00	
38	628102.61	3061151.54	5.00	
39	626368.77	3056690.11	30.00	few well points, cant estimate
40	629106.75	3054644.00	30.00	
41	636090.67	3054577.22	110.00	few well points, cant estimate
42	636993.68	3057526.66	210.00	out of KUKL service area

Calibration and validation without LULC change (2016)

RMSE		1.80	RMSE		1.98
Mean Absolute Error		1.35	Mean Absolute Error		1.63
Mean Error		-0.87	Mean Error		-0.44
Name	**Observed head (m)**	**Simulated Head (m)**	**Name**	**Observed head (m)**	**Simulated Head (m)**
W1	1291.04	1291.65	W1	1293.62	1293.41

RMSE		1.80	RMSE		1.98
Mean Absolute Error		1.35	Mean Absolute Error		1.63
Mean Error		-0.87	Mean Error		-0.44
Name	**Observed head (m)**	**Simulated Head (m)**	**Name**	**Observed head (m)**	**Simulated Head (m)**
W2	1298.72	1299.49	W2	1299.69	1303.63
W3	1297.11	1297.75	W3	1299.35	1301.50
W5	1270.69	1271.42	W5	1275.50	1271.99
W6	1281.37	1279.94	W6	1280.85	1280.45
W7	1285.75	1289.04	W7	1290.84	1289.64
W9	1293.80	1293.00	W8	1291.68	1295.76
W12	1287.94	1289.49	W9	1291.75	1294.91
W13	1297.92	1298.99	W10	1293.48	1296.59
W14	1288.74	1289.23	W12	1290.14	1290.58
W15	1290.36	1289.90	W13	1297.61	1299.15
W16	1292.69	1292.80	W14	1291.36	1289.77
W17	1289.03	1290.92	W15	1291.76	1290.70
W18	1320.18	1320.20	W16	1294.70	1293.15
W23	1306.83	1305.27	W17	1291.92	1291.30
W25	1329.17	1329.68	W18	1321.10	1320.56
W26	1329.37	1328.90	W22	1304.24	1307.91
W27	1288.33	1287.21	W23	1307.72	1309.36
W28	1348.01	1350.99	W24	1297.40	1298.02
W32	1293.64	1296.71	W25	1333.07	1333.72
W34	1305.34	1305.87	W26	1330.47	1332.64
W36	1294.40	1295.19	W27	1289.73	1288.08
W37	1290.79	1290.88	W28	1349.74	1351.12
W39	1298.52	1303.47	W34	1305.99	1307.44
W40	1292.52	1292.57	W36	1295.35	1296.25
W41	1288.83	1291.72	W38	1291.52	1292.71
W42	1290.26	1290.71	W40	1297.27	1295.03
W43	1346.27	1349.55	W41	1291.06	1291.97
W44	1361.12	1362.97	W42	1292.19	1292.34

RMSE		1.80	RMSE		1.98
Mean Absolute Error		1.35	Mean Absolute Error		1.63
Mean Error		-0.87	Mean Error		-0.44
Name	**Observed head (m)**	**Simulated Head (m)**	**Name**	**Observed head (m)**	**Simulated Head (m)**
W45	1359.45	1359.26	W43	1350.65	1349.66
W46	1331.24	1332.07	W44	1361.21	1363.09
W47	1336.17	1336.08	W47	1340.68	1336.19
W48	1329.97	1331.99	W48	1330.34	1332.10
W49	1315.77	1314.18	W49	1312.92	1314.29
W50	1322.67	1326.02	W50	1324.72	1327.37
W51	1315.18	1315.08	W51	1316.98	1315.57
W53	1309.34	1312.46	W53	1313.20	1312.61
W54	1304.79	1303.60	W54	1305.34	1304.32
W56	1289.83	1290.47	W56	1292.38	1291.32
W57	1304.49	1307.50	W57	1305.90	1307.64
W59	1289.56	1288.84	W59	1289.70	1289.35

Cross-sectional data

ALONG SECTION A_A (2016)							
DRY_SEASON			**WET_SEASON**				
Well	**Simulated Head**		**Well**	**Simulated Head**	**WID**	**RL. Ground**	**RL SA Bottom**
W28	1351.0		W28	1351.1	W28	1352.81	1338.707
W16	1292.8		W16	1293.2	W16	1296.38	1284.271
W17	1290.9		W17	1291.3	W17	1294.73	1282.945
W27	1287.2		W27	1288.1	W27	1290.93	1281.806
W7	1289.0		W7	1289.6	W7	1292.95	1276.390
W12	1289.5		W12	1290.6	W12	1292.54	1274.564
W34	1305.9		W34	1307.4	W34	1310.89	1300.734
W36	1295.2		W36	1296.3	W36	1295.60	1284.057
W18	1320.2		W18	1320.6	W18	1323.55	1312.576
W53	1312.5		W53	1312.6	W53	1314.69	1300.788

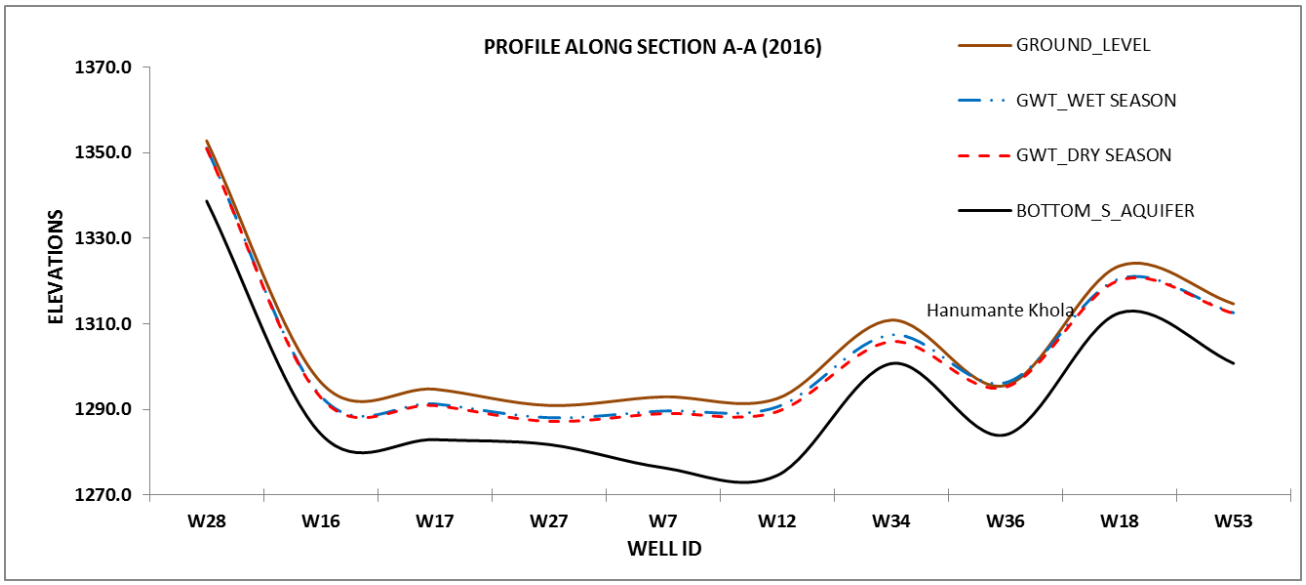

ALONG SECTION B_B (2016)							
DRY_SEASON			WET_SEASON		WID	RL. Ground	RL SA Bottom
Well	Simulated Head		Well	Simulated Head			
W9	1293.0		W9	1294.9	W9	1296.10	1286.528
W27	1287.2		W27	1288.1	W27	1290.93	1281.806
W7	1289.0		W7	1289.6	W7	1292.95	1276.390
W1	1291.6		W1	1293.4	W1	1297.64	1290.055
W2	1299.5		W2	1303.6	W2	1305.62	1296.242
W3	1297.8		W3	1301.5	W3	1305.10	1295.828
W59	1288.8		W59	1289.4	W59	1291.77	1279.717
W41	1291.7		W41	1292.0	W41	1292.08	1282.240
W13	1299.0		W13	1299.2	W13	1299.72	1288.732
W57	1307.5		W57	1307.6	W57	1308.40	1293.783

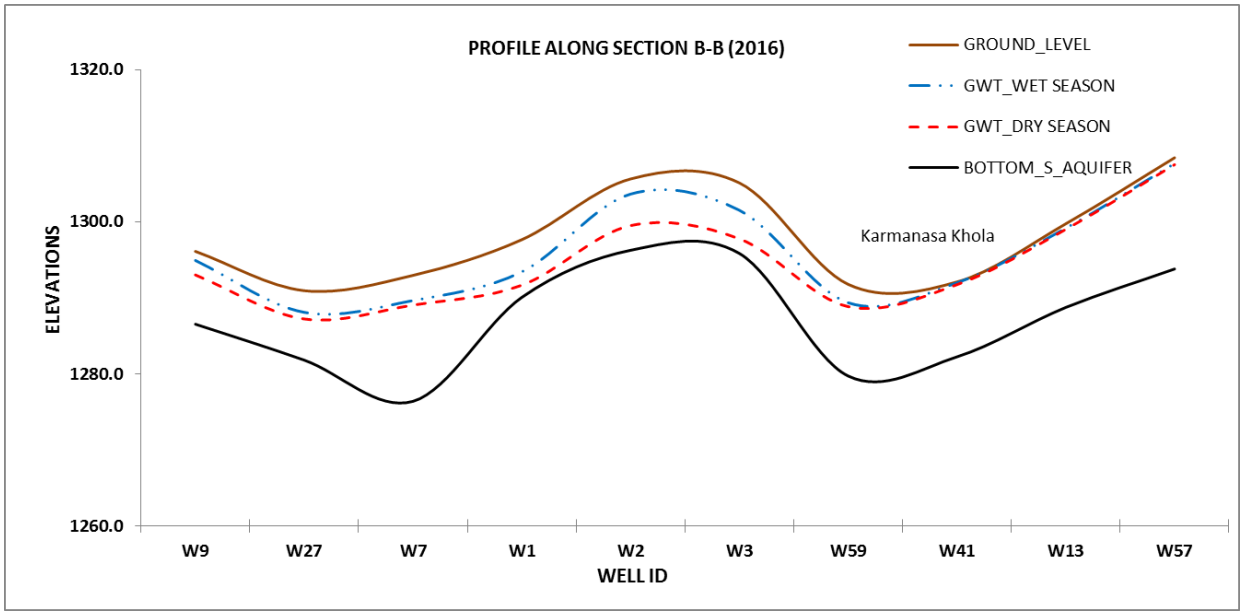

Decadal simulated head without LULC during 2020-2050

Well ID	Dry				Wet			
	2020	2030	2040	2050	2020	2030	2040	2050
W1	1291.90	1291.89	1291.87	1291.85	1292.20	1292.08	1292.06	1292.04
W2	1300.77	1300.75	1300.73	1300.69	1301.68	1301.55	1301.53	1301.50
W3	1298.74	1298.72	1298.70	1298.66	1299.78	1299.64	1299.62	1299.59
W5	1271.44	1271.44	1271.43	1271.42	1271.98	1271.93	1271.92	1271.91
W6	1279.96	1279.95	1279.94	1279.93	1280.44	1280.39	1280.38	1280.37
W7	1289.07	1289.06	1289.05	1289.04	1289.31	1289.19	1289.18	1289.17
W9	1293.08	1292.99	1292.88	1292.77	1295.75	1295.75	1295.75	1295.75
W12	1289.70	1289.69	1289.68	1289.67	1295.80	1294.62	1294.54	1294.45
W13	1299.00	1298.97	1298.94	1298.91	1296.94	1296.53	1296.50	1296.36
W14	1289.26	1289.25	1289.25	1289.23	1289.95	1289.84	1289.83	1289.82
W15	1289.92	1289.87	1289.81	1289.75	1299.38	1299.12	1299.10	1299.08
W16	1292.88	1292.88	1292.88	1292.88	1289.80	1289.70	1289.69	1289.68
W17	1291.00	1291.00	1291.00	1291.00	1291.18	1290.61	1290.57	1290.19
W18	1320.22	1320.20	1320.15	1320.13	1293.13	1293.13	1293.13	1293.13
W23	1305.46	1305.33	1305.19	1305.05	1291.28	1291.28	1291.28	1291.27
W25	1329.91	1329.89	1329.87	1329.84	1320.59	1320.53	1320.51	1320.50

W26	1329.11	1329.09	1329.06	1329.04	1307.98	1307.86	1307.82	1307.81
W27	1287.24	1287.20	1287.15	1287.11	1310.97	1308.77	1308.65	1308.52
W28	1350.99	1350.99	1350.99	1350.99	1298.15	1297.88	1297.81	1297.78
W32	1296.74	1296.72	1296.70	1296.68	1333.65	1333.44	1333.43	1333.42
W34	1305.96	1305.91	1305.84	1305.77	1332.64	1332.37	1332.35	1332.34
W36	1295.23	1295.19	1295.11	1295.07	1288.64	1287.88	1287.84	1287.79
W37	1290.90	1290.89	1290.88	1290.86	1351.11	1351.11	1351.11	1351.11
W39	1304.02	1304.01	1304.00	1303.98	1307.70	1307.31	1307.27	1307.23
W40	1293.08	1293.06	1293.04	1293.02	1296.48	1296.09	1296.01	1295.97
W41	1291.74	1291.71	1291.67	1291.62	1292.74	1292.70	1292.69	1292.69
W42	1290.78	1290.69	1290.60	1290.50	1293.40	1293.26	1293.24	1293.22
W43	1349.55	1349.55	1349.55	1349.55	1292.22	1291.93	1291.91	1291.88
W44	1362.98	1362.98	1362.97	1362.97	1292.99	1292.11	1292.05	1291.96
W45	1359.27	1359.24	1359.23	1359.21	1349.65	1349.65	1349.65	1349.65
W46	1332.12	1332.02	1331.97	1331.91	1363.08	1363.08	1363.08	1363.08
W47	1336.09	1336.09	1336.09	1336.09	1336.18	1336.18	1336.18	1336.18
W48	1332.00	1332.00	1332.00	1332.00	1332.09	1332.09	1332.09	1332.08
W49	1314.18	1314.18	1314.18	1314.18	1314.29	1314.28	1314.28	1314.28
W50	1326.39	1326.08	1325.47	1325.14	1327.43	1327.33	1327.31	1327.30
W51	1315.10	1315.08	1315.04	1315.02	1315.61	1315.50	1315.46	1315.45
W53	1312.46	1312.45	1312.43	1312.42	1312.67	1312.57	1312.55	1312.54
W54	1303.63	1303.61	1303.56	1303.54	1304.35	1304.21	1304.17	1304.15
W56	1290.51	1290.43	1290.35	1290.26	1291.97	1291.19	1291.14	1290.88
W57	1307.50	1307.49	1307.48	1307.47	1307.75	1307.62	1307.61	1307.60
W59	1288.86	1288.85	1288.83	1288.81	1289.47	1289.24	1289.22	1289.14

Decadal simulated head with LULC during 2020-2050

Well ID	Dry Season				Well ID	Wet Season			
	2020	2030	2040	2050		2020	2030	2040	2050
W1	1292.12	1292.10	1292.07	1292.06	W1	1293.06	1292.94	1292.93	1292.91
W2	1301.08	1301.05	1301.01	1300.99	W2	1302.91	1302.79	1302.76	1302.74

Well ID	Dry Season				Well ID	Wet Season			
	2020	2030	2040	2050		2020	2030	2040	2050
W3	1299.04	1299.01	1298.97	1298.95	W3	1300.95	1300.82	1300.80	1300.77
W5	1271.44	1271.43	1271.42	1271.41	W5	1272.04	1271.99	1271.98	1271.97
W6	1279.96	1279.95	1279.94	1279.93	W6	1280.49	1280.45	1280.44	1280.43
W7	1289.14	1289.13	1289.11	1289.11	W7	1289.60	1289.48	1289.48	1289.47
W9	1293.09	1292.99	1292.88	1292.77	W8	1295.76	1295.76	1295.76	1295.76
W12	1289.82	1289.80	1289.79	1289.78	W9	1295.94	1294.89	1294.79	1294.70
W13	1299.00	1298.97	1298.94	1298.91	W10	1296.95	1296.56	1296.53	1296.49
W14	1289.26	1289.25	1289.24	1289.23	W12	1290.40	1290.29	1290.28	1290.27
W15	1289.92	1289.87	1289.81	1289.75	W13	1299.39	1299.14	1299.12	1299.10
W16	1292.88	1292.87	1292.87	1292.87	W14	1289.86	1289.76	1289.75	1289.74
W17	1291.00	1291.00	1291.00	1291.00	W15	1291.23	1290.66	1290.63	1290.59
W18	1320.22	1320.20	1320.15	1320.13	W16	1293.15	1293.15	1293.15	1293.15
W23	1305.48	1305.33	1305.17	1305.05	W17	1291.30	1291.30	1291.30	1291.30
W25	1329.96	1329.93	1329.88	1329.89	W18	1320.60	1320.55	1320.53	1320.52
W26	1329.16	1329.13	1329.09	1329.08	W22	1308.02	1307.90	1307.87	1307.85
W27	1287.25	1287.21	1287.16	1287.12	W23	1311.38	1309.37	1309.15	1309.02
W28	1350.99	1350.99	1350.99	1350.99	W24	1298.27	1298.01	1297.94	1297.90
W32	1296.73	1296.71	1296.69	1296.67	W25	1334.06	1333.88	1333.87	1333.86
W34	1305.96	1305.90	1305.83	1305.76	W26	1333.04	1332.80	1332.78	1332.77
W36	1295.24	1295.19	1295.11	1295.07	W27	1288.79	1288.05	1288.01	1287.96
W37	1290.90	1290.88	1290.86	1290.85	W28	1351.12	1351.12	1351.12	1351.12
W39	1304.07	1304.06	1304.04	1304.03	W34	1307.83	1307.45	1307.41	1307.38
W40	1293.36	1293.34	1293.31	1293.29	W36	1296.62	1296.24	1296.16	1296.11
W41	1291.74	1291.70	1291.66	1291.61	W38	1292.75	1292.71	1292.70	1292.70
W42	1290.79	1290.70	1290.60	1290.50	W40	1294.50	1294.38	1294.36	1294.34
W43	1349.55	1349.55	1349.55	1349.55	W41	1292.23	1291.95	1291.93	1291.91
W44	1362.97	1362.97	1362.97	1362.97	W42	1293.08	1292.31	1292.24	1292.17
W45	1359.26	1359.24	1359.22	1359.21	W43	1349.66	1349.66	1349.66	1349.66
W46	1332.10	1331.99	1331.93	1331.88	W44	1363.09	1363.08	1363.08	1363.08
W47	1336.09	1336.08	1336.08	1336.08	W47	1336.19	1336.19	1336.19	1336.19

Well ID	Dry Season				Well ID	Wet Season			
	2020	2030	2040	2050		2020	2030	2040	2050
W48	1332.00	1331.99	1331.99	1331.99	W48	1332.09	1332.09	1332.09	1332.09
W49	1314.18	1314.18	1314.17	1314.17	W49	1314.29	1314.28	1314.28	1314.28
W50	1326.37	1326.03	1325.36	1325.09	W50	1327.46	1327.36	1327.34	1327.33
W51	1315.10	1315.08	1315.04	1315.02	W51	1315.67	1315.56	1315.53	1315.51
W53	1312.46	1312.45	1312.43	1312.42	W53	1312.69	1312.60	1312.58	1312.56
W54	1303.63	1303.60	1303.55	1303.53	W54	1304.44	1304.30	1304.25	1304.23
W56	1290.51	1290.43	1290.34	1290.25	W56	1292.03	1291.26	1291.22	1291.16
W57	1307.50	1307.49	1307.48	1307.47	W57	1307.76	1307.63	1307.62	1307.61
W59	1288.86	1288.85	1288.82	1288.81	W59	1289.54	1289.30	1289.29	1289.28

Cross section during 2020-2050 with LULC change

ALONG SECTION A - A (2020 - 2050)				
WET SEASON with LULC			WET SEASON without LULC	
Well ID	Simulated head (m) 2050	Simulated head (m) 2020	Simulated head (m) 2050	Simulated head (m) 2020
W16	1293.15	1293.15	1293.13	1293.13
W17	1291.30	1291.30	1291.27	1291.28
W27	1287.96	1288.79	1287.79	1288.64
W7	1289.47	1289.60	1289.17	1289.31
W12	1290.27	1290.40	1289.82	1289.95
W34	1307.38	1307.83	1307.23	1307.70
W36	1296.11	1296.62	1295.97	1296.48
W18	1320.52	1320.60	1320.50	1320.59
W53	1312.56	1312.69	1312.54	1312.67

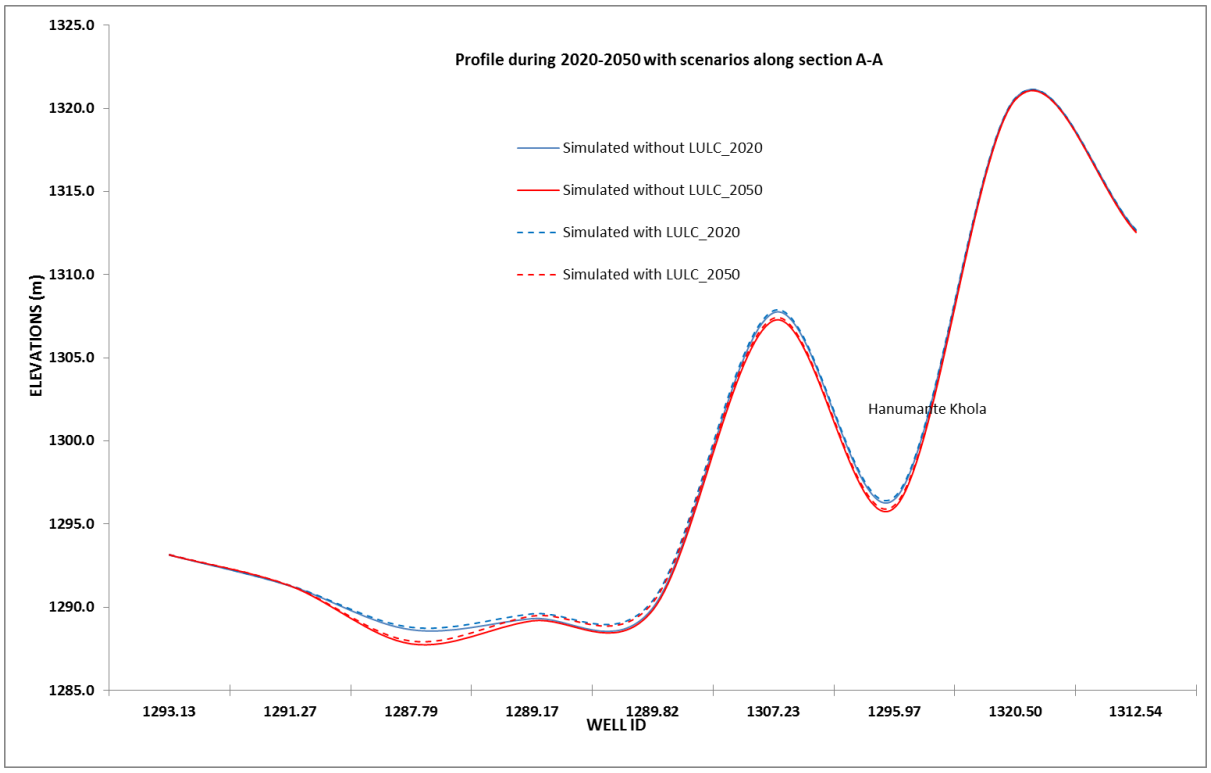

Hydraulic head map of 2020 and 2050 with and without scenario

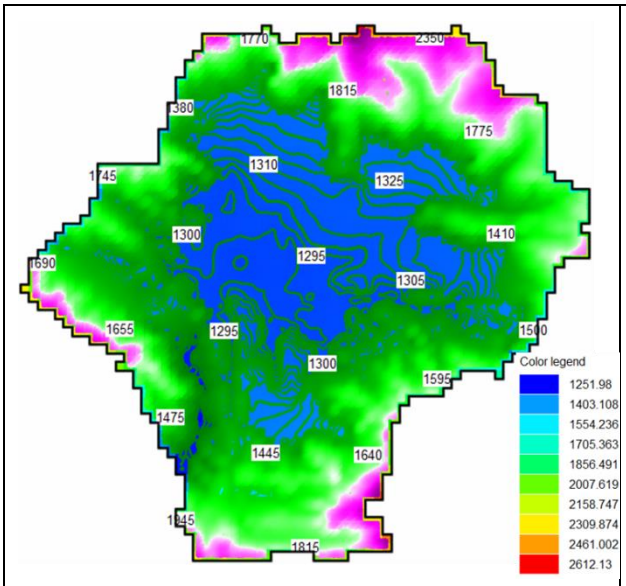

Pumping rate increase dry 2020

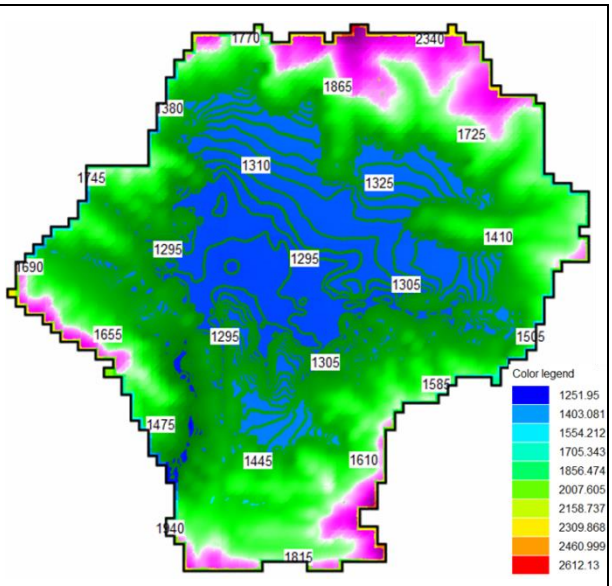

Pumping rate increase dry 2050

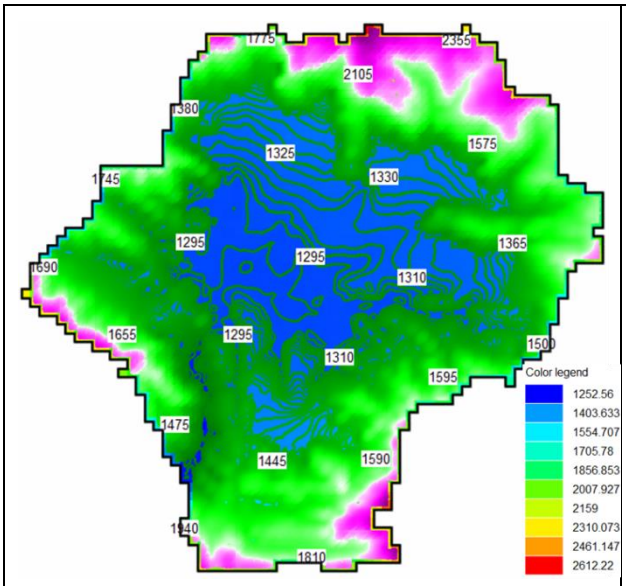

Pumping rate increase wet 2020

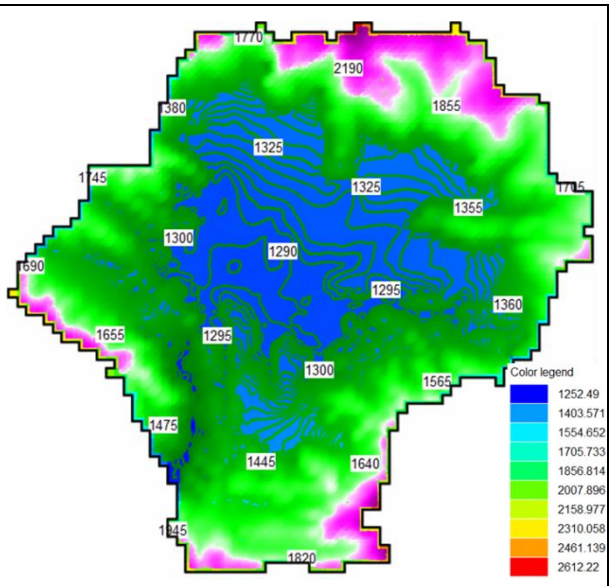

Pumping rate increase wet 2050